Geographia Technica

Geographia Technica

C o n t e n t s

Geographia Technica

CALCULATION OF THE RIVER FLOW WITH DIFFERENT PROBABILITIES OF OCCURRENCE USING ARTIFICIAL NEURAL NETWORK

A GIS-BASED MULTICRITERIA SPATIAL DECISION SUPPORT SYSTEM MODEL TO HANDLE HEALTH FACILITIES RESOURCES. CASE OF CRISIS MANAGEMENT IN BATNA, ALGERIA

COMPARISON OF THE EFFECTIVENESS OF TWO BUDYKO-BASED METHODS FOR ACTUAL EVAPOTRANSPIRATION IN UTTAR PRADESH, INDIA

Mărgărit-Mircea NISTOR[1] iD *, Praveen Kumar RAI[2]* iD *, Iulius-Andrei CAREBIA[3]* iD *, Prafull SINGH[2]* iD *, Arjun PRATAP SHAHI[4], Varun Narayan MISHRA[5]* iD

ABSTRACT:

Evapotranspiration is an important indicator in hydrology, agriculture, and climate. The classical methods to compute the evapotranspiration incorporate climate data of temperature and precipitation. Thornthwaite and Budyko approaches, therefore called here TBA, are the most applied methods for monthly potential evapotranspiration (ET0) respective actual evapotranspiration (AET0). In this study, we have compared the differences between ET0 and AET0 carried out with TBA methods with the crop evapotranspiration (ETc) and actual crop evapotranspiration (AETc) carried out with new methods of TBA applied at spatial scale (TBSS) including the land cover data. Mean monthly rainfall and mean monthly air temperature from 24 meteorological stations located in the Uttar Pradesh State from India were analyzed together with the land cover data to observe and analyse the spatial distributions and differences in evapotranspiration pattern. The study was conducted for 1951 – 2000 period including seasonal analysis. The results indicates that during the mid-season, the ET0 reaches highest values (856.25 mm) while in the same period, the ETc indicates values about 1343.44 mm. The differences between seasonal ET0 and ETc were observed also for the initial and end seasons, with significant increases in evapotranspiration (about 200 mm). Interestingly, during the cold season, the ET0 has higher values than ETc with about 20 mm. As consequences of seasonal increases of the ETc, the annual ETc and AETc indicate higher values than annual ET0 and AET0. These aspects may imply the reduction of runoff and water availability in the study area. Moreover, these findings highlight the importance of land cover pattern in the calculation of evapotranspiration and water balance. The results are illustrates that the applied methodology including the land cover data is more reliable for regional scale and water management investigation rather than the classic methods.

Key-words: *Climate change, Water balance, Evapotranspiration, Crop coefficient, Land cover, Uttar Pradesh.*

[1]*Nanyang Technological University, School of Civil and Environmental Engineering, Singapore. Email: renddel@yahoo.com,*

[2]*Amity Institute of Geo-Informatics and Remote Sensing, Amity University, Noida, India. Emails: rai.vns82@gmail.com, pks.jiwaji@gmail.com*

[3]*Department of Educational Technology, German European School, Singapore. Email: icarebia@gmail.com*

[4]*Department of Applied Geology, National Institute of Technology, Raipur, India. Email: arjunpratapshahi@gmail.com*

[5]*Centre for Climate Change and Water Research, Suresh Gyan Vihar University, Jaipur, India. Email: varun9686@gmail.com,*

1. INTRODUCTION

Evapotranspiration plays an essential role in the water balance and estimation of water renewals. Climatic components are often used in the studies regarding water availability, recharge of groundwater, and drought periods. Surface waters and groundwater represent precious resource that depend by precipitation regime. Climate change effects on different natural systems are an uncontested mater. Mostly, the impact of climate has negative (Parmesan & Yole, 2003; Kløve et al., 2014; Cox et al., 2013; Kløve et al., 2014; Prăvălie, 2014) consequences on the main resource of the Globe: water. However, the climate change affects directly and indirectly the hydrological cycle and groundwater resources as well. The main problems of freshwaters which occurs due to climate variations include the decrease of groundwater recharge, surfaces waters runoff reductions, melting of glaciers, decreased recharge of karst aquifers and decreased groundwater levels (Collins, 2008; Aguilera & Murillo, 2009; Hidalgo et al., 2009; Piao et al., 2010; Jiménez Cisneros et al., 2014). The Global and regional climate changes were claimed in many scientifically papers (Haeberli et al., 1999; IPCC, 2001; Oerlemans, 2005; IPCC, 2007; Cheval et al., 2014; IPCC, 2014; Čenčur Curk et al., 2015; Constantinescu et al., 2016; Nistor et al., 2016). The climate warming and high water consumptions may lead to reduction of spring's flow discharge in many regions of the Globe (Yustres et al., 2013; Kløve et al., 2014).

Up to present, in different countries and regions of the world, the scientists approve several methods to determine the evapotranspiration, including original or modified methods. The effects of climate change on evapotranspiration is mainly related to temperature regime and the water renewals are depending much by precipitation regime. Evapotranspiration in a certain territory may be estimated through calculations by empirical formula or by in-situ measurements. However, the last method is useful in particular locations and due to it's limits, the large territories should be estimates by formulas. During the last decades, numerous scientist estimated the evapotranspiration including the crops and land cover. Allen et al. (1998) proposed the standard methodology of ETc using crop coefficients (Kc) calculated for various types of vegetation and crops, in different zones of the Globe. One of the simplest and high applicability approach is Thornthawaite method (1948) for monthly ET0. In the end of 1990s, Grimmond & Oke (1999) examined the Kc in urban areas from United States. They have calculated the Kc not only for green areas, but also for urban, bare soil, and impervious lands. More recently, Nistor & Porumb-Ghiurco (2015) combined the Thornthwaite (1948) and Allen et al. (1998) methods to analyse the ETc at spatial scale for four seasons. Further, their method have been successfully applied for different regions from Europe and for Turkey (Nistor et al., 2017, Nistor et al., 2019). In the Grand Est region from France, Haidu & Nistor (2019a) used the ETc and precipitation for water availability calculation. The agriculture is the main function of the region and the study of evapotranspiration and water resources is necessary in the region.

The objective of this paper is to compare the classical evapotranspiration method of TBA with the new method TBSS carried out by climate data and land cover. As an example, in this study the spatial distribution of the climate variables over the Uttar Pradesh

State from India were used. The comparison consists in seasonal and annual maps of ET0, ETc, AET0, and AETc over 1951-2000 period.

2. STUDY AREA

Uttar Pradesh State is located in the North of India, close to the tropic zone (Figure 1). During the period 1951-2000, the mean annual temperature of the study area ranges between 24.41 °C and 26.16 °C, indicating the higher values in the eastern part of the region (Figure 2a). The annual precipitation regime varies from 253 mm to 1050 mm, with the much humid values in the East and South-East parts (Figure 2b).

According to Köppen-Geiger climate classification, the area has a warm temperate climate with warm summers (Cfb). Kottek et al. (2006) characterize the Cfb climate type as fully humid.

The land cover of the study area is mainly composed by crop lands, plantations and grass land. The northern and southeastern parts are covered by forest. I the region are presents numerous cities and artificial areas, while the surface water resources are present mainly by two long rivers Ganga and Yamuna and lakes in the southern part. The fallow and barren lands are extending much in the southern part.
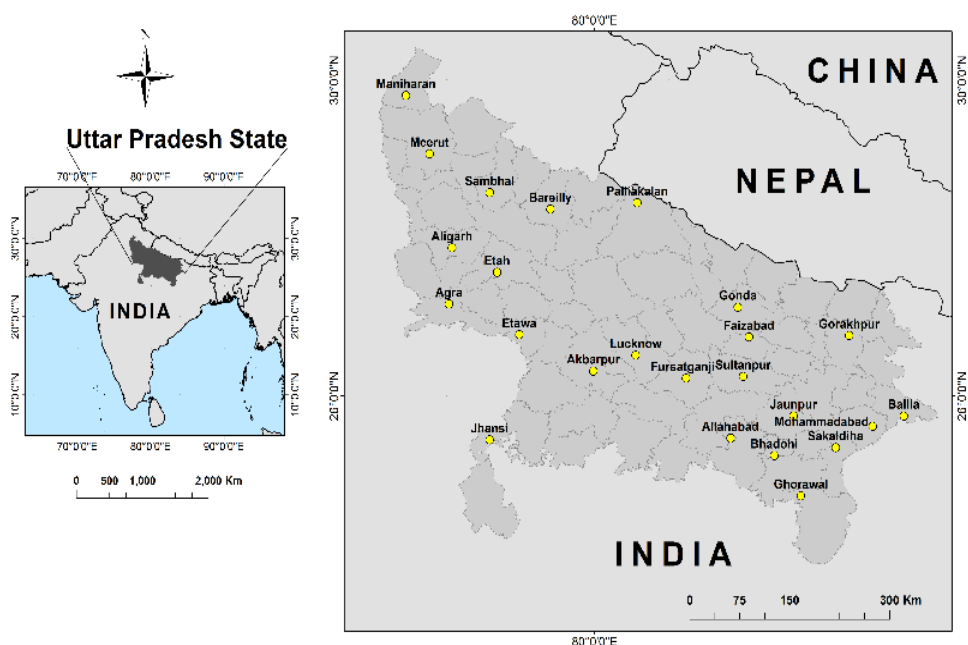
Fig. 1. Location of Uttar Pradesh State on the map of India.

3. MATERIALS AND METHODS

3.1. Overview of the methodology

This work is focusing on spatial procedures to estimate the distribution of evapotranspiration using different methods. Two methods (TBA and TBSS) were applied to for evapotranspiration using climate data from 24 meteorological stations.

In order to obtain the continuous surface of groundwater table over Singapore, Ordinary Kriging (OK) was used as it is recognized in the geostatistical analyses as one of the most important interpolator (Setianto & Triandini, 2013).
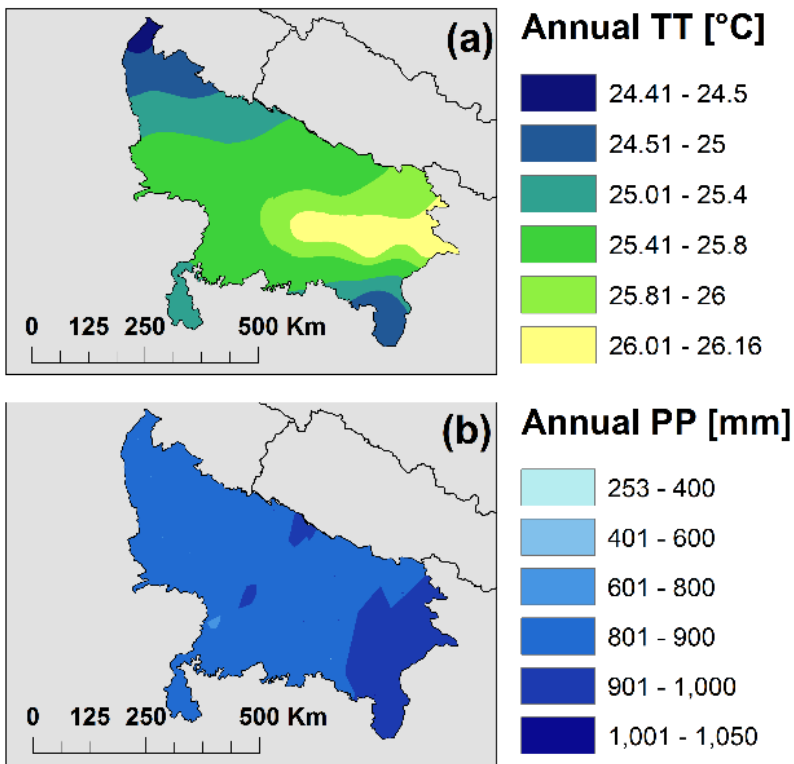
Fig. 2. Spatial variation of mean annual temperature and mean annual precipitation in Uttar Pradesh State. a. Temperature variation 1951-2000. b. Precipitation variation 1951-2000.

3.2. Climate data

Mean monthly air temperature and monthly precipitation from 1951-2000 were used in this study to calculate the ET0, ETc, AET0, and AETc. The climatic data belong to 24 meteorological stations located in the Uttar Pradesh State and these data are courtesy from Indian Meteorological Department at Pune, India (http://www.imdpune.gov.in/). The stations are well distributed in the territory and the data were homogenized and corrected for the long-term period. Table 1 shows the characteristics of climatological stations used in this study.

3.3. Land cover data

Land cover data in 12 classes was used to set up the seasonal Kc at spatial scale for each land cover type in Uttar Pradesh State. The data belong to Oak Ridge National Laboratory (ORNL) Distributed Active Archive Center (DAAC) and has a resolution of 100 m (Roy et al., 2015). Landsat data from 2005 was used as support for the land cover extraction. By supervised classification method, the land cover pattern was prepared.

Table 1.

The meteorological stations and their corresponding geographical co-ordinates (latitude and longitude) and elevations.

Station	Latitude N (decimal degrees)	Longitude E (decimal degrees)	Altitude above mean sea level (m)
Agra	27.17	78.03	169
Aligarh	27.88	78.07	187
Allahabad	25.45	81.73	698
Ballia	25.75	84.17	64
Bareilly	28.37	79.4	172
Sakaldiha	25.35	83.25	79
Etah	27.57	78.68	172
Etawa	26.78	78.98	197
Faizabad	26.75	82.08	102
Mohammadabad	25.62	83.75	77
Gonda	27.13	81.93	110
Gorakhpur	26.77	83.43	84
Juanpur	25.75	82.68	81
Jhansi	25.45	78.58	249
Akbarpur	26.32	79.98	200
Palliakalan	28.45	80.57	148
Lucknow	26.52	80.55	111
Meerut	29.07	77.77	237
Sambhal	28..58	78.58	293
Bhadohi	25.25	82.42	78
Fursatganji	26.23	81.23	88
Maniharan	29.81	77.45	264
Ghorawal	24.74	82.78	303
Sultanpur	26.25	82	96.8

3.4. Evapotranspiration

3.4.1. Potential evapotranspiration (ET0)

Thornthwaite (1948) method (Eq. (1)) was used to calculate the ET0 for Uttar Pradesh State during 1951-2000. This method implies the mean monthly air temperature data. Even if is old, this methods is used often in hydrology and climate studies at regional scale and for long period (Zhao *et al.*, 2013; Čenčur Curk *et al.*, 2014; Cheval *et al.*, 2017). Based on monthly ET0, the seasonal ET0 was calculated and further, the seasonal ETc was determined.

$$ET_0 = 16bi(\frac{10T_i}{I})^\alpha \quad \text{[mm/month]} \tag{1}$$

where:

ET$_0$ = potential evapotranspiration;

bi = radiation parameter for specific latitude (Table 2);
T$_i$ = monthly air temperature;
I = annual heat index (see Eq. 2);
α = complex function of heat index (see Eq. 3)

$$I = \sum_{i=1}^{12} \left(\frac{T_i}{5}\right)^{1.514} \tag{2}$$

where: T$_i$ = monthly air temperature

$$\alpha = 6.75 \times 10^{-7}I^3 - 7.71 \times 10^{-5}I^2 + 1.7912 \times 10^{-2}I + 0.49239 \tag{3}$$

where: I = annual heat index

Table 2.

Sunshine parameter (expressed in units of 30 days of 12 h).

Month	Jan	Feb	Mar	Apr	May	Jun	Jul	Aug	Sep	Oct	Nov	Dec
bi (25° N latitude)	0.93	0.89	1.03	1.06	1.15	1.14	1.17	1.12	1.02	0.99	0.91	0.91

Source: Thornthwaite (1948)

3.4.2. Seasonal and annual crop evapotranspiration (ETc)

In order to calculate the seasonal ETc, the ET0 of each season was multiplied by Kc of the respective season (Eqs. (4-7)). The annual ETc represents a sum of all seasons (Eq.(8)). The calculations were completed using raster grid data in ArcGIS environment. In this study were are using the standard Kc values following growth stages (Allen *et al.* 1998).

Therefore, four developmental stages of crop growth in one year were used in this present study and for each land cover type was assigned a specific value of Kc for that season. For the evapotranspiration rate in the areas with bare soil, open water and urbanization, the values of Kc were chosen accordingly to Grimmond and Oke (1999). They have calculated the Kc in base of studies in several cities from United States.

The seasons were divided as follow: initial season from March to May, mid-season from June to August, end season from September to November and cold season during January, February, and December. Table 3 reports the specific Kc for the land cover types from the study area. Figure 3 illustrates the spatial distribution of the seasonal Kc over Uttar Pradesh State.

$$ET_{c\,ini} = ET_{0\,ini} \times K_{c\,ini} \tag{4}$$

$$ET_{c\,mid} = ET_{0\,mid} \times K_{c\,mid} \tag{5}$$

$$ET_{c\,end} = ET_{0\,end} \times K_{c\,end} \tag{6}$$

$$ET_{c\,cold} = ET_{0\,cold} \times K_{c\,cold} \tag{7}$$

$$Annual\ ET_c = ET_{c\,ini} + ET_{c\,mid} + ET_{c\,late} + ET_{c\,cold} \tag{8}$$

Table 3.
Land cover classes and representative seasonal Kc coefficients for the Uttar Pradesh State

Corine Land Cover	Kc ini season	Kc mid season	Kc end season	Kc cold season
Land cover description	Kclc	Kclc	Kclc	Kclc
Built-up land	0.2	0.4	0.25	-
Wasteland	0.16	0.36	0.26	-
Plantation	0.3	1.05	0.5	-
Cropland	1.1	1.35	1.25	-
Deciduous broadleaf forest	1.3	1.6	1.5	0.6
Mixed forest	1.2	1.5	1.3	0.8
Grassland	0.3	1.15	1.1	-
Shrubland	0.8	1	0.95	-
Fallow land	0.4	0.6	0.5	-
Barren land	0.1	0.15	0.05	-
Permanent wetlands	0.15	0.45	0.8	-
Water bodies	0.25	0.65	1.25	-

Source: From Allen et al. (1998); Nistor and Porumb-Ghiurco (2015); Nistor (2017); Nistor et al. (2017)
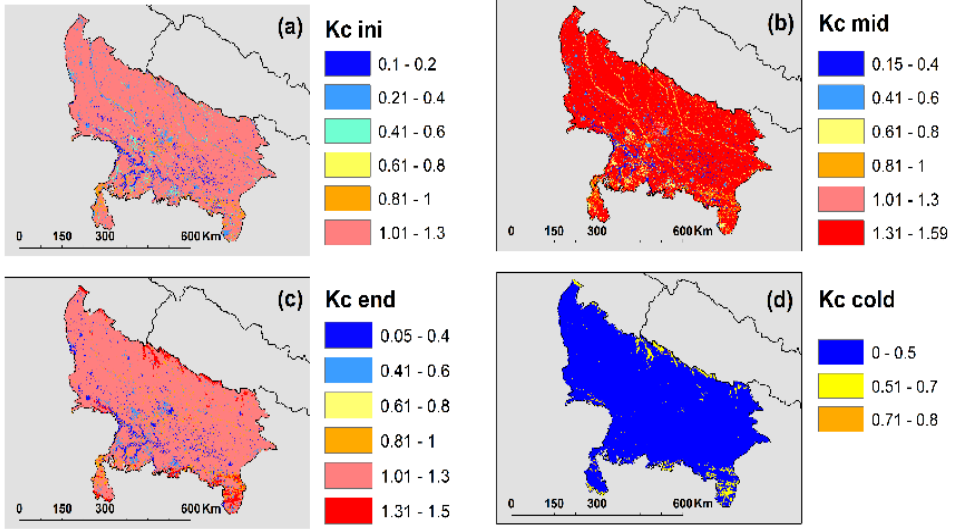
Fig. 3. Spatial distribution of crop coefficient (Kc) in Uttar Pradesh State. (a) Kc for initial season (Kc ini). (b) Kc for mid-season (Kc mid). (c) Kc for end season (Kc end). (d) Kc for cold season (Kc cold).

3.4.3. Determination of AET0 and AETc

The AET0 and AETc were calculated by Budyko (1974) approach (Eq. (9)). The method consists in aridity index φ calculation (Eq. (9)) and further in annual AET0 incorporanting also precipitation data. In case of AETc, the ETc was used instead of ET0 for the aridity index φ calculation. The Budyko's formula contributes to water balance determination and in the same time, it indicates if the heat energy is enough to produce the evaporation from the precipitation data (Gerrits *et al*., 2009; Cencur Curk *et al*., 2014). Recently, Haidu & Nistor (2019b) used Budyko approach to determine the climate change effect on groundwater resources in the Grand Est region, France.

$$\varphi = \frac{ET0}{PP} \tag{9}$$

$$\frac{AET0}{PP} = \left[\left(\varphi \tan\frac{1}{\varphi}\right)(1 - exp^{-\varphi})\right]^{0.5} \tag{10}$$

where:
AET0   actual land cover evapotranspiration [mm]
PP   total annual precipitation [mm]
φ   aridity index (Eq. (9))

4. RESULTS

4.1. Variation of seasonal and annual ET0 and Etc

Overall, the results carried out with the TBSS methods indicates higher maximum values in comparison with the TBA method both for seasonal and annual ETc. Thus, during the initial season, the ET0 ini shows values from 511.12 mm to 757.31 mm (Figure 4a). In the same season, the ETc ini indicates values between 56.32 mm to 968.61 mm (Figure 4b). For both ET0 ini and ETc ini, the high values were depicted in the South-central part of the region, while the low values were depicted in the northwestern part (ET0 ini) and in most of the urban and settlements areas.

The ET0 mid indicates values between 702.8 mm to 856.25 mm while the ETc mid shows values between 117.7 mm to 1343.44 mm. In this season, the higher values of ET0 mid were identified in the central and West-central parts of the Uttar Pradesh State (Figure 4c). The ETc mid recorded high values in the northern and northwestern parts of the region, mainly in the areas deciduous broadleaf forest (Figure 4d).

During the end season, the ET0 end values are ranging from 301.9 mm to 395.55 mm. In the same season, ETc end values varies from 15.19 mm to 588.99 mm. The ET0 end has high values in the West and East parts of the region (Figure 4e), while the ETc end shows higher values in the North and North-West of the region (Figure 4f).

Interestingly, the values of the ET0 cold are varying from 62.05 mm to 95 mm and the ETc cold vary from 0 mm to 75 mm. The higher values of ET0 cold were depicted in the eastern and southeastern part of the Uttar Pradesh State (Figure 4g), while the higher values of the ETc cold were depicted in few locations from the northern and southern parts (Figure 4h).

The annual ET0 varies from 1751 mm to 2003 mm, indicating higher values in the West, central, and East parts of the region. The lower values were identified in the North-West and South-East, but still these values are exceeding 1700 mm (Figure 5a). The variation of annual ETc is between 193 mm and 2869 mm, with most of the territory in the range of 2000 mm and 2500 mm. The higher values were identified in the northern and southern parts of the region. The lower values were depicted in the urban areas and wastelands (Figure 5b).

4.2. Variation of aridity index, AET0, and AETc

As ratio between evapotranspiration and precipitation, the aridity index indicates the drought and leak of water for the higher values of the index. In the Uttar Pradesh State, the aridity index was calculated as the basis for deriving the AET0 and AETc values. Thus, the aridity index calculated for AET0, incorporates the annual ET0 and it shows values between 1.7 and 7.6, but most of the territory has values between 2 and 3. For the AETc, the annual ETc was used in the ratio formula. The aridity index carried out for AETc shows values between 0.2 and 5.2.
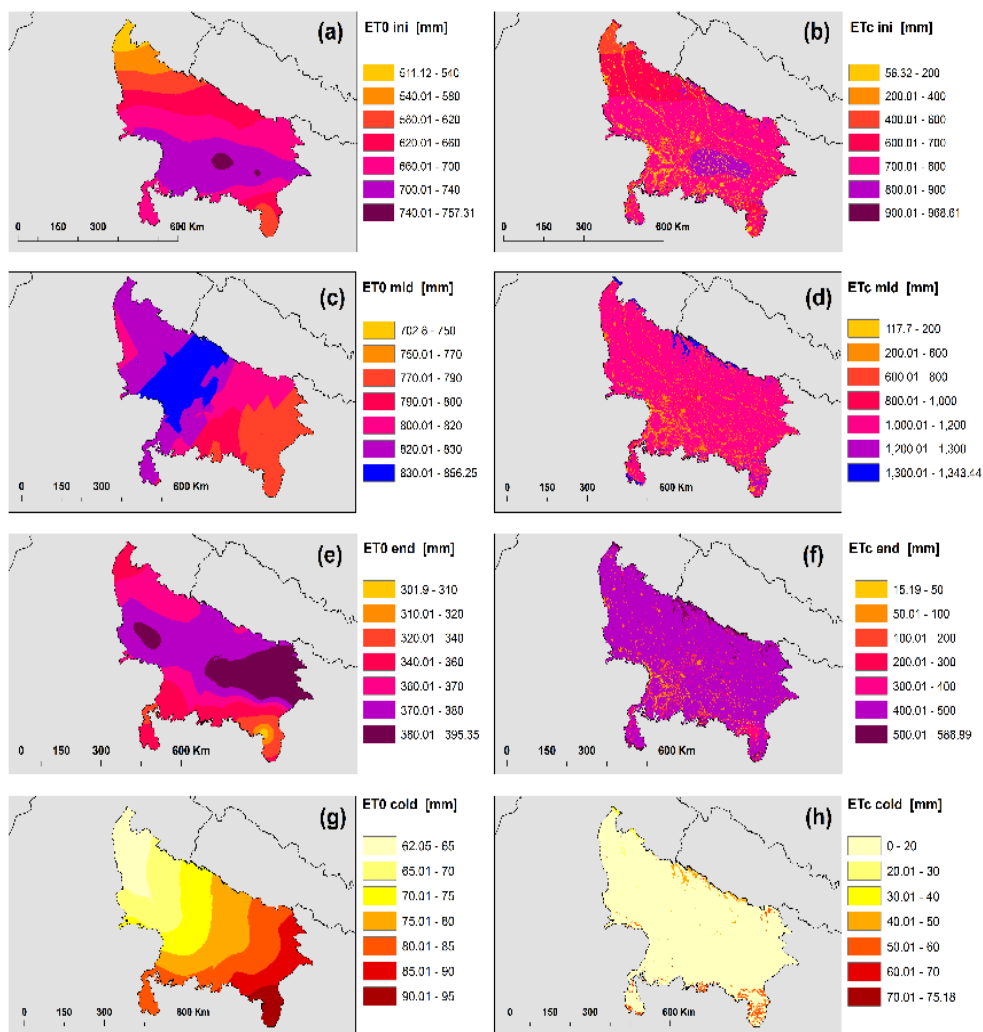
Fig. 4. Spatial distribution of seasonal potential evapotranspiration (ET0) and potential crop evapotranspiration (ETc) in Uttar Pradesh State. (a) ET0 for initial season (ET0 ini). (b) ETc for initial season (ETc ini). (c) ET0 for mid-season (ET0 mid). (d) ETc for mid-season (ETc mid). (e) ET0 for end season (ET0 end). (f) ETc for end season (ETc end). (g) ET0 for cold season (ET0 cold). (h) ETc for cold season (ETc cold).

The AET0 varies from 253 mm to 906 mm, indicating higher values in the eastern and central parts of the region. The lower values were identified in the northwestern and southwestern parts (Figure 6a). The variation of AETc is between 183 mm and 923 mm (Figure 6b). The higher values were identified in the northern and southern parts of the region. The lower values were depicted in the urban areas and wastelands.
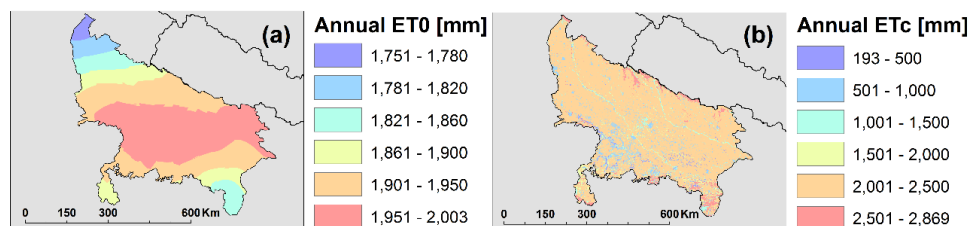
Fig. 5. Spatial distribution of annual potential evapotranspiration (Annual ET0) and annual potential crop evapotranspiration (Annual ETc) in Uttar Pradesh State. (a) Annual ET0. (b) Annual ETc.
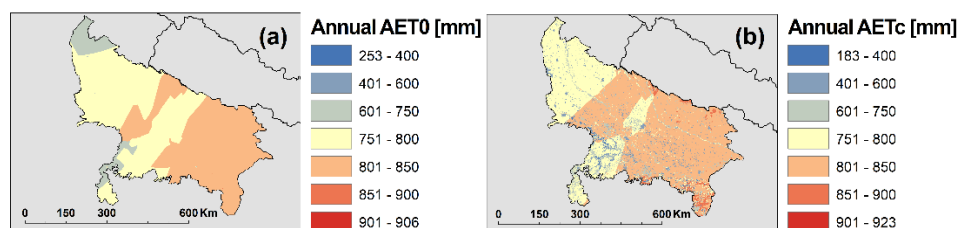
Fig. 6. Spatial distribution of annual actual evapotranspiration (AET0) and annual actual crop evapotranspiration (AETc) in Uttar Pradesh State. (a) Annual AET0. (b) Annual AETc.

5. DISCUSSION

The applied complex methods based on TBA and TBSS integrate the climate and land cover data for determination of seasonal and annual ET0 and ETc, and for annual AET0 and AETc. Based on the climatological data from the 1951-2000 recorded in Uttar Pradesh State, the application of the two methods for evapotranspiration was completed. Firstly, the TBA includes only the temperature and precipitation data, while the TBSS includes the vegetation pattern. The difference in findings of the two methods is obviously not only at numerical results but also at spatial scale. In fact, the TBSS method is much useful at the spatial scale analyses. Secondly, the last method (TBSS) returns values higher and lower for the maxima and minima with respect to the TBA method. For this reason, the seasonal ETc indicates higher values for ETc ini, ETc mid, and ETc end in comparison with the seasonal ET0. In contrast, due to the reduced plants activities during the cold season, the ETc cold has lower values in comparison with the ET0 cold. The contribution of another

three seasons (ETc ini, ETc mid, and ETc end) for evapotranspiration are influencing the higher values of the annual ETc in comparison with annual ET0.

Thus, according to the TBA the values of evapotranspiration are not reaching the maximum and are not fall to the minimum that the TBSS method are given. The performance of the TBSS may help better in the agriculture studies, in varies types of land cover and crops. In this way, the areas with high Kc and low precipitation, could be in deep investigated and, if necessary, prepared for irrigation. Looking in much details, the TBSS method could be also be used for the water resources investigations. In this sense, the runoff and water availability could be calculated at spatial scale and the areas with low runoff and water availability could be protected by some activities (i.e. water exploitation, intense agriculture).

The results of this study underline the importance of continuously improving the traditional methods (i.e. TBA) with much current approaches that cover nowadays requirements (i.e. spatiality analysis with TBSS). In addition, the groundwater resources recharge at spatial scale could be estimated and further, different groundwater models could be set up.

The analysis of the original maps that we provided here can be a substantial way to evaluate the proprieties of the evapotranspiration and water resources in a single locations, focusing on a single type of land cover. For instance, the variations of evapotranspiration by TBA and TBSS indicate higher values of the maximum calculations for the TBSS due to the incorporation of Kc. The Kc values contribute to the increases of evapotranspiration for ETc ini, ETc mid and ETc end because the plants and crops plantations are active during these seasons. Regarding the cold seasons, only forest and threes are consuming heat energy.

The present research demonstrates how the same methods could return different results if the land cover pattern is included in the analysis. Due to the specific Kc for various seasons, the TBSS method could be more useful in the applicability of agriculture and water resources pressure under the climate change. Thus, our work become an important task not only in the climatology, hydrology and agriculture, but also for the regional administration of the environment. As an example, the delimitation of protection areas with respect of low water resources could be done using the present results. In addition, the groundwater vulnerability and future planning strategies could be drawn based of the original maps developed in this study.

6. CONCLUSIONS

This paper aimed in the comparison of the TBA and TBSS methods for the evapotranspiration. The application of these methods was completed on the Uttar Pradesh State from India using the land cover and climate data from 24 stations. By comparing the results of both methods, the following conclusions could be drawn:

- The procedures and calculations of the four seasons ET0 and ETc were applied on the Uttar Pradesh State from territory. Further, the AET0 and AETc were carried out using both TBA and TBSS methods.
- For the spatial analysis of ETc and AETc, the specific Kc was assigned for each land cover types. In base of this, the contribution of vegetation pattern for evapotranspiration was taken into consideration.
- Both TBA and TBSS methods return reasonable results with respect to the evapotranspiration at seasonal and annual temporal scales. As the findings confirmation, the evapotranspiration reach higher values in the mid-season.
- The maximum values of evapotranspiration, were found for ETc and AETc by using TBSS method.
- TBA method is much consistent with the climate data, while the TBSS follows the climate data but the results are controlled by the Kc values. However, both methods could be useful for hydrological, climatological, and agricultural studies.

This comparison represents a contribution for the existing approaches with respect to the evapotranspiration. The methodology can be widely used for investigations at spatial scale. The results indicate that the TBSS method is much realistic due to the incorporation of the land cover data. Based on the findings of this paper and the spatial calculations of ET0, ETc, AET0, and AETc in the Uttar Pradesh State, the environmental plans for management could be implemented in this region.

REFERENCES

Aguilera, H. & Murillo, J.M. (2009) The effect of possible climate change on natural groundwater recharge based on a simple model: a study of four karstic aquifers in SE Spain. *Environmental Geology*, 57(5), 963–974.

Bettelli, G. & De Nardo M.T. (2001) Geological outlines of the Emilia Apennines (Italy) and introduction to the rocks units cropping out in the areas of landslides reactivated in the 1994-1999 period, Quaderni di Geologia Applicata, Volume 1, Publish no. 2131 GNDCI-CNR, Pitagora Editrice Bologna.

Budyko, M.I. (1974) Climate and life. Academic Press, New York, USA, pp. 508.

Čenčur Curk, B., Cheval, S., Vrhovnik, P., Verbovšek, T., Herrnegger, M., Nachtnebel, H.P., Marjanović, P., Siegel, H., Gerhardt, E., Hochbichler, E., Koeck, R., Kuschnig, G., Senoner, T., Wesemann, J., Hochleitner, M., Žvab Rožič, P., Brenčič, M., Zupančič, N., Bračič Železnik, B., Perger, L., Tahy, A., Tornay, E.B., Simonffy, Z., Bogardi, I., Crăciunescu, A., Bilea, I.C., Vică, P., Onuţu, I., Panaitescu, C., Constandache, C., Bilanici, A., Dumitrescu, A., Baciu, M., Breza, T., Marin, L., Draghici, C., Stoica, C., Bobeva, A., Trichkov, L., Pandeva, D., Spiridonov, V., Ilcheva, I., Nikolova, K., Balabanova, S., Soupilas, A., Thomas, S., Zambetoglou, K., Papatolios, K., Michailidis, S., Michalopoloy, C., Vafeiadis, M., Marcaccio, M., Errigo, D., Ferri, D., Zinoni, F., Corsini, A., Ronchetti, F., Nistor, M.M., Borgatti, L., Cervi, F., Petronici, F., Dimkić, D., Matić, B., Pejović, D., Lukić, V., Stefanović, M., Durić, D., Marjanović, M., Milovanović, M., Boreli-Zdravković, D., Mitrović, G., Milenković, N., Stevanović, Z. & Milanović, S. (2014) CC-WARE Mitigating

Vulnerability of Water Resources under Climate Change. WP3 - Vulnerability of Water Resources in SEE, Report Version 5. URL: http://www.ccware.eu/output-documentation/output-wp3.html. [Accessed 15th May 2017].

Čenčur Curk, B., Vrhovnik, P., Verbovsek, T., Dimkic, D., Marjanovic, P., Tahy, A., Simonffy, Z., Corsini, A., Nistor, M.M., Cheval, S., Herrnegger, M. & Nachtnebel, P.H. (2015) Vulnerability of Water Resources to Climate Change in South-East Europe, AQUA 2015 42nd IAH Congress, The International Association of Hydrogeologists, 218.

Cheval, S., Birsan, M.V. & Dumitrescu, A. (2014) Climate variability in the Carpathian Mountains region over 1961-2010. *Global Planet Change*, 118, 85–96.

Civita, M. (2005) Idrogeologia applicata ed ambientale. CEA, Milano, Italy, 794 pp.

Civita, M. (2008) An improved method for delineating source protection zones for karst springs based on analysis of recession curve data. *Hydrogeology Journal*, 16, 855–869.

Collins, D.N. (2008) Climatic warming, glacier recession and runoff from Alpine basins after the Little Ice Age maximum. *Annals of Glaciology*, 48(1), 119–124.

Constantinescu, D., Cheval, S., Caracaș, G. & Dumitrescu A. (2016) Effective monitoring and warning of Urban Heat Island effect on theindoor thermal risk in Bucharest (Romania). *Energy and Buildings*, 127, 452–468.

Cox, P.M., Betts, R.A., Jones CD. et al. (2000) Acceleration of global warming due to carbon-cycle feedbacks in a coupled climate model. *Macmillan Magazines Nature*, 408, 184–187.

Galleani, L., Vigna, B., Banzato, C. & Lo Russo S. (2011) Validation of a Vulnerability Estimator for Spring Protection Areas: The VESPA index. *Journal of Hydrology*, 396, 233–245.

Gerrits, A.M.J., Savenije, H.H.G., Veling, E.J.M. and Pfister, L. (2009) Analytical derivation of the Budyko curve based on rainfall characteristics and a simple evaporation model. *Water Resources Research*, 45(4), 1–15. https://doi.org/10.1029/2008WR007308

Giannini, E. & Lazzarotto A. (1975) Tectonic evolution of the Northern Apennines, Geology of Italy Volume II, Edited by Coy H. Squyres, Tripoli.

Haeberli, W.R., Frauenfelder, R., Hoelzle, M. & Maisch, M. (1999) On rates and acceleration trends of global glacier mass changes. *Physical Geography,* 81A, 585–595.

Haidu, I. & Nistor MM. (2019a). Groundwater vulnerability assessment in the Grand Est region, France. Quaternary International, https://doi.org/10.1016/j.quaint.2019.07.024.

Haidu, I. & Nistor MM. (2019b) Long-term effect of climate change on groundwater recharge in the Grand Est region, France. Meteorological Applications, doi: 10.1002/met.1796.

Hidalgo, H.G., Das, T., Dettinger, M.D. et al. (2009) Detection and attribution of streamflow timing changes to climate change in the western United States. *Journal of Climate,* 22(13): 3838-3855.

IPCC. (2001) Climate Change 2001: The Scientific Basis. Contribution of Working Group I to the Third Assessment Report of the Intergovernmental Panel on Climate Change [Houghton, J.T., Ding, Y., Griggs D. J. et al. (eds.)]. Cambridge University Press, Cambridge, United Kingdom and New York, NY, USA, 881 pp.

IPCC. (2007) Contribution of Working Group I to the Fourth Assessment Report of the IPCC. In „Climate Change 2007: The Physical Science Basis" [Solomon, S., Qin, D., Manning, M., Chen, Z., Marquis, M., Averyt, K.B., Tignor, M. and Miller, H.L. (eds.)] Cambridge University Press, Cambridge, United Kingdom and New York, NY, USA, 996 pp.

IPCC. (2014) Climate Change 2014: Impacts, Adaptation, and Vulnerability. Contribution of Working Group II to the Fifth Assessment Report of the Intergovernmental Panel on Climate Change.

Jiménez Cisneros, B.E., Oki, T., Arnell, N.W. et al. (2014) Freshwater resources. In: Climate Change 2014: Impacts, Adaptation, and Vulnerability. Part A: Global and Sectoral Aspects. Contribution of Working Group II to the Fifth Assessment Report of the Intergovernmental Panel on Climate Change [Field, C.B., Barros, V.R., Dokken, D.J. et al. (eds.)]. Cambridge University Press, Cambridge, United Kingdom and New York, NY, USA, 229–269.

Kløve, B., Ala-Aho, P., Bertrand, G., Gurdak, J.J., Kupfersberger, H., Kværner, J., Muotka, T., Mykrä, H., Preda, E., Rossi, P., Bertacchi Uvo, C., Velasco, E. & Pulido-Velazquez, M. 2014. Climate change impacts on groundwater and dependent ecosystems. *Journal of Hydrology*, 518, 250–266.

Meinzer, O.E. (1927) Large springs in the United States. In "Plants as indicators of groundwater. Water-Supply Paper 557". Published by United States Geological Survey.

Nistor, M.M. & Porumb-Ghiurco, C.G. (2016) Record year for annual retreat rate of Whittier Glacier from South Alaska in 2014. *GEOREVIEW Scientific Annals of Ştefan cel Mare University of Suceava Geography Series*, 25(1), 93 - 99. ISSN: 1583-1469. URL: http://georeview.ro/ojs/index.php/revista/article/view/269

Nistor, M.M., Dezsi, Şt., Cheval, S. & Baciu M. (2016) Climate change effects on groundwater resources: a new assessment method through climate indices and effective precipitation in Beliş district, Western Carpathians. *Meteorological applications*, 23, 554–561.

Nistor, M.M., Cheval, S., Gualtieri, A., Dumitrescu, A., Boţan, V.E., Berni, A., Hognogi, G., Irimuş, I.A. & Porumb-Ghiurco, C.G. (2017) Crop evapotranspiration assessment under climate change in the Pannonian basin during 1991-2050. *Meteorological applications*, 24, 84-91.

Nistor, M.M., Mîndrescu, M., Petrea, D., Nicula, A.S., Rai, P.K., Benzaghta, M.A., Dezsi, Şt., Hognogi, G. & Porumb-Ghiurco CG. (2019) Climate change assessment on crop evapotranspiration in Turkey during 21st century. *Meteorological Applications*, 26, 442-453.

Oerlemans, J. (2005) Extracting a Climate Signal from 169 Glacier Records. *Science,* 308: 675-677.

Parmesan, C. & Yohe, G. (2003) A globally coherent fingerprint of climate change impacts across natural systems. *Nature*, 421(2), 37–42.

Piao, S., Ciais, P., Huang, Y. et al. (2010) The impacts of climate change on water resources and agriculture in China. *Nature*, 467(7311), 43–51.

Prăvălie, R. (2014) Analysis of temperature, precipitation and potential evapotranspiration trends in southern Oltenia in the context of climate change. *Geographia Technica*, 9(2), 68–84.

Setianto, A. & Triandini T. (2013) Comparison of Kriging and Inverse Distance Weighted (IDW) interpolation methods in lineament extraction and analysis. *J. SE Asian Appl. Geol.,* 5(1), 21-29.

Thornthwaite, W. (1948) An Approach toward a Rational Classification of Climate. *American Geographical Society*, 38(1), 55–94.

Yustres, Á., Navarro, V., Asensio, L., Candel, M. & García, B. (2013) Groundwater resources in the Upper Guadiana Basin (Spain): a regional modelling analysis. *Hydrogeology Journal*, DOI 10.1007/s10040-013-0987-y.

Zhao, L., Xia, J., Xu, C., Wang, Z., Sobkowiak, L. and Long, C. (2013) Evapotranspiration estimation methods in hydrological models. *Journal of Geographical Sciences*, 23(2), 359–369.

GIS-BASED FLOOD HAZARD MAPPING USING HEC-RAS MODEL: A CASE STUDY OF LOWER MEKONG RIVER, CAMBODIA

Vanthan KIM[1], Sarintip TANTANEE[2], Wayan SUPARTA[3] (ID)

ABSTRACT:
Rivers are the main water sources for human and animals' lives. Unfortunately, they have been frequently damaged by flooding. Flooding has affected and threatened not only human's lives and infrastructures but also the environmental capital. This study aims to determine the application of flood frequency analysis integrated with the GIS and HEC-RAS models to prepare a multi-return period flood hazard map in the Lower Mekong River of Cambodia. A 30-year peak discharge (Kampong Cham gauging station) with a multi-return period of 10, 20, 50, and 100-years was estimated by using four distributions analysis. An EasyFit software is used to test the best distribution for the input of the HEC-RAS model to prepare the estimation of the corresponding floodplain areas. The results showed that Log-Pearson III distribution analysis of the return period of 10, 20, 50, 100 years is the best fits with the 52,208 m³/s, 54,990 m³/s, 59,381 m³/s, and 62,194 m³/s, respectively. The HEC-RAS calibration indicated a good agreement with observed data discharge 2011 and 2013. While the simulation model shows the return period of floods 10 and 20 years for the predicted depth of flooding is stable compared to the flood peaks of 2011 and 2013 discharges, but the conditions of other flood return periods are not stable. Overall, HEC-RAS with its flood hazard map is a model that can estimate the level of flood depth in the Lower Mekong River, Cambodia and is useful in providing information about the depth and characteristics of floods for river communities.

Key-words: *Flood Hazard Map, GIS, HEC-RAS, Flood Frequency analysis, Mekong River*

1. INTRODUCTION

Over the last decades, the flood has been the most common natural disaster worldwide, constructing many negative environmental and socio-economic consequences on people, infrastructures, properties, and indirectly impact the country's economy (Kheradmand et al., 2018). The conservative flood management approach focusing on structural flood mitigation measures have now been shifted to a risk-based flood mitigation concept (Romali et al., 2018). Furthermore, the severity of flood hazard around the world requires to continue prevention to reduce their impact (Azouagh et al., 2018). Because it is the most widespread, frequent, and costly natural disaster for human societies (Mihu-Pintilie et al., 2019). Each year, more than 140 million people across the world are affected by floods (OECD, 2016). Flood hazard is the probability of a flood event will take place (Vojtek & Vojtekova, 2016).

Flood modeling is very important for flood hazard assessment to show the magnitude of a flood with a convincing exceeded probability (Azouagh et al., 2018), while the purpose

[1,2] Naresuan University, Department of Civil Engineering, Faculty of Engineering, Phitsanulok 6500, Thailand, Corresponding author: sarintipt@nu.ac.th
[3] Universitas Pembangunan Jaya, Department of Informatics, South Tangerang City, Banten 15413, Indonesia, Corresponding author: wayan.suparta@upj.ac.id ORCID 0000-0002-6193-1867

of a vulnerability assessment is to provide hydrological characteristics to model the damage (Rahmati et al., 2016). Some researchers (e.g.,Shafapour et al., 2017; Mihu-Pintilie & Nicu, 2019) applied a GIS-based approach to conduct flood hazard mapping with different parameters (i.e. land use, land cover, DEM, soil, river network, and slop). Mostly, coupling GIS and hydraulic models (Haidu, 2016) have been recommended for studying flood analysis and flood prediction (Győri et al., 2016; Haidu et al., 2017; Vojtek et al., 2019). A combination of GIS (Geographic Information System) and HEC-RAS (Hydrologic Engineering Center-River Analysis System) has a great capability in the simulation of flood hazard maps. HEC-RAS is one of the most commonly used models to analyze channel flow and floodplain delineation (Maskong, 2019). River flood hazard mapping was first initiated in 1988 in the United States by the Hydrologic Engineering Centre (HEC) of the U.S. Army Corps of Engineers (USACE, 2018). The HEC-RAS model was found to give a good performance where the simulated results for both studies showed a close agreement with observed water surfaces.

In Cambodia, floods caused by the Mekong River in 2000 and 2011 killed 250 people, affected 350,000 households of over 1.5 million people, causing 52,000 households to be evacuated, costing the economy 521,000 million US dollars. These floods were ranked as the worst natural disasters in Cambodia over the last 70 years (CFE-DM, 2017). Moreover, report the Cambodian floods of 2013, which affected 20 out of 24 provinces, 377,354 households, claiming 168 lives, and forcing 31,314 households to be evacuated to safer areas (Rishiraj et al., 2015; Vichet et al., 2019). Mochizuki et al. (2015), who study the assessment of the natural disaster of flood and cyclone risks to public and private buildings including educational structures, health facilities, and housing, estimates that the total direct economic damage ranges from approximately 304 million US dollars for a 5-year return period event, to 2.26 billion US dollars for a 1000-year return period event. Furthermore, the annual records by the National Committee of Disaster Management of Cambodia (1996 to 2018) as well as (Yu et al., 2019) review of CRED, 2014, showed that extreme flooding from the Mekong River mostly affected the country in 1978, 1991, 1994, 1996, 2000-2002, 2011, and 2013. Likewise, Cambodia Disaster and Risk Profile (EM-DAT) 2017, who study floods caused by drought and storm based on frequency, mortality and economic issues, observe that flooding induced more complicated impact than drought and storm (CRED, 2019).

Flood hazard map is considered an important tool for tackling these problems. The study aims to prepare a flood hazard map that integrates flood inundation areas, flood extent, and flood depth in the study area. HEC-RAS and GIS-based methods are the main components in analyzing flood hazards of the lower Mekong River, Cambodia. The scope of the study is focused on the river floods, where investigate the ability of methods applied to design flood hazard maps and the length of the data series.

2. STUDY AREA AND DATA

Cambodia is one of the countries in South-East Asia located between 102.350 and 107.620 longitude and 9.910 and 14.690 latitudes. The total area is 181,035 km^2, 97.5 percent of which is the land while 2.5 percent is a water body (Vichet et al., 2019). The Mekong River is one of the world's longest river systems, flowing 4,909 km through six countries: China, Myanmar, Thailand, Lao PDR, Cambodia, and Vietnam, having a basin area of 795,000 km^2, and a mean annual discharge of 14,500 m^3/s or 475 km^3/ year. The flows are of a very large difference during the wet (June to October) and dry (November to May) seasons (Ang & Oeurng, 2018).

This study aims to develop a return period-based flood hazard map using the GIS and HEC-RAS models in the part of Kampong Cham (1,258 km^2), Tboung Khmum (87 km^2), and Kandal (518 km^2) province and Phnom Penh (85 km^2) city. The river division **(Fig. 1)** starts from the Mekong upstream Kampong Cham (KC) and reaches Chruy Changvar (CC) gauging station (Phnom Penh City), with the area of 1,948 km^2 and length 103.53 km in Cambodia.
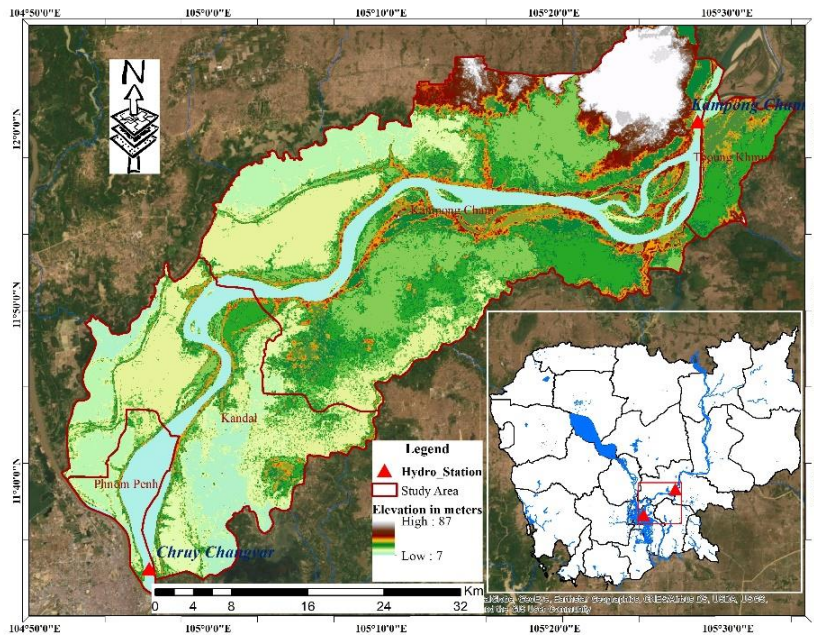
Fig. 1. Location of the study area (Source: authors).

Peak discharge in 30 years is collected from the Department of Meteorology and River Works, Cambodia. The peak discharge is used to calculate the different return periods of 10, 20, 50, and 100-years. Hence, the 30m resolution of Advanced Spaceborne Thermal Emission and Radiometer (ASTER) Digital Elevation Model (DEM) was downloaded free from the U.S Geological Survey website (https://earthexplorer.usgs.gov/) in order to extract basin geometry, stream networks, river geometry, Triangular Irregular Network (TIN), and 100 cross-sections.

3. METODOLOGY

3.1. Flood Frequency Analysis

To analyze the extreme values of different return periods 10, 20, 50, and 100-years using observed maximum historical discharge, a variety of methods can be applied, i.e. Log-Pearson type III, Log-Normal, Normal, and Gumbel's distribution (Tanaka et al., 2017; Farooq et al., 2018; Bhat et al., 2019). Moreover, the estimation of peak discharge is an important step for selecting flood events and different return periods to input model processing.

In this study, Log-Pearson type III, Log-Normal, Normal, and Gumbel's distribution were used in flood frequency analysis. The EasyFit software was used to select the base flood value to identify the peak flood of various historical records. 30 annual peak discharges of Kampong Cham station (ID: 198,02 and coordinate, X: 551,341, Y: 1,327,363) between 1989 and 2018 were used. The goodness of fit test (GOF) of Kolmogorov, Anderson, and Chi-Squared were employed to analyze and estimate the best-fitted distribution.

3.2. GIS and HEC-RAS Modeling

GIS provides a broad range of tools for determining areas affected by floods or for forecasting areas likely to be flooded due to high river water levels (Klemešová et al., 2014). A DEM offers the most common way of showing topographic information and even enables the modeling of flow across topography; a controlling factor in distributed models of landform processes (Toosi et al., 2019).

HEC-RAS is a widely used hydraulic software tool developed by the U.S Army Corps of Engineers (USACE, 2018). HEC-RAS employs 1-D flood routing in both steady and unsteady flow conditions by applying an implicit-forward finite difference scheme between successive sections of flexible geometry. The steady flow scheme is based on the solution of the 1-D energy equation or the momentum equation between two successive cross-sections (USACE, 2018). The energy equation is written as follows (Echogdali et al., 2018, p. 963):

$$Z_2 + Y_2 + \frac{a_2 V_2^2}{2g} = Z_1 + Y_1 + \frac{a_1 V_2^2}{2g} + h_e \qquad (1)$$

where Z_1 and Z_2 are the elevations of the main channel inverts, Y_1 and Y_2 are the depths of water at cross-sections, V_1, V_2 is the average velocities (total discharges/total flow area), a_1, a_2 are the velocity weighting coefficients, that account for non-uniformity of the velocity distribution over the cross-section, g: gravitational acceleration, and h_e: is the energy head loss.

The cross-section sub-division for the water conveyance is calculated within each reach using the following equations:

$$Q = KS_f^{1,2}, \text{while } K = \frac{1.486}{n} AR^{2/3} \qquad (2)$$

where K = conveyance for subdivision, n = Manning roughness coefficient, A = flow area subdivision, R = hydraulic radius for subdivision (wetted area/wetted perimeter), and S_f = friction slope.

DEM was used as input data to generate a watershed and drainage network in RAS Mapper. The channel, bank stations, flow direction, and cross-section cut lines were prepared in RAS Mapper and exported to the HEC-RAS model. An upstream (Kampong Cham) station of Lower Mekong River was selected for data input. Moreover, the multi return periods of the peak floods were obtained from Log-Pearson III and used as an input to the model in order to simulate results for each cross-section. At the same time, water surface profiles were run in the model for 10, 20, 50, and 100-years. After running input data in the HEC-RAS model, the outputs were exported to GIS in the format of the RAS GIS Export file. GIS was used to generate flood depth mapping for multi return periods. The overall methodology flow chart is shown in **(Fig. 2).**
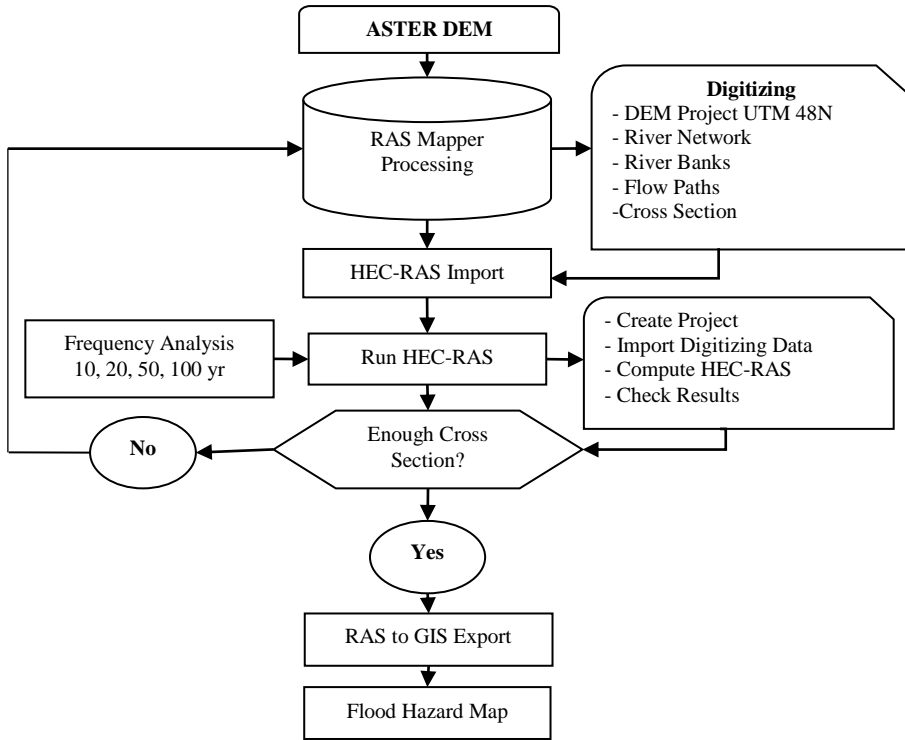
Fig. 2. Methodology framework of flood hazard mapping

3.3 Calibration of HEC-RAS Model

The calibration of the model has used three indicators including Nash-Sutcliffe model efficiency (NSE), percent bias (PBIAS), and coefficient of determination (R^2) were computed using daily average flow, as standard show in **(Table 1)** (USACE, 2018)

$$\text{NSE} = 1 - \frac{\sum_{i=1}^{n} \left(Q_{obs_i} - Q_{sim_i}\right)^2}{\sum_{i=1}^{n} \left(Q_{obs_i} - \overline{Q_{obs_i}}\right)^2} \tag{3}$$

$$PBIAS = \left[\frac{\sum_{i=1}^{n} \left(Q_i^{obs} - Q_i^{sim}\right) \times 100}{\sum_{i=1}^{n} \left(Q_i^{obs}\right)}\right] \tag{4}$$

$$R^2 = \frac{\sum\left(\left(Q_{sim}(t) - \overline{Q_{sim}}\right)\left(Q_{obs}(t) - \overline{Q_{obs}}\right)\right)^2}{\sum\left(Q_{sim}(t) - \overline{Q_{sim}}\right)^2 \sum\left(Q_{obs}(t) - \overline{Q_{obs}}\right)^2} \tag{5}$$

where Q $_{sim(t)}$ and Q $_{obs(t)}$ are the simulated and observed discharges at time step t, and $\overline{Q_{sim}}$ and $\overline{Q_{obs}}$ are the simulated and observed average discharges.

<div align="right">Table 1.</div>

<div align="center">Performance ratings for summary statistics.</div>

Performance Rating	NSE	PBIAS	R^2
Very Good	$0.65 < \text{NSE} \leq 1.00$	$\text{PBIAS} < \pm 15$	$0.65 < R^2 \leq 1.00$
Good	$0.55 < \text{NSE} \leq 0.65$	$\pm 15 \leq \text{PBIAS} < \pm 12$	$0.55 < R^2 \leq 0.65$
Satisfactory	$0.40 < \text{NSE} \leq 0.55$	$\pm 20 \leq \text{PBIAS} < \pm 30$	$0.70 < R^2 \leq 0.55$
Unsatisfactory	$\text{NSE} \leq 0.40$	$\text{PBIAS} \geq \pm 30$	$R^2 \leq 0.40$

Source: US Army Corps of Engineers (USACE, 2018)

4. RESULTS AND DISCUSSIONS

4. 1 Flood Frequency Analysis

The peak discharge for 10, 20, 50, and 100-year return periods, is calculated using Log-Pearson III, Log-Normal, Normal and Gumbel distributions as indicated in **Table 2**. The Easyfit software found that the value of predicted peak flood using Log-Pearson 3 distribution is the best goodness of fit. The predicted maximum flood using Gumbel's is the highest as, compared to Log-N and Normal. The smallest values were obtained by Log-Pearson III.

<div align="right">Table 2.</div>

<div align="center">Return periods based on Log-P3, Log-N, Normal, and Gumbel distributions analysis.</div>

Return Period (Years)	Estimated Peak Discharge in Deference Distribution at KC Station (m^3/s)			
	Log-P3	Log-Normal	Normal	Gumbel
10	52208	50701	50242	51523
20	54990	55158	53698	55160
50	59381	57459	55376	59869
100	62194	61510	58171	63397

<div align="right">Table 3.</div>

<div align="center">The performance ranking based on Kolmogorov, Anderson and Chi-Squared goodness of fit Test.</div>

Distribution	Kolmogorov		Anderson		Chi-Squared	
	Statistic	Rank	Statistic	Rank	Statistic	Rank
Log-Pearson III	0.0933	1	0.3371	1	0.2096	1
Normal	0.1053	2	0.4226	2	0.5162	2
Lognormal	0.1096	3	0.5972	3	2.0160	3
Gumbel Max	0.1419	4	1.4984	4	3.6242	4

Table 3 indicates the performance ranking based on Kolmogorov, Anderson and Chi-Squared test. Log-Pearson III is ranked first in terms of performance, followed by Log-N, Normal, and Gumbel distribution. The ranking is based on the p-value. A p-value closer to 1 indicates a goodness of fit distribution. The highest p-value of goodness of fit test is 0.1419 and the lowest is 0.0933. Based on the results **(Fig. 3)**, Log-Pearson III distribution was put into HEC-RAS hydraulic model. The peak flood estimated for 10, 20, 50, and 100-years are 52,208 m^3/s, 54,990 m^3/s, 59,381 m^3/s, and 62,194 m^3/s respectively of Kampong Cham gauge station.
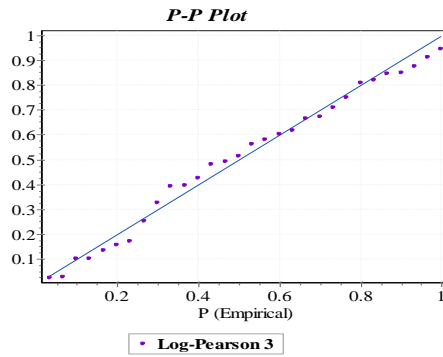
Fig. 3. Plot delineation goodness best fit of Log-Pearson III.

4.2 Performance Calibrated Model Simulation of Year 2011 and 2013

During the 2011 and 2013 flood events, there was a recorded highest hydrograph at the study area. The peak discharge of the observed hydrograph in KC upstream was 50,967 m³/s, whereas that in CC downstream was only 39,612 m³/s. Based on this approach and simulation, an upstream hydrograph was generated and the recorded hydrograph of the downstream from the HEC-RAS model to validate the hydrograph recorded at the CC station. These results were confirmed to correct this flood hydrograph; the new hydrograph was the simulated during the years 2011 and 2013 to adjust the peak observed hydrograph showed in (**Fig. 4** and **Fig. 5**).
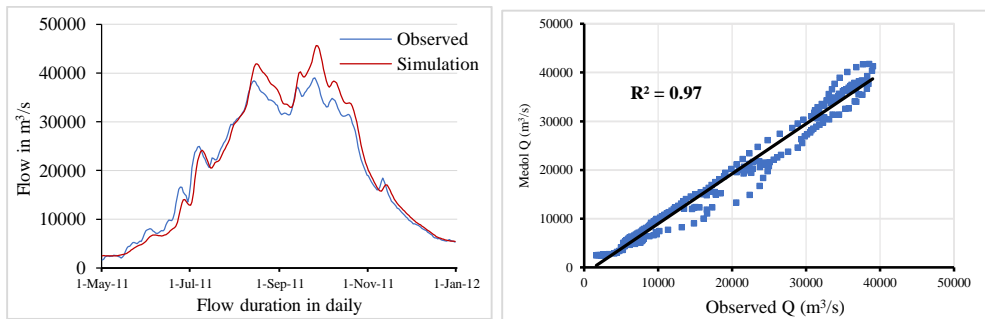
Fig. 4. Observed and simulated flow hydrograph at the downstream year 2011.
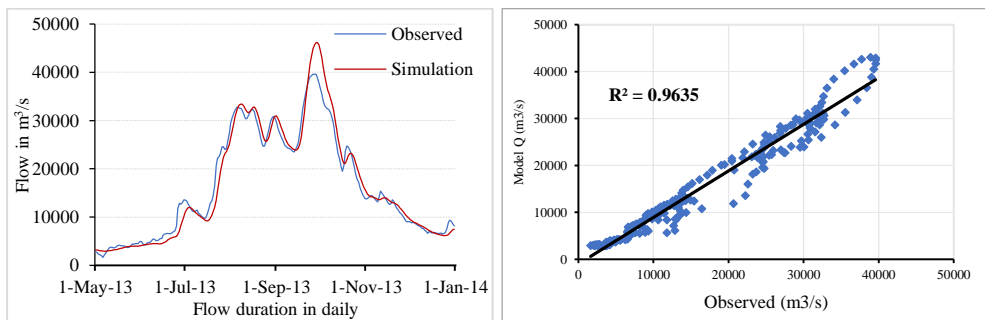
Fig. 5. Observed and simulated flow hydrograph at the downstream year 2013.

Hydraulic model performance (**Table 4**) was tested using NSE, PBIAS, and R^2 statistics with values of the year 2011 (0.91, 15.14, and 0.97) and the year 2013 (0.90, 15.38, and 0.96), respectively. The calibration with simulated flood depths from the HEC-RAS flow model shows a fairly good agreement with observations where their relationship shows very strong.

Table 4.

Model performance of the river discharge at the stations during calibration.

Years	Simulation period	Roughness coefficient Manning's n	Boundary condition Normal depth	NSE	PBIAS	R^2
2011	May-Dec, 2011	0.035	0.001	0.91	15.14	0.97
2013	May-Dec, 2013	0.035	0.001	0.90	15.38	0.96

4. 3 Flood Hazard Mapping

An HEC-RAS hydraulic modeling set-up was created to generate the water discharge due to the 2011 and 2013 flood and subsequently, the flood map for various returns simulated the 2011 and 2013 flood and the simulated 10, 20, 50 and 100-year periods. The comparison between the return periods is presented. The flood depth was reclassified to three levels such as 0.001 to 3 meters, 3 to 6 meters, 6 to 9 meters, and 9 to 14 meters, to identify little or no flood, medium flood, and high flood events. The results are presented in **Tabel 5**.

Table 5.

Flood depth extend the area of the return period 10, 20, 50, and 100-year.

Flood Depth (m)		Flood depth deference return periods (RP) study area (km^2)			
		10-year	20-year	50-year	100-year
< 3 (m)	very low	156	137	131	128
3-6 (m)	low	465	423	375	348
6-9 (m)	medium	741	727	788	812
9-12 (m)	high	294	371	358	353
> 12 (m)	very high	21	27	45	66

The following maps are the simulation of the results steady from flood return period 10, 20, 50, and 100-year, indicated as increase like **(Fig. 6).** The presented is classified as the layer based on depth values as per the criteria mentioned in Table 3. For floodplain exposure to the simulated flood depth and extent, 'Intersect' flood depth layer (vector format) with the flood depth layer. Then summarize the exposed flood depth in the form of graphs/maps while the river depth increases the highest from return period 10, 20, 50, and 100 as like 12.86 m, 13.10 m, 13.46 m, and 13.69 m. The following graph shows landcover exposure to the deference of flood return period 10, 20, 50, and 100-year events in the study.
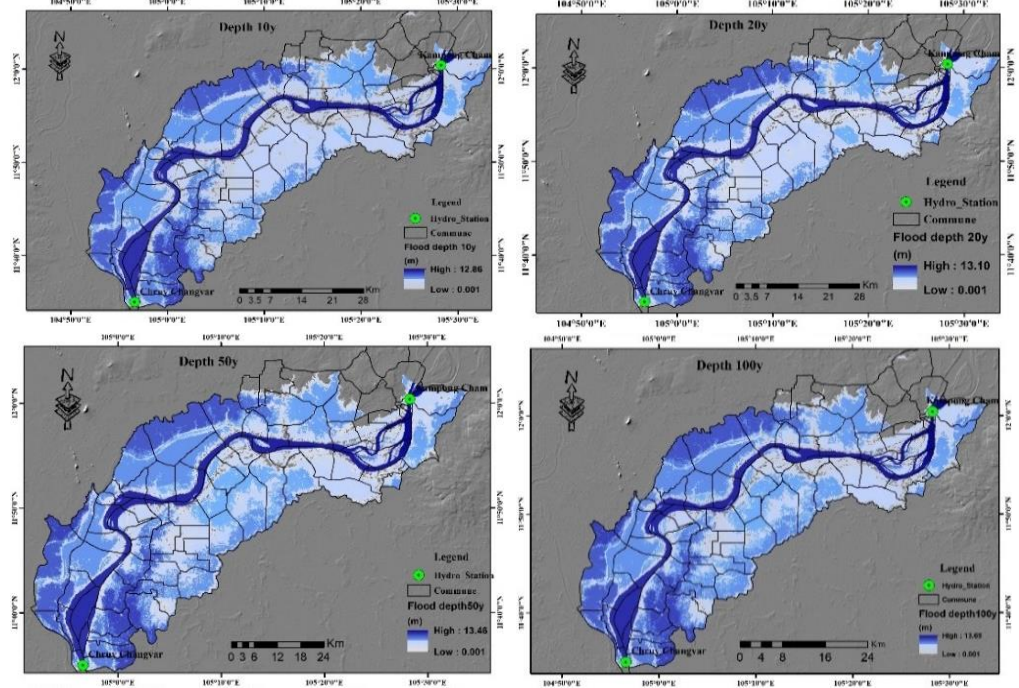
Fig. 6. Simulated flood depth area at the return period
$Q_{10yr}=52208$ m^3/s, $Q_{20yr}= 54990$ m^3/s, $Q_{50yr}= 59381$ m3/s, and $Q_{100yr}= 62194$ m^3/s.

5. CONCLUSIONS

The study is attempted to apply the HEC-RAS version 5.0.7 and GIS version 10.5 with peak discharge through a steady flow analysis. Thus, the output of modeling was generated into flood extent and flood depth in ArcGIS. Flood hazard maps from 10, 20, 50, and 100-year return period flood with the value of affected areas and flood depth along with the river study. According to the performance simulating of 2011 and 2013 with the downstream station, the value of NSE, PBIAS, and R^2 statistics with values of the year 2011 (0.91, 15.14, and 0.97) and year 2013 (0.90, 15.38, and 0.96) accuracy.

To construct a flood hazard map for the highest flood-affected area is the applicated model and validation value of Manning's ***n*** 0.035 for simulating 1D flood depth. Simulated flood hazard map based on input peak discharge of multi flood return periods confirms that the simulated flood hazard areas at 10, 20, 50, and 100-years are 52208 m^3/s, 54990 m^3/s, 59381 m^3/s, and 62194 m^3/s almost identical to the 2011 and 2013 (50295 m^3/s and 50295 m^3/s) observed peak discharge. The simulation suggests that most of the flood depth areas of the 10 and 20-years flood return periods were also affected by the 2011 and 2013 historical floods. But 50 and 100-year flood return periods, the simulation was unstable. The flood hazard map can be utilized as a tool to identify the priority of the area for the planning of flood prevention, flood mitigation, and flood risk management.

This study presents the methodology for improving the awareness of the flood events. The aim was to reduce the damage from floods and provide a better quality of life in the

study area. Coupling of GIS and hydraulic modeling provides a solution to sustainable flood protection and ensure a cleaner and safer environment. The present study mentions the successful combination of scientific and practical experiences to show the effectiveness of modeling techniques for engineering practice. In other words, it presents a successful functioning system of flood mitigation measures that increases sustainability and environmental protection of the territory. The outcome of the study could serve as an essential basis for a more informed decision and science-based recommendations in identifying river location and forming more effective policies in dealing with flood hazards.

ACKNOWLEDGEMENTS

R E F E R E N C E S

Ang, R., & Oeurng, C. (2018). Simulating streamflow in an ungauged catchment of Tonlesap Lake Basin in Cambodia using Soil and Water Assessment Tool (SWAT) model. *Water Science, 32*(1), 89-101. doi:10.1016/j.wsj.2017.12.002

Azouagh, A., El Bardai, R., Hilal, I., & Stitou el Messari, J. (2018). Integration of GIS and HEC-RAS in Floods Modeling of Martil River (Northern Morocco). *European Scientific Journal, ESJ, 14*(12), 130. doi:10.19044/esj.2018.v14n12p130

Bhat, M. S., Alam, A., Ahmad, B., Kotlia, B. S., Farooq, H., Taloor, A. K., & Ahmad, S. (2019). Flood frequency analysis of river Jhelum in Kashmir basin. *Quaternary International, 507*, 288-294. doi:https://doi.org/10.1016/j.quaint.2018.09.039

CFE-DM (2017). *Disaster Management Reference Handbook-Cambodia 2017*: Center for Excellence in Disaster Management & Humanitarian Assistance.

CRED (2019). EM-DAT, The International Disaster Database, (Centre for Research on the Epidemiology of Disasters).

Echogdali, F. Z., Boutaleb, S., Elmouden, A., & Ouchchen, M. (2018). Assessing Flood Hazard at River Basin Scale: Comparison between HECRAS-WMS and Flood Hazard Index (FHI) Methods Applied to El Maleh Basin, Morocco. *Journal of Water Resource and Protection, 10*(09), 957-977. doi:10.4236/jwarp.2018.109056

Farooq, M., Shafique, M., & Khattak, M. S. (2018). Flood frequency analysis of river swat using Log Pearson type 3, Generalized Extreme Value, Normal, and Gumbel Max distribution methods. *Arabian Journal of Geosciences, 11*(9), 216. doi:10.1007/s12517-018-3553-z

Győri, M. M., Haidu, I., & Humbert, J. (2016). Deriving the floodplain in rural areas for high exceedance Probability Having limited data source. *Environmental Engineering and Management Journal, 15*, 1879-1887. doi:10.30638/eemj.2016.201.

Haidu, I. (2016). What is Technical Geography - a letter from the editor. *Geographia Technica, 11*(1), 1-5. doi: 10.21163/gt_2016.111.01

Haidu, I., Batelaan, O., Crăciun, A.I., & Domnița, M. (2017). GIS module for the estimation of the hillslope torrential peak flow. *Environmental Engineering and Management Journal*, **16**(5), 1137-1144.

Kheradmand, S., Seidou, O., Konte, D., & Barmou Batoure, M. B. (2018). Evaluation of adaptation options to flood risk in a probabilistic framework. *Journal of Hydrology: Regional Studies, 19*, 1-16. doi:https://doi.org/10.1016/j.ejrh.2018.07.001

Klemešová, K., Kolar, M., & Andrasko, I. (2014). Using GIS in the Flood Management - Flood Maps (Troubky, Czech Republic). *Geographia Technica*, 9 (2), 44-53

Maskong, H. (2019). Flood Hazard Mapping Using on-Site Surveyed Flood Map, Hecras V.5 and Gis Tool: A Case Study of Nakhon Ratchasima Municipality, Thailand. *International Journal of GEOMATE, 16*(54). doi:10.21660/2019.54.81342

Mihu-Pintilie, A., Cimpianu, C. I., Stoleriu, C. C., Perez, M. N., & Paveluc, L. E. (2019). Using High-Density LiDAR Data and 2D Streamflow Hydraulic Modeling to Improve Urban Flood Hazard Maps: A HEC-RAS Multi-Scenario Approach. *Water, 11*(9), 1832.

Mihu-Pintilie, A., & Nicu, I. C. (2019). GIS-based Landform Classification of Eneolithic Archaeological Sites in the Plateau-plain Transition Zone (NE Romania): Habitation Practices vs. Flood Hazard Perception. *Remote Sensing, 11*(8), 915.

Mochizuki, J., Vitoontus, S., Wickramarachchi, B., Hochrainer-Stigler, S., Williges, K., Mechler, R., & Sovann, R. (2015). Operationalizing Iterative Risk Management under Limited Information: Fiscal and Economic Risks Due to Natural Disasters in Cambodia. *International Journal of Disaster Risk Science, 6*(4), 321-334. doi:10.1007/s13753-015-0069-y

OECD (2016). *Financial Management of Flood Risk.* Paris: OECD Publishing.

Rahmati, O., Zeinivand, H., & Besharat, M. (2016). Flood hazard zoning in Yasooj region, Iran, using GIS and multi-criteria decision analysis. *Geomatics, Natural Hazards and Risk, 7*(3), 1000-1017. doi:10.1080/19475705.2015.1045043

Rishiraj, D., Senaka, B., & Atiq, K. A. (2015). Assessing Gaps and Strengthening Early Warning System to Manage Disasters in Cambodia. doi:10.5595/idrim.2015.0104

Romali, N. S., Z., Y., & Ismail, A. Z. (2018). Application of Hec-Ras and Arc Gis for Floodplain Mapping in Segamat Town, Malaysia. *International Journal of GEOMATE, 14*(43). doi:10.21660/2018.43.3656

Shafapour, T. M., Shabani, F., Neamah, J. M., Hong, H., Chen, W., & Xie, X. (2017). GIS-based spatial prediction of flood prone areas using standalone frequency ratio, logistic regression, weight of evidence and their ensemble techniques. *Geomatics, Natural Hazards and Risk, 8*(2), 1538-1561. doi:10.1080/19475705.2017.1362038

Tanaka, T., Tachikawa, Y., Ichikawa, Y., & Yorozu, K. (2017). Impact assessment of upstream flooding on extreme flood frequency analysis by incorporating a flood-inundation model for flood risk assessment. *Journal of Hydrology, 554*, 370-382. doi:https://doi.org/10.1016/j.jhydrol.2017.09.012

Toosi, A. S., Calbimonte, G. H., Nouri, H., & Alaghmand, S. (2019). River basin-scale flood hazard assessment using a modified multi-criteria decision analysis approach: A case study. *Journal of Hydrology, 574*, 660-671. doi:10.1016/j.jhydrol.2019.04.072

USACE (2018). *Analyzing Flood Risk for Forecast Informed Reservoir Operations in the Russian River Watershed Using HEC-WAT*. Institute for Water Resources Hydrologic Engineering Center: Institute for Water Resources Hydrologic Engineering Center.

Vichet, N., Kawamura, K., Phan Trong, D., Van On, N., Gong, Z., Lim, J., . . . Bunly, C. (2019). MODIS-Based Investigation of Flood Areas in Southern Cambodia from 2002–2013. *Environments, 6*, 57. doi:10.3390/environments6050057

Vojtek, M., Petroselli, A., Vojtekova, J., & Asgharinia, S. (2019). *Flood inundation mapping in small and ungauged basins: sensitivity analysis using the EBA4SUB and HEC-RAS modeling approach*.

Vojtek, M., & Vojtekova, J. (2016). Flood hazard and flood risk assessment at the local spatial scale: a case study. *Geomatics, Natural Hazards and Risk, 7*(6), 1973-1992. doi:10.1080/19475705.2016.1166874

Yu, W., Kim, Y., Lee, D., & Lee, G. (2019). Hydrological assessment of basin development scenarios: Impacts on the Tonle Sap Lake in Cambodia. *Quaternary International, 503*, 115-127. doi:10.1016/j.quaint.2018.09.023

URBAN RECREATIONAL PARKS TO OFFSET THE FLOODING OF RIVERS: LA DEVESA OF GIRONA -CATALONIA- (19TH CENTURY)

Ramon RIPOLL [1], Jordi GOMIS [2] , Carlos TURÓN [3], Miquel-Àngel CHAMORRO [4]

ABSTRACT:

In the 18th and 19th centuries, hydraulic works played an important role in economic development throughout Europe. There has been much research into the construction of dikes, canals and bridges to protect against, harness, and control the unbridled power of rivers; but there is still a lack of insight into how these functional, productive and social goals combined for purely cultural purposes. The hydraulic engineering work that is the Devesa urban park of Girona (located near the confluence of the Ter, Onyar and Güell rivers) is a magnificent example that fuses territorial engineering and urban architecture. Its design involves 18th and 19th century solutions to resolve the continuous flooding of the city of Girona, combining perfectly with its citizens' social, cultural and recreational activities.

Key-words: *Hydraulic Geography, Urban Geography, Civil Engineering, City Planning.*

1. INTRODUCTION

The aim is to study the relationship between urban geography and the geography of rivers. There are historical examples of how harmonization between nature and construction is achieved by culturizing hydraulic engineering. The analysis of the city of Girona provides us with prolific documentation on such blended solutions. In this case, the construction during the second half of the 19th century of a large park at the confluence of four rivers enabled largely solving the urban destruction caused by river flooding. The work methodology used is based on the graphic study of surveying and a historical study of documents on the Devesa park. The research requires reviewing the works that cast doubt on both the technological training of academic architects and the humanistic view of engineers and of many master builders. The findings reveal that technology and humanism can complement each other perfectly. The documentary sources used are the Girona Municipal Archives, the Girona Historical Archive and the Archive of the Crown of Aragon.

Let us recall that many pre-industrial European cities are located near rivers. They are riverine settlements that take advantage of direct access to water for residential, manufacturing, agricultural, etc. purposes (Sambrico, 1990). Yet, many of them suffer from flooding, especially if they have been built unwisely in areas prone to flooding by rivers whose flow is irregular. In this case, river courses pose a constant threat of destruction and

---

[1,4] *Universitat de Girona, 61 Maria Aurèlia Capmany Street, 17003-Girona, Spain,*
ramon.ripoll@udg.edu, mangel.chamorro@udg.edu

[2,3] *Universitat Rovira i Virgili, 26 Països Catalans Avenue, 43007-Tarragona, Spain,*
jordi.gomis@urv.cat, carlos.turon@urv.cat

calamity. One such example is the city of Girona. During the late Medieval and modern periods, the city irresponsibly urbanized easily flooded areas implementing medieval and modern defensive walls as the only means of protection (AHM, 1820). The hydraulic situation was very serious because these historic settlements were located on both sides of two rivers -the Onyar and the Galligans- creating a major urban clamp strangling the hydraulic section, and at the same time on the banks of the confluence of the rivers Güell and Ter, creating the corresponding dam effect on the city (Ribas, 2006). Such organization was highly favourable and optimal in times of plenty and rather unfavourable and dramatic in periods of torrential rain (**Table 1**).

Table 1.
Floods between 1716 and 1970 (AMG 1716-1970).

FLOODS 1716-1970

#	Year	Rivers		#	Year	Rivers		#	Year	Rivers	
1	1716	Onyar and Ter	2	*31*	1814	Ter	1	*61*	1876	Onyar, Ter and Güell	3
2	1726	Onyar and Ter	2	*32*	1814	Ter	1	*62*	1882	Güell	1
3	1732	Galligans and Onyar	2	*33*	1816	Ter	1	*63*	1884	Galligans, Onyar and Güell	3
4	1735	Galligans	1	*34*	1819	Ter	1	*64*	1884	Galligans, Onyar, Ter and Güell	4
5	1736	Galligans, Onyar and Ter	3	*35*	1820	Ter	1	*65*	1885	Onyar and Ter	2
6	1738	Galligans	1	*36*	1822	Onyar and Ter	2	*66*	1898	Galligans, Onyar, Ter and Güell	4
7	1740	Onyar and Ter	2	*37*	1823	Ter	2	*67*	1898	Ter	1
8	1741	Ter	1	*38*	1826	Onyar and Ter	2	*68*	1902	Onyar and Ter	2
9	1742	Ter	1	*39*	1826	Onyar and Ter	2	*69*	1903	Onyar and Ter	2
10	1758	Ter	1	*40*	1827	Onyar	1	*70*	1907	Onyar	1
11	1759	Galligans and Güell	2	*41*	1828	Galligans, Onyar, Ter and Güell	4	*71*	1908	Onyar and Ter	2
12	1762	Ter	1	*42*	1829	Onyar, Teri and Güell	3	*72*	1919	Ter	1
13	1763	Ter	1	*43*	1829	Onyar and Güell	2	*73*	1920	Onyar and Ter	2
14	1765	Galligans, Onyar and Ter	3	*44*	1831	Onyar and Ter	2	*74*	1920	Onyar	1
15	1765	Galligans, Onyar and Güell	3	*45*	1832	Onyar	1	*75*	1921	Ter and Güell	2
16	1765	Onyar	1	*46*	1832	Onyar	1	*76*	1926	Güell	1
17	1772	Onyar	1	*47*	1833	Ter	1	*77*	1932	Ter	1
18	1776	Galligans, Onyar, Ter and Güell	4	*48*	1836	Ter	1	*78*	1939	Onyar	1
19	1777	Galligans, Onyar and Ter	3	*49*	1838	Ter	1	*79*	1940	Onyar, Ter and Güell	3
20	1777	Galligans, Onyar and Ter	3	*50*	1838	Ter	1	*80*	1943	Onyar	1
21	1783	Galligans, Onyar, Ter and Güell	4	*51*	1839	Onyar and Ter	2	*81*	1944	Onyar and Ter	2
22	1787	Onyar and Ter	2	*52*	1839	Onyar and Ter	2	*82*	1948	Galligans, Onyar and Ter	3
23	1790	Onyar	1	*53*	1840	Onyar	1	*83*	1962	Onyar, Ter and Güell	3
24	1791	Ter	1	*54*	1840	Onyar	1	*84*	1963	Onyar, Ter and Güell	3
25	1793	Onyar and Ter	2	*55*	1843	Galligans, Onyar, Ter and Güell	4	*85*	1963	Onyar	1
26	1795	Ter	1	*56*	1850	Galligans, Onyar, Ter and Güell	4	*86*	1965	Onyar	1
27	1798	Ter	1	*57*	1853	Onyar and Ter	2	*87*	1969	Onyar	1
28	1801	Galligans and Onyar	2	*58*	1861	Onyar	1	*88*	1969	Onyar	1
29	1802	Onyar and Ter	2	*59*	1861	Galligans, Onyar, Ter and Güell	4	*89*	1970	Galligans, Onyar, Ter and Güell	4
30	1804	Ter	1	*60*	1872	Onyar and Ter	2	*90*	1971	Onyar, Ter and Güell	3
									TOTAL FLOODS		**168**

The worst floods suffered by the city of Girona took place in 1732 with 11 houses destroyed, in 1763 with the evacuation of residents through the perforated dividing walls, in 1843 with 100 killed and 22 houses destroyed, in 1861 with two dead, one house destroyed and 72 houses severely affected, and so on. Year after year during the period of heavy rains, such destruction affected walls, dikes, embankments, riverbeds, dams, canals and bridges as well as houses, mills, factories, orchards, fields and plantations. Socially speaking, these situations were experienced with tension and drama because the citizens of the most affected neighbourhoods had to leave their homes hurriedly, both by day and at night.

Evacuations were conducted to the sound of the bells of the city announcing the flood, the lamplighters required double provisions of oil (AHM, 1814), those responsible for the city gates had to open them to allow the water to run freely (AHM, 1814) and, at the same time, churches and convents were called to offer supplications (AHM, 1814).

2. FLUVIAL REALITY AND TECHNOLOGY

The extensive documentation provided by Girona City Council manuals meticulously describes the damage caused by floods and the technical, constructive and economic means for their repair. Such information is repeated year after year, throughout the 18th and 19th centuries. The continued destruction surpassed the technical and economic resources of the city and each year the municipal authorities had to deal with an extreme situation to avoid paralysing the urban, productive and regional communications infrastructures. In all these cases a gap and dysfunction were noted between the reality of the river and the constructive means available to definitively solve the problem (Ripoll, 2005).

First, there was a clear lack of economic resources. Hence, the difficulties in seeking and raising funds, implementing and imposing new taxes on the population, funding and finding guarantors, disbursing and paying at the start, during and at the end of the work, etc. were reported. In addition, systems were sought that would allow the greatest possible cost savings, such as making plans and projects with effective solutions, drawing up more detailed job cost sheets on the works to be carried out, awarding the works by public auction to the highest bidder with a closed budget, or awarding the works by direct labour, if such meant lower costs. The economic insecurity is very clearly illustrated by the occasions on which requests were made to reduce the wages of the workers and labourers of the waterworks to one third (AHM, 1787). This lack of financial resources was compounded when the short duration of the effort made could be seen. According to the sources consulted, it was known in advance that the solutions adopted and the financial resources used often did not last long due to regular episodes of torrential rain. This idea of general precariousness is strengthened by the statement by the architect Cusanes on the futility of most of the repairs carried out on the river Ter (AHM, 1790). Nevertheless, among the most optimistic views is the analysis by the engineer Azara when he said that the most enduring means were the planting of trees and the implementation of strong stakes and planks, as they usually last up to a maximum of 50 years (AHM, 1778).

It is also interesting to note that most of the solutions adopted were based solely on technological means, ranging from the simplest to the most complex constructive proposals. The simplest constructive means included: cleaning the rivers, rebuilding the damage caused, strengthening the channels, building breakwaters, closing the new riverbeds opened by the rivers, replanting trees, and so forth. These works required moving sand and earth, driving oak, poplar or elm stakes, nailing oak planks, wedging stones, transporting ashlars or large stones, making dry stone or cobble embankments, etc. It is worth mentioning some reports that speak of the advantages provided by embankments made using river cobbles because they are more resistant to flash flooding than stakes or masonry. In this case, the engineer Boer (AHM, 1778) compared river water to a cannonball that does more damage to a masonry wall than to a dirt wall or sandbags. He also emphasized the importance of protective breakwaters at specific points, such as the royal walk in the district of Pedret (AHM, 1800), etc. The most striking observation is the assiduity of the floods, which brought many hydraulic constructions to a premature end. In these cases, materials and work tools were often carried away by flash floods (AHM, 1820). The technically more complex solutions

involved diverting the rivers Ter (AHM, 1769), Güell (AHM, 1796) etc. Among these proposals, the most difficult to build were those proposed in 1802, which consisted of returning the Ter to its original course at a cost of 3,463,200 reales, or lowering the bed of the river Ter at a cost of 12,720,000 reales, therefore four times more expensive than the proposal to return the Ter to its original course. The most expensive was to divert the river Ter fully behind the Turó de Roca hill, at a cost of 348,347,364 reales, a hundred times more expensive than returning the Ter to its original course. Other proposals included moving the Güell river away from the city by means of an earth embankment or diverting the Onyar around the city. Many of these studies were unachievable, as were most of the financial means proposed for their implementation: taxes, levies and urban tolls (AHM, 1803).

We should also mention some more realistic studies and analyses that provided affordable solutions to the problem. Such is the case of Girona City Council, when it recognized that cutting down all the trees of the Devesa would leave much of the city unprotected (AHM, 1796), or the orders issued by the commander-in-chief of the engineers forcing the replanting of the trees of the Devesa for this very reason, to protect the city (AHM, 1796). These observations considered the woodland of the Devesa at the confluence of the four rivers as being one of the most important means of protection the city could have against flooding (Aragó, 1980). This conclusion was reached after having cut all the trees of the Devesa to cover the costs of military works to recompose the city walls due to the proximity of the French Army of Occupation (AHM, 1795) (**Fig. 1**).
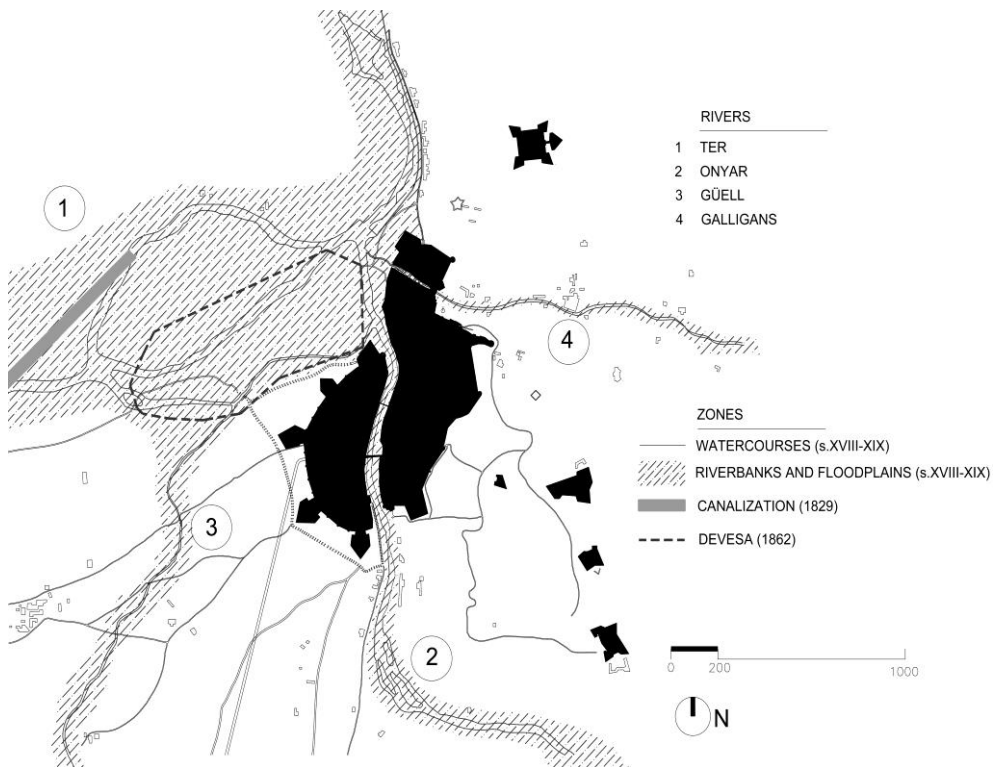

Fig. 1. Evolution of the Devesa park in the 18th and 19th centuries
(Drawing by R. Ripoll, private archive, 2018).

3. TECHNOLOGY AND URBAN PARK

The industrial revolution caused profound changes in the cities, especially in factory towns. Population growth and the concentration of large masses of population quickly turned them into "big-towns". However, there were no suitable planning responses to this problem, with purely speculative prevailing in new designs of towns (Gomis & Turón, 2015). As the 19th century progressed, it began to be seen that the most affordable solution in terms of finance and construction processes largely involved combining, harmonizing and blending technological proposals to improve the Ter river course hydraulic section and social proposals to transform the Devesa into an urban park (Ripoll, 2005). The former aimed to improve the river course section and the latter to stabilize the soil. For the first time, complementarity between river technology, moving the Ter river away from the city, and the architecture of the landscape, building a large urban park, were entertained (**Fig. 2**).
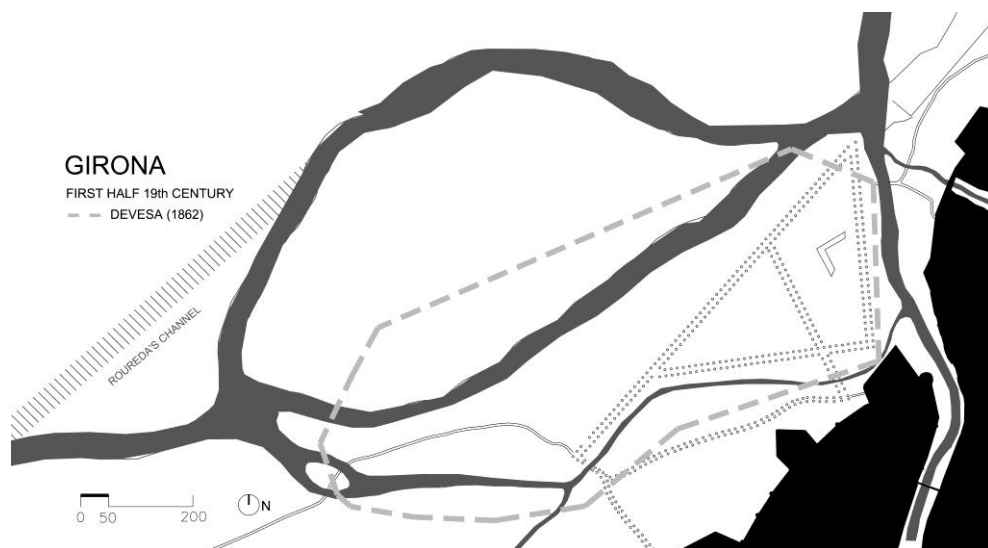
Fig. 2. Devesa Park at the start of the 19th century (Drawing by R. Ripoll, private archive, 2018).

The first aspect of this new approach began in 1826, when there was a project to move the Ter river back to its original course. This involved the construction of an 856 m-long, 1.6 m-deep channel, called the Roureda, and of an embankment, or dam, to direct the river water to the new channel. The project was led by the expert master builders Miguel Fàbrega and Benito Santigosa with a budget of 4,210,740 reales. This amount could be interpreted as relatively tight as it represented 20% more than the budget of a similar project carried out 24 years earlier, in 1802. The aim was to again move the river away from the city and the farmland of the Girona plain (AHM, 1826). Following the refusal by the king (AHM, 1827) to help financially with funds raised by the land registry (AHM, 1826), local and municipal authorities struggled to find the financial resources to carry out the works (AHM, 1827). In this case, the construction of the works of the Roureda canal and the planting of trees to consolidate the works to construct the canal started to be combined (AHM, 1829). The works were directed by the geometrician Luis Barnoya and the architect José Cabot.

As of 1830, works began to drain, fill in, normalize and consolidate the areas freed by the new course of the Ter. Actions also began to find more compatible functions for this new fluvial land. For example, there was an initiative to purge the area of agricultural uses by tenants farming the land (AHM, 1837). Years later this same operation was repeated to put an end to using the land for grazing animals (AHM, 1865). In parallel, there was increased tree planting (AHM, 1850). According to reports, the result, in the second half of the 19th century, was the existence of slender, lush plantains measuring 1.5 m in circumference with a 5 m branchless trunk standing between 15 and 20 metres high. These reports also describe how the trees were arranged in a grid 22.5 m apart. They also describe the existence of a nursery of plantains (AHM, 1882).

Thus, in the second half of the 19th century, the Devesa described in these reports was very similar to what we find today and followed the characteristics of the Devesa urban park as proposed by the architect Martí Sureda in 1862, a project for an urban park covering a surface area of 388,377 m2 which accounted for 82% of the surface area of the entire city of Girona at the time (459,757 m2) and consisted of six large squares of gardens, measuring between 8,340 m2 and 10,912 m2 each, bounded by avenues of large trees (**Fig. 3**). We should also mention the Field of Mars, or a rectangular open space of 63,842 m2. Finally, the entire assembly is flanked on three sides by irregularly-shaped neighbouring gardens located in the north, west and south covering 14,966 m2, 55,115 m2 and 49,949 m2 respectively (Ferrer, 1994).
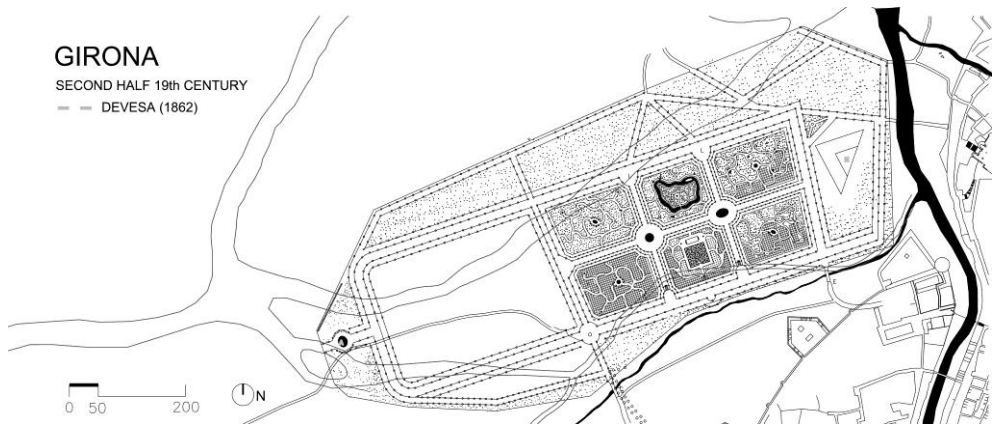
Fig. 3. The project for the Devesa park by Martí Sureda, 1862
(Drawing by R. Ripoll, private archive, 2018).

The park designed by Sureda was in keeping with the design of French gardens, perfectly combining the overall composition of totally geometrical longitudinal and transversal avenues. The alignments defined closed inner spaces with pleasure gardens containing erratic walkways. Each of these spaces had its corresponding centres of interest formed by ponds, canals, musicians' platforms, or even the odd pergola (Desimini & Waldheim, 2016). Similarly, Martí Sureda's project defined a maze made of perfectly geometrical tree-lined walls symbolizing the certainty and disorientation of life. The maze has four entrances, three of which are intertwined (**Fig. 4**).
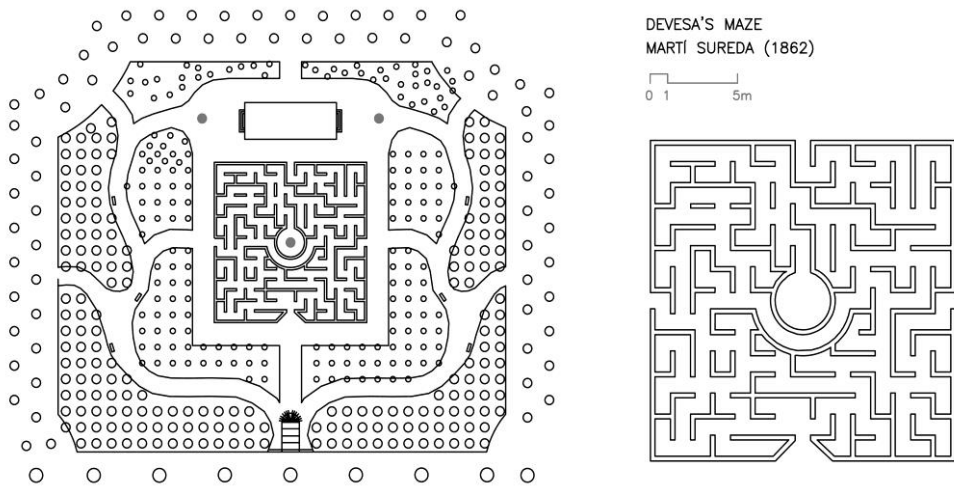
Fig. 4. Detail of the project for the urban park by Martí Sureda, 1862
(Drawing by R. Ripoll, private archive, 2018).

It should be highlighted that the Devesa urban park has lasted until today preserving most of the general characteristics described in Martí Sureda's project of 1862. Only four of the six inner gardens and a few specific complementary elements have not been implemented. During the last century and a half, the Devesa park has not only played the role of allaying the most dramatic dangers of flooding on the city of Girona, but also of partially urbanizing the Ter river as it passes through the city. In this case, the Devesa urban park has helped update river-related vocabulary in the city of Girona. For example the expressions found in historical documents prior to 1862 such as banks, warpage, bed, pasture, field or grove have been replaced successively by such contemporary expressions after 1862 as recreational, social relations, stroll and urban park.

4. CONCLUSIONS

The example studied is paradigmatic in two ways. First, the intention to put sophisticated leisure gardens that were reserved in Europe for the nobility, such as the royal gardens of the palace of Drottningholm (Stockholm, 1811), the oldest in the world in use, at the service of all citizens of a secondary population of southern Europe in 1862.

And secondly, already during the second half of the 19th century, it anticipated the unlimited complementarity between technology and architecture, a dual feature that allows building a luxurious, perfect park on the most counterproductive, deteriorated and punished land.

REFERENCES

ACA: Archive of the Crown of Aragón.

AHG: Girona Historical Archive.

AHM: Girona Municipal Historical Archive.

Aragó, N. (1980). La Devesa paradís perdut. Girona: COAC.

Desimini, J. & Waldheim, C. (2016). Cartographic Grounds: Projecting the Landscape Imaginary. New York NY: Princeton Architectural Press.

Ferrer, M. (1998). Martí Sureda Deulovol (1822-1890). Girona. COAC.

Gomis, J. & Turón C. (2015). Conceptual and instrumental influences in the graphic representation of urbban planning: The industrial Revolution and the 19tk Century. *Geographia Technica,* 10 (1), pp 44-50.

Ribas, A. (2006). Les inundacions de Girona. Girona: Girona City Council.

Ripoll, R. (2005). L'arquitecte, l'arquitectura i la ciutat. Girona 1760-1835. Barcelona: Publications of Montserrat Abbey.

Sambrico, C. (1990). El "Límite" de la ciudad ilustrada: La ordenación de un espacio urbano. *ARQUITECTURA (Revista del Colegio Oficial de Arquitectos de Madrid).* Issue September-December 1990, No. 286-287 pp. 168-183.

ANALYSIS OF WATER AWARENESS, ACCOUNTABILITY, AND GOVERNANCE TO IMPROVE SUSTAINABILITY OF FIRM'S PERFORMANCE IN URBAN AREAS

Agustine DWIANIKA[1] ![ID], *Etty MURWANINGSARI[2,]*, *Wayan SUPARTA[3]* ![ID]

ABSTRACT:
Managing water efficiency will cut costs and promote the environment and increase public awareness of the importance of water in governance. Water conflicts and the increasing phenomenon of water scarcity will result in business stagnation, especially for sustainable firm's performance. The purpose of this research is to find a new measurement model to improve the sustainability of a firm's performance through awareness of water and environmental management. This study was conducted on 20 manufacturing firms in Indonesia where 100 respondents were taken from the firm. The questionnaire was used as a tool to collect data on water awareness, accountability awareness, and water governance. Explanatory research is also carried out to analyze the effect of these three variables on the sustainability of firm performance. The results showed that water awareness, accountability awareness and corporate governance by the measurement of the ASEAN Corporate Governance (CG) Scorecard supported firm performance. This result can be recommended to improve the firm's sustainability performance, especially in urban areas.

Keywords: Water awareness, Accoutability awareness, ASEAN CG Corecard, Sustainable Firm's Perfomance

1. INTRODUCTION

According to the World Resources Institute (WRI), Indonesia is one of the countries expected to experience water stress in 2040 as shown in **Fig. 1**. This is partly due to a lack of awareness of tree planting, the use of water for households is increasing, exploration and use of water for industrial, especially manufacturing. Recent research on the problem of water in various regions has been observed by Biocchi et al. (2015) and Boutera et al. (2012). Climate change such as heat waves also plays an important role in influencing water availability especially in urban areas (Suparta & Yatim, 2019).

Due to the lack of land capacity to absorb water due to reduced forest area and rainwater absorption, good corporate governance now plays an important role in the possibility of accounting fraud and companies that have weak governance structures are becoming more vulnerable to fraud (Brigham et al., 2009). Company performance can be achieved by enhancing an organizational culture that can be done by applying the principles of Good Corporate Governance (GCG). One of the rankings of corporate governance is to

[1] Universitas Pembangunan Jaya, Accounting Department, Jl. Cendrawasih Raya Block B7 / P, Sawah Baru, Ciputat, Tangerang Selatan, Banten 15413, Corresponding author: agustine.dwianika@upj.ac.id

[2] Trisakti Universiti, Accounting Department, Jl. Kyai Tapa, Grogol, Jakarta Barat 11440 Indonesia, etty_nasser@yahoo.com

[3] Universitas Pembangunan Jaya, Department of Informatics, South Tangerang City, Banten 15413, Indonesia, Corresponding author: wayan.suparta@upj.ac.id

use the ASEAN Corporate Governance Scorecard. This ranking is often used as a measurement of Corporate Governance practices. This refers to the provisions of the ASEAN Capital Market Forum (ACMF) as an association of ASEAN capital market authorities. The ASEAN Corporate Governance Scorecard is based on the OECD Principles and will increase the investor's trust to public companies (Globe Telecom, 2019).
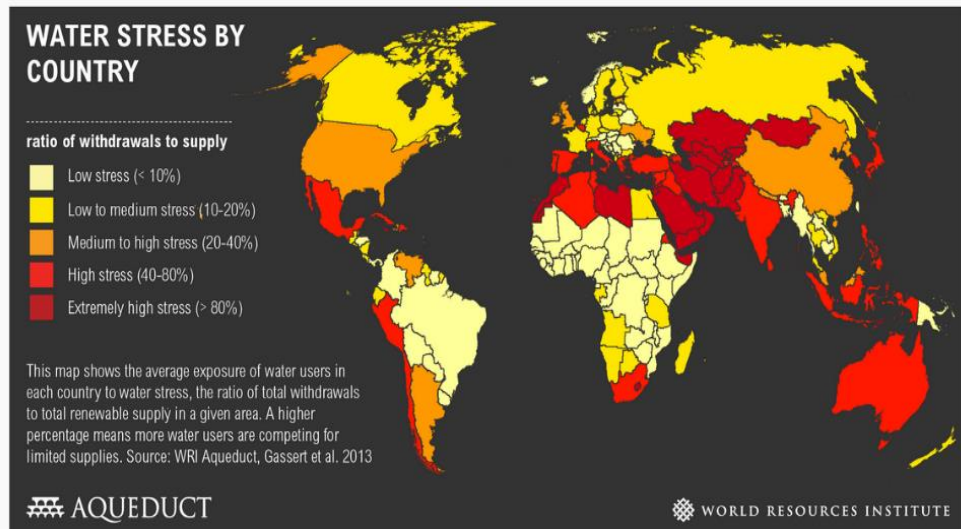
Fig. 1. Water stress by country where Indonesia is in high stress level (WRI Aqueduct, 2013).

Awareness of the preservation of natural resources for the next generation has become an international concern, especially highlighting water exploration for the manufacturing sector in the production process. In countries facing water shortages, water conservation education is one of the targets at the school level. By introducing the program to students about the importance of water conservation and economic value, it will increase awareness among the community to know that a good percentage of people are students (Gilley et al., 2006). At present, water awareness and accountability are widely studied and linked to water accounting systems for water management strategies. One of them is the framework of the water accounting system as stated by Turner et al. (2010).

The recent financial crisis is creating new or recent emphasis on risk management which is important for financial and non-financial companies. For many companies, the focus on risk management is still a new thing, and they found the right place to start is to identify and manage strategic risk companies; risk the most impact on the organization's ability to execute its strategy and achieve its goals. Richard et al. (2009) identified 207 different performance variables from 213 reviewed articles from 2006 to 2009. They stated that the performance of the organization consists of the actual output of an organization as measured against its intended output, which includes three specific areas, namely corporate results profitability, return on assets (ROA) and return on equity (ROE). However, a recent study intensively looks at the company's performance is not only financial but also non-financial. Kaplan and Norton (2004), shows that non-financial performance measures are a better indicator of future financial performance.

The objective of this research is to find a new measurement model to improve the sustainability of company performance through water and environmental management. Therefore the relationship between water awareness and accounting awareness is expected to influence the implementation of the ASEAN CG Scorecard company and have a positive impact on company performance. Awareness of water sustainability is very important to be motivated to increase stakeholder control over the application of good governance.

2. METHODS

This study uses the population of all companies listed in the Indonesia Stock Exchange (ISE) in 2017 which publishes the Financial Statements. Samples were obtained by using a purposive sampling method with the criterion of manufacturing companies listed in ISE in 2017. This sample is considered to use water resources which are relatively large compared to other types of companies and are located in an urban area. To recommend the firm's performance to achieve water sustainability, variable used to be analyzed in this research are water awareness refers to ten indicators belonging to Jawad (2012), accounting awareness refers to seven indicators of Turner et al. (2010), and Firm's Governance refers to the measurement of ASEAN CG Scorecard. The expected output is the firm's performance refers to Kotane (2012). The expected model developed in this study is using the multiple linear regression (MLR) method as shown in the following equation.

$$Y = \alpha + \beta_1 X_1 + \beta_2 X_2 + \beta_3 X_3 + \mathcal{E} \tag{1}$$

where α, β_1, β_2, and β_3 are constant, while X_1 is the water awareness, X_2 is the accounting awareness and X_3 is the corporate governance. The output Y is firm's performance. The three constants are obtained by ANOVA (Analysis of Variance) approach. Besides using MLR equation, explanatory research is also used to explain the effect of three variables on the firm's performance.

Fig. 2 shows the research process in obtaining an adoption model. The first step will design measurement tools for data collection. Secondly, the instrument developed will be tested and validated, analyzed and discussed. For the validation and to test the reliability of the instrument, Cronbach Alpha is employed. Cronbach's alpha is a measure of internal consistency that is how closely a set of items is correlated with other items as a group. An SPSS 25 software is employed to analyze the three variables above. This study used 100 respondents to representing 20 manufacturers firm In Indonesia as shown in **Fig. 3** which cover Java and Kalimantan Islands. Each firm is represented by five respondents which are one respondent at the top level of managerial, two respondents as middle level, and two respondents as junior staff. The criteria for selecting respondents are employees in corresponding positions in sample firms with a minimum working period is one year.
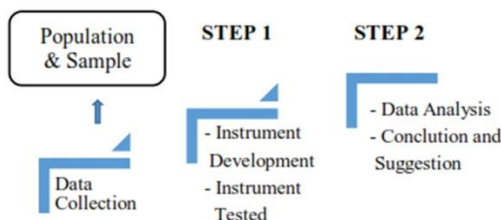
Fig. 2. Research Process in determining water sustainability to firm's performance.
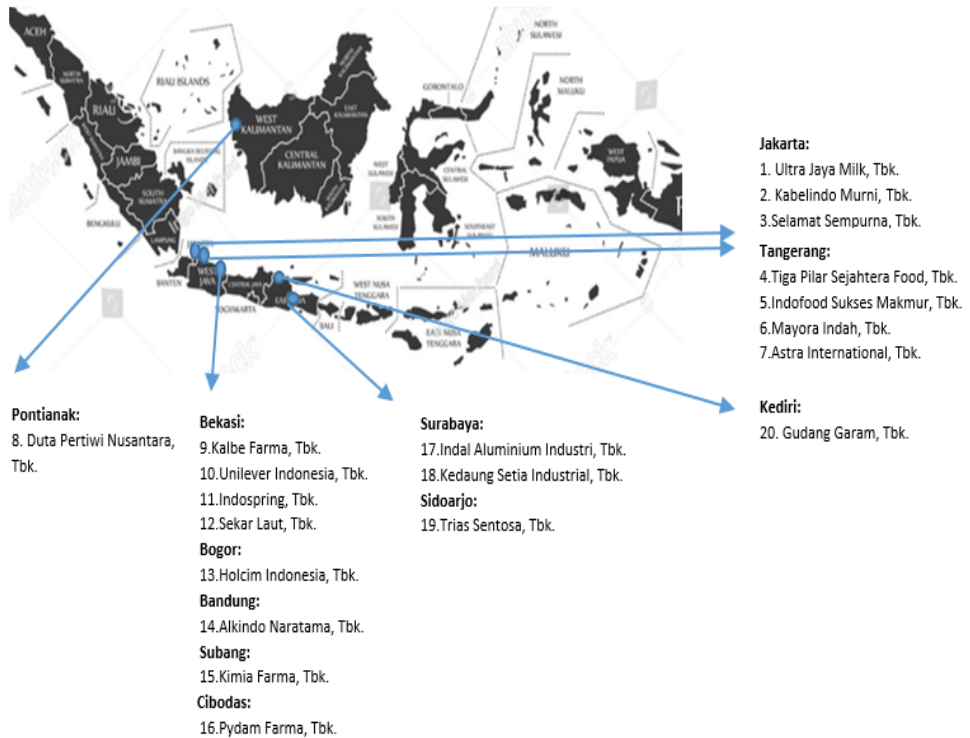
Fig. 3. Firm's study case location in Indonesia.

3. RESULT AND DISCUSSION

From the data obtained, several test data analysis was conducted. Initial analyzes related to the demographic data of respondents such as gender, education level, age and the length of the respondents working with companies in the sample showed an ascending trend. Most of the respondents are male as much as 70% as shown in **Table 1**. It is very reasonable considering the company sample is manufacturing, which does have a tendency to take longer to work without a lot of distractions and allow to work overtime.

The respondent demographic showed that the level of education are 15% certificated, 15% diplomas , 65% degrees, and 5% postgraduates. Note that the manufacturing business selected as a sample is likely more focused on human resources which have a good working experience compared to the high level of education. The majority of respondents aged between 35-44 (55%), 45-54 (20%), 25-34 (15%), and the last age of the respondents is above 55 (10%). While the mayority of finance department employee is aged between 35-44 years old, where this age is an ideal for a productive performance. A 60% of respondents have worked at the company between 6-10 years, above 10 years, and the last is 1-5 years. In ifdeal organization, expertise employees can minimize the errors that occur

in the company's business processes, especially in terms of financial reporting by using water awareness adoption.

Table 1.

Demography for 100 Respondens.

	Gender	Frequency	Percent
	Male	70	70%
	Female	30	30%
Age	25-34	15	5%
	35-44	55	55%
	45-54	20	20%
	>= 55	10	10%
Domicile	Jakarta	20	20%
	Bogor	25	25%
	Depok	16	16%
	Tangerang	32	32%
	Bekasi	7	7%
	Certified	15	15%
	Diploma	15	15%
	Degree	65	65%
Level of education	Post Graduate	5	5%
Experience	> 10 years	35	35%
	6 - 10 years	60	60%
	1 – 5 years	5	5%

Source: SPSS Data (2019)

To test the instrument developed, 20 respondents is used as a pilot study to indicate the measuring instrument developed (questionnaire) is valid. The result for this validity test for each variable is presented in **Table 2**. The result shows the consistency of the variable tested with a reliability value (Cronbach's Alpha) of 0.750. The results also showed the value of the coefficient of determination Adjusted R Square (R2) is approximately 0.492. This means that 49.2% of non-financial performance was influenced by the sample companies studied and the rest is possibly by other factors.

Table 2.

The Validity Test with N = 20.

No.	Variable	r^{count}	r^{table}	Remark
1	Water Awareness	0.514	0.360	valid
2	Accounting Awareness	0.527	0.360	valid
3	Corporate Governance	0.511	0.360	valid
4	Firm's Performance	0.553	0.360	valid

The pilot test result show consistency and reliably of measurement with moderate correlation and then 100 respondents now is used to collect data for data analysis to produce a model as shown in **Table 3**. The correlation (r^{count}) between items and the total items show a stronger correlation with r above 0.7 except for Water Awareness.

To ascertain the value of the influence of the three variables, the MLR test is carried out using 100 data that have been collected where the results are shown in **Table 4**. This important step is intended to test the hypothesis that water awareness and accountability will influence the implementation of the ASEAN CG Scorecard and its impact on the firm's performance. The results of this test are illustrated in **Table 5**. The table shows that

the F test was 5,096 to 0.001 lower than 0.05. This means the hypothesis is accepted where the three variables are a very clear influence on the firm's performance.

Table 3.

The Validity Test with N=100.

No.	Variable	r^{count}	r^{table}	Remark
1	Water Awareness (WA)	0.627	0.165	valid
2	Accounting Awareness (AA)	0.726	0.165	valid
3	Corporate Governance (CG)	0.856	0.165	valid
4	Firm's Performance (Y)	0.859	0.165	valid

Tabel 4.

The result of Multi Linier Regression (MLR) Coefficient[a]

Model		Unstandardized Coefficients	Standardized Coefficients	F	Sig.
1	Constant	3673.623	576.380	2.976	0.000
	WA	125.482	159.161	0.215	0.001
	AA	629.105	117.550	1.015	0.000
	CG	567.225	221.026	4.966	0.001

a. Dependendent Firm's Performance

Tabel 5.

F Statistical Test Result from ANOVA[a]

Model		Sum of Squares	df	mean Square	F	F Table	Sig.
1	Regression	1.634	4	0.408	5.096	2.724	0.001[b]
	residual	2.805	35	0.080			
	Total	4.438	39				

[a] Dependent Variable: Company Performance
[b] Predictors: (Constant), Water Awareness, Awareness Accounting, Corporate Governance

From **Table 4**, the equation's value obtained from equation can be formulated as below.

$$Y = 3.673,623 + 125,482\ WA + 629,105\ AA + 567,225\ CG \qquad (2)$$

It shows that three variables effect on Firm's Performance. WA affects 9.5%, AA affects 47.59% and CG affects 42.91%. The contribution of these parameters can be illustrated as in **Fig. 4**. Results about water awareness, accoutability awareness and corporate governance on firm's performance showed a significance of 0.047 < 0.05. This means that the hypoteses tested is accepted.
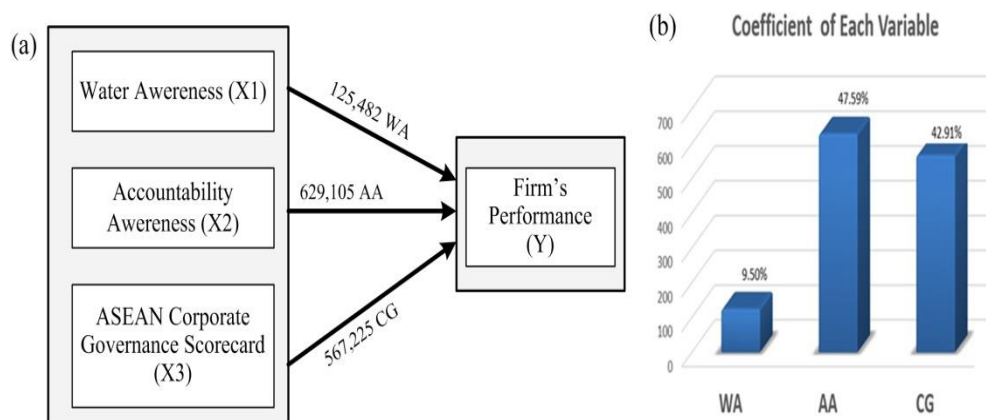
Fig. 4. (a) the influence of three variables on the Firm's Performance and
(b) the percentage influence in each variable

5. CONCLUSIONS

In general, the manufacture firms listed on the ISE have water awareness. They also count this awareness on reporting corporate governance to gain the firm's sustainability. The result indicates that each variable significantly influences on Sustainability Firm's performance. Water awareness, accountability awareness, and corporate governance showed a positively correlation to increase the firm's performance. According to this finding, this research contributes to suggest new measurement of Firm's Sustainability Performance by considering water and accountability awareness. Manufacturing firms are suggested to adopt this model by applying water-based governance principles.

Further research to improve the measurement of sustainability performance has been identified by comparing the results with other sectors and experiences from other countries. The contribution of water awareness is moderately correlated for this case, however, in larger and more complex urban areas, it is important to expand the scope of the research area.

R E F E R E N C E S

ACCA 2010 Disclosures on water. *Accountants for Business*. http://www.accaglobal.com/sustainabilityreporting
Water Supply Regulatory Agency of Jakarta 2018 *Jakarta drinking water crisis*. http://www.brpamdki.org
Baiocchi, V., Lelo, K. & Vatore, F. 2015 Boolean logic model for an environmental protection plan on a local administration terriotry. *Geographia Technica*, 10, 2/2015, pp 1-8.

Brigham, Eugen F. and Joel F. Houston. 2009. *Fundamentals of Financial Management*. Jakarta: Four Salemba.

Boutera, M., Roubhia, A., Lakheneche, D. & Xeereg, S. 2012 Wastewater rejection impact on groundwater wuality in a semi arid region. Case of Tebessa Aquifer. *Geography Technica*, 1, 19-27.

Freeman, RE 2004. A Stakeholder Theory of Modern Corporations. *Ethical Theory and Business*, 7th edn.

Gilley, R., Sullivan, R., Tang, S. & Tarbet, A., 2006. Water Conservation in Windhoek Schools, *City of Windhoek: The Department of Infrastructure*, Water and Technical Services.

Globe Telecom 2019 *ASEAN Corporate Governance Scorecard*. https://www.globe.com.ph/about-us/corporate-governance/asean-corporate-governance-scorecard.html.

Gujarati, D. 2003. *Basic Econometrics*. Jakarta: Erland.

Jawad A. D. 2012 Water issues and accounting awareness. *American Journal of Scientific Research* 60, 46-53, http://www.eurojournals.com/ajsr.html,

Jensen, M. C. & William, H. M.1976 Theory of the Firm: Managerial Behavior, Agency Costs, and Ownership Structure. *Journal of Financial Economics*, 3, 305-360.

Kotane, I. & Merlino 2012 Non financial indicator for evaluation of business activity. *Riga International School of Economics and Business Administration*. DOI 10.5755/j01.eis.0.5.1099.

Richard, P. J., Devinney, T. M., Yip, G. S. & Johnson, G. 2009 Measuring ORGANIZATIONAL PERFORMANCE: TOWARDS BEST PRACTICE methodological. *Journal of Management*, 35, 3, 718-804.

Suparta, W. & Yatim, A. N. M. 2019 Characterization af heat waves: a case study for Peninsular Malaysia. *Geographia Technica*, 14 (1), 146 - 155.

Turner, G., Baynes, T. M., McInnis, B.C. 2010 A Water accounting system for strategic water management. *Water Resouces Management Journal*. DOI: 10.1007/s11269-009-9457-7.

Wiersma, E. 2008 An exploratory study of the relative and incremental information content of two non-financial performance measures: Field study evidence of absence on frequency and on-time delivery. *Accounting, Organizations and Society*, 33, 249-265.

GNSS CORS NETWORK OF THE UNIVERSITY OF PALERMO: DESIGN AND FIRST ANALYSIS OF DATA

Gino DARDANELLI [1] , Mauro LO BRUTTO [1] , Claudia PIPITONE [1]

ABSTRACT:
Nowadays, technical and scientific researches are focused on the use of Global Navigation Satellite System (GNSS) Continuously Operating Reference Stations (CORS) networks due to their global impact on the satellite positioning. This study aims to describe the main steps developed by the University of Palermo for the realization of the GNSS CORS network distributed in the western part of Sicily (Italy). Specifically, it focuses on data availability, preliminary studies and analyses involving the GNSS CORS network, the geodetic framework used, the coordinates and displacements time series retrieved over time and the statistical analysis with the Cumulative Distribution Function (CDF). The analyses allowed to verify the network operating service and the quality of the recorded data during the first period of testing procedure (2008 – 2012).
Key-words: GNSS; CORS; data analysis; time series

1. INTRODUCTION

In the last few decades, many investigations have been developed for the analysis of the three-dimensional (3D) positioning by using the Global Navigation Satellite System (GNSS) Continuously Operating Reference Stations (CORS). The scientific and technical applications developed in different parts of the continents (Snay and Soler, 2008) involved the CORS networks to evaluate the 3D positioning in real-time (Network Real-Time Kinematic, NRTK) and in post-processing analyses. Indeed, the innovative framework of the GNSS CORS networks allowed receiving the most reliable differential corrections over an area by using the Virtual Reference Station (VRS, Wanninger, 2003), the Flächen-Korrektur-Parameter (FKP, Kim et al., 2017) or the Multi Reference Station (MRS, Fotopoulos and Cannon, 2001) approaches. As a consequence, the use of CORS networks allowed increasing the distances between the reference stations, reducing contemporary the total amount of CORS distributed over the same area. Also, many advantages have been observed in terms of economic impact and network management (Grejner-Brzezinska et al., 2005a).

The scientific implementations using the CORS networks were also focused on the analysis and correction of the ionospheric and tropospheric errors (Grejner-Brzezinska et al., 2005a; Zhang and Lachapelle, 2001); the latter, in particular, through the Zenith Tropospheric Delay (ZTD) estimation. Many analyses have been developed to evaluate the use of a global reference system and its inconstancy (Bruyninx et al., 2012; Kenyeres and Bruyninx, 2004) and worldwide the geodynamic studies, over seismic areas (Altiner et al., 2013). Other technical implementations have been also developed in different fields, such as agriculture (Osório and Cunha . 2013), mining (Jing-xiang and Hong, 2009), structures monitoring, utilities, surveying and land cadastral management (Rizos and Satirapod, 2011;

---

[1] *Department of Engineering, University of Palermo, Viale delle Scienze, 90128 Palermo, Italy (e-mail: gino.dardanelli@unipa.it; mauro.lobrutto@unipa.it; claudia.pipitone02@unipa.it)*

Erenoglu 2017; Abidin et al., 2015), Mobile Mapping Systems (MMS, Gordini et al., 2007), Geographical Information System (GIS, Huang et al., 2011) or mapping and airborne Unmanned Aerial Vehicle (UAV, Forlani et al., 2018; Ebolese et al., 2019), road and rail transport and logistics (Marais, 2017), maritime navigation (Angrisano et al., 2013), and aviation (Zhang and Zhan, 2016). Recently, the emerging GNSS framework proposed by the Beidou and Galileo Constellations will further augment CORS demand through use with dual-frequency mobile phones (Dabove and Di Pietra, 2019; Radicioni and Stoppini, 2019; Robustelli et al., 2019).

Nowadays, worldwide, the GNSS CORS networks are widely distributed and they are classified as global, regional, national and local networks based on the covered region (Soler, 2011).

In Italy, several distributed CORS networks are managed by public or private institutions, known as national CORS networks and local level based networks, respectively. In 1994, the first national CORS network, called Geodetic Data Archiving Facility (GeoDAF), has been installed by the Agenzia Spaziale Italiana (ASI). The network (Vespe et al., 2000) is managed by ASI's Space Geodesy Center "Giuseppe Colombo" (ASI/CGS), belonging to the International Laser Ranging Service (ILRS), of International VLBI Service (IVS) and International GNSS Service (IGS). All stations belonging to the GeoDAF are able to provide daily and hourly recorded data in Receiver INdependent Exchange (RINEX) format; most of them are also able to supply data in real-time within the EUREF IP project. Since 1996, all data, available from GeoDAF and other CORS networks distributed in Italy, are able to support all users through an EUREF Local Analysis Center (GeoDAF, 2020). Since 2004, in Italy, the Istituto Nazionale di Geofisica e Vulcanologia (INGV) has managed a national CORS network, made up of ≈ 200 CORS (Avallone et al., 2010), called Rete Integrata Nazionale GPS (RING) mainly devoted to tectonic studies; this network provides the availability of RINEX data at 30 second online.

In 2009, the Istituto Geografico Militare Italiano (IGMI, the Official Italian geodetic entity) has developed the national CORS network, called Rete Dinamica Nazionale (RDN), made up of 99 CORS; 21 of those were included in the EUREF Permanent Network (EPN), and other 14 stations were used for the computation of the International Terrestrial Reference Frame 2005 (ITRF2005) solution (Baroni et al., 2009). The ITRF2005 coordinates of these stations are also converted to the ETRF2000 frame by using the Helmert parameters (Boucher and Altamimi, 2011). Indeed, the RDN also provides the European Terrestrial Reference Frame (ETRF2000, epoch 2008.0), updating the previous reference system ETRS89 of the static GPS geodetic network, called IGM95; these reference stations belong to different Research Centres, Universities and Public Institutions. Consequently, in 2013, the IGMI has monitored the GNSS network, re-computing periodically the stations' positions and analysing the time series of the stations over the first five years of their activity. It was found that ≈20% of the 99 RDN stations were not able to transmit data correctly and many of those have been dismissed (Maseroli, 2015). This breakdown caused the inactivity of several distributed areas. Thus, a new version of the RDN network, called RDN2, restoring the correct geometry between the stations, has been materialised by the IGMI replacing the old CORS and re-computing their updated positions (epoch 2014.4). In Italy, other two private national CORS networks are also available. Specifically, 133 of these CORS are managed by Hexagon Geosystems, Italian Positioning Service (ItalPoS) (HxGN SmartNet 2020) and more than 200 CORS are managed by Topcon Italia, (NetGeo 2020). These private national CORS, referred to the ETRF2000-RDN reference frame, were developed to make available real-time corrections in the 3D

positioning with VRS, FKP, MRS approaches and RINEX data for post-processing analyses and technical research.

Many other local level based networks, managed by Universities, public and private institutions are also available in Italy, improving the NRTK positioning for technical research, increasing the number of available CORS in the whole country. Data from these stations are also used for scientific and experimental research (**Fig. 1**).

Since 2014, the University of Padua has recomputed the weekly position of GeoDAF, RING, RDN, ItalPos, Netgeo and other local networks, based on the combination of seven daily solutions with Bernese 5.2 software. All these CORS belong to the so-called Italian GNSS Network, made up of ≈700 GNSS CORS, available in Italy and the neighbouring countries. The time series and the horizontal and vertical velocity fields of these stations are made available on a specific website (Italian GNSS Network 2020).
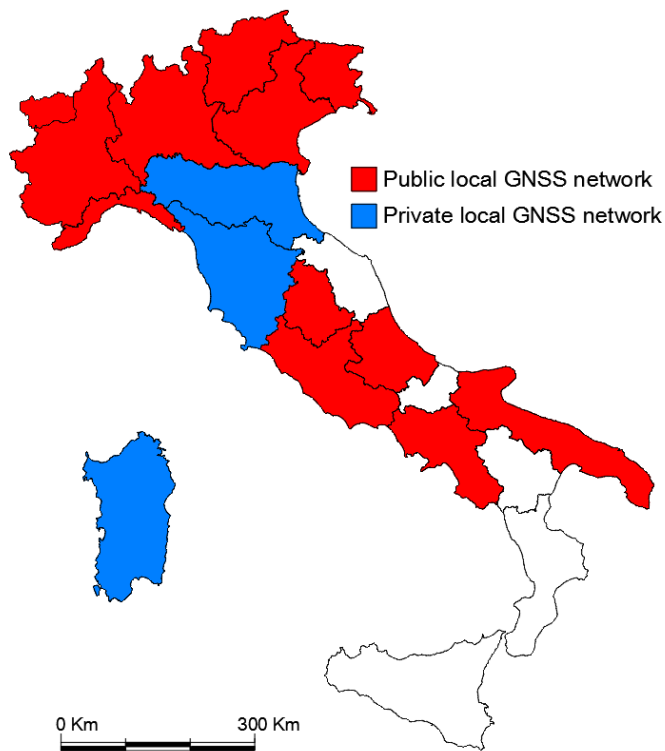
Fig. 1. Map of the local level based network in Italy.

Up to 2008, in Sicily there was not a local GNSS network; thus the University of Palermo has designed and realised the first local level based network in the central-western part of the island. The management of the GNSS CORS network, made up of 8 stations, used for technical and scientific purposes, was preliminary entrusted to the University (until 2013); later, the stations were included in the Netgeo GNSS network, managed by Topcon Italy, due to the scientific collaboration between the latter and the University of Palermo, aimed to realize the first local level based network in Sicily.

The CORS network set up in the western part of Sicily has been tested and data was used for several scientific works focused on: dams monitoring (Pipitone et al., 2018; Dardanelli and Pipitone, 2017; Dardanelli et al., 2014), geological analyses (Stocchi et al., 2017), trajectories calculation of MMS (Dardanelli et al., 2015; Dardanelli and Carella, 2013), integrated survey in archaeological context (Fazio et al., 2019; Ebolese et al., 2019) and also geodynamic research (Barreca et al., 2020).

The aim of this study is the description of the developments of a new infrastructure able to support scientific and technical research by Universities, private users and National Agencies for the site monitoring and control, realized by the University of Palermo. Specifically, the study points out the main activities related to the data availability and its preliminary use for scientific purposes, the geodetic frame, the time series and the statistical analyses; the latter developed through the implementation of a Cumulative Distribution Function (CDF).

This study focuses on the analysis of the GNSS CORS network over the first period of operability of approximately 5 years (from 2008 to 2012); the choice of this preliminary dataset is based on different motivations. Firstly, for each GNSS CORS, it is important to verify the quality of the data obtained throughout the analysis of the GNSS observations during the first period. This approach allows the validation of the infrastructure for technical and scientific applications according to the network's installation purposes. Moreover, the analysis of the correctness of this preliminary dataset was important because since 2013 the data retrieved from UNIPA GNSS CORS network has been used for the computation of the RDN2 network (EPN subnetwork), managed by the most important Italian cartographic institute (IGMI). In addition, from this period (2013), data has been made available for the evaluation of the national reference framework by the IGMI and for technical researches able to investigate the horizontal and vertical velocity map (Maseroli, 2015). Specifically, the EPN recommends the use of the first five years of data for the inclusion of a CORS within a network (Bruyninx, 2019).

The use of RINEX files since the first years of data acquisition is common in the scientific field, as demonstrated by several studies, e.g. the analysis conducted in 2009 for homogeneous reprocessing of the EUREF permanent network based on the 1996-2003 dataset (Kenyeres et al., 2009) or the analysis of the performances and the time series of CORS local network (Baniulis, 2017). Specifically, in the latter, the authors analysed in a succeeding period (2017) the data collected during a previous one, between 2008 and 2011.

The paper is organized as follows: the description of the CORS network (preliminary analyses, network project design and its materialization, description of the instrumentation) is discussed in Section 2. The software used for the preliminary analyses, the computation of the GNSS time series and the geodetic frame are described in Section 3; the results of the analyses are presented in Section 4. Finally, the conclusions and future applications are reported in Section 5.

2. GNSS CORS NETWORK DEVELOPED BY UNIVERSITY OF PALERMO

2.1 Preliminary studies and network project design

Preliminary studies for the materialization of the GNSS network have deeply analysed the importance of fixing a minimum number of CORS and the distance between them, assuming that no specifications are available in literature. Only few recommendations are available from experimental tests developed for NRTK applications. Some of those have considered the maximum distance to be used between the reference stations of

approximately 200 km (Grejner-Brzezinska et al., 2005b); but generally, the distances to be used between the stations are within the range 50-80 km, to avoid exceeding the maximum value ($\approx$200 km) (Benciolini et al., 2006).

The geometric configuration of the GNSS CORS network proposed by the University of Palermo (UNIPA) considered the shape of the area to be monitored; specifically, the distribution of the CORS was conceived along the boundary of the western part of the island. Just to avoid exceeding more than 100 km between the CORS, another reference station has been installed in the hinterland, approximately barycentric between the CORS.

Other two existing CORS have been included in the network project design, one installed on the top of a building at the University of Palermo (PALE), the other in Termini Imerese (TERM). Other three CORS have been installed in the main cities of the western part of Sicily. Specifically, they are located in Trapani (TRAP), Agrigento (AGRI) and Caltanissetta (CALT); while the remaining were installed in little cities or towns: Partinico (PART), Campobello di Mazara (CAMP) and Prizzi (PRIZ). Totally, 8 CORS belong to the UNIPA GNSS network; the distances between the reference stations, influenced by the position of the buildings allocating the GNSS instrumentations, are included within the range 22 - 83 km (**Fig. 2**).

Almost all UNIPA CORS (TRAP, TERM, PART, CAMP, PRIZ) have been installed at Institutions interested in the collaboration with the University for scientific research, mainly secondary schools. The schools made available suitable areas where the instrumentation and the internet connection have been only used for the project. Only PALE and AGRI CORS have been installed at the Universities, while CALT CORS has been installed at the *Genio Civile* office.
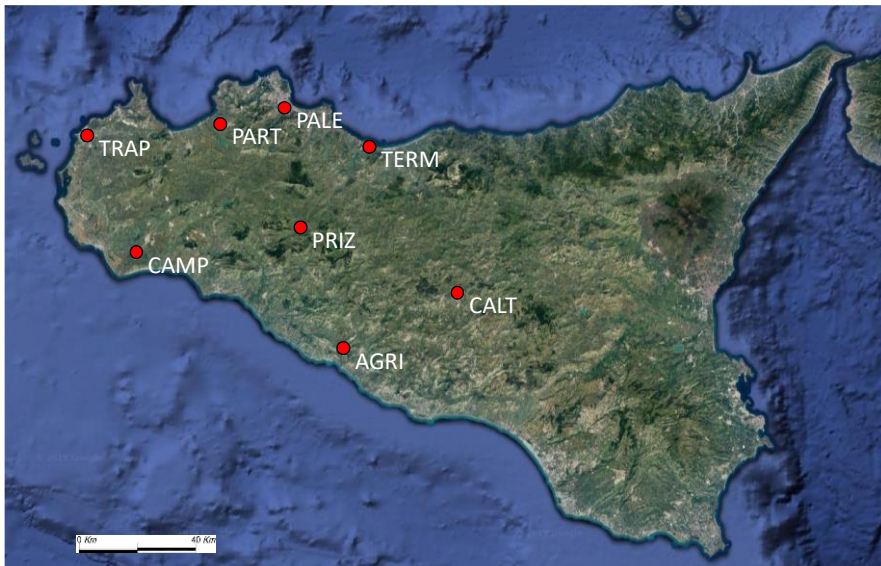

Fig. 2. Location of the UNIPA GNSS CORS (from Google Maps©).

2.2 Materialization and installation of the CORS

The materialization of the GNSS CORS was relatively easy to be installed. This steps could be realised using different solutions; indeed many GNSS Institutions, for example,

the International GNSS Service (IGS), the University NAVSTAR Consortium (UNAVCO) and the National Geodetic Survey (NGS, Anderson et al., 2000) have made standard procedures for this purpose.

Depending on the use of the GNSS CORS, the instrumentations can be fixed directly on the ground, (*e.g.* for geodynamic analyses), or on the top of the buildings (*e.g.* for technical purposes), but generally, the instrumentation is fixed with concrete or steel pillars, three-dimensional structures or also invar and steel beams (Anderson et al., 2000).

To determine the correct position of the GNSS instrumentation, some requirements needed to be satisfied, such as preventing the presence of obstacles that could restrict the satellites' visibility with cut-off angles more than five degrees, or preventing the presence of mirroring surfaces that could cause the multipath effect, or moreover preventing the presence of TV or mobile repeaters that could cause electromagnetic disturbances on the GNSS signal. Indeed, as discussed in previous works (Edwards et al., 2010), some investigations have been developed to preliminary investigate and analyse the quality of the signal with acquisitions of few hours.

Specifically, the UNIPA GNSS CORS have been installed on steel pillars placed on the top of selected buildings. Some of them have been fixed on reinforced concrete bases (PALE, TRAP, PRIZ), the others have been fixed with steel clamps and flanges (**Fig. 3**). Both materializations allowed obtaining strong and resistant structures over time.
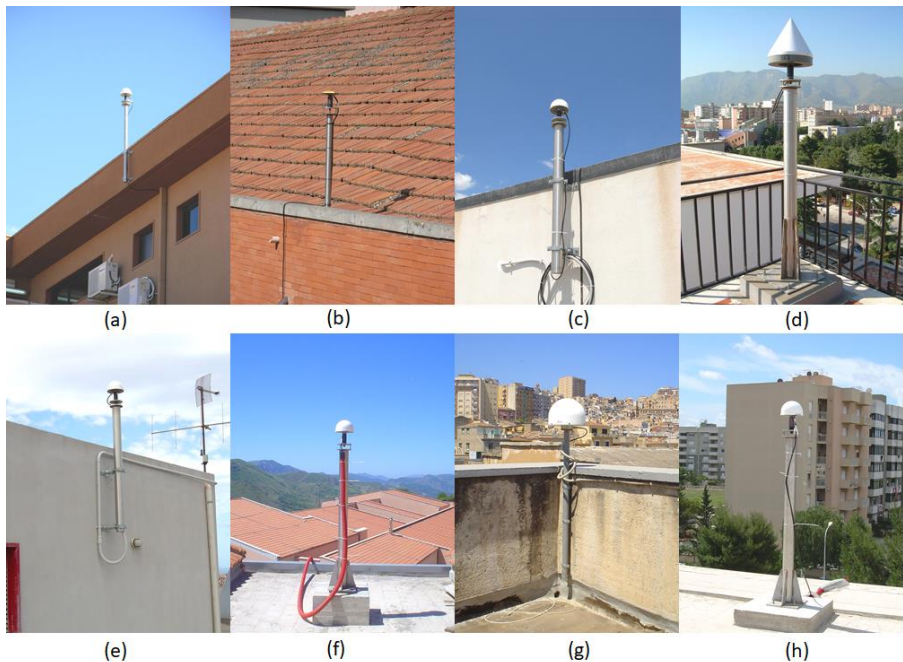
Fig. 3. Monumentation of the UNIPA CORS. From left to right and from up to bottom: (a) AGRI; (b) CALT; (c) CAMP; (d) PALE; (e) PART; (f) PRIZ; (g) TERM; (h) TRAP.

2.3 Main characteristics of GNSS receivers and antennas

As discussed before, the materialization of the UNIPA GNSS CORS network has been guaranteed by the collaboration with Topcon Italy that supported the scientific research with GNSS receivers and all instrumentation. This collaboration allowed the

University to reduce costs, guaranteeing the use of the GNSS CORS data by private institutions for commercial purposes (especially for NRTK corrections). This approach is widely used in literature (Rizos, 2007), for example in the United Kingdom (UK) the Ordnance Survey Network (OSNet) permits the use of CORS data to Leica Geosystems and Trimble companies (Edwards et al., 2010; Henning, 2011).

All GNSS CORS were equipped with Topcon NET-G3 GNSS receivers, able to receive signals from both GPS and GLONASS constellations, but also Galileo frequencies. They are also equipped with an Ethernet door for their management from remote by using the Transmission Control Protocol/Internet Protocol (TCP/IP) protocol and a data storage to archive two weeks of data collected with a rate of 1 second. They were allocated within plastic lockers with more long-lasting batteries to be used when the electricity is not available.

All UNIPA CORS were also equipped with Topcon G3-A1 antennas with plate-ground and radome, excepting for the two CORS (PALE and TERM) already existing before the network's materialization. The first one is equipped with choke-ring antenna Topcon CR-3, the other GPS-GLONASS choke-ring antenna was already furnished by Leica (Leica AT504). All antennas and receivers were connected with RG-58 cables longer than 30 meters, installed within external pipes made of polyvinyl chloride (PVC).

2.4 Network design, data transmission, products and available services

All UNIPA GNSS CORS are monitored from remote and they are able to transmit data by using the Asymmetric Digital Subscriber Line (ADSL), exclusively used for the project. This technology, low-cost and easily installable, is configured with static Internet Protocol (IP) address by *Telecom Italia* for all available GNSS CORS, excepting for PALE CORS, directly connected to the server of the University and AGRI CORS, connected with another technology by *Gruppo di Armonizzazione delle Reti della Ricerca* (GARR). The routing of the network allows connecting each reference station to the main server of the *Centro Universitario di Calcolo* (CUC) of the University of Palermo.

In the preliminary stage of activity, from 2008 to 2012, the management was exclusively entrusted to the University of Palermo, specifically to the Geomatic Laboratory of the Department of Engineering. The software managing the network was GNSS State Monitoring And Representation Technique (Geo++® GNSMART) allowing a continuous monitoring system, recording and storing GPS data, computing and sending the differential corrections *via* FKP or VRS. This software is also able to record data from all GNSS CORS in Radio Technical Commission for Maritime Services (RTCM) format, checking the quality and the entirety of the data, estimating the ambiguity phase in real-time and the disturbances and the errors of the phase and code measurements.

The distribution of the data in RTCM format, used for real-time positioning, is guaranteed by Networked Transport of RTCM via Internet Protocol (NTrip), developed by EUREF to promote and spread GNSS data *via* internet. For post-processing positioning, GNSS data are available in RINEX format at 1, 5, 30 seconds rate. The latter are stored on the server of the University and made available to private users only after specific requests.

Since 2013, Topcon Italy has also used its software to manage the GNSS data available from UNIPA CORS. Specifically, the software Topnet was used for sending the corrections of Netgeo network in real-time (Nearest, VRS, MRS, FKP, DGPS), while the *Meridiana Sat Enterprise* software, implemented with "Megaserver" module, is only used for post-processing positioning systems, specifically for data recording, transferring, storing and making available online the RINEX format of the data.

3. MATERIALS, SOFTWARE USED AND METHODS

3.1 Data availability

For this case study, the dataset refers to the period 2008 - 2012 and consists of all available data in RINEX format daily acquired (24h) from UNIPA GNSS CORS. The data availability was analysed with Network Deformation Analysis (NDA) Lite software, specifically, with the graphic interface NDA Data Quality Evaluation (DQE), developed by Galileian Plus S.r.l.

The quality check of the data with NDA Lite software was analysed over the entire time span, specifically from the Modified Julian Date (MJD) 54400 to the MJD 56400.

Other specifications were also considered for the analysis:

- The ratio between expected and collected data acquired in RINEX format;
- The ratio between the number of acquired data in dual-frequency and the amount of acquired data;
- The number of cycle slips for each session.

3.2 Preliminary analysis

For the preliminary analysis, two software have been used: Translation Editing Quality Check (TEQC) and QC2SKY, both open-source and available from UNAVCO website. The first one is a powerful tool for the preliminary processing of GPS, GLONASS but also Galileo observations. It also allows modifying the data format and implementing the quality check, modifying and extracting metadata. The main functions of the software are reported below and can be used separately or combined:

- Translation: conversion of the data from the original binary format to RINEX files in American Standard Code for Information Interchange (ASCII) format;
- Editing: transformation and/or extraction of metadata from RINEX files and RINEX files formatting;
- Quality Control: quality check of RINEX data.

Results from TEQC software are then processed with QC2SKY software, implemented and made freely available online by the Polytechnic of Turin (Italy). Results from these analyses are shown in bitmap format, describing the Signal-to-Noise Ratio (SNR) values and the multipath skyplots on both frequencies, the ionosphere and the first derivative of ionospheric delay. The quality check of RINEX data is based on the use of Estey and Meertens equations (Estey and Meertens, 1999).

3.3 Geodetic framework and time-series computation

The NDA Professional software, developed by Galileian Plus s.r.l., in collaboration with the Polytechnic of Milan and the *Agenzia Spaziale Italiana* (ASI), has been used to determine the geodetic framework and the time-series of all UNIPA CORS. NDA has been used in many technical-scientific applications in Italy; in particular, in 2013 for SISMA (Seismic Information System for Monitoring and Alert) project, comparing the results obtained by NDA with those of GAMIT/GLOBK to obtain a combined solution (Panza et al., 2013). In 2014 a GNSS continuous monitoring system for earth-dam deformations has been developed using NDA; the NDA results were also validated through Bernese ver 5.0 (Dardanelli et al., 2014).

The tropospheric corrections involving Saastamoinen and Niell mapping functions (Saastamoinen, 1972; Niell, 1996) and the ionospheric error determined by using the

Klobuchar model (Klobuchar, 1996) are both implemented within the software; but also the ocean tides corrections are available, based on the Schwiderski model (Schwiderski, 1980).

NDA software adopts this correction model regardless of the receiver type. In particular, for ionosphere modelling users can select the ionosphere model available to compute and remove the ionospheric path delay. Possible choices are:

1) *Zero*: no ionospheric residual is added on double differenced data. It is recommended for baseline length < 5 Km;

2) *Euler-Goad*: the dispersive delay is estimated using the Euler-Goad algorithm;

3) *Absolute*: the Euler-Goad estimation average is replaced with the Klobuchar's model average;

4) *Klobuchar (broadcast)*: the dispersive delay is computed using the Klobuchar's model and the eight model parameters are obtained from broadcast ephemerides files;

5) *Klobuchar (CODE)*: the eight model parameters are computed by the European Centre for Orbit Determination (CODE), and distributed in RINEX navigation file data header format. If Klobuchar model with CODE parameters is selected, a valid path for CODE Global Ionospheric Map (GIM) file repository must be provided.

Additional parameters such as the Earth's rotation parameters (ERP), the ephemerides relative to the sun and the moon, the precise ephemerides (sp3 format) and the antenna phase centre position retrieved from the International GNSS Service (IGS) were also used for the analysis. Sun ephemerides are mandatory to remove the antenna satellite offset and fully exploit the sub centimetre precision of IGS precise ephemeris, while, moon ephemerides are used (together with sun ephemerides) to compute the antenna displacements.

A single baseline was used for the connection between the UNIPA and IGS CORS (Noto, Cagliari, Matera and Lampedusa). Based on the design project of the network, totally 32 baselines (with lengths between 105 and 478 km) have been developed, connecting separately four UNIPA CORS to each of the IGS stations. For the baselines processing, the zenith troposphere estimation (affecting the baseline coordinates estimation) was enabled on both stations (recommended for baseline over 15 km). According to the multi-frequency strategy, double-differenced observation data coming from L5 (wide-lane) and L3 (ionospheric-free) frequencies combination were used. This option is recommended within the software for baseline lengths higher than 10 km. The Least-Squares Ambiguity De-correlation Adjustment (LAMBDA) method was used to fix the phase ambiguity (Teunissen, 2005). To estimate the final solution, the Wide-lane observation estimating the Wide-lane ambiguity and then, the ionospheric-free observations estimating the remaining Narrow-lane ambiguity were also used. Finally, the time range and the cut-off angle were set to 30 s and 10 degrees, respectively.

3.4 Statistical analysis

The statistical analysis of GNSS data has been computed by using Matlab software. In particular, the software allowed analysing the robustness of data, removing the outliers and plotting the time series over time. Then, according to the literature (Feng and Jokinen, 2017; Prikry et al., 2013; Olivares-Pulido et al., 2019) a CDF has been applied to the coordinates (X, Y, Z) of each GNSS CORS. Preliminary, an adjustment test has been also conducted on the dataset ("*Lillietest*"), to verify its Gaussian distribution. Then, results from GNSS analysis have been preliminary averaged applying a simple moving average (SMA) over a temporal moving window (~1 month), during the whole period (2008 - 2012) to retrieve the long-term trend of the coordinates.

4. RESULTS AND DISCUSSION

As mentioned previously, this study focuses on the analysis of the GNSS CORS network over the first period of 5 years (2008 – 2012) in which RIXEX data was collected; indeed, other experimental research by EPN, UNAVCO or IGS did not reveal the minimum time span mandatory for the GNSS CORS network analyses (Kenyeres et al., 2019). Preliminary, the coordinates and the velocities (both absolute and relative) of all GNSS CORS have been computed in the IGb08 reference frame, by using the Geo++® GNSMART and NDA Professional software. Since 2013, the collaboration with Topcon Italy for the management of the network has started and six UNIPA GNSS CORS have been included in the RDN2 network (EPN network), managed by IGMI. From this period, data was available for the national reference frame evaluation, conducted by the IGMI but also for technical research, to analyse the CORS time series, the map of horizontal and vertical velocities, weekly published on the *Bollettino Bernese* by the Italian GNSS Network (Italian GNSS Network 2020).

4.1 Data availability

The availability of the dataset was checked analysing the RINEX files during the monitored period (from MJD 54400 to MJD 56400); specifically, the RINEX files have been daily analysed over a period of 5 years, while the daily mean has been retrieved from the observation data, during the same period. Availability of single GPS satellite day by day is shown in **Fig. 5** and **6**; the percentage of daily satellite availability for all CORS is generally over 90%. **Fig. 7** and **8** show instead the number of cycle slips per single satellite day by day; the values are very low for all CORS. The total amount of expected RINEX files to be downloaded (expR), the number of files actually acquired (acqR) and their ratio (R1%) have been reported in **Table 1**. In the same table, also the amount of expected observations (expO), the number of files really acquired (acqO) and their ratio (R2%), the average value of cycle slips (Cs) for each session and another parameter called CSR have been resumed. The latter parameter is computed as follows:

$$CSR = \frac{cycle\ slips}{n^{o} of\ observation} \ 1000 \qquad (1)$$

Results confirmed the highest values of R1 for CAMP, PALE, PART, PRIZ CORS (ranging between 82 and 89%), while values between 69% and 78% of the same parameter have been found for AGRI, CALT, TERM and TRAP CORS. The lowest value of R1 has been found for CALT CORS (69%), because the CORS has been moved from the original site for technical reasons and a loss of data has been verified during the repositioning of the instrumentation. In general, referring to previous studies already analysing the percentage of transmitted data, the R1 values seem to be satisfactory for all GNSS CORS (Barbarella et al., 2018). Results confirmed also a strong percentage of R2 values for all GNSS CORS (R2 > 92%), while the CSR parameter is generally less than 5 for all CORS, according to EUREF and IGS prescriptions (Boucher and Altamimi, 2011; Barbarella et al., 2018), despite the reference stations have been included in the EPN network (B classification).

Fig. 5. Availability of single GPS satellite day by day; the x-axis represents the time (Epochs-MJD), the y-axis represents the percentage of data availability.
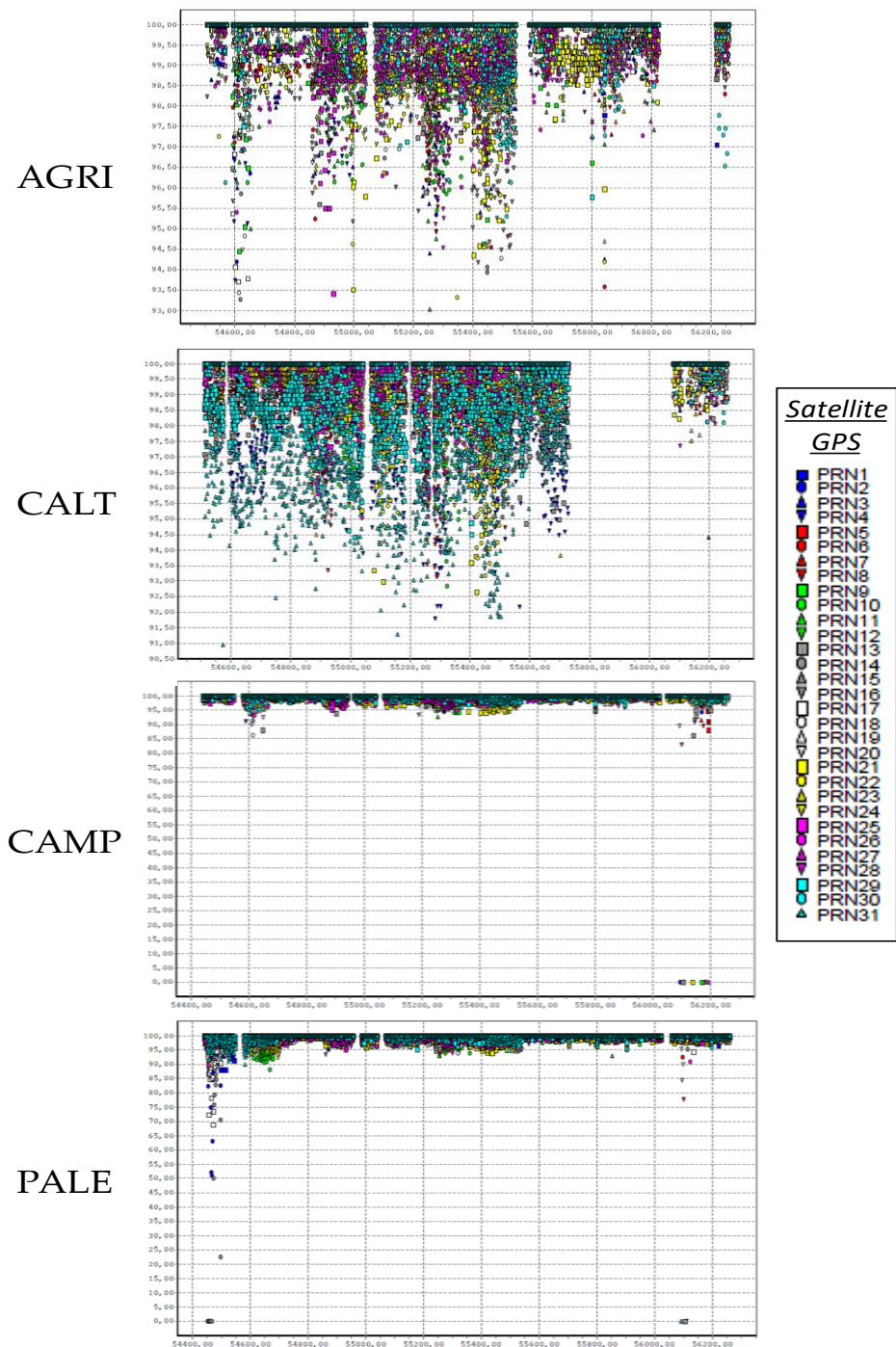
Fig. 6. Availability of single GPS satellite day by day; the x-axis represents the time (Epochs-MJD), the y-axis represents the percentage of data availability.

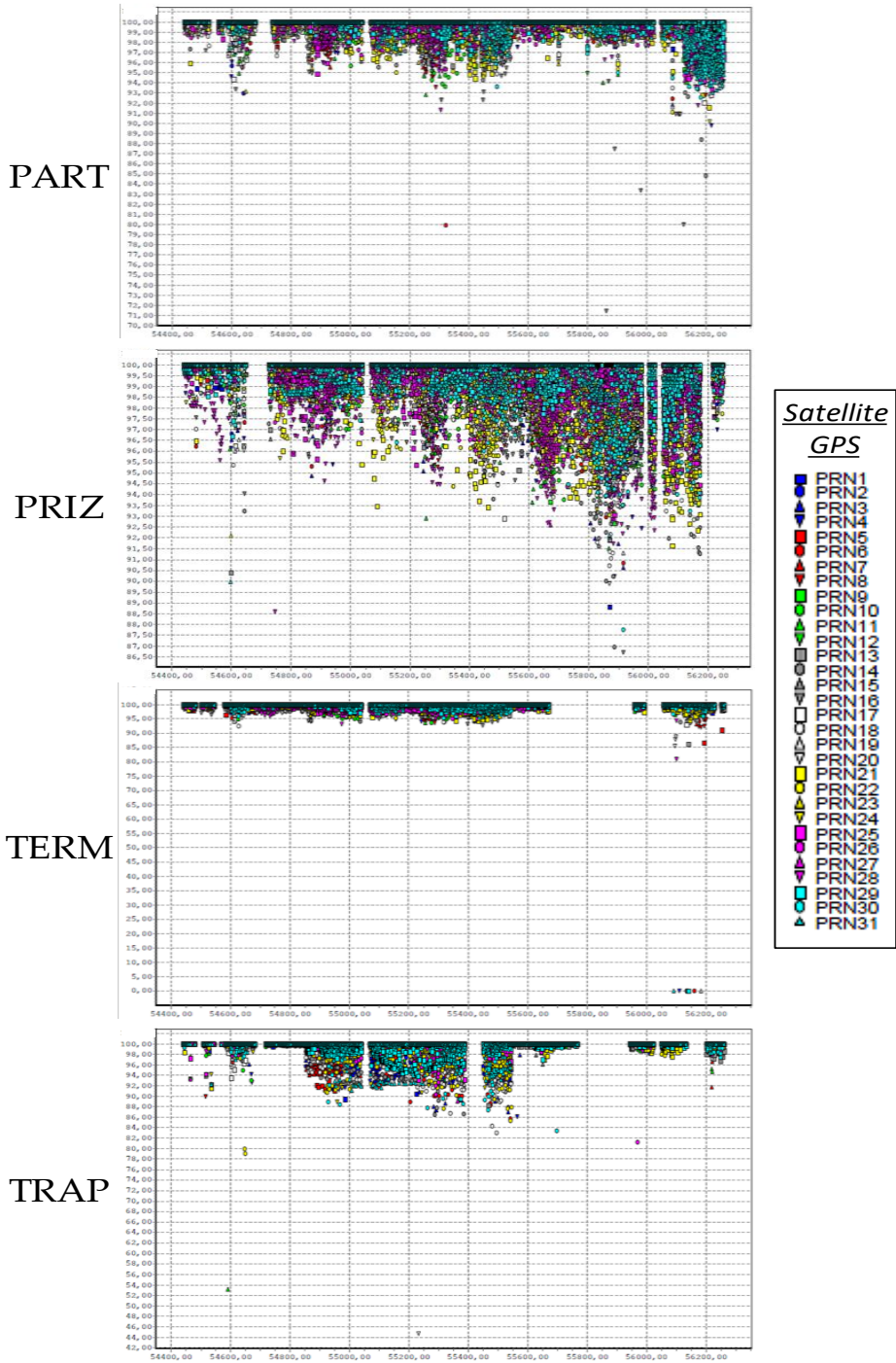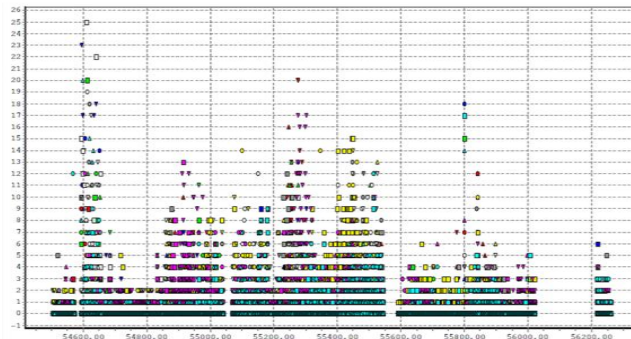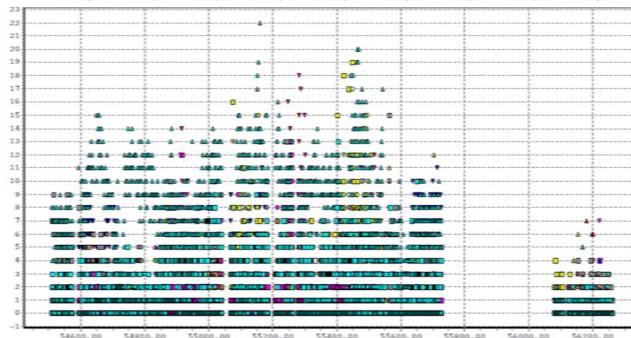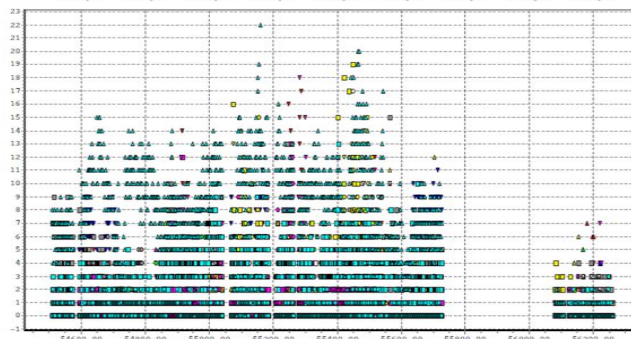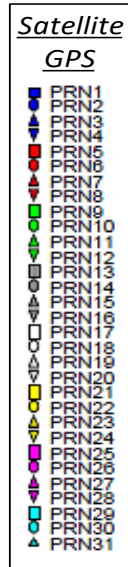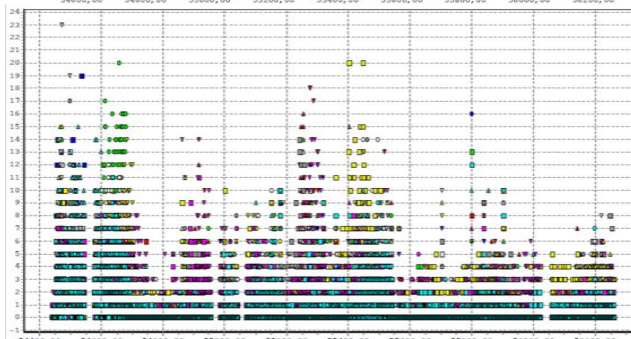**Fig. 7.** Cycle slips per single satellite; the x-axis represents the time (Epochs-MJD), the y-axis represents the number of cycle slips.
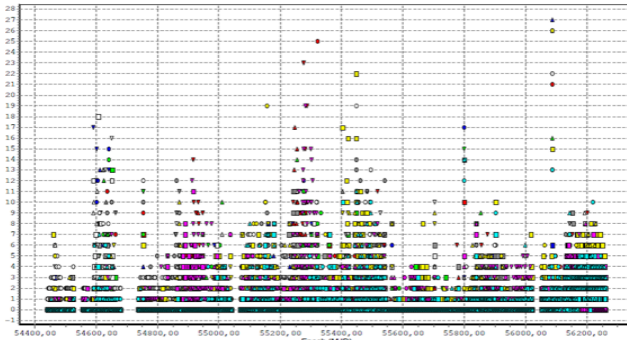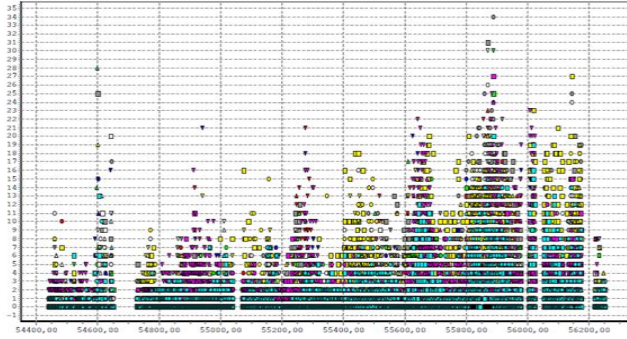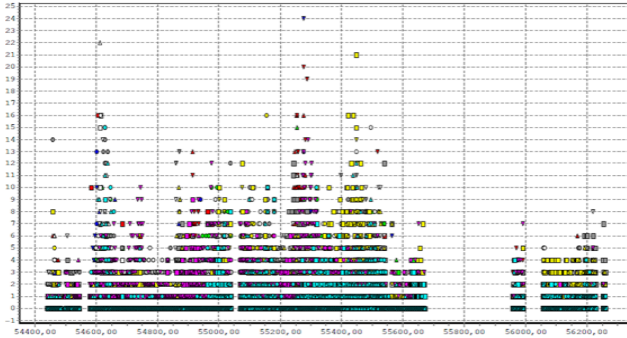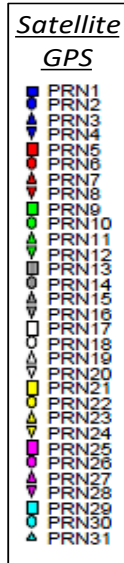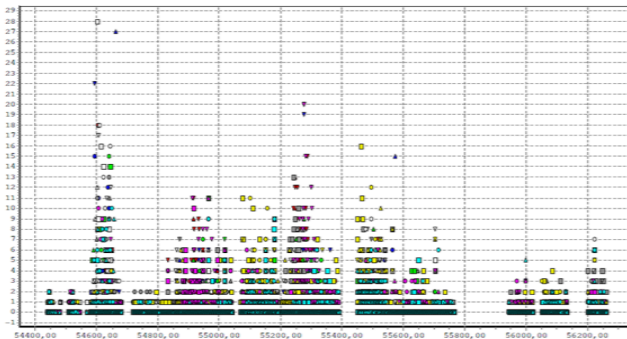
Fig. 8. Cycle slips per single satellite; the x-axis represents the time (Epochs-MJD), the y-axis represents the number of cycle slips.

RINEX and observation data from MJD 54400 to MJD 56400

CORS	RINEX data			Observation data				
	exp_R	acq_R	R1 (%)	exp_O	acq_O	R2 (%)	Cs	CSR
AGRI	1827	1428	78	22795	22458	99	6730	0.1
CALT	1827	1253	69	22639	21042	93	2635	0.4
CAMP	1827	1623	89	23355	22945	98	9126	0.1
PALE	1827	1635	89	23321	22898	98	5101	0.2
PART	1827	1608	88	25030	23908	96	14404	0.1
PRIZ	1827	1507	82	25260	24254	96	3456	0.3
TERM	1827	1300	71	23308	22908	98	5350	0.2
TRAP	1827	1334	73	25277	24943	99	15660	0.1
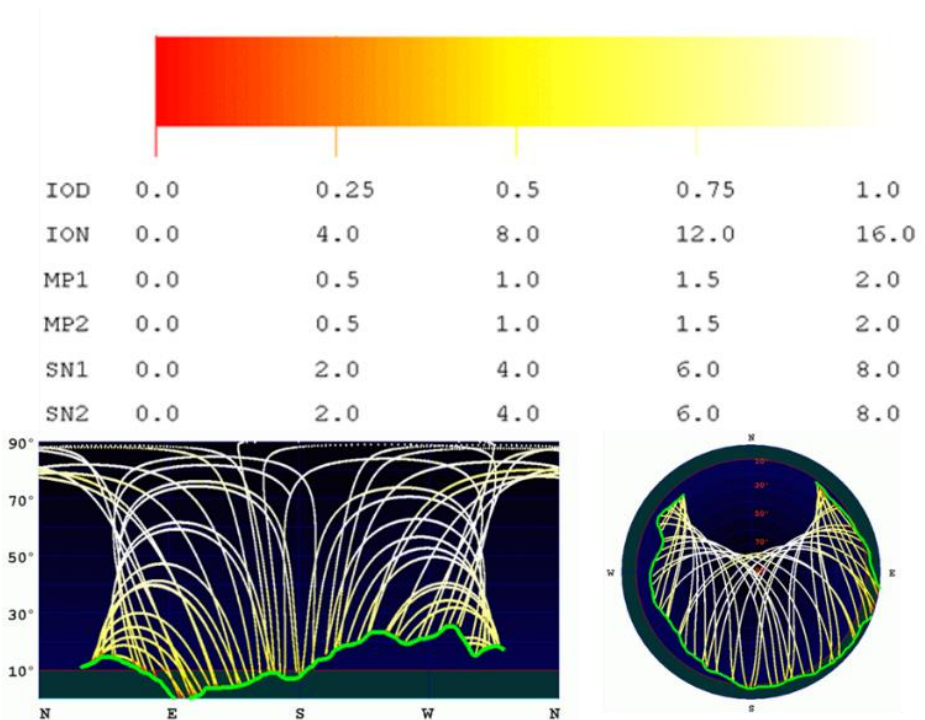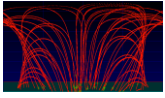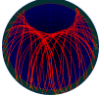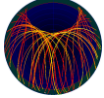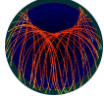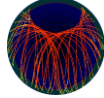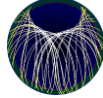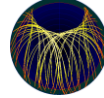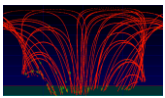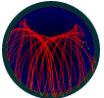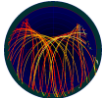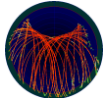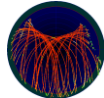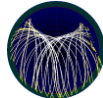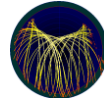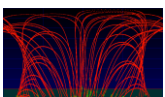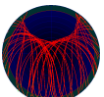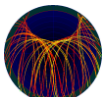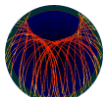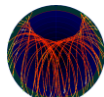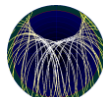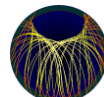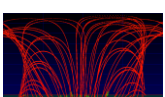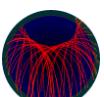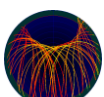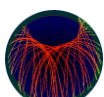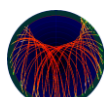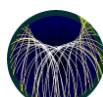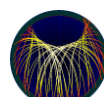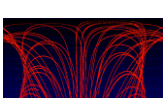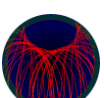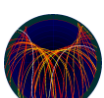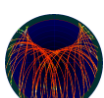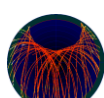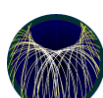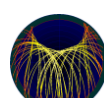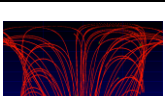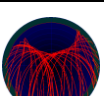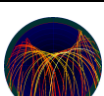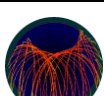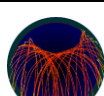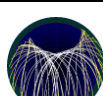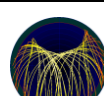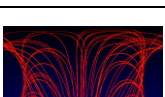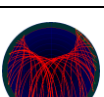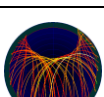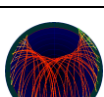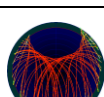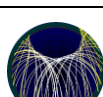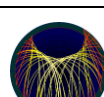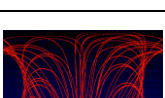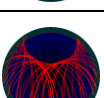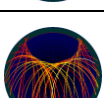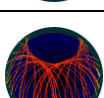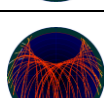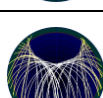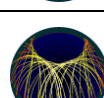
Fig. 9. QC2SKY color scale.

QC2SKLY skyplot (cartesian and polar).

CORS	Cartesian L1	IOD	ION	MP1	MP2	SNR1	SNR2
AGRI							
CALT							
CAMP							
PALE							
PART							
PRIZ							
TERM							
TRAP							

4.2 Preliminary analyses

The preliminary analyses have been conducted with TEQC and QC2SKY for all UNIPA GNSS CORS. Results obtained with TEQC software are plotted as functions of the elevation angle and the azimuth of the satellites at the time of observation; they refer to two different coordinate systems: polar and cartesian. In the latter, the azimuth is represented on the x-axis and the elevation angle is on the y-axis. The SNR of L_1 frequency is represented in colour scale in TEQC, specifically, in green the obstructions on the horizon are represented. The output from QC2SKY software shows only one colour scale for each panel, only changing the upper limit as reported in **Fig. 9**; the units of the ION (ionospheric delay, in meters), IOD (first derivative of ionospheric delay, in meters/minute), and MP1

and MP2 (multipath, in meters) values are uniformly displayed. SN1 and SN2 are reported for L1 and L2 signals in dBHz units. The units in TEQC can not be modified, the software QC2SKY schematically shows the TEQC outputs, resampling all values in the same color scale. In particular, in **Fig. 9** the skyplot of only one casual day is represented, corresponding to the date 30-06-2010, because too many representations were available from the analysis (more than 250 graphs). **Fig. 9** and **Table 2** show that the ionospheric delay (IOD) is always included within the range 0.00 - 0.25, first derivative of ionospheric delay (ION) (Kang et al., 2019; Mitch et al., 2013) within the range 0.00 - 4.00, the multipath values (for both MP1 and MP2) are included within the range 0.00 - 0.50, while SNR1 and SNR2 values range between 6.00 – 8.00 and 4.00 – 6.00, respectively. These values are in agreement with literature (Hu et al., 2016; Baniulis et al., 2017); indeed, the Root Mean Square (RMS) MP1 of half of IGS stations is lower than 0.4 m and 2/3 have less than 0.5 m; the absolute values of multipath RMS, however, do not necessarily correlate with site performance. Finally, the RMS MP2 values of half of IGS stations are lower than 0.6 m and less than 0.75 m for 2/3 of IGS stations (IGS 2020).

4.3 Geodetic reference framework analysis and CORS time-series computation

Preliminary, the coordinates of all UNIPA GNSS CORS, referred to February 2008 have been computed in the International GNSS Service, epoch 2008.0 (IGb08) reference frame. The coordinates of the reference stations have been also computed in the European Terrestrial Reference Frame, epoch 2008.0 (ETRF2000) reference frame, by using the "Altamimi and Boucher" equations ((Boucher and Altamimi, 2011). The computation of the coordinates has been processed, analysing the available monthly dataset from GPS week 1465 to 1469. The analysis included other IGS reference stations, such as Noto, Cagliari, Matera and Lampedusa. A prori precision of these CORS was 2 mm and 4 mm, for the planimetric and altimetric components, respectively. Results obtained from the analyses are in agreement with IGS standard recommendations (IGS 2020). The weekly solutions are computed from the daily ones, evaluating for the latter the network balance with double differences. Specifically, several parameters have been evaluated for each reference station and each daily solution, such as data quality indicators, the amount of cycle slips, the amount of initial ambiguity phase, the percentage of fixed ambiguity phase and the fixing quality, the standard deviation (σ) of the float and the final solutions. The coordinates and the standard deviations for each GNSS CORS are reported in **Table 3**. Also for the GNSS time-series estimation, the IGS CORS of Noto, Cagliari, Matera and Lampedusa have been considered. **Fig. 10** show the geocentric components (X, Y and Z) of all GNSS CORS coordinates corresponding to the GPS epochs (MJD). Preliminary, the outliers have been removed from the time-series and the evolution of the scattered behaviour has been plotted within the range ±3σ, as reported in literature (Barbarella et al., 2018; Gandolfi et al., 2016). In **Table 3** also the average errors related to the X, Y, Z components of the CORS coordinates have been reported. As shown, these values are lower than 0.4 mm, excepting for those referred to PALE CORS. Indeed, for this station, the values are included within the range 2.9 - 6.5 mm, but they are even in agreement with EPN recommendations suggesting the limits up to 10 – 20 mm (Gülal et al., 2013). According to the strategy explained in section 3.3, after removing the outliers, reporting the time series within the range ±3σ, the behaviour of the CORS coordinates is mainly considered linear, in agreement with (Gülal et al., 2013) (**Fig. 10**).

UNIPA CORS geodetic positions in IGb08 and ETRF2000 systems.

CORS	IGb08 epoch 2008.0			ETRF2000 epoch 2008.0		
	X (m)	Y (m)	Z (m)	X (m)	Y (m)	Z (m)
AGRI	4936330.975± 0.0006	1194330.805± 0.0004	3845901.113± 0.0005	4936331.298	1194330.469	3845900.834
CALT	4915665.317± 0.0009	1230635.627± 0.001	3861348.553± 0.0007	4915665.644	1230635.292	3861348.275
CAMP	4933160.640± 0.0007	1115797.477± 0.0002	3873025.139± 0.0004	4933161.054	1115797.238	3873024.868
PALE	4889534.164± 0.0065	1160203.926± 0.0038	3914738.891± 0.0029	4889534.473	1160203.648	3914738.514
PART	4898768.541± 0.0029	1140863.11± 0.0010	3909130.693± 0.0020	4898768.970	1140862.867	3909130.415
PRIZ	4914033.044± 0.0023	1174032.102± 0.0006	3881406.106± 0.0008	4914033.464	1174031.855	3881405.827
TERM	4890360.965± 0.0014	1192337.292± 0.0002	3904013.365± 0.0004	4890361.337	1192337.028	3904013.032
TRAP	4911562.977± 0.0009	1092566.697± 0.0003	3906586.062± 0.0006	4911563.389	1092566.455	3906585.782

Table 4 highlights that some of the analysed CORS exhibit more frequent gaps due to missing data and post-processing analysis failure, e.g. AGRI, TERM and TRAP CORS (**Fig. 10**).

Gaps, missing acquisitions or post-processing analysis' failure and outliers range (MJD).

CORS	Gaps, missing acquisitions or post-processing analysis' failure	Outliers range (MJD)
AGRI	Dec 11-Jan 12, Apr 12-Oct 12	54590-54510, 55750-55820
CALT	Dec 09, Jun 11-May 12	54650-54800, 55500-55650
CAMP	Apr 08-May 08, Apr 09-May 09, Jul 10-Aug 10, Apr 12-May 12	56050-56200
PALE	May 09, Aug 09, Apr 12-May 12	56100-56150
PART	Mar 08, Aug 08-Sep 08, Apr 12-May 12	55380-54000
PRIZ	Jun 08, Jul 08, Aug 08-Sep 08, Aug 09, Feb 12-Oct 12	54300-54800, 55750-55820
TERM	Mar 08-Apr 08, Jul 09, Apr 11, May 12	56100- 56200
TRAP	Aug 08-Sep 08, Aug 09, Jul 12-Sep 10, Jul 11-Jan 12, Apr 12-May 12, Aug 12-Sep 12, Dec 12	54490-54510
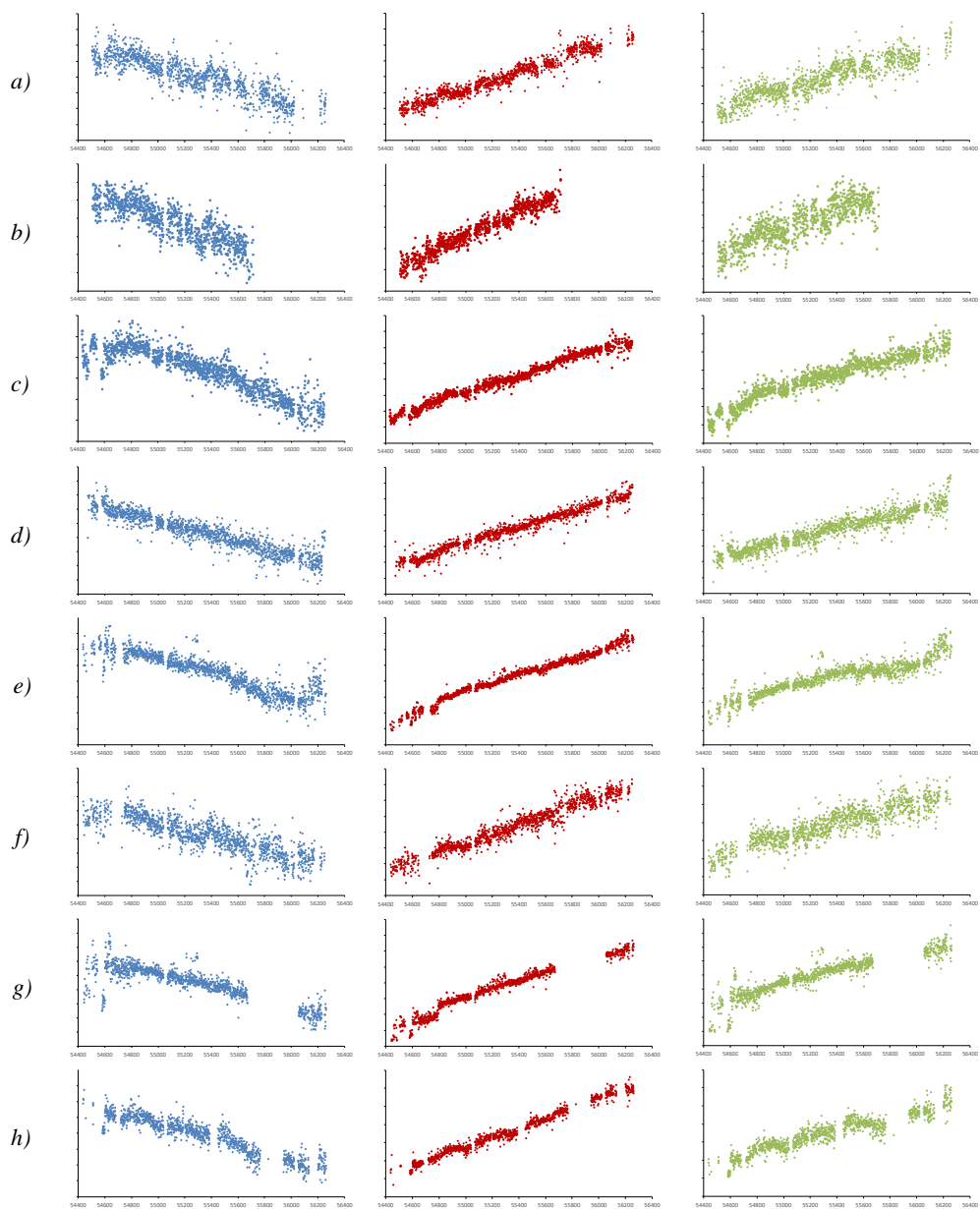
Fig. 10. Time series diagrams. *a)* AGRI (X, Y, Z), *b)* CALT (X, Y, Z), *c)* CAMP (X, Y, Z); *d)* PALE (X, Y, Z), *e)* PART (X, Y, Z), *f)* PRIZ (X, Y, Z), *g)* TERM (X, Y, Z), *h)* TRAP (X, Y, Z). In horizontals axis MJD (time), in vertical axis geodetic component (X in blue, Y in red, Z in green).

However, the time series of some UNIPA CORS is not continuously represented in this figure; indeed, several gaps, due to missing acquisitions or post-processing analysis' failure, were identified and separately shown within another table (**Table 4**). Best results describing the linear trend of the CORS have been found for CAMP, PALE and PART stations, where just few missing data over short periods are observed (**Fig. 10**). The CORS of PRIZ looks more scattered than the others. Also, some blunders not rejected by the analysis have occurred for the three components (X, Y, Z); in this case, maybe the lower accuracy of the measurements can be associated to imprecise solutions derived from the post-processing analysis. Generally, the other CORS clearly show a linear trend over the long-term period. Most critical results have been obtained for CALT CORS. Specifically, for this reference station, the time series shows a long gap, from MJD 55727 to MJD 56079 (**Fig. 10**). In this period, indeed, data was not recorded because the CORS was not active. Only in this case, after MJD 56079 (6th January 2012), a jump occurred for the three components (X, Y, Z) after changing the materialization site of the antenna, far approximately 1.5 km from the previous one; also, at the beginning of the time series, data was missing because the station started acquiring data since MJD 54510, corresponding to the 14th February 2008.

4.4 Statistical analysis (CDF)

Fig. 11 shows the Gaussian distribution of the CDF obtained for all GNSS CORS coordinates (X, Y, Z). Specifically, a deep analysis allowed the comparison and the overlapping between the theoretical Gaussian distribution and the real distribution of the CDF obtained for each CORS. **Fig. 12** shows that no significant variation concerns the Z components for all CORS.

Results shown in **Fig. 11** highlighted a good agreement between the theoretical Gaussian and the real CDF distributions obtained for all UNIPA CORS. Thus, another adjustment test has been improved to confirm the results, the so-called "*Lilliefors*" test. The latter is based on the "*Kolmogorov–Smirnov*" model (Massey, 1951; Lilliefors, 1967) and it is implemented by using the Matlab software.

This test is able to verify if data is retrieved from a Gaussian distribution (initial hypothesis, h=0), without any other specifications about the mean value and the variance of the distribution.

Specifically, the test has been implemented for each variable and each CORS, considering three different significance levels (α = 1%, 5%, 10%) and the solution is able to reveal if the hypothesis is confirmed (h=0) or rejected (h=1). In the first case, the Gaussian distribution of the dataset will be confirmed, otherwise, the distribution of the dataset will not follow the Gaussian distribution.

Results confirmed the rejection of the initial hypothesis (h=1) for all CORS coordinates (X, Y, Z). This is probably due to the analysis of a long time series evolution, indeed, little shifts between the theoretical and the real CDF distributions allow rejecting the initial hypothesis.
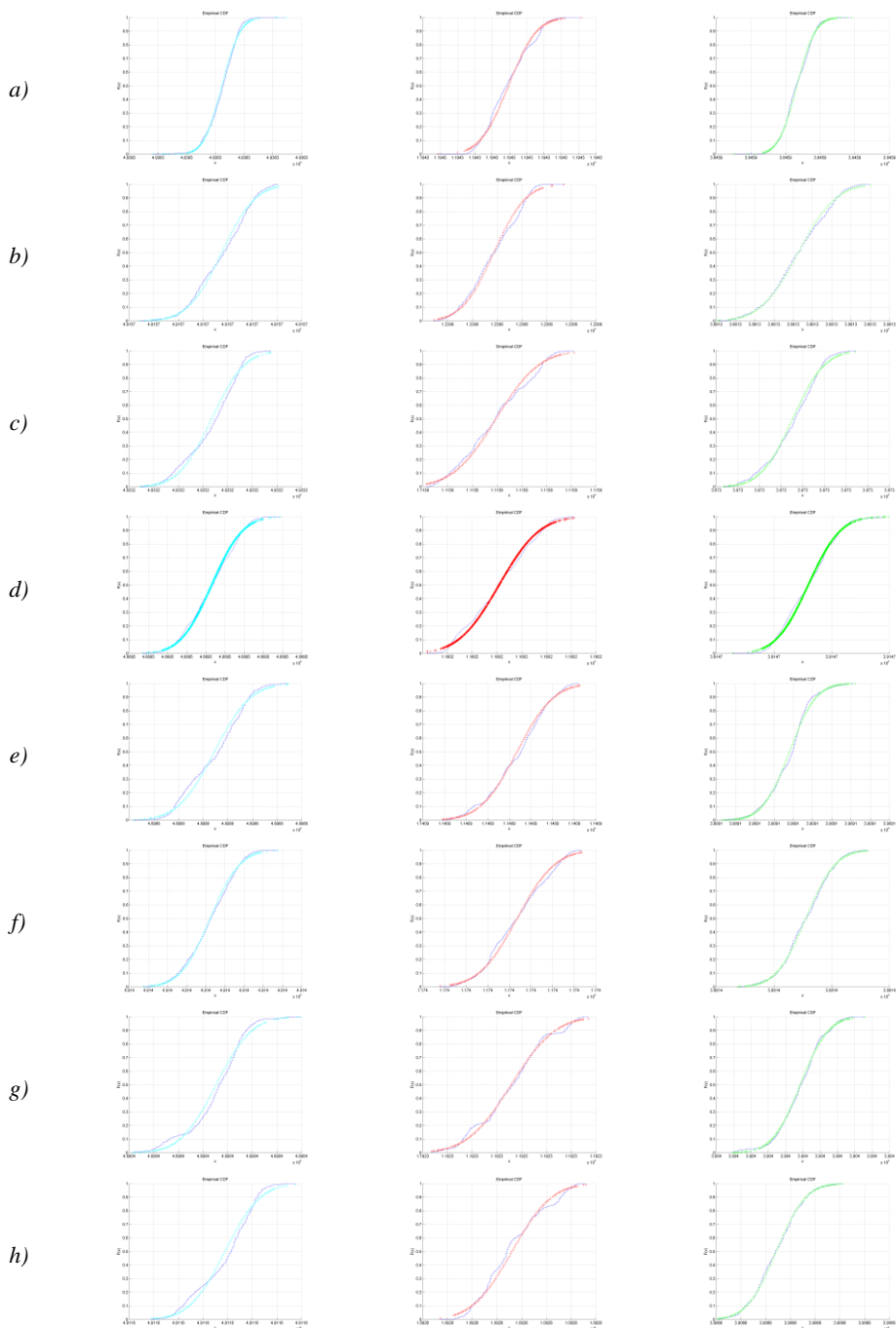
Fig. 11. CDF diagrams; in x-axis the coordinates values (X, Y, and Z), in y-axis the percentage of probability density functions. In blue the real CDF, in cyan, red and green the empirical CDF for X, Y and Z respectively. *a)* AGRI, *b)* CALT, *c)* CAMP; *d)* PALE, *e)* PART, *f)* PRIZ, *g)* TERM, *h)* TRAP.
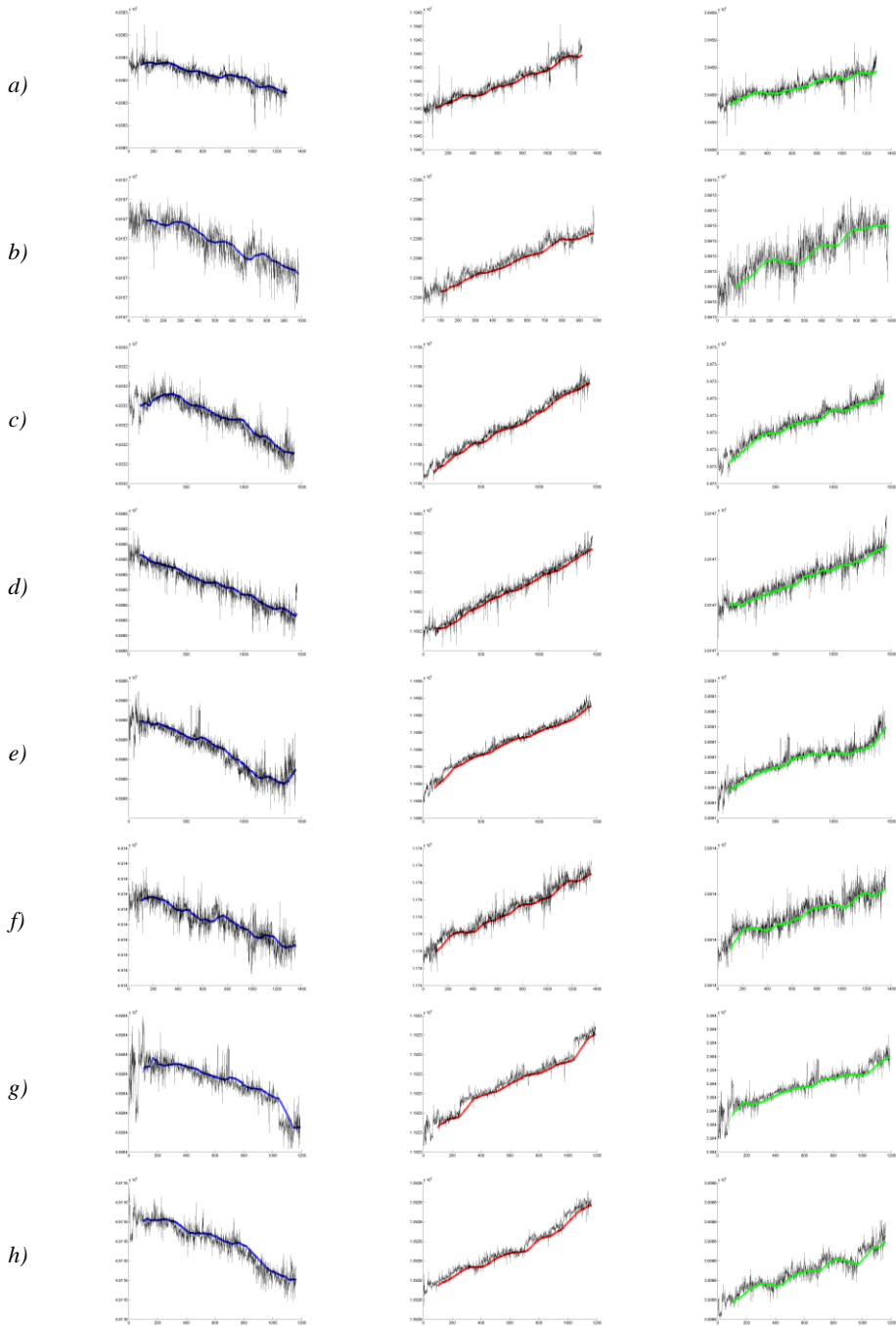
Fig. 12. Diagrams of the single moving average of time series; black line the time series data (X, Y, Z), coloured line the moving average (X in blue, Y in red, Z in green). *a)* AGRI, *b)* CALT, *c)* CAMP; *d)* PALE, *e)* PART, *f)* PRIZ, *g)* TERM, *h)* TRAP.

Considering also the scattered behaviour of all CORS coordinates reported in the same figure (**Fig. 12**), a moving average has been overimposed on the GNSS time-series to determine the long-term trend of the coordinates, without considering the variations over short periods.

Finally, a t-Student test has been implemented on the average values of the coordinates to analyse the significance of the GNSS coordinates' variations. The comparison has been made with the mean of the previous year, with α=0.05, considering as initial hypothesis (h=0) that the variations between the average values were not statistically relevant. Results confirmed the rejection of the initial hypothesis (h=1), indeed the average values significantly change for all GNSS CORS, year by year. More generally, the statistical analysis of the GNSS time-series during the period 2008 - 2012 highlighted substantial statistical changes of the CORS positions.

5. CONCLUSIONS

This study describes the main steps for the development of a new infrastructure, to realize a GNSS CORS network in the central-western part of Sicily (Italy), during the period 2008-2012.

The analysis of the data availability highlighted a relevant percentage of acquired data, compared to those expected, for CAMP, PALE, PART, PRIZ CORS; lower values have been found for AGRI, CALT, TERM and TRAP CORS, but generally satisfactory. All UNIPA CORS, instead, have shown a substantial amount of acquired data (also in double frequency). The CSR parameter, for each CORS, is also in agreement with the recommendations available for the reference stations involved for the determination of the EUREF reference system. The preliminary analyses of the dataset demonstrated that the ionospheric delay, the first derivative of ionospheric delay, the multipath and SNR values are included within a range already confirmed by other similar experimental research. The residual values of the coordinates for the geodetic reference framework are generally sub-millimetric, excepting for two CORS with millimetric residuals. The precisions of the CORS coordinates are in agreement with those required by the RDN2 national network managed by the IGMI. The trend of the time series is almost linear for all GNSS CORS over the analysed period. Only for one CORS the analysis highlighted a gap within the time series, due to the change of the installation site. The statistical tests based on the CDF and the moving average analyses highlighted a good agreement of the coordinates with the Gaussian distribution over time.

These analyses validated the use of CORS within wider networks (e.g. RDN2) already used for the materialization of the geodetic framework (Maseroli, 2015) and for the new realization of more recent European reference systems (ITRF2014, Kenyeres et al., 2019).

Currently, other researches are being developing to analyse the GNSS time series of UNIPA CORS network over a wider period (10 years at least) by using innovative techniques, such as the use of Precise Point Positioning (PPP) with freely available software (*RTKlib*). From these results, more details about the horizontal and vertical velocity fields will be investigated to analyse the geodynamic evolution of a highly seismic land (Sicily).

The authors are grateful to the developer also for his technical support. The authors would like to thank the anonymous reviewers for their constructive comments and useful suggestions.

R E F E R E N C E S

Abidin, H.Z., Haroen, T.S., Adiyanto, F.H., Andreas, H., Gumilar, I., Mudita, I., Soemarto, I. (2015) On the establishment and implementation of GPS CORS for cadastral surveying and mapping in Indonesia. *Survey Review*, 47 (340), 61-70.

Altiner, Y., Söhne, W., Güney, C., Perlt, J., Wang, R., Muzli, M. (2013) A geodetic study of the 23 October 2011 Van, Turkey earthquake. *Tectonophysics*, 588, 118-134.

Anderson, R., Chin, M., Cline M., Hoar, D., Murray O., Stone W. (2000) NATIONAL CONTINUOUSLY OPERATING REFERENCE STATION (NATIONAL CORS) SITE MONUMENTATION FINAL REPORT December 20, 2000 Available online: URL https://kb.unavco.org/kb/assets/285/CORS_Monumentation.pdf [Accessed Feb 2020].

Angrisano, A., Gaglione, S., Gioia, C. (2013) Performance assessment of aided global navigation satellite system for land navigation. *IET Radar, Sonar and Navigation*, 7 (6), 671-680.

Avallone, A., Selvaggi, G., D'Anastasio, E., D'Agostino, N., Pietrantonio, G., Riguzzi, F., Serpelloni, E., Anzidei, M., Casula, G., Cecere, G., D'Ambrosio, C., De Martino, P., Devoti, R., Falco, L., Mattia, M., Rossi, M., Obrizzo, F., Tammaro, U., and Zarrilli, L. (2010) The RING network: Improvements to a GPS velocity field in the central Mediterranean. *Annals of Geophysics*, 53 (2), 39-54.

Baniulis, R.; Galinauskas, K.; Marozas, L.; Parseliunas, E.; Petniunas, M.; Puskorius, V. (2017) An Analysis of the Performance and Coordinates Time Series of CORS Network LitPOS (2017). *Proceedings - 2017 Baltic Geodetic Congress (BGC) Geomatics*, art. no. 8071443, 45-48.

Barbarella, M., Gandolfi S., Tavasci L. (2018) Monitoring of the italian GNSS geodetic reference frame. *Lecture Notes in Geoinformation and Cartography*, 59-71.

Baroni, L., Cauli, F., Farolfi, G., Maseroli, R. (2009) Final results of the Italian «Rete Dinamica Nazionale» (RDN) of Istituto Geografico Militare Italiano (IGMI) and its alignment to ETRF2000. *Bollettino di Geodesia e Scienze Affini*, 68 (3), 287-317.

Barreca G., Bruno V., Dardanelli G., Guglielmino F., Lo Brutto M., Mattia M., Pipitone C., Rossi M. (2020) An integrated geodetic and InSAR technique for the monitoring and detection of active faulting in southwestern Sicily. Annals of Geophysics, 63, art. no. EP03.

Benciolini, B., Biagi, L., Crespi, M., Manzino, A., Roggero, M. (2006) Linee guida per la realizzazione di reti di stazioni permanenti di servizio. *Bollettino di Geodesia e Scienze Affini,* 65 (2), 90-121.

Boucher, C., Altamimi Z. (2011) Memo: Specifications for reference frame fixing in the analysis of EUREF GPS campaign; 18-05-2011, Version 8. 2011. Available online: URL http://etrs89.ensg.ign.fr/memo-V8.pdf [Accessed Feb 2020].

Bruyninx C. (2019) GUIDELINES FOR EPN STATIONS & OPERATIONAL CENTRES EPN. Available on line :URL:http://epncb.oma.be/_documentation/guidelines/guidelines_station operationalcentre.pdf. [Accessed Feb 2020].

Bruyninx, C., Habrich, H., Söhne, W., Kenyeres, A., Stangl, G., Völksen, C. (2012) Enhancement of the EUREF permanent network services and products. *International Association of Geodesy Symposia*, 136, 27-34.

Dabove, P., Di Pietra, V. (2019) Single-Baseline RTK Positioning Using Dual-Frequency GNSS Receivers Inside Smartphones. *Sensors*, 19, 430

Dardanelli, G., Carella, M., Integrated surveying with mobile mapping system, EGNOS, NRTK and laser technologies in the park "Ninni Cassarà" in Palermo. (2013) *ISPRS Annals of the Photogrammetry, Remote Sensing and Spatial Information Sciences*, 2 (2W1), 95-100.

Dardanelli, G., Pipitone, C. (2017) Hydraulic models and finite elements for monitoring of an earth dam, by using GNSS techniques. *Periodica Polytechnica Civil Engineering*, 61 (3), 421-433.

Dardanelli, G., Paliaga, S., Allegra, M., Carella, M., Giammarresi, V. (2015) Geomatic applications tourban park in Palermo. *Geographia Technica*, 10 (1), pp. 28-43.

Dardanelli, G., La Loggia, G., Perfetti, N., Capodici, F., Puccio, L., Maltese, A. (2014) Monitoring displacements of an earthen dam using GNSS and remote sensing. *Proceedings of SPIE - The International Society for Optical Engineering*, 9239, art. no. 923928.

Ebolese, D., Lo Brutto, M., Dardanelli, G. (2019) Uav survey for the archaeological map of lilybaeum (Marsala, Italy). In the ISPRS Annals of the Photogrammetry, Remote Sensing and Spatial Information Sciences, 42 (2/W11), 495-502.

Edwards, S.J., Clarke, P.J., Penna, N.T., Goebell, S. (2010) An examination of network RTK GPS services in great Britain. *Survey Review*, 42 (316), 107-121.

Erenoglu, R.C. (2017) A comprehensive evaluation of GNSS- and CORS-based positioning and terrestrial surveying for cadastral surveys. *Survey Review*, 49 (352), 28-38.

Estey, L.H., Meertens, C.M. (1999) TEQC: The Multi-Purpose Toolkit for GPS/GLONASS Data. *GPS Solutions*, 3 (1), 42-49.

Fazio, L., Lo Brutto, M., Dardanelli, G. (2019) Survey and virtual reconstruction of ancient roman floors in an archaeological context. In the ISPRS Annals of the Photogrammetry, Remote Sensing and Spatial Information Sciences, 42 (2/W11), 511-518.

Feng, S., Jokinen, A. (2017) Integer ambiguity validation in high accuracy GNSS positioning. *GPS Solutions*, 21 (1), 79-87.

Forlani, G., Dall'Asta, E., Diotri, F., di Cella, U.M., Roncella, R., Santise, M. (2018) Quality assessment of DSMs produced from UAV flights georeferenced with on-board RTK positioning. *Remote Sensing*, 10 (2), art. no. 311.

Fotopoulos, G., Cannon, M.E. (2001) An Overview of Multi-Reference Station Methods for cm-Level Positioning. *GPS Solutions*, 4 (3).

Gandolfi, S.; Tavasci, L.; Poluzzi, L. (2016) Improved PPP performance in regional networks. *GPS Solutions*, 20 (3), 485-497.

GeoDAF. Available online: URL http://geodaf.mt.asi.it/gps_page.html [Accessed Feb 2020].

Gordini, C., Abbondanza, C., Barbarella, M. (2007) GNSS network real time positioning: Testing procedure to evaluate the accuracy of a geodetic moving antenna. In International Archives of the Photogrammetry, Remote Sensing and Spatial Information Sciences - ISPRS Archives, 36 (5C55).

Grejner-Brzezinska, D.A., Kashani, I., Wielgosz, P. (2005) On accuracy and reliability of instantaneous network RTK as a function of network geometry, station separation, and data processing strategy. *GPS Solutions*, 9 (3), 212-225.

Grejner-Brzezinska, D.A., Kashani, I., Wielgosz, P., Smith, D.A., Spencer, P.S.J., Robertson, D.S., Mader, G.L. (2005) The impact of the external ionospheric models on the accuracy of RTK position estimation. *Proceedings of the Institute of Navigation*, National Technical Meeting 2005, 462-470.

Gülal, E.; Erdoğan, H.; Tiryakioğlu, I. (2013) Research on the stability analysis of GNSS reference stations network by time series analysis. *Digital Signal Processing*, (6), 1945-1957.

Henning, W. (2011) Best methods for high accuracy real time GNSS positioning from a single reference station. *CORS and OPUS for engineers: Tools for surveying and mapping applications*, 173-180.

Hu, Y.; Cheng, L.; Wang, X. (2016) Quality analysis of the campaign GPS stations observation in Northeast and North China. *Geodesy and Geodynamics*, 7 (2), 87-94.

Huang, Z., Huang, D., Xu, Z., Xu, Z. (2011) GPS vehicle positioning monitoring system integrated with CORS and Mobile GIS. In Procedia Environmental Sciences, 10 (PART C), 2498-2504.

HxGN SmartNet. Available online: URL https://hxgnsmartnet.com/it-it/ [Accessed Feb 2020].

Italian GNSS Network. Available online: URL http://retegnssveneto.cisas.unipd.it/gpsitn/ [Accessed Feb 2020].

IGS. Available online: URL https://kb.igs.org/hc/en-us/articles/204229743-Questions-about-the-data-quality-graphs [Accessed Feb 2020].

Jing-xiang, G., Hong, H. (2009) Advanced GNSS technology of mining deformation monitoring. *Procedia Earth and Planetary Science*, 1 (1), 1081-1088.

Lilliefors, H.W. (1967) On the Kolmogorov-Smirnov Test for Normality with Mean and Variance Unknown. *Journal of the American Statistical Association*, 62 (318), 399-402.

Marais, J., Beugin, J., Berbineau, M. (2017) A Survey of GNSS-Based Research and Developments for the European Railway Signaling. *IEEE Transactions on Intelligent Transportation Systems,* 18 (10), art. no. 7857080, 2602-2618.

Massey, F.J. (1951) The Kolmogorov-Smirnov Test for Goodness of Fit. *Journal of the American Statistical Association*, 46 (253), 68-78.

Maseroli, R. (2015) Evoluzione del Sistema Geodetico di Riferimento in Italia: la RDN2. *Bollettino della Associazione Italiana di Cartografia*, (153), 19-44.

Mitch, R.H., Psiaki, M.L., Tong, D.M. (2013) Local ionosphere model estimation from dual-frequency global navigation satellite system observables. *Radio Science*, 48 (6), 671-684.

Niell, A.E. (1996) Global mapping functions for the atmosphere delay at radio wavelengths. *Journal of Geophysical Research*, 101, 3227–3246.

NetGeo. Available online: URL http://www.netgeo.it/page.php?Id=62 [Accessed Feb 2020]. Italian GNSS Network. Available online: URL http://retegnssveneto.cisas.unipd.it/gpsitn/ [Accessed Feb 2020].

Kang, S., Song, J., Han, D., Kim, B., So, H., Kim, K.-J., Kee, C. (2019) A new method to improve the detection of co-seismic ionospheric disturbances using sequential measurement combination. *Sensors*, 19 (13), art. no. 2948.

Klobuchar, J.A. (1996) *Ionospheric Effects on GPS. In Global Positioning System: Theory and Applications*, American Institute of Aeronautics and Astronautics: Reston, VA, USA; Chapter 12; Volume 1, 485–515.

Kenyeres, A., Bellet, J.G., Bruyninx, C.,Caporali, A., de Doncker F., Droscak, B., Duret, A., Franke, P., Georgiev, I., Bingley, R., Huisman, L., Jivall, L., Khoda, O., Kollo, K., Kurt, A.I., Lahtinen, S., Legrand, J., Magyar, B., Mesmaker, D., Morozova, K., Nágl, J., Özdemir, S., Papanikolaou, X., Parseliunas, E., Stangl, G., Ryczywolski, M., Tangen, O.B., Valdes, M., Zurutuza, J., Weber, M. (2019) Regional integration of long-term national dense GNSS network solutions. *GPS Solutions*, 23 (4), art. no. 122.

Kenyeres, A., Bruyninx, C. (2004) EPN coordinate time series monitoring for reference frame maintenance. *GPS Solutions*, 8 (4), 200-209.

Kim, J., Song, J., No, H., Han, D., Kim, D., Park, B., Kee, C. (2017) Accuracy improvement of DGPS for low-cost single-frequency receiver using modified Flächen Korrektur parameter correction. *ISPRS Int. J. of Geo-Information*, 6 (7), art. no. 222.

Kenyeres, A., Figurski, M., Kamiński, P., Legrand, J., Bruyninx, C., Habrich, H. (2009) Homogeneous reprocessing of the EUREF permanent network: First experiences and comparisons. *Bollettino di Geodesia e Scienze Affini*, 68 (3), 207-218.

Olivares-Pulido, G., Terkildsen, M., Arsov, K., Teunissen, P.J.G., Khodabandeh, A., Janssen, V.A (2019) 4D tomographic ionospheric model to support PPP-RTK. *Journal of Geodesy*, 93 (9), 1673-1683.

Osório, I., Cunha, M. (2013) The Role of the TRS in Precision Agriculture: DGPS with EGNOS and RTK Positioning Using Data from NTRIP Streams. In International Association of Geodesy Symposia, 138, 277-282.

Panza, G.F., Peresan, A., Magrin, A., Vaccari, F., Sabadini, R.; Crippa, B.; Marotta, A.M., Splendore, R., Barzaghi, R.; Borghi, A., Cannizzaro, L., Amodio, A.; Zoffoli, S. (2013) The SISMA

prototype system: Integrating Geophysical Modeling and Earth Observation for time-dependent seismic hazard assessment. *Natural Hazards*, 69 (2), 1179-1198.

Prikry, P., Sreeja, V., Aquino, M., Jayachandran, P.T. (2013) Probabilistic forecasting of ionospheric scintillation and GNSS receiver signal tracking performance at high latitudes. *Annals of Geophysics*, 56 (2).

Pipitone, C., Maltese, A., Dardanelli, G., Brutto, M.L., Loggia, G.L. (2018) Monitoring water surface and level of a reservoir using different remote sensing approaches and comparison with dam displacements evaluated via GNSS. *Remote Sensing*, 10 (1), art. no. 71.

Radicioni, F., Stoppini A (2019) Umbria's new multi-constellation GNSS network. *Geomedia* (23), 4, 6-11.

Rizos, C. (2007) Alternatives to current GPS-RTK services and some implications for CORS infrastructure and operations. *GPS Solutions*, 11 (3), 151-158.

Rizos, C., Satirapod, C. (2011) Contribution of GNSS CORS infrastructure to the mission of modern geodesy and status of GNSS CORS in Thailand. *Engineering Journal*, 15 (1), 25-42.

Robustelli, U., Baiocchi, V., Pugliano, G. (2019) Assessment of Dual Frequency GNSS Observations from a Xiaomi Mi 8 Android Smartphone and Positioning Performance Analysis. *Electronics*, 8, 91.

Saastamoinen, J. (1972) Atmospheric correction for troposphere and stratosphere in radio ranging of satellites. In The Use of Artificial Satellites for Geodesy; Henriksen, S.W., Mancini, A., Chovitz, B.H., Eds.; AGU: Washington, WA, USA, 1972; Volume 15, 247–252.

Stocchi, P., Antonioli, F., Montagna, P., Pepe, F., Lo Presti, V., Caruso, A., Corradino, M., Dardanelli, G., Renda, P., Frank, N., Douville, E., Thil, F., de Boer, B., Ruggieri, R., Sciortino, R., Pierre, C. (2017) A stalactite record of four relative sea-level highstands during the Middle Pleistocene Transition. *Quaternary Science Reviews*, 173, 92-100.

Soler, T. (2011) CORS and OPUS for engineers: Tools for surveying and mapping applications, 1st ed.; American Society of Civil Engineers (ASCE), Reston (USA), 1-186.

Snay, R.A., Soler, T. (2008) Continuously operating reference station (CORS): History, applications, and future enhancements. *Journal of Surveying Engineering*, 134 (4), 95-104.

Schwiderski, E.W. (1980) On charting global ocean tides. *Reviews of Geophysics*, 18, 243–268.

Teunissen, P.J.G. (2005) Integer aperture bootstrapping: A new GNSS ambiguity estimator with controllable fail-rate. *Journal of Geodesy*, 79 (6-7), 389-397.

Vespe, F., Bianco, G., Fermi, M., Ferraro, C., Nardi, A., Sciarretta, C. (2000) The Italian GPS Fiducial Network: Services and products. *Journal of Geodynamics*, 30 (3), 327-336.

Wanninger, L. (2003) Virtual reference stations (VRS). *GPS Solutions*, 7 (2), 143-144.

Zhang, J., Lachapelle, G. (2001) Precise estimation of residual tropospheric delays using a regional GPS network for real-time kinematic applications. *Journal of Geodesy*, 75 (5-6), 255-266.

Zhang, Z., Zhan, X. (2016) GNSS spoofing network monitoring based on differential pseudorange. *Sensors (Switzerland)*, 16 (10), art. no. 1771.

ANALYSIS OF STATIC MORPHOSTRUCTURE CONDITIONS WITH DYNAMIC MORFOSTRUCTURE (LANDSLIDE TYPE)

SUWARNO[1] , MISNAH[2], MUJIARTO[3]

ABSTRACT:
Landslides occur in many types of Tuff rocks and Tertiary-aged andesite sandstones which can cause changes in the shape of the earth's surface, which shows the development of dynamic morphostructure. The purpose of this study was to determine the relationship of static morphostructure with dynamic morphostructure landslide type in Pekuncen Banyumas District. The research method used a survey method which included fieldwork (for inventory of static morphostructure and dynamic morphostructure landslide type) and laboratory work (for interpretation of aerial and satellite photo, and analysis of static morphostructure relationships with dynamic morphostructures landslide type). The results of the study found many observable landslides and geological structures. The geological structure that contained are in the structure of folds, fractures, and volumes. There is a relationship between landslide and geological structures. In fault structures, folds and layers sloping with patterns of clustered landslide, while in volcanic structures, the patterns of landslide are spread.

Key-words: *Static morphostructure, Dynamic morphostructure, Landslide, Indonesia*

1. INTRODUCTION

Based on the reading of the Geological Map of the Purwokerto and Tegal sheets, on a scale of 1:100,000, Pekuncen District is composed of Tertiary to Holocene rocks and consists of several geological structures. The age of these rocks shows the old one to young, Tertiary rocks are older rocks than the Holocene. Old-aged rocks with intensive weathering levels indicated by the thickness of weathering and more landslide (Suwarno, 2014). In areas with geological structure in form of faults and sloping rock layers which are composed of sedimentary rocks which have undergone weathering and changes in vegetation cover occur, then the area has many landslides (Kevin, *et al.,* 2017; Luigi, *et al.,* 2014). Landslides are a form of the manifestation of dynamic morphostructures, while the appearance of geological structures is an embodiment of active morphostructures (Verstappen, 2014).

 Landslides are the results of relationships reciprocal between systems in nature, including geological, geomorphological, hydrological, climate, and land use systems (Irimus *et al.,* 2017; Suwarno *et al.,* 2019). The geological factor in this case is rock and geological structure, while geomorphological factors are slopes (Pacione, 1999). The factors that cause landslides are human activities and physical conditions. Physical conditions include rocks,

---

[1]* *Geography Education Department of Universitas Muhammadiyah Purwokerto, Jl. Raya Dukuh Waluh Kembaran, Purwokerto, Jawa Tengah, Indonesia, *Corresponding author: suwarnohadimulyono@gmail.com*

[2]*Tadulako University, Jl. Soekarno Hatta Km. 9, Palu, Sulawesi Tengah 94148, Indonesia*

[3]**Universitas Muhammadiyah Tasikmalaya, Jl. Tamansari KM. 2,5, Tasikmalaya 46196, Indonesia, *Corresponding author: mujiarto@umtas.ac.id*

geological structures, and slopes. The human activities influential include cutting slopes for construction road, houses, agriculture and mining of rocks and sand (Sartohadi, 2008).

Knapen et al. (2005) explain that landslides are caused by several factors including slope, rock, soil and land use. Landslides and landslide densities are influenced by factors such as morphology form of land surface, geological conditions, the distance between river channels, earthquakes (Havenith, *et al.,* 2015). Suwarno & Sutomo (2012) conducted a study in Pekuncen Subdistrict indicating that there were landslides that could still be observed in 98 locations and found several waterfalls and rocks outcrops with sloping layer structures. Landslides occur in many types of tuff rocks and andesite sandstones that are Tertiary. Landslide are influenced by several factors, they are geological factors consisting of material type/rock, major fault distance, rock mass structure, while other factors consist of morphology, elevation, slope angle, slope aspect, avalanche type, soil type, land use and rain (Glenn, *et al.,* 2006; Nadim, *et al.,* 2006; Thapa and Esaki, 2007; Lan, *et al.,* 2004).These landslides can cause changes in the shape of the earth's surface, it means that the area shows the development of dynamic structure morphostructure. The development of the dynamic morphostructures is influenced by the static morphostructures found in the area, therefore an in-depth study of the active and dynamic morphostructure relationships is needed.

2.   METHODS
2.1   Materials and Research Tool

a. The material included:
1) 1: 50,000 in panchromatic aerial photographs of 1: 50,000 in 1994
2) Indonesian topographical maps of Ajibarang sheets, Paguyangan scale of 1: 25,000
3) a sheet of geological maps of Purwokerto - Tegal scale of 1: 100,000
4) satellite imagery of Banyumas Regency in 2005

b. Research Tools
5) GPS (global positioning system), used to determine the coordinates of the measuring point.
6) Geological hammer, for identifying the rocks.
7) Geological compass, for measuring dip, strike, and measurement direction.
8) Camera, for making documentation of important phenomena in the field.
9) Mirror stereos, for interpreting of aerial photographs.
10) Meter, for measuring the slope length, depth of weathering rock.
11) Abney level, for measuring the slope.

2.2   Research Path
a. Pre-fieldwork.

At this stage doing interpretation of aerial or satellite photos and other material maps in order to compile a map of the temporary used for material reference land field work.

b. Fieldwork

In this field work, it is intended to look for data both primary and secondary data to test the results of interpretations of aerial photographs or from m aps carried out in the laboratory. The field survey in this case is conducting observations and measurements on geomorphological aspects which include static morphostructures, and dynamic morphostructures.

c. Laboratory Analysis

Laboratory analysis is the reinterpretation of aerial and satellite photos, the making of landform maps, static morphostructural maps, and dynamic structure morphostructure maps in the form of landslides.

2.3   Variables and Data

a. Variables

The variables needed in this study include the influence variables namely static morphostructural aspects and the affected variables namely dynamic structure morphostructures. Static morphostructures include geological structures such as folds, fractures or horizontal layers, and dynamic morphostructures structures in the form of landslides and types. Primary data include slope length, slope, slope shape, valley shape, valley width, valley length, rock type, geological structure, weathering depth. Secondary data related to this study include landslide events data, rainfall data and thematic maps.

b. Data acquisition

Data acquisition is a way to obtain data from each variable either directly or indirectly. The way to obtain data on each variable varies, among others, by making observations, measurements in the field or in the laboratory, analyzing thematic maps and secondary data. The following is the method of obtaining the data needed in the study:

1) slope length, obtained from measurements of field
2) slope, obtained from DEM analysis of RBI maps,
3) slope shape, obtained from interpretation of aerial photographs and satellite imagery,
4) valley shape, obtained from interpretation of aerial photographs and imagery Satellites,
5) rock types, obtained from field observations,
6) geological structures, obtained from the interpretation of maps geological and field observations,
7) weathering depths, obtained from field measurements,
8) characteristics of mass movement, obtained from measurements and field observations
9) mass movement events and mass movement types, obtained from secondary data, rainfall data, obtained from secondary data.

2.4   Analytical approaches

a. Analysis of Geomorphological aspects consists of static morphostructure, dynamic morphostructure with geomorphological analytical approach presented in the form of static morphostructure maps, and distribution maps of landslide.

b. The analysis to determine the relationship between static morphostructure and dynamic morphostructure landslide type using quantitative descriptive by *overlaying /*overlapping arrangement of static morphostructure maps, and distribution maps of landslide.

3. RESULTS AND DISCUSSIONS

3.1 Research Area Description

a.   Location and wide scale

The study was administratively located in Pekuncen District, Banyumas Regency. The astronomical position of the study area is located between 109˚ 01 '39 "BT to 109˚ 09' 22" BT and 7˚ 15 '25 "LS to 7˚ 24' 37" LS or is located between 282,831 mT to 294,317 mT

and 9,180,805 mU up to 9,193,344 mU at UTM coordinates. The research area is 8,277.69 ha, divided into 16 villages, Cibangkong, Petahunan, Semedo, Cikawung, Karangklesem, Candinegara, Cikembulan, Tumiyang, Glempang, Pekuncen, PasiramanLor, PasiramanKidul, Banjaranyar, Karangkemiri, Kranggan, and Krajan.

b. *The rocks type*

The rocks type in the study area is determined based on the reading of the Geological Map of Purwokerto and Tegal Sheets, 1: 100,000 scale and the results of field observations. The results of map reading and field observations in the study area consisted of 5 rock formations. Lava sediment of Slamet Volcano (Qls) is Quaternary (Holocene) age. This formation consists of lava with volcanic rocks composed of andesite-basalt, with a diameter of 10-50 cm, produced by Slamet Tua Volcano, the distribution includes flat areas. **Fig.1** shows the Slamet Volcanic sedimentary rock.

Fig.1. Photograph of Slamet volcanic deposits (Source: Suwarno, 2014).

Slamet Rocks volcano does not decompose (Qvs) Quaternary age (Pleistocene). In this formation, there are volcanic breccia, lava, score and tuff, the distribution of which forms the terrain and hills. Tread formation (Tpt) age Tertiary (Pliocene), consisting of sandstone coarse-grained greenish, calcareous marl, greenish sandstone, calcareous tufa and marl greenery. Tertiary age (Tmph) Formation (middle-end Miocene), consisting of sandstone andesite, tuff, breccia, sand, and napal, inserts sandstones. Tertiary age (Tmr) Formation (Middle Miocene), consisting of marl. Sedimentary materials of Tertiary age from a combination of sand and clay have the highest intensity of avalanches (Luigi Borrelli, *et al.,* 2014). **Fig. 2** photos of the following marbles.

Fig.2. Photograph of marl rocks, (Source: Suwarno, 2014).

Rocks in the study area are composed of five rock formations and consist of 14 rock types. The fourteen types of rock are 1) Andesite lava, 2) Volcanic breccia, 3) Lava, 4) Skoria, 5) Quaternary Tuff, 6) Greenish sandstone, 7) calcareous marlstone, 8) Greenish marl, 9) Andesite sandstone, 10) Tufa gampingan, 11) Tertiary Tufa, 12) Tertiary Breccia, 13) Sandstone, and 14) Marl. Sandstone and clay are one of the causes of high landslide events (Barančoková, *et al.,* 2014).

c. *Stratigrafi*

Suwarno (2014) explained that based on observations in the field and reading of the Geological Map of Purwokerto and Tegal Sheets, a scale of 1: 100,000. The results of reading the Geological Map of the stratigraphy in the western part of the sequence from the bottom up are propagation formation (Tmr), Halang (Tmph) formation, and Tread formation (Tpt). In the eastern region, the sequence of stratigraphy from the bottom up is the Creation formation (Tmr), Slamet Volcanic lava deposits (Qls), and unregulated Slamet Volcanic rocks (Qvs).

The appearance in the field of Tapak formation is seen in Karangkemiri Village and Petahunan Village. In the formation there are 20 landslides, this is caused by the Tread formation located above the Halang formation in the form of sandstone andesite. The andesite sandstone layer becomes a field of landslide slip. The andesite sandstone layer which is part of the Halang formation is seen in Karangkemiri Village. The Halang Formation which is located under the visible Tapak formation in Semedo Village and Cibangkong Village. The Halang Formation in the lower layer is composed of andesite sandstones and above it, there are tuff stones, breccias, sandstones, and marl, therefore in the Halang formation, there are 49 landslides. Andesite sandstones can be seen at the bottom of the Penjalin River Cibangkong Village (Suwarno, 2014).

d. *Geological Structure*

Identification of geological structures based on contour patterns, appearance on aerial photographs and results of field observations. Contour patterns in the study area have a straight contour pattern and this meeting indicates a fault structure. Topography is a good guide to estimating fault structures (Barnes & Lisle, 2004). Topography can be seen in patterns contour, aerial photographs and in the field. The appearance of aerial photographs shows the shape of a long, steep slope. Appearance in the field found six waterfall points in Karangkemiri, Petahuan and Cibangkong Villages. It shows the pattern of straightness and many springs found.

Fig.3. Photograph of the appearance of a fault structure (Source: Suwarno, 2014)

Outcrops of andesite sandstone are found in several locations with the direction and slope of the layers can be used to characterize the structural origin of the land, and the top layer of rock used for naming units of land. **Fig. 3** shows the layers of rock that are truncated and not in line with the slope of this slope can be used as evidence of fault structures. The appearance of the geological structure is like a fault found in Karangdlima Hamlet, Petahuan Village. Barnes & Lisle (2004) explains that to estimate the fault structure is by knowing the presence of elongated valleys, cracked rock layers that suddenly dropped. The fault is seen in the river valleys that extend along the river channel assault shown in **Fig. 4**.

Fig.4. The appearance of a fault (Source: Suwarno, 2014).

The appearance of a sloping rock coating structure that shows the structure of the fold, for example in Klapajejer Hamlet, CibangkongVillage with a slope of 10º coating and N79ºE coating direction is shown in **Fig. 5**.

Fig.5. The appearance of a sloping/fold layer on Tuff rocks (Source: Suwarno, 2014)

e.   Static Morphostructures

Static morphostructure can be assessed from the landform actual aspects. The actual landforms reflect static morphostructures in the form of geological structures (HT Verstappen, 1983). The geological structure can be in the form of horizontal structures, tilts, folds, faults, and volumes. Both the synclinal and anticlinal fold structures are found in Petahuan and Cibangkong Villages, fault structures are in Petahuan Village, oblique and structures horizontal are found in Petahuan, Semedo, and Cibangkong Villages, while volcanic structures are found in most areas in DistrictPekuncen.

Based on the geological structure in the study area, there are two landform genesis, namely structural landform units, and volcanic landform units (Suwarno, 2014). Structural origin landform are produced by endogenous processes and layered rock structures. Structural landforms are characterized by changes in the slope of rock layers. At the

beginning of the rock layers formation is flat, then by the endogenous processes it cause the rock layer to be tilted or shifted. Volcanic origin landform is produced by magma activities, this landform in the study area are located on the slopes below Volcano Slamet. Identification of this volcanic origin is based on the results of field observations and aerial photo interpretation. The results of field observations found that there were materials or rocks originating from the activity of the Slamet Volcano in the form of lava deposits, score rocks, volcanic breccias, and tuffs.

f. Dynamic Morphostructure

Verstappen (2014) explains that dynamic geomorphology studies the processes and short-term changes in the landforms depicted in dynamic morphostructure. The processes in this case are exogenous processes which consist of weathering, mass movement, erosion, and sedimentation. Weathering of rocks mainly occurs in structural forms. **Fig. 6** is an example of weathering of rounded type rocks found in a unit of structural hilly landforms of rocks sandstone, on the slope class IV in Cibangkong Village. **Fig. 7** shows the weathering process of rocks in structural landforms units of tufa rocks, on the slope class IV in Semedo Village. The process of weathering that takes place intensively will cause the weathering zone to become thicker. Weathered zones get thicker causing increased slope loads and effecting on landslide.

Fig.6. Appearance of sphereoidal weathering onionon sandstone rocks
(Source: Suwarno, 2014)

Fig.7. Photo of weathering appearance which is controlled by a system of cracks,
(Source: Suwarno, 2014)

The process of erosion, especially surface erosion occurs a lot. The slope factor is one reason for surface erosion. Surface erosion is seen in units of landforms structural of tufa rocks, on slope III class in Cibangkong Village (see **Fig. 8**). These hills look bald and have only been planted with teak plants, and many surface rocks such as gravel and grit are found. Splash erosion takes place and develops to form rill erosion. Worosuprojo (2002) explains that landslides are preceded by rill erosion. Landslide is one of the most common forms of mass movement, 98 landslides were found and in the field survey in this study found the location of 98 new landslides (Suwarno, 2014). **Fig.9** is an example of a landslide appearance in the study area.

Fig.8. Photos of surface erosion appearance, (Source: Suwarno, 2014)

1   2

Fig.9. Landslide appearance photos in 1.Krajan Village, 2. Village Semedo,
(Source: Suwarno, 2014)

3.2 The Relationship of Static Morphostructural and Dynamic Morphostructures

The analysis of relationship of static morphostructure and dynamic morphostructures is carried out by spatial analysis. The spatial analysis to overlay interchanges between maps of landform units with distribution maps of landslide. Static morphostructure is reflected in landforms units of origin structural and volcanic. Structural origin landform are characterized by the presence of geological structures of folds and faults. The fold structure found in the study area is the synclinal fold and the outcrop of rock that is sloping, while the fracture structure is a broken down. The most landslide are found in structural land, this is due to their older age, there are many cracks, and the sloping position is in the direction of the slope (Suwarno, 2018).The results of the overlay arrangement of maps are presented in Figure 10. Based on the analysis, it is illustrated that landslide are related to geological structure patterns. Landslides are clustered on fault structures, folds, and sloping layers, while on the volcanic structure patterned landslides occur.
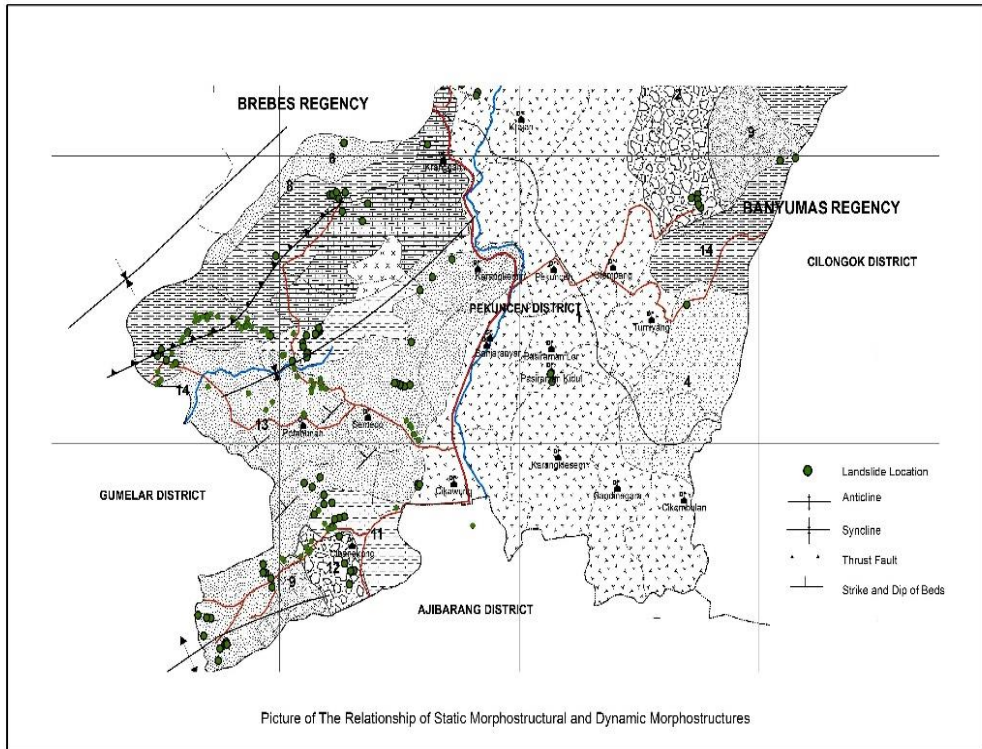
Fig.10. Relationship between Static Morphostructures and Dynamic Morphostructures

(Source: Source: Suwarno, 2014)

4. CONCLUSION

Based on the results of the study, it can be concluded that in the study area there were many landslide that could be observed in each unit of land. The geological structure contained is the structure of folds, fractures, and volcano. Many landslides are found in origin structural landforms units which are steep slopes. There is a relationship between landslide and geological structures, in fault structures, folds, and layers sloping with patterns of clustered landslide, while in volcanic structures, the patterns of landslide are spread. In the geological structure of the synclinal folds, many landslides occur in the synclinal valley. In the fault structure, many landslides occur in the fault field.

R E F E R E N C E S

Barančoková, M., Kenderessy, P. (2014) Assessment of landslide risk using GIS and statistical methods in the Kysuce region. Ekológia (Bratislava), **33**(1), 26–35.

Barnes, J.W., Lisle, R.J. (2004) *Basic Geological Mapping*. West Sussex PO19 8SQ, England: John Wiley & Sons Ltd.

Glenn, F.N., David, R.S., John, C.D., Glenn, D.T., Stephen, J.D. (2006) Analysis of Characteristic Topographic Information for Characterizing Landslide Morphology and Activity. *Geomorphology, **73**,* 131-148.

Irimuș, I.-A., Roșca, S., Rus, M.-I., Marian, F.L., Bilașco, Ș. (2017) Landslide susceptibility assessment in Almas basin by means of the frequency rate and GIS techniques. *Geographia Technica*, **12**(2), 97-109.

Knapen, A., Kitutu, MG, Poesen, J., Breuggelmans, W., J., D., &Muwanga, A. (2005) Landslides in Densely Populated County at the Footprint of Mount Elgon (Uganda): Characterstics and Causal Factors, *Geomorphology*, **77**, 149-165.

Roback, K., Clark, M.K., West, J.A., Zekko, D., Li, G., Gallen, S.F., Chamlagain, D., Godt, J., (2017) The size, distribution and mobility of landslides Gorkha earthquake, Nepal, *Geomorphology, journal homepage: www.elsevier.com/locate/geomorph*

Lan, H.X., Zhou, C.H., Wang, L.J., Zang, H.Y., Li, R.H. (2004) Landslide Hazard Spatial Analysis and Prediction Using GIS in The Xiaojiang Watershed, Yunnan, China, *Geology Engineering, **76**,* 109-128.

Borrelli, L., Antronico, L., Gullà, G., Sorriso–Valvo, G.M. (2014) Geology, geomorphology and dynamics of the 15 February 2010 Maierato landslide (Calabria, Italy), *Journal of Geomorphology.*

Nadim, F., Rodolf, P., Herbert, E., Herbert, K., and Steven, K. (2006) An Introduced Methodology for Estimating Landslide Hazard for Seismic and Rainfall-Induced Landslides in a Geographical Information System Environment, *ECI Conference on Geohazards, Lillehammer, Norway.*

Pacione, M. (1999) *Applied Geography: Principles and Practice*. London and New York: Routledge.

Sartohadi, J. (2008) The Landslide Distribution in Loano Sub-District, Purworejo District Central Java Province, Indonesia.*Geography Forum*, **22**(2), 129–144.

Suwarno (2014) *Land management models in Longsorlahan Prone Areas in District Pekuncen Banyumas*. Gadjah Mada University Yogyakarta.

Suwarno (2018) An Analysis of Landslide Occurrence Distribution and Geomorphological Conditions of River Flow Sub-Watershed in Banyumas Regency. *5th International Conference on Community Development (AMCA 2018). Advances in Social Science, Education and Humanities Research,* **231.**

Suwarno & Sutomo (2012) *Landslide Mitigation Modeling Based on Geographic Information System Technology in Ajibarang Subdistrict, Banyumas Regency*. Purwokerto.

Suwarno, Sutomo & Aditama M.R. (2019) The analysis of the landslide vulnerability sub watersheds Arus in Banyumas Regency. *Geographia Technica*, **14**(2), 112-119, DOI: 10.21163/GT_2019.142.10

Thapa, BP, and Esaki, T. (2007) GIS-based Quantitative Landslide Hazard Prediction Modeling in Natural Hills, Agra Khola Watershed, Central Nepal, *Bulletin of the Department of Geology,* Tribhuvan University, Kathmandu, Nepal, **10**, 63-70.

Verstappen, H.T. (1983) *Applied Geomorphology: Geomorphological Surveys for Environmental Development*. Amsterdam: Elsevier.

Verstappen, H.T. (2014) *Applied Geomorphology : Geomorphological Survey for Environmental Development*. Yogyakarta: Waves.

Worosuprojo (2002) *Study of Erosion of Trenches and Landslides with a Geomorphological Approach in the Oyo River Basin of the Special Province of Yogyakarta*. Gadjah Mada University Yogyakarta.

FACTORS INFLUENCING THE UPTAKE OF FLOOD MITIGATION MEASURED IN BUDALANGI, KENYA

Sylvan ODIDI[1], Sarintip TANTANEE[2] ID, Korakod NUSIT[3] ID, Panu BURANAJARUKORN[4]*

ABSTRACT:
The severe climate change necessitates the people who live in the flood prone areas, to implement the flood mitigation measures in their communities. There are various factors that influence the uptake of mitigation measures; these factors are very vital in the design of community development plans. This research aims to assess the relationship between socio-psychological factors and the people's uptake of flood mitigation measures in Budalangi, Kenya. The socio-psychological factors include - (1) the perceived self-efficacy, (2) the flood experience, (3) the perceived response cost, (4) the worry, and (5) the perceived flood consequences. Primary data was obtained from one hundred households in Budalangi through face-to-face interviews. The statistical analysis and Spearman correlation test were employed for evaluating the interviewed data. The analysis results revealed that the uptake of mitigation measures is greatly affected by the self-efficacy. The flood experience and worry contribute moderate and weak positive influences, respectively. The perceived response cost has negative influences. The perceived consequence is statistically insignificant factor. The identified barriers of mitigation schemes implementation include - incentive, financial issue, lack of technology, communication and information transferred. These impediments required immediate attentions to improve the mitigation management at household's level. The future research should focus on household's perspectives if the effective mitigation measures are implemented.

Key-words: *Socio-psychological factors, Flood, Protection Motivation Theory, Flood Mitigation Measures.*

1. INTRODUCTION

The previous research shown that, in 2050, approximately two billion people or more will be affected by flood from the frequent rainfall, snow and ice melting (Bogardi, 2004). Globally, communities along the rivers are experiencing an exponential rise in flood risks (Ceola et al., 2014; Costache, 2014). The anthropogenic factor has a high impact on the degree of flood damages (Elme et al., 2012). The flood risk potential increases with the rise in the number of properties in floodplains (Taki et al., 2013; Nusit et al., 2019). Moreover, flooding event impedes social and financial developments.

[1]*Department of Industrial Engineering, Naresuan University, 65000, Tha-Po, Mueang, Phitsanulok, odidisylvan@gmail.com*

[2]*Centre of Excellence on Energy Technology and Environment, Department of Civil Engineering, Naresuan University, 65000, Tha-Po, Mueang, Phitsanulok, Thailand, sarintipt@nu.ac.th*

[3]*Centre of Excellence on Energy Technology and Environment, Department of Civil Engineering, Naresuan University, 65000, Tha-Po, Mueang, Phitsanulok, Thailand, korakodn@nu.ac.th*

[4] *Department of Industrial Engineering, Naresuan University, 65000, Tha-Po, Mueang, Phitsanulok, Thailand, korakodn@nu.ac.th*

The floods significantly influence the country developments and people well-beings. They pose a profound threat to education, health, infrastructure, economic growth, and environment.

Budalangi in Busia County, Kenya, located at the mouth of Nzoia river. According to its geographical conditions, the area is prone to be affected by flooding disasters, which may result in huge economic and financial losses. For example, in May 2018, 4,000 farmers were affected by flood and 39,000 acres of crop were destroyed (NTV, 2018). In response to that incident, Government of Kenya has initiated and implemented the flood mitigation projects. The Western Kenya CDD and Flood Mitigation Project (2007-2016) was one of the projects equipped by the Government of Kenya at that time. The project includes many components such as dike and weir dam constructions. The public mitigation measures could not eradicate the entire damages; however, private mitigation measures contribute a significant role in damages reduction. Private mitigation measures formed the part and parcel of contemporary flood risk management. (Osberghaus, 2015).

The previous studies related to floods and flood mitigation measures within the Budalangi Constituency focused on - (1) comparative study of flood resilience (Atieno, 2015), (2) understanding the extreme climatic events (Huho & Kosonei, 2014), (3) the flood root causes and community interventions (Okumu, 2017), (4) the analysis of flood impact based on gender differences (Mukuna, 2015), and (5) the perceptions of household on impacts (Opondo et al., 2014). However, very little attention has been directed to the detailed assessment of the factors that influences the uptake of mitigation measures at household level. Therefore, the objective of this study is to evaluate the relationship between the socio-psychological factors and the uptake of flood mitigation measures in Budalangi, Kenya.

In this research, the socio-psychological factors include the perceived self-efficacy, the flood experience, the worry, the perceived response cost, and the perceived flood consequences.

2. PROTECTION MOTIVATION THEORY

This research was characterized based on the Protection Motivation Theory (PMT), which was developed by Rogers in 1975 (1983). At first, the PMT was used to explain the self-protection behavior of people based on their health risks. The PMT was later improved by Miler et al. (2000). Even though, the PMT was initially developed for health protection scheme, its uses were extended to other fields of study. Grothmann et al. (2006) adopted the PMT for assessing the personal protection plan on flood disaster. According to the Grothmann's framework, individual who have ability to protect themselves from flood will implement more measures. In addition, individual who perceives the mitigation measure will effectively reducing flood damages and losses.

The flood-experienced people are likely to implement the mitigation measures, to avoid or reduce the damages associated with floods. In addition, households that worry about the flood consequences will be motivated to implement mitigation measures to protect themselves. The individual who perceive that the cost of implementing mitigation measure is high and time consuming is unlikely to take mitigation measures.

Regarding to the perceived flood consequences, individual who perceive the impacts of flood will be encouraged to implement the mitigation measures. On the other hand, the perceived flood damage does not influence these intentions, because it does not automatically convert to high levels of preparedness. However, the implementation barriers

are exit. This includes the lack of incentives, limited information transferred, and the financial status of the household. The example of previous research which employed the PMT for the household behaviors assessment includes Grothmann, et al. (2006), Bubeck et al. (2013), Poussin et al. (2014), Osberghaus (2015), and Babcicky et al. (2017).

3. MATERIALS AND METHODS

3.1. The study area

Budalangi located in the Western part of Kenya, in Busia County (see **Fig. 1**). It lies between the latitude 0º 30" S and 0º 11' 30" N, the longitudes 33º 56' 30" W and 34º 10' 30" E (Muku et al., 2013). The study area was selected because of it situated in the flood prone area (Opere, 2013; Opondo, 2013). The study area has a very flat topography. The average annual rainfall of the area ranges from 750 – 1,015 mm (Onywere, 2011). It is about 185 square-meter wide. The total population of the study area is 66,732 with the number of households standing at 15,245 (KNBS, 2010).
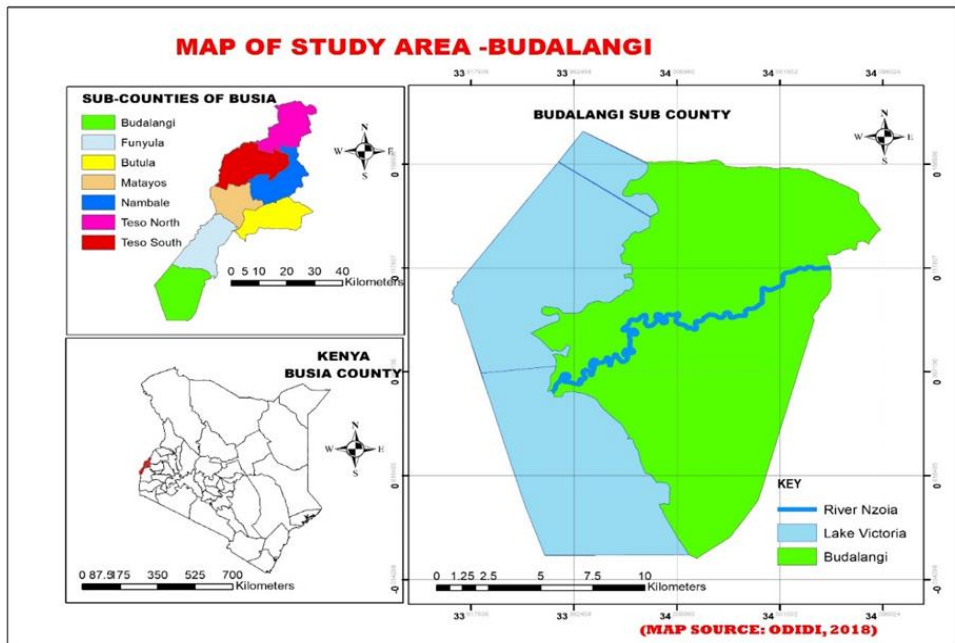
Fig. 1. The study area.

3.2. The sample sizes

To determine the sample size, Yamane's sampling method was adopted (Yamane, 1973). The sample size calculation based on Yamane's method is expressed in Eq. 1.

$$n = N/(1+Ne^2) \tag{1}$$

in which, n is the sample size, N is the population (households), and e is the margin of error (0.1, 0.05 or 0.01).

The sample size in this research was calculated with e = 0.1. Therefore, one hundred household was obtained from Eq. 1.

3.3. Sampling method

Scientific research attaches great importance to the problem of sampling, nowadays there are specific procedures according to each field (Şarpe and Haidu 2017 – an example in hydrology; Nistor *et al.,* 2019 – an example in soil sciences). The present study employed a multistage sampling method for the selection of the sampling sites and the sizes of sample at each site. Multistage Sampling is one of the sampling techniques which the size of sample is reducing for the subsequent analysis stage. In the first stage, Busia county was chosen. In the second stage, Budalangi constituency was purposively chosen because it is prone to flood event. Then, Budalangi was divided into four strata – central Bunyala, south Bunyala, west Bunyala, and north Bunyala. In the third stage, 10 sub-locations were randomly selected. These sub-locations were previously affected by the flood events. In the final stage, the sample size of the interviewed household was calculated according to the number of households within each sublocation as shown in **Table 1.**

Table 1.

Sample sizes of the 10 sub-locations in Budalangi.

Wards (strata)	Sublocation	Population	Number of households	Sample size	Percentage
North Bunyala	Mudere	1,665	339	4	4
	Budalangi	5,608	1,247	15	15
	Mudembi	4,113	936	11	11
	Ruambwa	5,022	1,135	14	11
South Bunyala	Rukala	3,071	680	9	9
	Lugale	2,325	520	6	6
	Mabinju	3,225	756	9	9
Central Bunyala	Magombe West	4,344	1,063	13	13
	Magombe Central	3,458	785	10	10
West Bunyala	Singinga	3,531	779	9	9
	Total		8,240	100	100

3.4. Questionnaire design

The questionnaire contains close-ended questions for socio-psychological factor assessment (see **Table 2**). The socio-psychological factors considered in this study included the perceived self-efficacy, the perceived response cost, the flood experience, the worry, and the perceived flood consequences. In this research, every interviewed household were assumed to be influenced by one-time flooding each year. The interviewees were also asked to state the flood mitigation measures that they had implemented to protect themselves from flooding.

3.5. Data collection, entry, and analysis

Household survey was conducted during a period of December 2018 and January 2019 using face-to-face interview technique, from 100 households. Data collected from the field was coded on the variable view of Statistical Package for the Social Sciences (SPSS). The socio-psychological variables were coded as indicated in **Table 2**. The dependent variable (flood mitigation measures) was ranked from 0 to 9. The Spearman correlation was used in this research, since the collected data was not normally distributed. In addition, the Spearman correlation is suitable for ordinal data. The Spearman correlation was determined by the SPPS and used for evaluating the relationship between socio-psychological variables and the number of mitigation measures. A method developed by Dancey, et al. (2007) was used to interpret Spearman correlation coefficient as presented in **Table 3.**

Table 2.

Summary of field data questions and their coding values.

Independent Variable	Question	Coding
Perceived Self-Efficacy	Do you agree with this statement? I can cope up with negative impacts of floods.	1. Strongly disagree, 2. Disagree, 3. Neutral, 4. Agree, 5. Agree, 6. Strongly agree
Perceived Response Cost	How do you perceive the overall cost of implemented mitigation measure?	1. Not costly, 2. Slightly costly 3. Costly, 4. Very costly
Flood Experience	How many times have you experience flooding event?	0. No experience, 1. Once, 2. Twice, 3. Thrice, 4. 4 times, 5. 5 times, 6. over 5 times
Perceived Consequences	How likely do you perceive an increase of material/ financial or health damage due to future flood occurrence for your	1. Very unlikely, 2 Rather unlikely, 3. Moderate likely, 4. Rather likely, 5. Very likely
Worry	Are you worried about flood risk in your village?	1. Not worried, 2. Slightly worried, 3. Worried, 4. A lot

Table 3.

Interpretation of spearman correlation coefficient in psychology (Dancey et al. 2017).

Level of Strength	Correlation Coefficient	
Zero	0	0
Weak correlation	+0.1 to +0.3	-0.1 to -0.3
Moderate correlation	+0.4 to +0.6	-0.4 to -0.6
Strong correlation	+0.7 to +1.0	-0.7 to -1.0

4. RESULTS AND DISCUSSIONS

4.1. The study area

4.1.1 Socio-economical characteristics

The percentage of male and female interviewees were 51% and 49%, respectively. Most of the interviewed households have the family size of 6-10 people. The 74% of the households were home owners.

4.1.2 Number of Flood Experience

The heads of the household were asked to state the number of flood events they have experienced from the past. The interviewed results show that, 3% of the households had no flood experiences, 8% of them had experienced once, 7% of the interviewed households stated that they had experienced twice. Majority of the household mentioned that they experienced flooding three times, which equivalent to 41% of the interviewed households. The 17%, 11%, and 13% of the interviewed households experienced flooding 4 times, 5 times and over five times, respectively. The interviewed household experienced floods in 1997, 2000, 2002, 2003, 2010, 2017, 2018. Others also stated that they experienced floods yearly. Majority of the households stated that the impacts of floods included – properties damages, the death of people and animals, outbreak of the water-borne diseases (such as cholera and malaria), high remedial investment, and famine.

4.1.3 Perceived Response Cost

The household's representatives were asked to rate their perceived response cost in term of overall cost of flood mitigation. The 9% of the interviewed household stated that it was not costly, while 21% of them stated that it was slightly costly. On the other hand, 10% percent of them stated that it costly and 60% of them stated that it was very costly. The households with the perception of high response cost may attribute by their low incomes.

4.1.4 Perceived Self- Efficacy

The household representatives were asked to confirm that they can deal with flood impacts. The 26 % of them stated that they strongly disagree, 29% of them stated that they disagree, while 26% of them stated that they agree. The agreed households believed that they could apply the mitigation measures to protect themselves and properties. On the other hand, the disagreed households cited their financial constraints as a huge impediment.

4.1.5 Perceived Consequences

In this research, the perceived consequences refer to expected flood consequences, such as property destruction and death. The 5% of household stated that it is unlikely to experience the increase damages from the future flooding events. The 15% of them stated that it is likely, while 80% of them stated that it is very likely to cause more damages. The high perceived consequences are caused by the of lack of permanent dykes to act as a protective barrier and the increased intensity of flooding events.

4.1.6 Worry

The household heads were asked whether they worried about the flood risk in Budalangi. The 60% of the household representatives stated that they worried a lot, while 32 % of them stated that they worried. On the other hand, 2% and 6 % of them stated that they slightly worried and not worried, respectively. Many households stated that, they

worried about the floods because it had severe impacts on their lives, properties, crops and their financial.

4.2. Flood mitigation measures

The interviewees were asked to provide (more than one of) their mitigation measure during the flood events. According to the face-to-face interview results, the mitigation techniques implemented by the local are as followed – (1) constructing the drainage channels to improve the drainage system (73%), (2) raising the house floors (35%), (3) raising the electrical wiring system (29%), (4) constructing the water resistant walls (31%), (5) plating trees as a flood mitigation measures (57%), and (6) relocating their houses (66%). The 34% of households had precaution savings. Only 6% of the households had flood emergency plans. The 19% of the households had implemented at least 4 measures, while 2% of them had implemented a total of nine measures as presented in the **Fig. 2.**
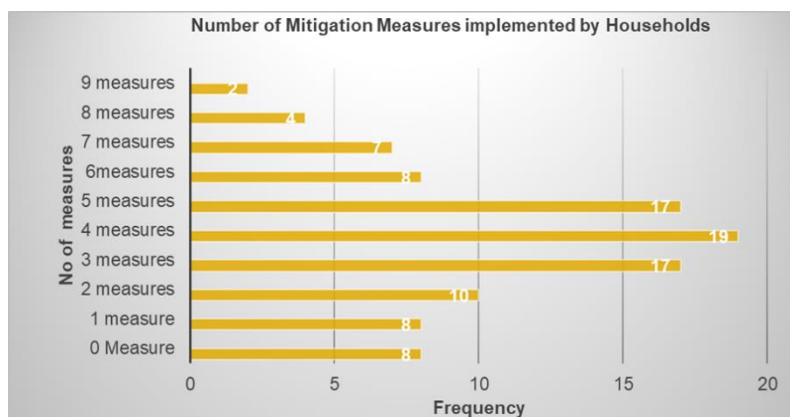
Fig. 2. The number of flood mitigation measures implemented by the interviewed households.

4.3. Statistical analysis

4.3.1 Perceived Self-Efficacy

It is strong positive correlation between perceived self-efficacy and the total number of implemented mitigation measures ($r = 0.815^{**}$). This correlation is statistically significant ($p < 0.01$) as shown in **Table 4**. The results suggest that the number of implemented flood mitigation measures increases with the rise in self-efficacy. It means that the individuals who can cope with flood impacts are usually implemented more mitigation measures compared to the other. This finding is similar to the study results determined by Grothmann et al. (2006); Peak et al. (2010); Loke et al. (2012); Mishra et al. (2012); and Bubeck et al. (2013). The previous studies discovered that the perceived self-efficacy positively influences the uptake of mitigation measures due to their financial status or skill wise.

4.3.2 Perceived Response Cost

Table 4 illustrates that the perceived cost negatively correlated with a total number of mitigation measures at moderate level ($r = -0.522^{**}$). The correlation is also statistically significant ($p < 0.01$). The perceived response cost of mitigation measures increases with

the decrease in flood mitigation measures implementation. Therefore, perceived response cost negatively influences the uptake of flood mitigation measures implementation. The findings also similar to the works done by Poussin et al. (2014).

4.3.3 Flood Experience

Flood experience positively correlated with the number of flood mitigation measures implemented by households in Budalangi (r = 0.444*). The correlation was statistically significant p < 0.01 as indicated in **Table 4.**

The findings showed that experienced households implemented more flood mitigation measures. This finding is consistent with the works done by Poussin et al. (2014); Cameron, et al. (2012); and Kousky (2010). The results from previous research also show that flood experience positively impacts the mitigation behaviours. In addition, Grothmann, et al. (2006); Siegrist et al. (2008); and Brubeck et al. (2012) also found out that flood experience is statistically significance and positively correlates with the adoption of mitigation measures. Therefore, having flood experience increases the willingness to implement more measures.

Table 4.

Influence of socio-psychological variables on flood mitigation measures implementations

Socio-psychological variables	Total number of flood mitigation measures implemented.	
	Correlation coefficient	**Significant level (p)**
Perceived self-efficacy	0.815**	0.000
Perceived cost of response	-0.522**	0.000
Number of flood experience	0.444**	0.000
Worry	0.320**	0.001
Perceived consequences	0.109	0.140
*Statistically significant at 0.01***		

4.3.4 Perceived Consequences

It is evidently clear that the perceived consequence is not statistically significant (p>0.01) when correlated with the total number of mitigation measures. This result is in line with the works done by Poussin, et al. (2014). The level of flood consequences was not related to the level of household preparedness to mitigate flooding.

4.3.5 The worry

The worry positively correlates with the total number of mitigation measures (0.320**). It is also statistically significant (p <0.01). The results suggested that worry about flood risk increases the willingness to implement more mitigation measures.

4.4. The barriers to implementing the flood mitigation measures

Majority of the households (71%) stated that financial issue was the key obstacle to implementing the flood mitigation measures. This was evidently true because most of the interviewees were low-income earners. The only 10 % of the interviewed households stated that communication was a barrier. This because the local radio station regularly broadcasts necessary flood information in Kinyala language. The 53% of the households reported the lack of technology to build flood-protection houses with reasonable cost. The 30% of the

households stated the lack of cost-effectiveness information on the specific mitigation measures. In addition, 32% of the households also stated the lack of mitigation tools, such as sandbags and trees seedling.

5. CONCLUSIONS AND RECOMMENDATIONS

The research study revealed that simple canal, tree plantation and temporary relocation are the most practical mitigation measures in Budalangi, Kenya. The interviewed results show that perceived self-efficacy has positive impacts to the uptake of mitigation measures. The flood experience and worry have moderate and weak influences, respectively. The perceived response cost has negative influence on the uptake of mitigation measures. On the other hand, perceived consequences are not correlated with the uptake of mitigation measures. The identified barriers to mitigation measures implementation include – (1) incentives, (2) financial issue, (3) lack of technology, (4) communication and information transferred. Future research should focus on household's perspectives on effectiveness of the mitigation measures implementation.

REFERENCES

Babcicky, P., and Seebauer, S. (2017) The two faces of social capital in private flood mitigation: Opposing effects on risk perception, self-efficacy, and coping capacity. *Journal of Risk Research*, 20(8), 1017-1037.

Becker, G., Aerts, J., and Huitema, D. (2014) Influence of flood risk perception and other factors on risk-reducing behavior: a survey of municipalities along the Rhine. *Journal of Flood Risk Management*, 7(1), 16-30.

Bogardi, J. J. (2004) Hazards, risks and vulnerabilities in a changing environment: the unexpected onslaught on human security? *Global Environmental Change*, 4(14), 361-365.

Bubeck, P., Botzen, W. J., and Aerts, J. C. (2012) A review of risk perceptions and other factors that influence flood mitigation behavior. *Risk Analysis: An International Journal*, 32(9), 1481-1495.

Bubeck, P., Botzen, W. J., Kreibich, H., and Aerts, J. C. (2013) Detailed insights into the influence of flood-coping appraisals on mitigation behavior. *Global Environmental Change*, 23(5), 1327-1338.

Ceola, S., Laio, F., and Montanari, A. (2014) Satellite nighttime lights reveal increasing human exposure to floods worldwide. *Geophysical Research Letters*, 41(20), 7184-7190.

Costache, R. (2014) Estimating Multiannual Average Runoff Depth in the Middle and Upper Sectors of Buzau River Basin. *Geographia Technica*, 9(2), 21-29.

Coumou, D., and Rahmstorf, S. (2012). A decade of weather extremes. *Nature Climate Change*, 2(7), 491.

Dancey, C. P., and Reidy, J. (2007) *Statistics without maths for psychology*. Pearson Education.

Elmer, F., Hoymann, J., Düthmann, D., Vorogushyn, S., and Kreibich, H. (2012) Drivers of flood risk change in residential areas. *Natural Hazards and Earth System Sciences*, 12(5), 1641-1657.

Grothmann, T., and Reusswig, F. (2006) People at risk of flooding: why some residents take precautionary action while others do not. *Natural hazards*, 38(1-2), 101-120.

Huho, J. M., and Kosonei, R. C. (2014) Understanding extreme climatic events for economic development in Kenya. *IOSR Journal of Environmental Science, Toxicology and Food Technology*, 8(2), 14-24.

Kousky, C. (2010) Learning from extreme events: Risk perceptions after the flood. *Land Economics*, 86(3), 395-422.

Laska, S. B. (1990) Homeowner adaptation to flooding: an application of the general hazards coping theory. *Environment and Behavior*, 22(3), 320-357.

NTV (2018, May 27) 39,000 acres of crops destroyed by Budalangi floods [Video file] retrieved from https://www.youtube.com/watch?v=qPZbFETClkE

Mishra, S., and Suar, D. (2012) Effects of anxiety, disaster education, and resources on disaster preparedness behavior. *Journal of Applied Social Psychology*, 42(5), 1069-1087.

Muku, L. O., and Nyandwaro, G. (2013) River Flood Modelling with Mike 11: Case of Nzoia River (Budalangi) in Kenya. *Civil and Environmental research*, 3(12), 103 – 111.

Mukuna, T. E. (2015) Vulnerability Analysis of the Gender-Differentiated Impact of Flooding in Budalangi Flood Plains, Kenya. *Journal of Emerging Trends in Educational Research and Policy Studies*, 6(2), 201-216.

Mulilis, J. P., and Lippa, R. (1990). Behavioral change in earthquake preparedness due to negative threat appeals: A test of protection motivation theory. *Journal of Applied Social Psychology*, 20(8), 619-638.

Nistor, M-M., Rahardjo, H., Satyanaga, A., Leong, E.C., Hao, K.Z., Sham, A.W.L. and Wu, H. (2019) GIS-based approach to identify the suitable locations for soil sampling in Singapore. *Geographia Technica*, **14**(1), 103-117, DOI: 10.21163/GT_2019. 141.08.

Nusit, K., Tantanee, S., Subsomboon, K., Leungvichcharoen, S. and Yiemwattana, S. (2019) The Design of Flood Protection along Nan River, Phitsanulok Province, Thailand *Geographia Technica*, **14**, A special Issue On Sustainable Urban Development, 129 – 137.

Okumu, M. (2017). Assessing the Root Cause of Persistent Floods and Strategic Community-based Interventions in Bunyala, Busia County, Kenya. *International Journal of Innovative Research and Development*, 6(6), 250 - 254.

Opere, A. (2013) Kenya: A Natural Outlook: Chapter 21. Floods in Kenya, *Developments in Earth Surface Processes*, 16, 315 – 330.

Opondo, D. (2013) Loss and Damage from Flooding in Budalangi District, Western Kenya Loss and Damage in Vulnerable Countries Initiative, *Case study report*. Bonn: United Nations University Institute for Environmental and Human Security.

Onywere, S.M., Getenga, Z.M., Mwakilala, S.S., Twesigye, C.K. and Nakiranda, J.K. (2011) Assessing the challenge of settlement in Budalangi and Yala swamp area in Western Kenya using Landsat satellite image. *The Open Environmental Engineering Journal*, 4, 97 – 104.

Opondo, D. O. (2013) Erosive coping after the 2011 floods in Kenya. *International Journal of Global Warming*, 5(4), 452 - 466.

Osberghaus, D. (2015) The determinants of private flood mitigation measures in Germany—Evidence from a nationwide survey. *Ecological Economics*, 110, 36 - 50.

Otiende, B. (2009) The economic impacts of climate change in Kenya: riparian flood impacts and cost of adaptation. online] adapt. org/knowledge-base/files/758/4e25a4b8c8bf61C-kenyariparian-floods-case-study. pdf (accessed August 2013).

Poussin, J. K., Botzen, W. W., and Aerts, J. C. (2014) Factors of influence on flood damage mitigation behaviour by households. *Environmental Science & Policy*, 40, 69 - 77.

Richert, C., Erdlenbruch, K., and Figuières, C. (2017) The determinants of households' flood mitigation decisions in France-on the possibility of feedback effects from past investments. *Ecological Economics*, 131, 342 - 352.

Rippetoe, P. A., and Rogers, R. W. (1987) Effects of components of protection-motivation theory on adaptive and maladaptive coping with a health threat. *Journal of personality and social psychology*, 52(3), 596 - 604.

Rogers, R. W. (1975) A protection motivation theory of fear appeals and attitude change. *The journal of psychology*, 91(1), 93-114.

Rogers, R. W. (1983) Cognitive and psychological processes in fear appeals and attitude change: A revised theory of protection motivation. *Social psychophysiology: A sourcebook*, 153-176.

Siegrist, M., and Gutscher, H. (2008). Natural hazards and motivation for mitigation behavior: People cannot predict the affect evoked by a severe flood. *Risk Analysis: An International Journal*, 28(3), 771-778.

Şarpe, C.A., and Haidu, I., (2017) Temporal sampling conditions in numerical integration of hydrological systems time series. *Geographia Technica*, **12**(1), 82- 94, DOI: 10.21163/GT_2017.121.09

Kenya National Bureau of Statistics. (2010) *The 2009 Kenya population and housing census*: Kenya National Bureau of Statistics Kenya.

Taki, K., Matsuda, T., Ukai, E., Nishijima, T., and Egashira, S. (2013) Method for evaluating flood disaster reduction measures in alluvial plains. *Journal of Flood Risk Management*, 6(3), 210 - 218.

Wiegman, O., Taal, E., van den Bogaard, J., Gutteling, J. M., Winnubst, J., and Maes, S. (1992) Protection motivation theory variables as predictors of behavioral intentions in three domains of risk management, in J.A.M. Winnubst and S. Maes (eds.), *Lifestyles, stress, and health: New developments in health psychology*, DSWO/Leiden University Press, Leiden, The Netherlands, 55-70.

Yamane, T. (1973) *Statistics: An introductory analysis*. 3rd Edition, Harper and Row, New York.

A STUDY ON THE EFFECTS OF LAND USE CHANGE ON FLOODING RISKS IN NIGERIA

Eseosa Halima IGHILE[1] , *Hiroaki SHIRAKAWA[2]*

ABSTRACT:
This paper aims at identifying the drivers of land use change and their effects on flood risks in Nigeria. The study presumed that changes to land use and their drivers could affect the level of risks to natural disasters. From the research; we identified the factors responsible for land use changes in Nigeria between 2000 and 2013 and their effects on the level of flooding risks. The multinomial logistic regression models the probability of land use changes and their impact on flooding risks, as a function of explicit independent variables. The results show that Economic, biophysical, demographic and climatic variables were the significant determinants of land use change. Additionally, while assessing the relationship between the changes in land use and flood risks, agricultural, settlement and forest land use had the most significant contributions to the changes in the level of flood risks. The result of this study would aid in the contribution and improvement of efficient countermeasures for flooding disasters. Therefore ensuring the prioritisation of the flood hazard areas and future land development.

Key-words: *Land use, Flood Risks, Regression, Nigeria.*

1. INTRODUCTION

Nigeria, in the last 40 years, has witnessed significant changes in land-use/land cover(LULC) across various regions due to both natural and human-made factors. These changes have occurred in the areas of infrastructural development, resource extraction, crop cultivation, and human development. As continuous land use changes are one of the prominent attributes of a developing country (Meyer & Turner, 2003), like Nigeria; due to its rapid urbanisation, population growth, increased inflow of population to urban centres, climate change and the frequent modification by both natural and anthropogenic factors (Peter et al., 2012).

Aside the changes to land use, the frequent occurrence of flooding disasters in Nigerian cities have become a major social, economic and environmental problem which has greatly affected the overall functioning of the urban environment (Bashir et al., 2012). Moreover, over the years, this has forced millions from their homes, wrecked businesses, contaminated water resources and amplified the risk of diseases (Baiye, 1988, Akinyemi, 1990; Nwaubani, 1991; Edward-Adebiyi, 1997, UNECA, 2015). Over time, these changes and amplified pressure on land and the frequent occurrence of disasters has affected the socioecological resilience of the country (Baiye, 1988, Akinyemi, 1990; Nwaubani, 1991; Edward-Adebiyi, 1997, UNECA, 2015). Furthermore, the lack of the relevant management plans to respond effectively to disasters, and with the ever-growing possibility that each

[1]*Nagoya University, Graduate School of Environmental Studies, Environmental Engineering and Architecture,464-8601, Nagoya, Japan, ighileeseosa1@gmail.com;*
[2]*Nagoya University, Graduate School of Environmental Studies, Environmental Engineering and Architecture, 464-8601, Nagoya, Japan. sirakawa@urban.env.nagoya-u.ac.jp*

change to the existing land use having the likelihood of altering the ability of ecosystem services to function and combat impending disasters (Khan et al., 2014). Efforts to understand the role of land-use, its drivers and their relationship to flooding disaster risks and management are now necessary. Therefore, estimating and understanding what drives the changes to land use is crucial for the sustainable growth, management and development of Nigeria. Similarly, assessing the contribution of each land use class to changes in flooding disaster risks levels is vital for a practical land resource, disaster management, and mitigation against the underlying vulnerability of human systems. Asides having proper knowledge on the drivers and contributions of the changes to land use on disaster risks, this study would assist in enabling the creation of appropriate land use-land cover plans which focuses on mitigating the impacts of each environmental stressor on disaster risks. This study also aims at enumerating the drivers of LULC change, and the contributions of each historical LULC class to the increased risk of disasters for the affected areas. The purpose of this study firstly is to investigate the main drivers of land-use change using analytical modelling techniques. Secondly, analyse the relationship and impacts of the changes in the LULC types and their drivers on flood disaster risks in Nigeria.

2. STUDY AREA

The Federal Republic of Nigeria is in Western Africa (**Fig. 1**). It occupies an area of 923,768 sq.km, including the land surface area of about 910,770 sq.km, and the maritime area covering approximately 200 nautical miles. Nigeria consists of 36 states, and the federal capital territory Abuja.
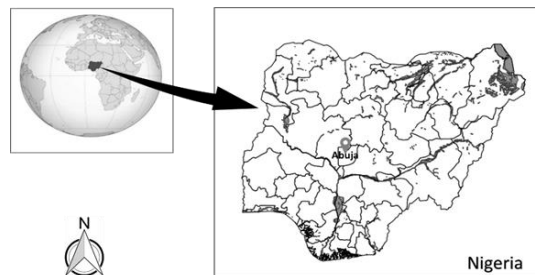
Fig. 1. Geographical Location of Nigeria (Source of data: Authors)

The population of Nigeria is approximately 190 million (UN,2017), with about 48.6% of the entire population living in urban areas distributed across eleven(11) cities having a population above a million(1,000,000) residents and more than 70 cities having over one hundred thousand (100,000) inhabitants (USGS, 2015). The significant contributions to the Nigerian economy is attributed to different sectors; Agriculture (21.65%), Trade (17.06%), Information & Communication (12.41%), Manufacturing (9.91%), Mining & Quarrying (9.67%), Oil (9.61%), Real Estate Services (5.63%), Construction (4.04%), Finance & Insurance (3.55%), Professional, Scientific & Technical Services (3.51%), (World Bank, 2017). Even as Nigeria continues to experience major economic growth, with a GDP of about 500 billion US dollars in 2015 (National Bureau of statistics, 2017), a large number of citizens in Nigeria still live in abject poverty. The dynamics of wealth

distribution in Nigeria according to the world poverty clock indicates that the level of inequality in Nigeria is at a record high, with about 46.5% of the total population are living in multidimensional /extreme poverty (world poverty clock,2018).

The trends in land use in Nigeria between the period 1975 and 2013 shows that there have been significant changes to the land use types in Nigeria. Agriculture, settlement and forest land use, have undergone the most noteworthy changes. The total area of agricultural land use experienced a massive increase from about 21 per cent in 1975 to 41 per cent in 2013, of the entire land territory (**Fig. 2**). That is, the area initially covered by agricultural land use increased from about 192,000 square kilometres to 379,000 square kilometres. The implication of this massive change indicates that agricultural land use conversion doubled within thirty-eight years. Apart from the rapid agricultural land use expansion, settlements land use also experienced enormous growth from an estimated average of 1-2 per cent per annum between 1975 and 2000 to a rate of 2-4 per cent between 2000 and 2013. Subsequently, although agricultural and settlement land use shows an increase in the land coverage area, forest land use, on the other hand, decreased by about 45 per cent between the period 1975 and 2013.
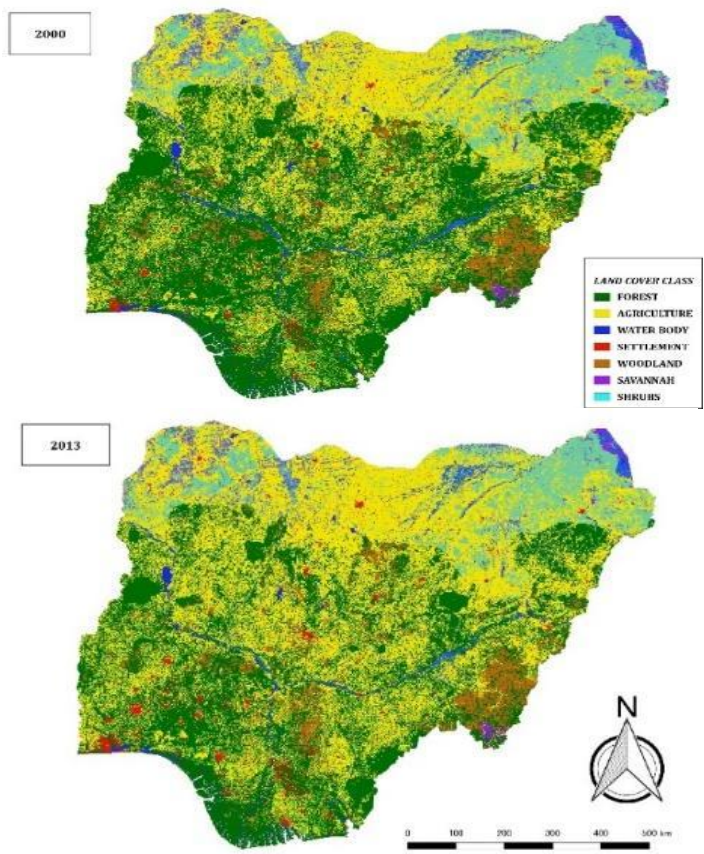
Fig. 2. Land use maps of Nigeria (2000 and 2013) (Source of data: USGS,2015)

Nigeria frequently experiences flooding incidents, especially during the peak summer months between June and August, which is the most predominant natural disaster event in Nigeria (Olorunfemi & Adebimpe, 2011). The trend in disaster occurrence across the country can be observed, in most of the large and densely populated areas and neighbouring regions having a higher frequency of disasters. The observed reason for the increased reoccurrence of flooding incidents in Nigeria's major urban centres results from the increased influx of new residents into the major cities, the high population growth and population density. Aside from the increased migration to urban centres, the limited arable land for human settlement has resulted in overcrowding, slum formation, increased pollution. The increase experienced in the level of uncontrolled and unsustainable land use conversions, when combined with the existing flood hazards, potentially increases the risk to urban flooding disasters (Oladokun & Proverbs, 2016).

3. METHODOLOGY AND DATA

3.1. Modelling the Drivers of Land Use Change

We assessed the drivers of land use change in Nigeria with the aid of the multinomial logistic regression, to model the probability of land use conversion as a function of various selected independent variables. According to Suwarno et al. (2019), several factors can be used to understand the impacts of each driver such as the geologic, hydrologic, biologic, climatologic, geographic, social, economic, and technologic characteristics when modelling probabilistic changes. In the study, the variable selection for the land use model was chosen based on several factors, such as economic, biophysical, demographics, climatic and accessibility, which influence land use pattern formation (Kim & Heung, 2016). The selection of the multinomial logistic regression model for this research aids in determining the patterns and factors for each land use class and their response due to several social, economic and environmental interactions. We analysed the land use maps of two separate years 2000 and 2013 respectively. The equation for the land use probability (πij) is;

$$\pi_{ij} = \frac{exp(x_i\beta_j)}{\sum_{k=1}^{J} exp(x_i\beta_k)} \ j = 1,\dots,J. \tag{1}$$

where;

i: index of the location.   j: type of LULC
π_{ij}: the probability of j at 1 x: vector of variables
β: vector of parameters   k: index of the hazard risk level
J: total number of LULC types

For the assessment of the index of the hazard risk level used in the land use model, the existing flood risk data from the UNEP study (2011) classified into five categories; low, low/medium, medium, high and extreme using GIS (**Fig.3**), and further calculated the percentage of each risk level under each land use type. The risk level is classified based on the magnitude of the total number of persons affected in the event of a flooding incident. The purpose of the classification is to rank the risk levels based on the severity scale that would allow for an understanding of the areas most affected by flooding disasters (Klemešová et al., 2014).
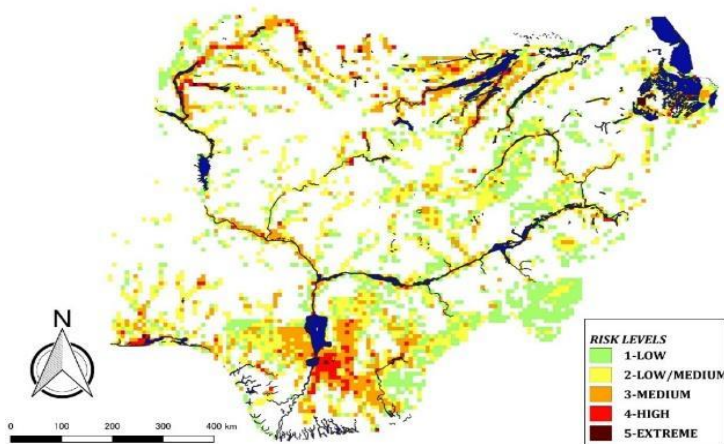
Fig. 3. Multilevel Hazard risk classification in Nigeria (Source of data: UNEP, 2011)

3.2. Data

This study utilised an extensive range of datasets. The type and nature of the data used include both temporal and spatial resolutions comprising of land use maps, and other datasets categorised under climatic, biophysical, neighbourhood, demographics and economics respectively. The pre-processed land use maps for the period 2000 and 2013, were obtained from the United States Geological Survey (USGS,2015), digital elevation model (DEM) with a resolution of 30 × 30 m, downloaded from the STRM30 (https://earthexplorer.usgs.gov/). The soil datasets were classified into seven categories (N1-N7) to represent the seven major categories of soil types in Nigeria, including the proportions of sand, silt, loamy and clay, and the soil depths extracted from the Harmonized World Soil Database version 1.2 (HWSD) (Nachtergaele et al., 2009). Demographic information consisting of Population density is from LandScan, which is the global population distribution data made by ORNL. The sociological data such as migration and the economic variable: gridded Gross Regional Product (GRP) (in US$) and poverty ratio, downloaded from, http://sedac.ciesin.columbia.edu/data/set/spatialecon-gecon-v4 (2005 and 2010). Climatic data, including annual average temperature, and precipitation obtained from the GPCC Global Precipitation Climatology Centre at https://www.esrl.noaa.gov/psd/data/gridded/data.gpcc.html). Flood risks maps are from the United Nations Environment Programme; http://www.grid.unep.ch (UNISDR, UNEP,2011, & Umvoto Africa, 2004). The neighbourhood indices; calculated from randomly generated points, and the other datasets, such as the official administrative maps, were obtained from GADM (https://gadm.org/).

3.2.1. Analysis

The data used for the regression analysis is through the generation of 10000 randomly generated points within the Nigeria administrative boundary map, and each point sampled off the selected independent variables in the QGIS environment. The extracted data from each location is then processed, first by correlation analysis to eliminate variables that are closely correlated from the model to ensure good results. All the statistical analytical computations are in the r studio environment. The Likelihood-ratio (LR), then compares the log-likelihood from the model with that of the reduced model ignoring the explanatory

variables. In this case, the multinomial logistic regression models of multi-dimensional conversions for settlements, agricultural and forest land use types during the periods of 2000-2013, is used to determine the pattern and factors responsible for the changes in land use cover change. The model significance is at 5%. A back-step approach is applied during the final model calibration process to assign only variables with importance in the final regression results.

4. RESULTS AND DISCUSSIONS

4.1. Drivers of Land Use Change

4.1.1. Agricultural Land Use

Table 1 shows the result of the regression analysis for the drivers of agricultural land use and the probability of agricultural land use. The results indicate that population density, temperature, the rate of internal migration, precipitation, poverty, distance to water bodies, soil quality and the GRP per capita, have a positive impact on the probability of conversion to agricultural land. That is; with a unit change in any of those above, there is a high likelihood of the changes to the land use type around the surrounding and existing land cover class would be agricultural. On the other hand, elevation, distance from the road, and distance from the railway line, all have negative coefficients on the probability of agricultural land use conversion. The negative values show that; they do not influence the likelihood of agricultural land conversion.

Table 1.
Multinomial Logistic Regression for the probability of Agricultural Land (n=10000).

Variables		Estimate	Standard Error	Z Value	Significant Probability (pr>[z])
Population density		7.37	1.67	4.41	1.03 ***
Elevation		-6.34	1.47	-4.31	1.60 ***
Gross Regional Product		7.11	2.63	2.71	0.01 **
Railway		-1.75	6.23	-2.81	0.01 **
Temperature		9.82	7.89	12.44	0.00 ***
Road		-1.61	1.56	-10.26	0.00 ***
migration		5.94	1.03	5.79	7.22 ***
Precipitation		3.43	7.45	4.61	4.05 ***
Poverty		6.67	9.21	7.24	4.37 ***
Water		-1.38	8.45	-0.16	0.87 *
Soil quality		5.24	1.42	0.37	0.71
Soil type	N1(1 if yes, otherwise 0)	3.26	7.17	4.54	5.62 ***
	N2(1 if yes, otherwise 0)	1.76	4.47	-	-
	N3(1 if yes, otherwise 0)	-1.25	6.23	-2.00	0.05 *
	N4(1 if yes, otherwise 0)	-3.11	9.94	-3.13	0.00 **
	N5(1 if yes, otherwise 0)	2.60	8.30	3.13	0.00 **
	N6(1 if yes, otherwise 0)	-3.55	1.02	-3.48	0.00 ***
	N7(1 if yes, otherwise 0)	-6.30	1.13	-5.56	2.66 ***
Low risk		-2.01	4.15	-0.48	0.63
Medium risk		-1.65	4.16	-0.40	0.69

Significant. codes: 0 '***' 0.001 '**' 0.01 '*' 0.05 '.'

The results explain that the higher the poverty ratio (**Table 1**), the higher the likelihood of agriculture production as a source of revenue, leading to agriculture land expansion. Migration with a positive coefficient (**Table 1**) for agriculture land use change explains that as the rate of movement from rural to urban areas continues to increase, the demand for agricultural products in the urban centres will continue to grow. Additionally, the result explains the income (economic character) is also a key driver of agricultural land use change. The phenomenon will require more agriculture land conversion around urban settlements and a reduction in the productivity of some of the existing agricultural land in rural areas due to the low labour force.

4.1.2. Settlement Land Use

The results (**Table 2**) show that Population density, Elevation, Gross Regional Product, temperature, internal migration, distance to water bodies and soil quality, have positive coefficients on the likelihood of settlement land use change. Of the seven variables that positively influence settlement land use changes, population density, the Gross Regional Product, and temperature have the most significant impact on settlement land use change (p>0.05). On the other hand, poverty ratio, precipitation, distance from the road, distance from the railway line and the population density, gives a negative estimate value or the probability of settlement land use change. The rate of migration, gross regional product) and elevation is an indication that the drivers of settlement land use change, result from a combination of both demographics, economic and biophysical characteristics.

Table 2.

Multinomial Logistic Regression for the probability of settlement Land Use (n=10000).

Variables		Estimate	Standard Error	Z Value	Significant Probability (pr>[z])
Population density		1.28	2.14	5.99	2.12 ***
Elevation		7.96	4.38	1.82	0.07
Gross Regional Product		1.34	3.00	4.45	8.43 ***
Railway		-2.14	2.35	-0.91	0.36
Temperature		1.68	2.35	7.18	7.19 ***
Road		-2.61	7.02	-3.72	0.00 ***
migration		6.55	3.33	0.20	0.84 ***
Precipitation		-3.59	2.08	-1.73	0.08 .
Poverty		-1.72	2.36	-7.29	3.10 ***
Water		4.04	2.26	0.18	0.86 *
Soil quality		2.94	3.38	-	-
Soil	N1(1 if yes, otherwise 0)	3.27	9.70	3.38	0.00 ***
type	N2(1 if yes, otherwise 0)	1.75	4.47	0.04	0.97
	N3(1 if yes, otherwise 0)	-1.37	1.15	-1.19	0.23
	N4(1 if yes, otherwise 0)	-1.29	7.31	-1.76	0.08
	N5(1 if yes, otherwise 0)	4.87	2.55	1.91	0.06
	N6(1 if yes, otherwise 0)	-1.86	1.02	-1.82	0.07
	N7(1 if yes, otherwise 0)	-2.60	3.97	-0.66	0.51
Low risk		-9.49	5.40	-1.76	0.08
Medium risk		-1.10	5.52	-1.99	0.05 *

Significant. codes: 0 '***' 0.001 '**' 0.01 '*' 0.05 '.'

In the results in **Fig. 4**, we can easily understand how each of the selected drivers affects the probability of each respective land use class. **Fig. 4** explains when a change occurs in one variable and all other variables been held constant. The results show that; with an increase in the population density (**Fig. 4a**), we can observe that settlement land use continues to grow and whereas, the probability of agricultural and forest land conversion diminishes. GDP (**Fig. 4b**) also plays a vital role in land use conversion.
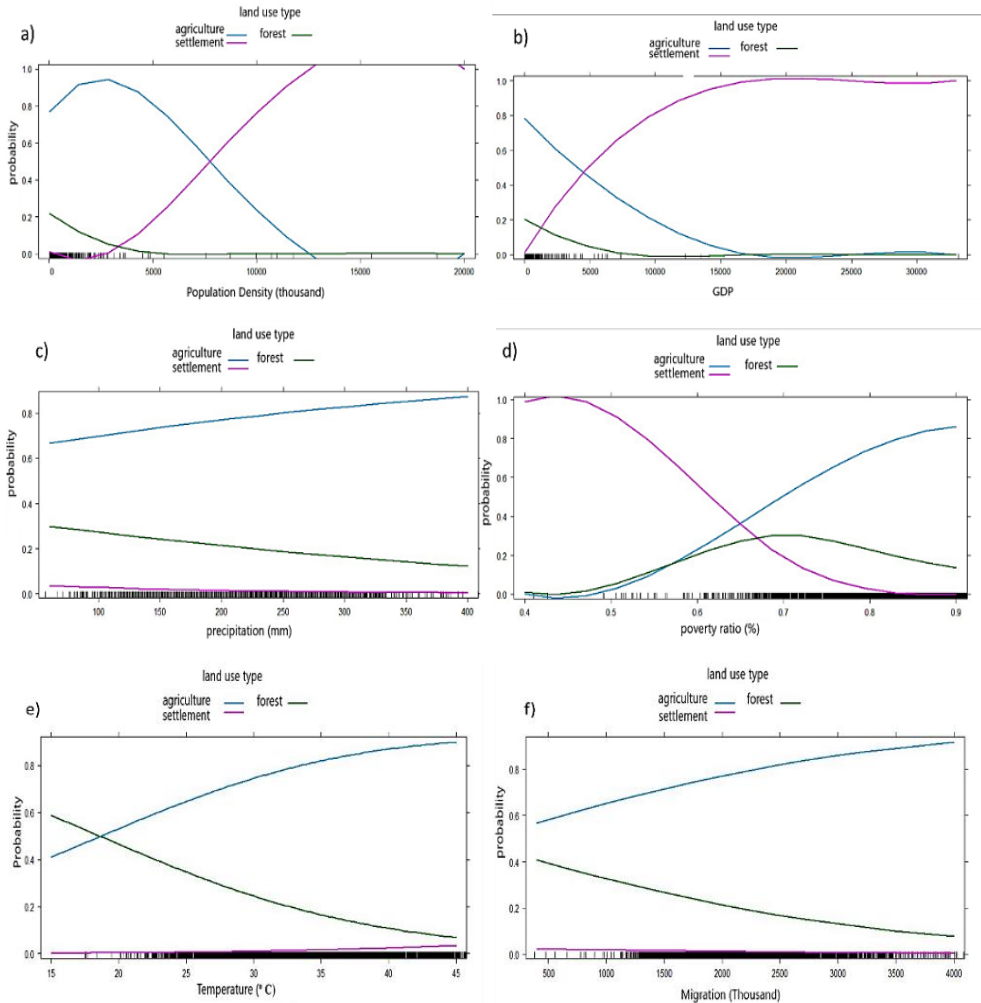
Fig. 4. The effects of the drivers of land use change a) population density, b) GDP, c), precipitation d), poverty ratio e) temperature and f) migration.

The higher the GDP, the higher the rate of settlement conversion, and while the GDP falls under $5000, the observed trend is that there is an increased probability of agriculture land expansion. In contrast, forest land declines due to agriculture land expansion. As income is perceived to play a vital role in the development of any society, we can equally compare the trend in income growth, with the growth rate of poverty. However, for

precipitation (**Fig. 4c**), there is a minimal impact on the changes experienced in land use. On the other hand, with every other variable been constant while a change occurs in the poverty ratio, we can notice that as the percentage of the total population in poverty rises (**Fig. 4d**), so does agricultural land increase, forestry and settlement expansion declines rapidly. The reason for this phenomenon is because an increase in poverty levels would lead to more individuals engaging in primary production to cater for their basic needs, and less focus is on infrastructural development (Meyer & Turner, 2003). For the case of the climatic variables, increasing temperature levels would lead to the further expansion of agricultural land areas and a decline in forest cover an indirect impact of climate change.

4.2. Percentage distribution of land use class in each risk zone

Fig. 5 explains the results of the percentage distribution of each land use class in each risk level zone. According to (Furtună & Holobâcă, 2013), the benefit of the risk probability analysis assists in comparing the current information on land use around each risk zone. In the low-risk zones, agriculture land use takes the largest share of 59.3%, while the settlement is set at 0.8% and forest 39.8% respectively. The same trend in agriculture land use is possessing the largest share in each risk zone (61.8% in low/medium,70.2% in medium and 59.8% in the high risk) level zones, respectively. In the case of settlement land use, for the low to medium risk zones, the percentage distribution falls between 0.8-2.5% respectively. However, for the high and extreme risk levels, settlement land use tends to have a more considerable margin in the distributive scale falling between 14.6 and 66.7% respectively. The indication is that the settlement land areas are mostly in the high and extremely high-risk zones, which may increase the mortality ratio and overall damage to the socio-economic dynamics of Nigeria in the event of a natural disaster.

Distribution of Land Use class in each Risk Zone

Land Use Class	LOW	LOW/MED	MEDIUM	HIGH	EXTREME
AGRICULTURE	59.3	61.8	70.2	59.8	16.7
SETTLEMENT	0.8	1.2	2.5	14.6	66.7
FOREST	39.8	37.0	27.3	25.6	16.7
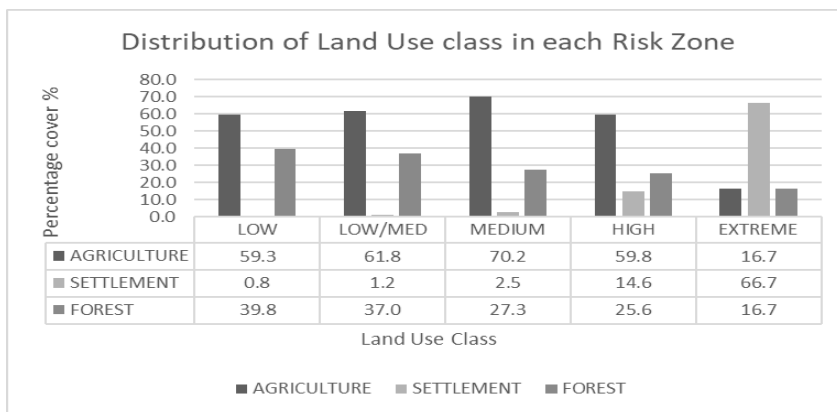
Fig. 5. Percentage distribution of land use type against each hazard level

In **Fig. 6**, we observe how the individual land use probabilities influence the risk levels. In the case of agriculture land use, as the probability increases, there would be a reduction in the areas with lower disaster risks. Whereas medium risk areas would increase, and the high-risk areas remain constant. For settlement land use probability, settlement land use expansion tends to increase the high- risk areas, while low and medium risk areas gradually reduce. However, for forest land use probability, the changes in the level of risk are negligible.
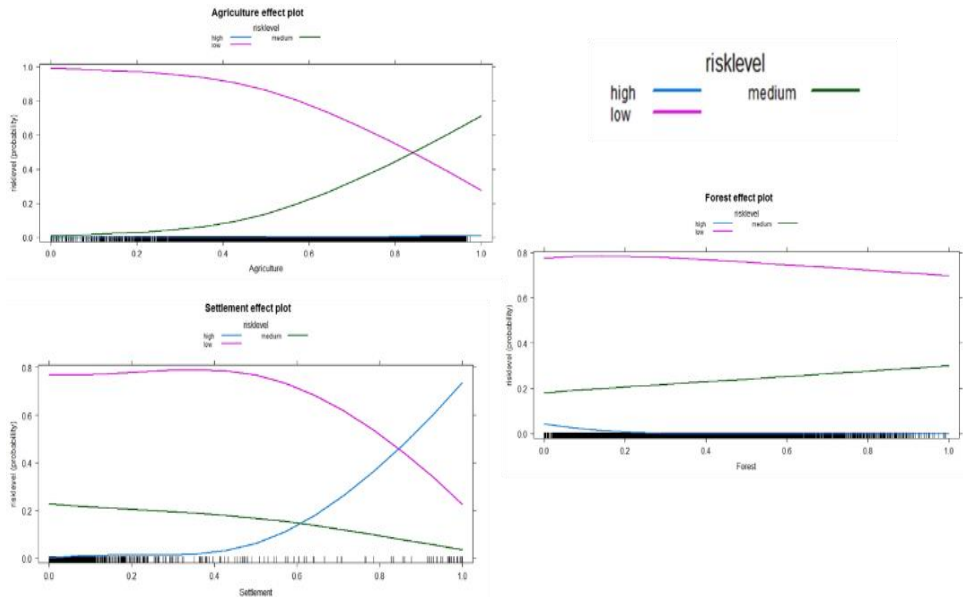
Fig. 6. The effects of the probability of each land use type on risk levels

5. CONCLUSIONS

The objective of the study is to determine the drivers of land use change and the effects of the probability of each LULC change on flood risk levels. This study successfully confirmed the drivers of land use and the effects of land use on each risk level. The results showed that the drivers of land use changes in Nigeria were the gross regional product, average temperature, migration and population density, in which the gross regional product and migration had the highest impacts on land use change. We further analysed how the drivers of land use change in conjunction with the likelihood of each changing land use class impacted on the level of risks in Nigeria. The results show that settlement land use changes increase the high-risk zones. In contrast, agriculture land use increases the medium risks areas and forest land use did not significantly influence the level of risks. The evidence from the research suggests that the use of variables of diverse characteristics is crucial for understanding the implications of the social, climatic, economic and demographics variables directly impacts land use changes and indirectly on disaster risks conditions (Fujiki & Renard, 2018). Therefore, this study highlights the relevance of developing and promoting effective land use management systems, through a consideration of natural and social systems for both land use changes and existing disasters which can enable the promotion of disaster resilience and achieve a sustainable society (Klemešová et al., 2014). The study result advocates for the introduction and implementation of proper policies that regulate land use conversion and promotes sustainable land use management. The methodology applied in this study showcases the importance of the application and consideration of different techniques in proffering solutions to land use and disaster management in Nigeria, as it enables the compilation of vital information from different sources in achieving the desired goals.

REFERENCES

Bashir, O., O., Oludare H., A., Johnson O., O., & Aloysius, B. (2012). Floods of Fury in Nigerian Cities. *Journal of Sustainable Development*. https://doi.org/10.5539/jsd.v5n7p69

Fujiki, K., & Renard, F. (2018). A geographic analysis of post-disaster social impacts on a municipal scale – A case study of a potential major flood in the paris region (France). *Geographia Technica*. https://doi.org/10.21163/GT_2018.132.03

Furtună, P., & Holobâcă, I. H. (2013). Forest fires study using remote sensing and meteorological indicators. Study case. *Geographia Technica*, *18*(2), 23–37.

Khan, M. M. H., Bryceson, I., Kolivras, K. N., Faruque, F., Rahman, M. M., & Haque, U. (2014). Natural disasters and land-use/land-cover change in the southwest coastal areas of Bangladesh. *Regional Environmental Change*, *15*(2), 241–250. https://doi.org/10.1007/s10113-014-0642-8

Kim, I., & Heung, C. (2016). Development of integrated modeling framework of land use changes and ecosystem services in mountainous watersheds, (October 1980).

Klemešová, K., Kolář, M., & Andráško, I. (2014). Using gis in the flood management – flood maps (Troubky, Czech Republic). *Geographia Technica*, *9*(2), 44–53.

Meyer, W. B., & Turner, B. L. (2003). Human Population Growth and Global Land-Use/Cover Change. *Annual Review of Ecology and Systematics*. https://doi.org/10.1146/annurev.es.23.110192.000351

Oladokun, V. O., & Proverbs, D. (2016). Flood risk management in Nigeria: A review of the challenges and opportunities. *International Journal of Safety and Security Engineering*, *6*(3), 485–497. https://doi.org/10.2495/SAFE-V6-N3-485-497

Olorunfemi, F. B., & Adebimpe, R. U. (2011). Sustainable Disaster Risk Reduction in Nigeria: Lessons for Developing Countries. *African Research Review*. https://doi.org/10.4314/afrrev.v2i2.41050

Peter, E., Samuel, D., & Olatunji, B. (2012). Land Use Change Modelling In Developing Countries: Issues And Prospects. *International Journal of Geography and Geology*, *1*(1), 23–41.

Suwarno, Sutomo, & Aditama, M. R. (2019). The analysis of the landslide vulnerability sub watersheds arus in Banyumas regency. *Geographia Technica*. https://doi.org/10.21163/GT_2019.142.10

UNISDR, UNEP, & Umvoto Africa. (2004). *Environmental Protection & Disaster Risk Reduction - A Community Leader's Guide , Volume 2, Issue 2*. UN/ISDR Africa Educational Series

SO₂ DISPERSION MODELING EMITTED FROM HONGSA COAL-FIRED POWER PLANT TRANSBOUNDARY TO NAN PROVINCE, THAILAND

Supawan SRIRATTANA[1], Kitsanateen PIAOWAN[2,3]

ABSTRACT:
Coal-fired power plant in general is a major source of sulfur dioxide (SO_2) emission. SO_2 is a primary pollutant and known as a respiratory irritant. The aim of this paper is to present the methodologies and results of an application of the dispersion modelling AERMOD as a potential model to predict the air quality impacts of SO_2 released by the flue stack of Hongsa coal-fired power plant (HCPP) located in Lao People's Democratic Republic (Lao PDR) transboundary to five villages in Chaloem Phra Kiat district, Nan province, Thailand during dry season (October to February) between 2015 and 2017. The results show that the hourly and daily modeled maximum ground-level concentrations of SO_2 were lower than Thailand's air quality standard, at 780300 and μg/m³, respectively. The highest hourly and daily SO_2 concentration were found at Ban Nam Ree village in January as high as 92.254 and 5.021 μg/m³, respectively. In contrast, SO_2 deposition, Ban Huai khon village was modeled to suffer from the highest impact from SO_2 deposition as 0.003 g/m² via dry deposition.

Key-words: *Coal-Fired Power Plant, AERMOD, Transboundary, SO₂.*

1. INTRODUCTION

HCPP operated by Banpu Power Limited (BPP), RATCH Group (formerly named as Ratchaburi Electricity Generating Holding Public Company Limited (RATCH)), and Lao Holding State Enterprise (LHSE) in Sayabouri province, Lao PDR (Banpu Power Limited, 2007) **(Fig. 1)**. At this time, Lao PDR's highest-capacity power plant, providing a sustainable source of energy for both Laos and Thailand. It consists of three 626 MW-generating units with a total electric generating capacity of 1,878-MW. The lignite from the Hongsa mine is used as the primary fuel for this power plant, at approximately 14.3 million tons per year - of which its lignite reserves were initially estimated at 436.9 million tonnes (Banpu Power Limited, 2007). The power plant is 20 km from Thai-Loas border in Nan province of Thailand **(Fig. 2)**.

According to the HCPP's EIA, HCPP has the flue gas desulfurization (FDG) system, selective catalytic reduction (SCR) system, and electrostatic precipitator (ESP) system to control emission of air pollutant. The series of emission abatement can eliminate 97-99 %

[1]*Naresuan University, Department of Civil Engineering, 65000 Phitsanulok, Thailand,*
supawan.sritat@gmail.com;

[2] *Naresuan University, Research Unit for Integrated Natural Resources Remediation and Reclamation* (*IN3R*)*, Department of Civil Engineering, 65000 Phitsanulok, Thailand,*
Piaowan.k@hotmail.com;

[3] *Naresuan University, Center of Excellence for Sustainability of Health, Environment and Industry (SHEI), 65000 Phitsanulok, Thailand, Piaowan.k@hotmail.com.*

of SO_2 (Breeze, 2019), lignite from the Hongsa Mine has contains substantial concentration of sulfur (S) 0.72% (Banpu Power Limited, 2007). Therefore, HCPP will release 2,110 tons of sulfur per year into the atmosphere. For this reason, fossil fuel combustion at power plants or even other industrial facilities are become largest sources of SO_2 emissions (Thepanondh et al., 2016).

Fig 1. Hongsa coal-fired power plant in Sayabouri province, Lao People's Democratic Republic
(Source of data:
http://www.hongsapower.com/index.php?model=cms&view=item&layout=page&id=1).

Importantly, SO_2 not only affects the atmosphere, but it also causes irritation to the human respiratory system (Charlene Marie Becka, 2014). Thus, monitoring of transboundary SO_2 from Lao PDR to Thailand is essential for risk management of the two countries. However, Thailand's air quality monitoring station is unable to service to all areas in Chalerm Phrakiat District. Therefore, the dispersion modeling is the best alternative method for checking and predicting the concentration of SO_2 emitted from HCCP's stack which may effected to air quality of Chalerm Phrakiat District (Cimorelli et al., 2005)) and the American Meteorological Society-Environmental Protection Agency Regulatory Model (AERMOD) is the standard model used by the EPA when evaluating pollutant dispersion from an industrial source (Charlene Marie Becka, 2014). Moreover, the dispersion modeling is a potential method of solution for many types of air pollutant such as PM_{10}, $PM_{2.5}$, Mercury, Arsenic, NO_X and NO_2 (Hysenaj, 2019).

The AERMOD model has been used in many research to predict or evaluate the air pollutant dispersion such as Mr. Khanh T. Tran (2011) was used AERMOD to predict the air quality impacts of SO_2 emitted by Luminant Martin Lake Coal Plant in Texas (Mr. Khanh T. Tran, 2011) ; Mark D.Gibson et al. (2013) was used AERMOD to evaluate concentration of $PM_{2.5}$, NO_X and SO_2 from traffic in Nova Scotia, Canada (Gibson et al., 2013); Nattawut Jittra et al. (2015) was used AERMOD to evaluate of NO_x and SO_2 dispersion in Maptaphut Industrial Complex Area, Thailand (Jittra Nattawut et al., 2015) ; Thepanondh et al. (2016) was used AERMOD to forecast SO_2 concentrations from petroleum refinery complex in Thailand (Thepanondh et al., 2016).

Consequently, in this paper describes the methods and results of air dispersion modeling that predict the ground-level concentrations of hourly and daily of SO_2 from

continued operation of flue stack of the HCCP couple with the study monthly deposition of SO_2 into the area of Chaloem Phra Kiat district. Finally, SO_2 impacts predicted by the AERMOD model will be compared against the hourly and daily of Thailand's air quality standard (PCD, 2001).

2. STUDY AREA AND DATA

Fig 2(A) was represented the location of HCPP. As can be seen in **Fig. 2(B)**, the modeling domain was 50 km x 50 km, centered at the HCPP's stack, it was covered five villages in Thailand as followed; Ban Huai Khon village (23 km from the power plant), Ban Kiew Chan village (22 km from the power plant), Ban Nam Chang village (18 km from the power plant), Ban Nam Ree village (20 km from the HCPP), and Ban Mom Chao Charoen village (26 km from the HCPP), respectively **(Fig. 2(C))**. The description of study area was shown in **Table 1**.
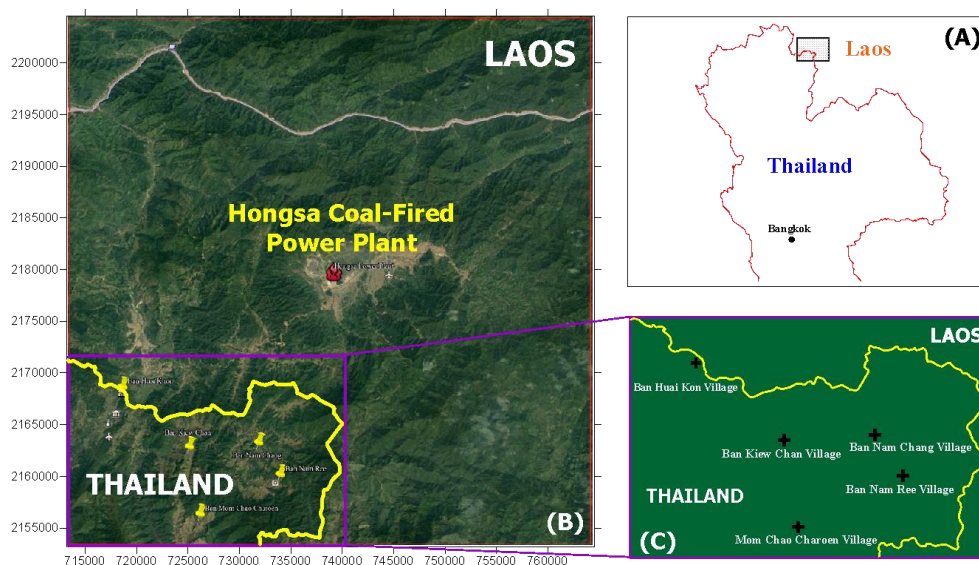
Fig. 2. Location of HCPP and five receptor areas in Chaloem Phra Kiat district, Nan Province, Thailand (Ban Huai Khon village, Ban Kiew Chan village, Ban Nam Chang village, Ban Nam Ree village, and Ban Mom Chao Charoen village).

Table 1.

Description of study area.

Location Name	°N (latitude)	°E (longitude)	Elevation (above sea level)
Hongsa Power Plant's stack	19.689909	101.282035	569.51 m
Ban Huai Khon village	19.596120	101.085101	561.04 m
Ban Mom Chao Charoen village	19.486062	101.154309	884.41 m
Ban Nam Chang village	19.546757	101.208972	919.17 m
Ban Nam Ree village	19.519160	101.228409	923.33 m
Ban Kiew Chan village	19.543990	101.145521	974.50 m

3. METHODOLOGY

3.1. AERMOD Dispersion Modeling

AERMOD is relatively a recent model developed by the American Meteorology Society (AMS) and United States Environmental Protection Agency (US EPA). The steady-state plume model of AERMOD assumes that a plume spreads both vertically and horizontally, leading to Gaussian concentration distributions (U.S. EPA, 2004). The concentration algorithm of AERMOD considers the effects of vertical variation of wind, temperature, and turbulence profiles. It is recommended by the US EPA for examining the effects of sources on receptor that are generally within 50 km of the source. For distances up to 50 km from the source of emission, AERMOD results are considered accurate because AERMOD is the models for demonstrating regulatory compliance in the near field (less than 50 km) (Rood, 2014). This study employed the AERMOD dispersion model (version 9.6.5) to predict and compare ambient air concentrations and deposition of SO_2. This version is currently the latest version of the model that has been approved by the US Environmental Protection Agency.

AERMOD required two preprocessors, AERMAP View and AERMET View, in order to run data. The preprocessor AERMAP View (Version 9.6.5) has been employed to obtain terrain elevations at these receptors using the GTOPO30/SRTM30 data with a resolution of 1,000 meters (U.S. EPA, 2018). The meteorological data preprocessor AERMET View (version 9.6.5) has been employed to prepare the meteorological data. The meteorological data in this study ordered from webpage of Lakes Environmental Software (https://www.weblakes.com /services/met_order.html). Meteorological data formats has been processed by Weather Research and Forecasting (WRF) model, Grid Resolution 4 km. WRF model can compute accurate windfields anywhere in the world. It is comprised of surface met data file, upper air met data file and AERMET input files for 3 years, 2015 to 2017.

3.2 Receptors

The multi-tier grid receptors and discrete cartesian receptors with a total discrete cartesian receptors of 65 places were used as a tool for SO_2 concentration monitoring in modeling domain **(Fig. 4)**. Note that in AERMOD, when specifying discrete cartesian receptors, it is necessary to specify the position of a source relative to the receptor is assigned (Jittra Nattawut et al., 2015). The multi-tier grid receptors have varying resolutions from the center by a total of 5,081 receptors: 250 m within the first 5 km, 500 m between 5 km and 10 km, and 1,000 m between 10 km and 25 km.

3.3 Input parameters

The input data were obtained from the information provided in the HCPP's EIA (Banpu Power Limited, 2007). The modeling domain was 50 km x 50 km centered at the HCPP (19.69068 °N (latitude), 101.2782°E (longitude)). The emission rate has been converted to grams per second (g/s) in as required by the AERMOD model by assuming that the boilers operate continuously, i.e. 8,760 hours per year. Furthermore, stack heights and exit velocities were identified as important factors that may affect pollutant dispersion and atmospheric concentrations in the region (Lee et al., 2014). The input parameters for the AERMOD model are summarized in **Table 2**.

The input parameters for the AERMOD model (Banpu Power Limited, 2007).

Parameter	Value
Stack elevation	569.51 m (above sea level)
Stack inside diameter	7.5 m
Physical stack height (meter above ground)	250 m
Stack exit temperature	75 ^{0}C
Stack exit velocity	26 m/s
Stack SO_2 emission	263.56 g/s

4. RESULTS AND DISCUSSIONS

4.1 Main wind from Laos to Thai

The wind field distribution plays an important role in the study of air distribution model (Boulghobra et al., 2016).

The wind field distribution plays an important role in the study of air distribution model. Therefore, the wind field distribution were evaluated for 12 months between 2015 and 2017. The average wind field distribution at the HCPP station was dominated by northeast and southwest winds. From October to February, wind obtained from measured data were blown from northeast to southwest while from March to September were blown from southwest to northeast (**Fig. 3**).
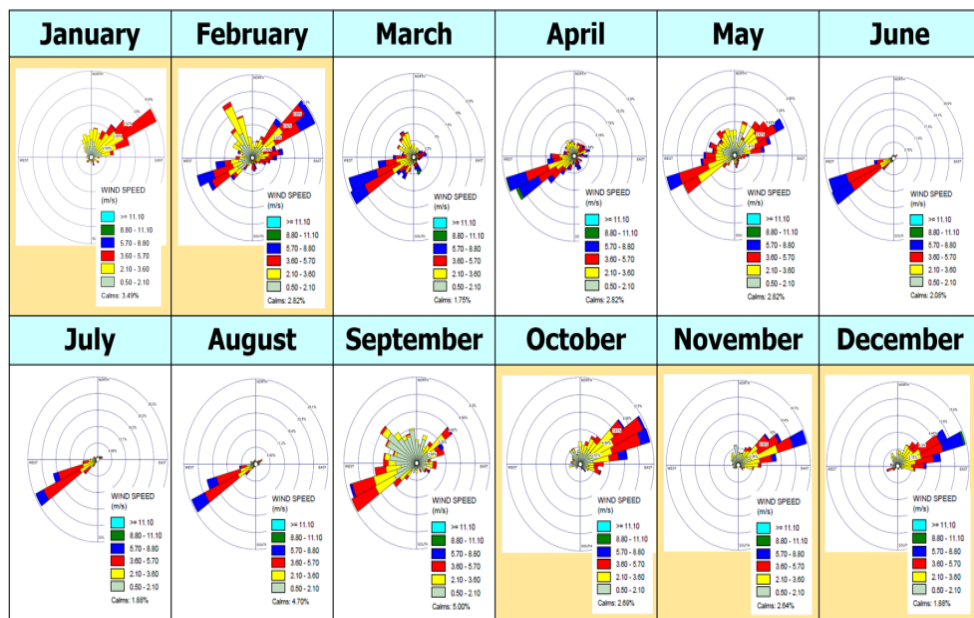
Fig. 3. Main wind from Lao PDR to Thai for 12 months between 2015 and 2017.

4.2 Modeled concentrations of SO₂

Hourly and daily maximum ground-level concentrations of SO_2 at each of the villages were computed. **Fig. 4** presented the hourly and daily concentrations contour map of SO_2 over a period of 3 years, the modeled concentration was calculated as 99th percentile. The both concentration of SO_2 per hourly and daily were lower than Thailand's air quality standard, at 780 and 300 μg/m³, respectively (PCD, 2001). The modeled results were focused on the day season (October to February) of each year because the wind is blow from Lao PDR to Thailand, Chaloem Phra Kiat district will suffered from HCPP's air pollution (**Fig. 3**).
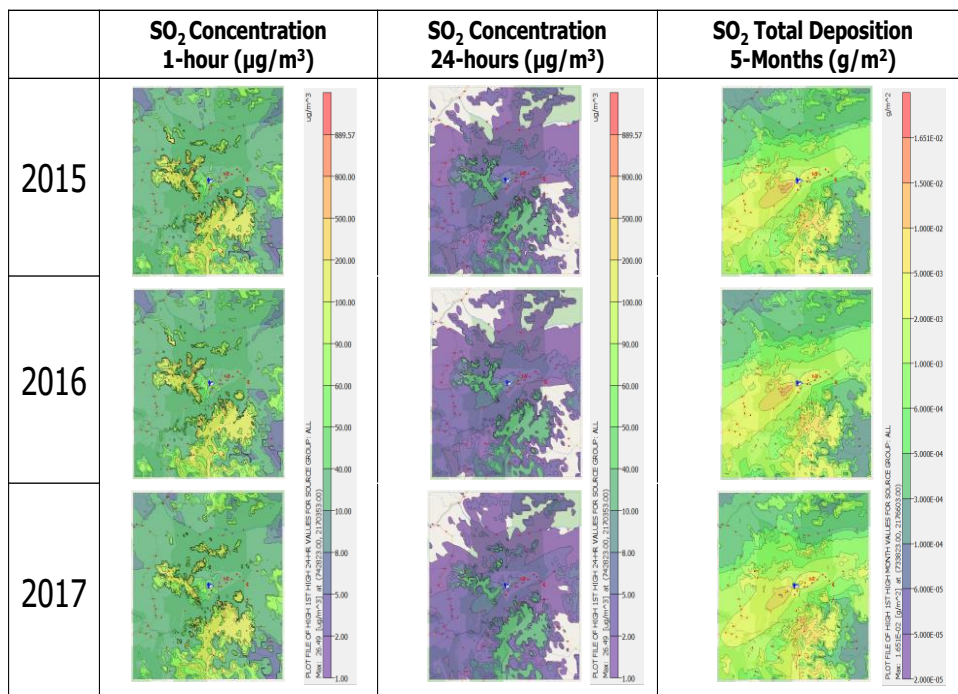
Fig. 4. The hourly and daily concentrations contour map, and monthly deposition of SO₂ based on emissions from the HCCP's stack during the dry season (October to February) between 2015 and 2017.

The highest hourly SO_2 concentration were found at Ban Nam Ree village in January as high as 92.254 μg/m³. The data of hourly concentration of each month can be explained as follows: 92.254 to 8.796 μg/m³ in January, 32.830 to 9.246 μg/m³ in February, 51.041 to 12.352 μg/m³ in October, 68.001 to 14.955 μg/m³ in November, and 54.703 to 15.698 μg/m³ in December, respectively (**Fig. 5(A)**). For daily concentration, the data trends were similar to hourly concentration, the highest concentration was 5.201 μg/m³ displayed at Ban Nam Ree village in January as well (**Fig. 5(B)**).

Although, the amount of SO_2 in air is at acceptable low levels in this area. However, SO_2 causes irritation to the human respiratory system when it is breathed in. It irritates the nose, throat, and airways to cause coughing, wheezing, shortness of breath, or a tight

feeling around the chest. The effects of sulfur dioxide are felt very quickly and most people would feel the worst symptoms in 10 or 15 minutes after breathing it in (Brian Chi-ang Lin and Zheng, 2017). Therefore, every dry season (October to February) people living in Chaloem Phra Kiat district should prepare for facing with SO_2. Interestingly, the concentration of SO_2 can change significantly with season, location, and geography. Ban Kiew Chan Village, Ban Nam Ree village and Ban Nam Chang village are located in higher geography than Ban Huai Khon village and Ban Mom Chao Charoen village (**Table 1** and **Fig. 6**).
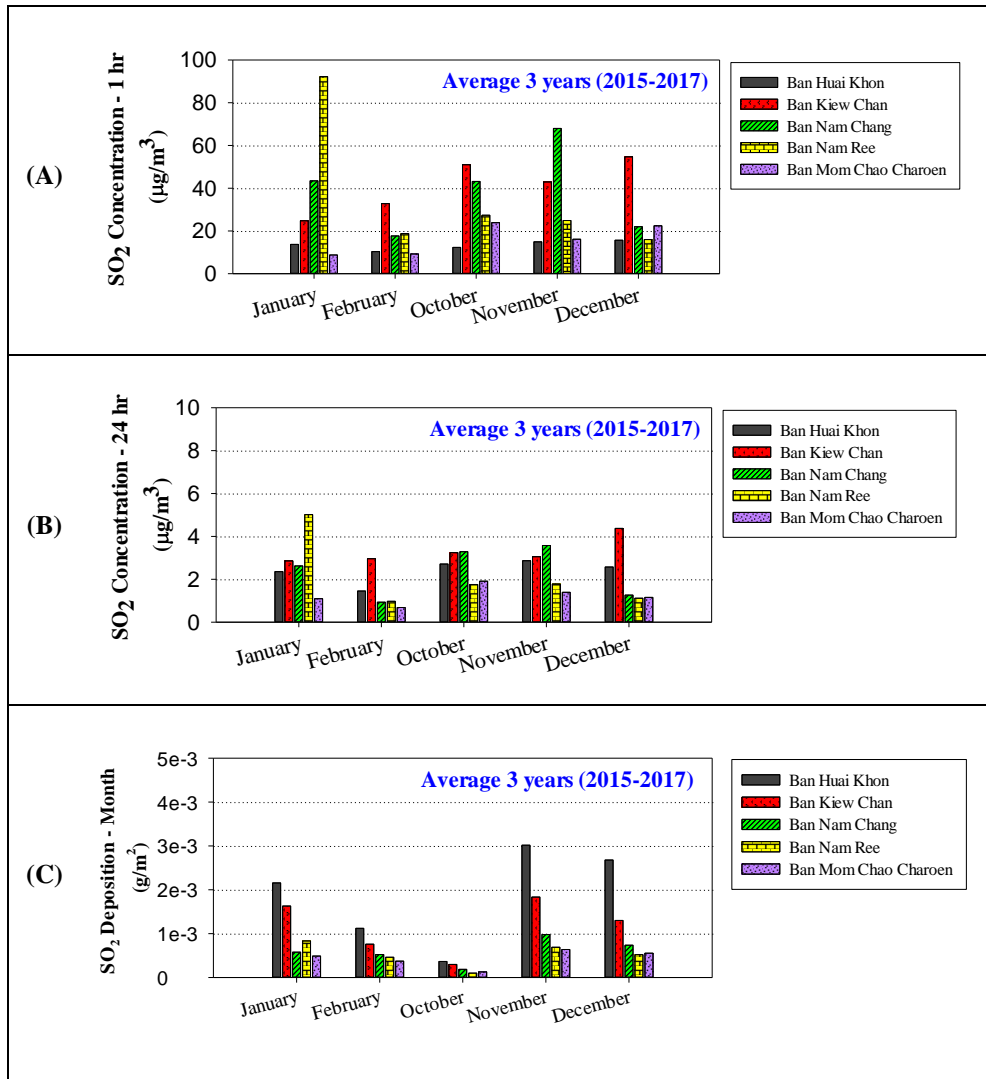
Fig.5. Modeled results of hourly concentrations, daily concentrations and SO_2 deposition at five villages in 5 months based on emissions from the HCCP's stack during the dry season (October to February) between 2015 and 2017.

Therefore, if considering the topography height of the HCPP' stack combined with stack height (569.51m + 250m = 820 m) and turbulent in air. the plume can be risen up to same altitude of the three which high SO_2 concentration. This hypothesis can support why the three villages have high modeled concentrations of SO_2.

4.3 SO₂ Deposition

The behavior of SO_2 after releasing into the air, it can be transform into acid rain by mix and react with water, oxygen, and other chemicals. Acid was eliminated from atmosphere by wet deposition (snow, rain, fog, mist, sleet, hail, dew, and etc.) and dry deposition (gas, dry particles, vapor, and aerosols) (Baedecker et al., 1992; U.S. EPA, 2008). The harmful effect of acid rain is considered as one of the most serious environmental problems and it becomes a major local ecological problem in most of the countries of the world (Haradhan Kumar Mohajan, 2018).

Acid Rain is a local environment pollution but global concern (Haradhan Kumar Mohajan, 2018) because it can damage plants, animals, soil, water, and building materials (U.S. EPA, 2008). Moreover, acid rain causes trees in forests to grow more slowly, and in some sensitive species it can even make the leaves or needles turn brown and fall off (U.S. EPA, 2008). At the same time, acid rain causes the release of substances such as aluminum from the soil. Aluminum can be very harmful to trees and plants. Once released into soil, aluminum can end up in streams, rivers, and lakes, where it can harm or even kill fish (U.S. EPA, 2008). Acid rain possesses higher levels of hydrogen ions (H^+) that can effected decreases the pH (potential hydrogen) scale of ecosystems (Katar Singh, 2007). Typical pH values of acid rain for anthropogenic emissions may be in the range of 3.5–5. The pH value between 5 and 8 is the ideal pH range for the plants' growth, and out of these ranges in soils, plants face difficulties to germinate or grow (Lazarus et al., 2006).
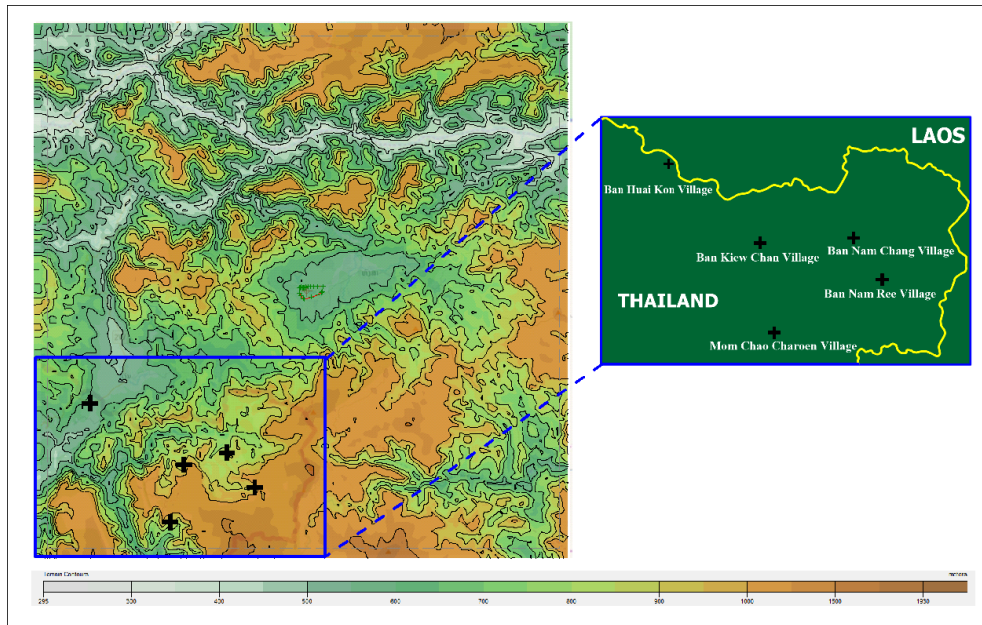
Fig. 6. Terrain characteristic of the study domain.

As can be seen in **Fig. 5(C)**, it is clear that Ban Huai khon village was predicted to suffer from the highest impact from SO_2 deposition emitted from the HCCP's stacks. The highest monthly SO_2 deposition during a period of 5 months was predicted as high as 0.003 g/m^2 in November via dry deposition. Unfortunately, Ban Huai khon village has many important sensitive areas such as Thai-Laos immigration border, school, hospital and agricultural area which is the main occupation of the people who live in this area.

5. CONCLUSIONS

AERMOD air dispersion model was evaluated for its performance to predict ground level SO_2 concentrations as emitted from the HCPP's stack. This model processed information about the emission rates of SO_2, local meteorological conditions, and other local information, such as terrain data, land use, and the location of receptors to predict maximum hourly, daily, period average concentrations, and deposition. Wind rose diagrams analysis showed that the wind directions is blow from HCCP through study area from October to February every year. Location and topography are plays important role on the SO_2 concentration. The highest predicted SO_2 concentrations was projected at Ban Nam Ree village in January while highest SO_2 deposition was found at Ban Huai khon village. The results from this study were more useful for understanding the SO_2 concentration distributions in this study case.

REFERENCES

Baedecker PA, Reddy MM, Reimann KJ, et al. (1992) Effects of acidic deposition on the erosion of carbonate stone — experimental results from the U.S. National Acid Precipitation Assessment Program (NAPAP). *Atmospheric Environment. Part B. Urban Atmosphere* 26: 147-158.

Banpu Power Limited. (2007) Environmental Impact Assessment of Hongsa Power Plant, Mining Development and Transmission Line Priject (Final report).

Boulghobra N, Koull N and Benzaoui T. (2016) Four decades period of climatic data for assessing the aeolian hazard in the region of Touggourt (Low Algerian Sahara). *Geographia Technica,,* **11**(1),13-22.

Breeze P. (2019) Chapter 3 - Coal-Fired Power Plants. In: Breeze P (ed) *Power Generation Technologies (Third Edition).* Newnes, 33-70.

Brian Chi-ang Lin and Zheng S. (2017) *Environmental Economics and Sustainability,* New York City, United States: John Wiley & Sons

Charlene Marie Becka. (2014) A case study of sulfur dioxide concentrations in Muscatine, Iowa and the ability for AERMOD to predict NAAQS violations. *Civil and Environmental Engineering.* MS (Master of Science): University of Iowa.

Cimorelli AJ, Perry SG, Venkatram A, et al. (2005) AERMOD: A dispersion model for industrial source applications. Part I: General model formulation and boundary layer characterization. *Journal of applied meteorology* 44: 682-693.

Gibson MD, Kundu S and Satish M. (2013) Dispersion model evaluation of PM2.5, NOx and SO2 from point and major line sources in Nova Scotia, Canada using AERMOD Gaussian plume air dispersion model. *Atmospheric Pollution Research* 4: 157-167.

Haradhan Kumar Mohajan. (2018) Acid Rain is a Local Environment Pollution but Global Concern. *Open Science Journal of Analytical Chemistry* 3: 47-55.

Hysenaj M. (2019) Dispersion Model Prospective of Air Pollution in Tirana. *Geographia Technica,* **14** (2), 10-19.

Jittra Nattawut, Pinthong Nattaporn and Thepanondh Sarawut. (2015) Performance Evaluation of AERMOD and CALPUFF Air Dispersion Models in Industrial Complex Area. *Air, Soil and Water Research* 8: 87-95.

Katar Singh. (2007) *Environmental Economics: Theory and Applications* New Delhi: SAGE Publications Pvt. Ltd.

Lazarus BE, Schaberg PG, Hawley GJ, et al. (2006) Landscape-scale spatial patterns of winter injury to red spruce foliage in a year of heavy region-wide injury. *Canadian Journal of Forest Research* 36: 142-152.

Lee HD, Yoo JW, Kang MK, et al. (2014) Evaluation of concentrations and source contribution of PM10 and SO2 emitted from industrial complexes in Ulsan, Korea: Interfacing of the WRF–CALPUFF modeling tools. *Atmospheric Pollution Research* 5: 664-676.

Mr. Khanh T. Tran. (2011) AERMOD Modeling of SO2 Impacts of the Luminant Martin Lake Coal Plant.

PCD. (2001) Ambient air quality standard of Thailand. Pollution Control Department (PCD).

Rood AS. (2014) Performance evaluation of AERMOD, CALPUFF, and legacy air dispersion models using the Winter Validation Tracer Study dataset. *Atmospheric Environment* 89: 707-720.

Thepanondh S, Outapa P and Saikomol S. (2016) Evaluation of dispersion model performance in predicting SO2 concentrations from petroleum refinery complex. 11: 2129-2135.

U.S. EPA. (2004) AERMOD: DESCRIPTION OF MODEL FORMULATION. September 2004 ed.

U.S. EPA. (2008) Learning About Acid Rain: A Teacher's Guide for Grades 6 through 8. April 2008 ed.: U.S. EPA,.

U.S. EPA. (2018) User's Guide for the AERMOD Terrain Preprocessor (AERMAP). April, 2018 ed.: U.S. EPA,.

THE POTENTIAL OF GREEN INFRASTRUCTURE (GI) FOR REDUCING STORMWATER RUNOFF IN A PHNOM PENH NEIGHBORHOOD

Chanrachna NOU[1], Sasima CHAROENKIT[2] ID

ABSTRACT:
Any increase in impervious ground surfaces due to urban growth tends to intensify stormwater management problems. Partial urban flooding can occur any time when the volume of stormwater exceeds local drainage capacity. Phnom Penh has suffered from urban flooding for more than a decade because of the limited capacity of the city's drainage system. Numerous studies have investigated and proposed the use of green infrastructure (GI) as a tool for mitigating flooding due to stormwater runoff. The purpose of this study is to investigate the potential of proposed GI features for reducing stormwater runoff in central Phnom Penh. By using the Rational method, the peak discharge was analyzed and estimated for Tuol Svay Prei Pir, a central Phnom Penh neighborhood that experiences frequent flood problems. The runoff peaks produced by the current practices (S1), and the proposed practices that integrate with the GI features (S2) were compared. The results show that an increase in pervious surface up to 48.14% by implementing the four GI features; trees, bioswales, permeable pavements, and green roofs, the runoff rate will be reduced by 37.90%, which is equivalent to a reduction of 1.55 m^3/s during peak runoff.

Key-words: Green Infrastructure (GI), Stormwater runoff, Rational method, Phnom Penh.

1. INTRODUCTION

Urban growth affects urban hydrology. Dramatic changes in land use in urbanized processes, from a natural landscape covered by vegetation to a built environment, leads to an increase in runoff volume due to larger areas of impermeable surfaces. Increases in urban development have become a major challenge in urban hydrology (Li et al., 2018). Extensive urban impermeable surfaces, particularly the construction of buildings, parking lots, roads, and sidewalks are the result of human activity (Malik et al., 2019). These activities disturb the urban hydrological cycle by reducing infiltration and increasing stormwater runoff. Higher amounts of runoff are likely to contribute to flood damage in urban areas.

Stormwater runoff has become one of the challenges for cities coping with floods. Once the rainfall intensity is greater than the water conductivity of impervious surfaces, urban floods occur because it is difficult for water to percolate into the subsoil. An excess runoff not only provokes urban flooding, but it also results in other environmental problems related to water pollution, local drought conditions and erosion in streams. Accordingly, many cities in the world are adapting themselves to become more resilient to flooding by applying concepts related to sustainable stormwater runoff reduction, such as green infrastructure (GI), low impact development (LID), best management practices (BMPs), sustainable urban drainage systems (SUDS), and water-sensitive urban design (WSUD) (Fletcher et al., 2014). All these concepts share similar principles based on vegetation-based

---

[1]*Naresuan University, Faculty of Architecture, Phitsanulok, Thailand, chanrachnanou@gmail.com;*

[2]*Naresuan University, Faculty of Architecture, Phitsanulok, Thailand, sasimacharoenkit@gmail.com.*

systems to alter urban hydrologic behavior and mitigate the environmental impact of stormwater runoff.

The integration of green infrastructure (GI) is promoted to minimize the drainage burden of cities. A variety of GI features are used to alleviate the negative impacts of extreme precipitation include street trees, bioretention system/rain gardens, permeable pavements, bioswales, the constructing of wetland systems, rainwater harvesting/rain barrels, and green roofs. The capacity of these GI features in absorbing stormwater is determined from the amount of water captured through subsurface infiltration and evapotranspiration rate. In addition, the potential of GI features for the reduction of runoff varies across climate zones. The retention's performance of GI reduce runoff volume by 48%, 67%, 34% when green roofs are applied in London Ontario (humid continental), Calgary Alberta (semi-arid, continental), and Halifax Nova Scotia (humid, maritime), respectively (Sims et al., 2016).

Despite the high rainfall intensity, less than 10 percent of studies were undertaken (Parker & Baro, 2019). Phnom Penh, Cambodia, annually suffers from stormwater runoff issues due to increasing population and urban development occurring on the low-lying areas. Covering an area of 678.47 Km^2 with inadequate stormwater management systems, this city is highly vulnerable to urban flooding. Flood characteristics in Phnom Penh caused by two patterns: Monsoon rains (flood level reaches 1.5 m in some parts during rainy season), and Mekong river floods (with the depth of 12 m between dry and rainy seasons and last for weeks) (Doyle, 2012). Therefore, to reduce flooding problems, GI can be the potential measure integrating with existing drainage systems. This study aims to investigate the potential of GI features for stormwater runoff reduction in central urban area of Phnom Penh.

2.   PERFORMANCES OF GI FEATURES FOR REDUCING STORMWATER RUNOFF

In this study, four GI features including trees, bioswales, permeable pavements and green roofs were selected to be implemented since they are common features of GI networks in several cities worldwide. Trees are basically composed of tree canopies, stems, and tree pits. These components intercept, infiltrate, and evaporate to reduce stormwater runoff and decrease rainfall intensity. Coniferous trees intercept 30% of rainfall more than deciduous trees because of tree properties (leaves, bark, and branches) (Zabret & Šraj, 2015) and the tree canopies can evaporate form 6.5% to 27% of the total rainfall (Kirnbauer et al., 2013). In urban areas, trees and pits could reduce runoff from asphalt with the maximum of 62% (Armson et al., 2013).

Bioswales are vegetated drainage channels designed with underlying engineered soil structures to capture and treat stormwater runoff. Three components of bioswales include vegetation, substrate, and soil. The ability to reduce stormwater runoff of bioswales integrating with engineered soil and trees is up to 88.8% from parking lot in a Mediterranean climate (Xiao & McPherson, 2011), while approximately 48 – 96% of storm events were captured in humid continental climate (Shrestha et al., 2018).

Permeable pavements are typically pervious concretes (PCs) and porous asphalts (PAs). Other types of permeable pavements are block pavers with mixed design material like concrete and plastic; either side joint with fine sand or grasses planted in open surface (e.g. permeable interlocking concrete pavers (PICPs), concrete grid pavers (CGPs), and plastic reinforcement grid pavers (PRGPs).

They reduce runoff through three mechanisms: storage in the subbase, an evaporation of pavement basecourse, and an exfiltration into subgrade soils. The percentage of runoff reduction of porous pavements varied between 45% to 55% for peak discharge and 50% to 60% for runoff volume reduction (Jayasuriya & Kadurupokune, 2010).

Green roofs, due to the depth of substrate, commonly divided into two types: extensive green roofs and intensive green roofs. The extensive green roofs basically have a substrate depth less than 150 mm and more than 150 mm of substrate depth for the intensive green roofs which allow a variety of vegetations to be planted (Uhl & Schiedt, 2008). The typical layers in green roofs; vegetation, substrate, filter fabric, and drainage plate, reduce rainwater through retaining and evaporating. The capacities of rainfall reduced by evapotranspiration for these green roofs were from 49.9% to 57.2% in tropical climates (Viola et al., 2017).

3. METHODOLOGY

3.1. Study area

A neighborhood in the center of Phnom Penh, Tuol Svay Prei Pir (TSPP) (11°33'11.84"N, 104°54'21.21"E) has a total area of 35.80 ha, was selected as our case study, because it has experienced severe flooding for more than a decade, and represents a typical residential area characterized by linked housing and streets as shown in **Fig. 1**. Due to the large impervious surfaces, which accounts to approximately 90 - 95% of the total area, TSPP is usually flooded during heavy rain. The estimated flood depth commonly ranges from $0 – 1$ m (Hong et al., 2016) and lasts between $1.5 – 3.0$ hours. The average annual temperature is 28 ^{0}C, ranging from 17 ^{0}C to 38 ^{0}C, and the average rainfall of 1400 mm annually, and is governed by a monsoon tropical climate, characterized by two major seasons; rainy (May – Oct) and dry (Nov – April) (Thoeun et al., 2014).
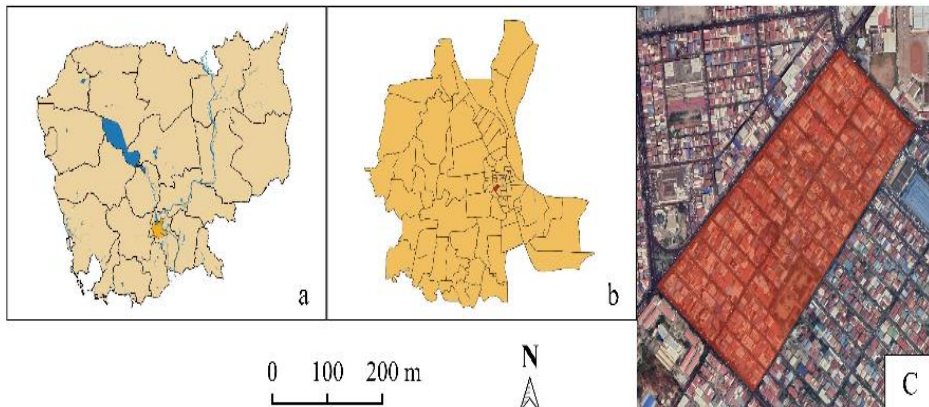
Fig. 1. Cambodia (a), Phnom Penh (b), and study area: Tuol Svay Prei Pir (c) *(Source: Open Development Cambodia, ODC)*

3.2 Overall framework

The investigation of GI's performance in this study was conducted by comparing runoff peaks between two scenarios. Scenario 1 (S1) referred to the existing practices without GI implementation, named as non-GI. Scenario 2 (S2) referred to the proposed practices in which GI features are integrated as illustrated in **Fig. 2**.
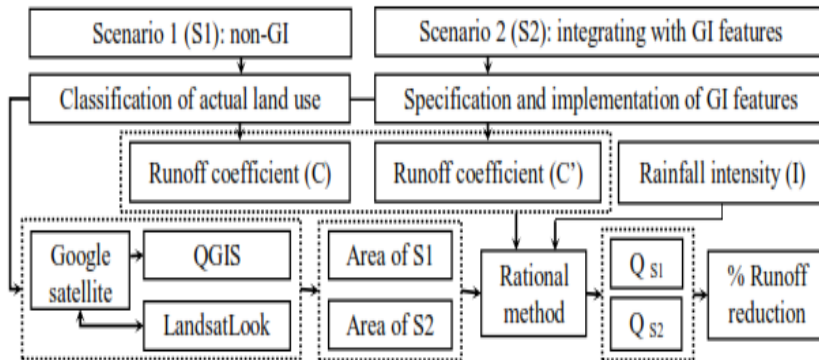
Fig. 2. Overall framework for quantifying the percentages reduction of stormwater runoff.

We want to note that the idea of scenarios is not new in hydrology. Haidu *et al*. (2017) developed a GIS module in order to elaborate stormwater runoff scenarios for different hypothetical storms.

3.2. Scenario 1 (non-GI)

3.2.1.   Land use/cover classification

Land use/cover classification of the study area was obtained by using QGIS version 3.4 with an overlay of Google satellite, which was confirmed by LandsatLook, made by USGS (2019) for achieving clearer views.

The impervious and pervious surfaces of the study area were further identified by using Google earth pro to determine the land cover types. Houses/buildings, paths, parking lots, campuses, sidewalks, roads, boulevards, and bare land were classified as impervious surfaces, while pervious surfaces were referred to those areas covered by tree canopies and grasses.

3.2.2.   Runoff coefficient (C)

There are many manuals, articles and references for equivalent runoff coefficient formulas, that can be used in the rational method (Costea, 2013; Győri *et al*., 2016; Haidu & Ivan, 2016; Voda *et al*., 2018).

In scenario 1, the selection of C values for each part of land covered is based on the Hydraulic Design Manual of Texas Department of Transport (Garcia, 2016). Some of the C values of the land covers that appear in scenario 1 are identical to the ones mentioned in the design manual. Therefore, C of similar land covers were selected and determined by their mean values, as shown in **Table 1**.

<div align="center">**Runoff coefficient (C) of actual land covers**</div>

<div align="center">*(source: Garcia, 2016: chapter 4: Hydrology, section 12— Rational method, p. 4-53 & 4-54).*</div>

Land use/cover		Runoff coefficient (C)	
		From mentioned hydraulic design manual	This study
Trees: tree canopies	Over impervious concrete	$C_{\text{unimproved area (steep grassed slopes)}} = 0.70$ $C_{\text{streets (concrete)}} = 0.90\text{ - }0.95$	0.8125
	Over impermeable pavers	$C_{\text{unimproved area (steep grassed slopes)}} = 0.70$ $C_{\text{streets (drives and walks)}} = 0.75\text{ - }0.95$	0.775
	Over impervious asphalt	$C_{\text{unimproved area (steep grassed slopes)}} = 0.70$ $C_{\text{streets (asphalt)}} = 0.85\text{ - }0.95$	0.80
Parks	Grass	$C_{\text{lawn (sandy soil, flat 2\%)}} = 0.05\text{ - }0.10$	0.075
Houses/buildings	Sloped roofs	$C_{\text{roofs}} = 0.75\text{ - }0.95$	0.95
	Flat roofs		0.75
Paths/campuses/ parking lots/bare lands	Impervious concrete	$C_{\text{streets (concrete)}} = 0.90\text{ - }0.95$	0.925
Sidewalks	Impermeable pavers	$C_{\text{streets (drives and walks)}} = 0.75\text{ - }0.95$	0.85
Roads/boulevards	Impervious asphalt	$C_{\text{streets (asphalt)}} = 0.85\text{ - }0.95$	0.90

3.3. Scenario 2 (integrating with GI features)

3.3.1.   Specification of GI features

Trees are mainly grown on/near sidewalks, parking lots (alone or in bioswales), and roadways. In this study, sidewalks are divided into two types: one-side along boulevards with 4 - 6 m wide and two-side along roads, which are 2 m, 2.5 m, 4 m, 6 m wide (measured by calculating the existing tiles through Google Earth Pro, street view). Therefore, the sizes of pits were 4 m^2 for one-side along boulevards and 1 m^2 for two-side along roads and were placed 8 m from each on sidewalks. The average radius of street trees canopies ranges from 1.8 -5.2 m (Pretzsch et al., 2015). Hence, 1.8 m and 3 m of tree canopies radius are applied on one-side along the boulevards and two-sides along roads in term of sidewalks' width. In these values, the tree canopies may cover sidewalks, roads, and boulevards. We assumed that tree canopies cover over roads and boulevards with one-third and two-thirds of total tree canopies, respectively.

Bioswales are suitable for implementing alongside streets/roadsides, residential roadways and on parking lots. In this study, the width of boulevards measured in QGIS, with an overlay of Google satellite, were between 18-20 m for four lanes, and the four boundaries were in the middle of boulevards and roads (**Fig. 1 (c)**). Thus, the bioswales with a half width of 2.4 m can be replaced an existing concrete median barrier on boulevards since the width of each traffic lane on residential streets must be at least 3.35 m (MacAdam, 2012). The other land use such as paths, campus, and parking lots are not applicable for bioswales because they were too narrow. **Table 2** summarizes GI features applied for the study area.

Permeable pavements are commonly installed in pedestrian areas/sidewalks, low volume roads, and parking areas. Here, the replacement of permeable pavements was based on the existing surfaces. For example, impervious concrete/asphalt and impermeable pavers were replaced by pervious concrete/porous asphalt and permeable pavers, respectively.

Specification of GI features on actual land use/cover, *(*) no GI features.*

S1		S2	
Land use	Land covers	GI features	Specification
Houses/buildings	Sloped roofs	*	*
	Flat roofs	Green roofs	Fully covered
Two sides of sidewalks along roads	Tree canopies over impermeable pavers	Tree canopies over permeable pavers	Tree canopies radius = 1.8 m Two-third of tree canopies
	No pits	Pits	1 m^2, placed 8 m each
	Impermeable pavers	Permeable pavers	Area without pits and tree canopies area
One side of sidewalks along boulevards	Tree canopies over impermeable pavers	Tree canopies over permeable pavers	Tree canopies radius = 3 m Two-thirds of tree canopies
	No pits	Pits	4 m^2, placed 8 m each
	Impermeable pavers	Permeable pavers	Area without pits and tree canopies area
Boulevards	Impervious asphalt	Porous asphalt	Area without bioswale and tree canopies area
		Bioswales	1.2 m wide
	Tree canopies over impervious asphalt	Tree canopies over boulevards	One-third of total tree canopies
Roads	Impervious asphalt	Porous asphalt	Area without tree canopies
	Tree canopies over impervious asphalt	Tree canopies over porous asphalt	One-third of tree canopies
Parks	Grass	*	*
Paths, campus, parking lots, and bare land	Tree canopies	*	*
	Impervious concrete	Pervious concrete	Fully covered

To facilitate water flow, the slope of the extensive green roof should be limited up to 45^0 and 10^0 for intensive green roofs (Mentens et al., 2006). Particularly, green roofs are applied on only flat roofs due to a difficulty to identify the degree of sloped roofs in this study. Some land uses/covers remain the same according to the specification designs of GI features.

3.3.2. *Runoff coefficient (C') of GI features*

Runoff coefficient (C') of GI features were acquired from other literatures and determined by mean values of each features as illustrated in **Table 3**.

3.4. Rational method

Rational method was originally proposed by Mulvany (1850). It is used to calculate peak rate runoff in urban or suburban watershed and it is suitable for calculating runoff peak in urban and suburban area with drainage areas less than 80 ha.

$$Q = \frac{1}{360} \, CIA \quad \text{(S.I unit)} \tag{1}$$

where,

Q = maximum rate of runoff (m³/sec.);   I= average rainfall intensity (mm/hr.);

C = runoff coefficient;   A = drainage area (ha).

Then,

$$\% \, Runoff \; reduction = \frac{Q_{S1} - Q_{S2}}{Q_{S1}} \tag{2}$$

The average rainfall intensity (I) is constant while runoff coefficient (C) and drainage area (A) are variables. Due to a lack of data of design rainfall intensity (I), this study used (I) that acquired from Pochentong meteorological station in Phnom Penh *(JICA, 2016)*. Hence, a 2-year storm return period, equals to 44.8 mm/h, was used to input in (1).

Table 3.

Runoff coefficient (C') of GI features.

Scenario 2		Runoff coefficient (C')	
GI features		From other studies	This study
Trees: tree canopies	Over pits	C $_{trees}$ = 0.20 – 0.26 (Armson et al., 2013)	0.23
	Over permeable pavers	C $_{trees}$ = 0.20 – 0.26 (Armson et al., 2013) C $_{Block\ pavers}$ = 0.20 - 0.50 (Hunt et al., 2002) C $_{Plastic\ grid\ pavers}$ = 0 – 0.26 (Dreelin et al., 2006)	0.47
	Over porous asphalt	C $_{trees}$ = 0.20 – 0.26 (Armson et al., 2013) C $_{porous\ asphalt}$ = 0.23 (NYC, 2012)	0.465
	Over pervious concrete	C $_{trees}$ = 0.20 – 0.26 (Armson et al., 2013) C $_{pervious\ concrete}$ = 0.20 (Dietz, 2007)	0.45
Bioswales		C $_{bioswales}$ = 0 – 0.06 (Xiao & McPherson, 2011) and 0.227 (Sun et al., 2014)	0.13
Permeable pavements	Porous asphalt	C $_{porous\ asphalt}$ = 0.23 (NYC, 2012)	0.23
	Pervious concrete	C $_{pervious\ concrete}$ = 0.20 (Dietz, 2007)	0.2
	Permeable pavers	C $_{block\ pavers}$ = 0.20 - 0.50 (Hunt et al., 2002) C $_{plastic\ grid\ pavers}$ = 0 – 0.26 (Dreelin et al., 2006)	0.24
Green roofs		C $_{green\ roofs}$ = 0 - 0.44 (Pimentel-Rodrigues & Silva-Afonso, 2017) and 0.19 - 0.39 (Uhl & Schiedt, 2008)	0.255

4. RESULT AND DISCUSSION

4.1. Area and ratio of actual land use/cover

With a total area of 35.80 ha, TSPP is divided into houses/buildings, transports, and the other areas are parks, paths, campuses, parking lots, and bare lands for 57.43% (20.56 ha), 33.83% (12.11 ha), 8.74% (3.13 ha), respectively, as shown in **Fig. 3 (a)**.

4.2. Implementation of GI features on actual land use

Land covers on actual land use are changed after applying GI features as shown in **Fig. 3 (b)**. **Table 4** illustrates the area and ratio change between S1 and S2. The ratio of tree canopies is high, ranges from 163% - 250%, after trees are planted every 8 m on sidewalks. In total, 1,668 trees (and pits) are placed on sidewalks, 189 trees on one-side along

boulevards and 1,479 trees on two-side along roads. Furthermore, the ratio changes of permeable pavements in S2 is lower than S1 because plenty of trees were implemented on sidewalks. Bioswales as well as green roofs are new features (100% change), in this study area.
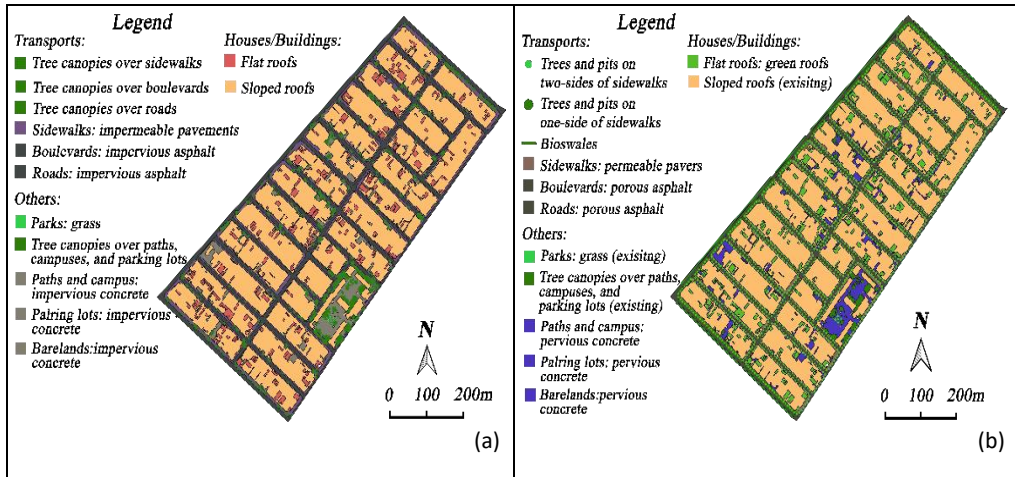
Fig. 3. Land use/cover: scenario 1 (a), scenario 2 (b).

Table 4.

Area and ratio changes between S1 and S2, *(*) no GI features.*

S 1			S 2		Changed (%)
Land use/cover		Area (ha)	Land cover	Area (ha)	
Houses/buildings	Sloped roofs	18.55	*	*	0
	Flat roofs	2.01	Green roofs	2.01	100
Sidewalks	Impermeable pavers	6.35	Permeable pavers	5.18	82
Roads/boulevards	Impervious asphalt	5.75	Porous asphalt	5.31	92
			Bioswale	0.18	100
Park	Grass	0.01	*	*	0
Trees	Tree canopies over impervious concrete	0.46	Tree canopies over pervious concrete	0.75	163
	Tree canopies over impermeable pavers	0.63	Tree canopies over permeable pavers	1.58	250
	Tree canopies over impervious asphalt	0.34	Tree canopies over porous asphalt	0.60	176
			Tree pits	0.22	100
The others	Impervious concrete	1.69	Pervious concrete	1.40	83

Tab. 5 shows the total area and ratio of each GI features in S2. It is obvious that permeable pavements have the highest ratio (34.03%) comparing to the other features. The ratio of bioswales is minor (0.51%) and this may be due to the limited space available in the area.

Table 5.

Area and ratio of GI features in S 2.

GI features	Trees (pits and canopies)	Bioswales	Permeable pavements	Green roofs
Area (ha)	2.86	0.18	12.18	2.01
Ratio (%)	8	0.51	34.03	5.61

4.3. Runoff reduction

The results attained from a quantification of peak runoff using Rational method are shown in **Table 6**. Peak runoff in S1 in 2-year return period is 4.09 m^3/s. This value was similar to those computed by Heng et al. (2016) who quantified peak runoff rate of 1.42 – 5.36 m^3/s on a catchment next to ours (in the same district) (Heng et al., 2017). It can be observed that land use/cover type as well as urbanization reflecting a high-density residential area which tended to large runoff volumes. Meanwhile, a significant increase in pervious surface from 4.17% to 48.14%, approximately decreased 1.55 m^3/s of peak runoff and yielded a reduction of 37.90% of stormwater runoff peaks by using trees, bioswales, permeable pavements, and green roofs with a ratio of 8%, 0.51%, 34.03%, and 5.61%, respectively.

Table 6.

The runoff reduction after the implementation of GI features.

Scenario		Ratio (%)	Q (m^3/s)	Q reduction (m^3/s)	Runoff reduction (%)
S1	Pervious	4.17	0.27	1.55	37.90
	Impervious	95.83	3.81		
S2	Pervious	48.14	0.57		
	Impervious	51.86	1.96		

The percentage of stormwater runoff reduction reported here is larger than in previous studies. A study of US cities which have a diversity of climate zones, presents lower runoff reduction rates which varied between 18 - 29% after implementing swales/infiltration (12%), bioretention (23%), and green roof (33%) (Sarkar et al., 2018). This rate can be expected because of a mean reduction of 11 locations with different climates, rather than an individual location (as with this study).

5. CONCLUSION

The aim of this study is to investigate the potential of proposed GI features for reducing stormwater runoff in central Phnom Penh. By using Rational method, the runoff peaks were estimated for Tuol Svay Prei Pir (TSPP), a central Phnom Penh neighborhood. The runoff peaks produced by the current practice (S1), and the proposed practices that integrate with the GI features (S2) were compared. The total runoff reduction was 37.90%, which is the equivalent to a reduction of 1.55 m^3/s during peak excess, due to an increase in pervious surfaces up to 48.14% of total area. Permeable pavements are the most effective feature in this study as they account for one-third (34.03%) of the total area, followed by green roofs (5.61%), trees (8%), and bioswales (0.51%), which demonstrate that GI features

are effective in the reduction of stormwater. These features can be applied to all existing developments and integrated into new ones for urban flood control and storm water management planning. Our future research will investigate the potential of using the GI features in commercial and service zones and mixed land areas for runoff reduction.

Land cover changes have significant influences on urban hydrology, especially discharge, and surface runoff. The value of runoff coefficients (C and C') used in this study were derived from other literatures. To achieve more accurate values, runoff coefficients derived from site surveys, such as the slope of the land and its uses, and the soil types need to be considered.

Climate regions alter the quantity of the total runoff reduction performed by GI features. For example, the capacity of rainwater reduced by green roofs was estimated according to the value of rainfall and potential evapotranspiration. What is obvious is annual rainfall is high in a tropical monsoon climate; the runoff volume would be high after heavy daily rainfall. Therefore, throughout evapotranspiration (potentially, high evaporation in rainy season), GI features may perform better when they are properly implemented in a tropical climate, subject to soil depth.

This study proposes GI assessment and implementation regarding stormwater runoff reduction, as well as enhancing esthetics and the ecosystem. The construction of GI as a retrofit can be difficult, but it is accomplishable, and will influences private and public participation willingness. Our suggestions on these matters, particularly in Phnom Penh are:

a. Green roofs would be more promotable in such residential areas if sloped roofs were modified (Rachmansyah et al., 2019). so that runoff could be reduced more than the recent results. On an individual level, citizens need to collaborate for GI spatial benefits.
b. Once sidewalks are reorganized to be pedestrian-friendly (recently used for illegal parking and commercial activities), there would be opportunities to install bioswales along both sides of sidewalks, according to national regulations.

REFERENCES

Armson, D., Stringer, P., & Ennos, A. R. (2013). The effect of street trees and amenity grass on urban surface water runoff in Manchester, UK. *Urban Forestry & Urban Greening, ***12**(3), 282-286. doi:10.1016/j.ufug.2013.04.001

Costea, G. (2013). Deforestation process consequences upon surface runoff coefficients. Catchment level case study from the Apuseni mountains, Romania. *Geographia Technica*, **8**(1), 28-33.

Dietz, M. E. (2007). Low Impact Development Practices: A Review of Current Research and Recommendations for Future Directions. *Water, Air, and Soil Pollution, ***186**(1-4), 351-363. doi:10.1007/s11270-007-9484-z

Doyle, S. E. (2012). City of water: architecture, urbanism and the floods of Phnom Penh. Nakhara Journal of Environmental Design and Planning.

Dreelin, E. A., Fowler, L., & Ronald Carroll, C. (2006). A test of porous pavement effectiveness on clay soils during natural storm events. *Water Res, ***40**(4), 799-805. doi:https://doi.org/10.1016/j.watres.2005.12.002

Garcia, R. (2016). *Hydraulic Design Manual*.

Gyori, M.M., Haidu, I. & Humbert, J. (2016)**.** Deriving the floodplain in rural areas for high exceedance Probability Having Limited Data Source. *Environmental Engineering and Management Journal*, **15**(8), 1879-1887.

Haidu, I., & Ivan, K. (2016). Évolution du ruissellement et du volume d'eau ruisselé en surface urbaine. Étude de cas: Bordeaux 1984-2014, France. *La Houille Blanche*, **5**, 51-56.

Haidu, I., Batelaan, O., Crăciun, A.I., & Domnița, M. (2017). GIS module for the estimation of the hillslope torrential peak flow. *Environmental Engineering and Management Journal*, **16**(5), 1137-1144.

Heng, S., Hong, P., & Ly, S. (2017). *Assessment of an Urban Drainage System in Phnom Penh Using Storm Water Management Model*. Paper presented at the THA 2017 International Conference on "Water Management and Climate Change Towards Asia's Water-Energy-Food Nexus", Bangkok, Thailand.

Hong, V., Ly, S., & Heng, S. (2016). *Application of MIKE FLOOD Model to simulate inundation map in Phnom Penh*. Paper presented at the Proceedings of the Second Seminar Urban Water Resource Management (JSPS Core-to-Core Program), Tokyo, Japan.

Hunt, B., Stevens, S., & Mayes, D. (2002). *Permeable pavement use and research at two sites in Eastern North Carolina*.

Jayasuriya, N., & Kadurupokune, N. (2010). *Comparative performance of permeable and porous pavements*. Paper presented at the International Conference on Sustainable Built Environment (ICSBE-2010), Kandy, Sri Lanka.

JICA (2016). The study on drainage and sewerage improvement project in Phnom Penh metropolitan area (Vol. Final report).

Kirnbauer, M. C., Baetz, B. W., & Kenney, W. A. (2013). Estimating the stormwater attenuation benefits derived from planting four monoculture species of deciduous trees on vacant and underutilized urban land parcels. *Urban Forestry & Urban Greening,* **12**(3), 401-407. doi:10.1016/j.ufug.2013.03.003

Li, C., Liu, M., Hu, Y., Shi, T., Qu, X., & Walter, M. T. (2018). Effects of urbanization on direct runoff characteristics in urban functional zones. *Sci Total Environ,* **643**, 301-311. doi:10.1016/j.scitotenv.2018.06.211

MacAdam, J. (2012). Green Infrastructure for Southwestern Neighborhoods. In J. D. Tory Syracuse, Karilyn Roach (Ed.): Watershed Management Group.

Malik, I. B. I., Suparta, W., & Dewancker, B. J. (2019). A Study of Population Density in Developing Countries. *Geographia Technica, 14*(Special Issue), 201-212. doi:10.21163/GT_2019.

Mentens, J., Raes, D., & Hermy, M. (2006). Green roofs as a tool for solving the rainwater runoff problem in the urbanized 21st century? *Landscape and Urban Planning, 77*(3), 217-226. doi:10.1016/j.landurbplan.2005.02.010

NYC, E. P. (2012). *Green Infrastructure Pilot Monitoring Report*. Retrieved from NYC Environmental Protection

Parker, J., & Zingoni de Baro, M. E. (2019). Green Infrastructure in the Urban Environment: A Systematic Quantitative Review. *Sustainability, 11*(11), 3182. doi:10.3390/su11113182

Pimentel-Rodrigues, C., & Silva-Afonso, A. (2017). Determination of Runoff Coefficients with a View to Integration of Green Roofs with Rainwater Harvesting Systems. *International Journal of Environmental Science, 2*, 366-372.

Pretzsch, H., Biber, P., Uhl, E., Dahlhausen, J., Rötzer, T., Caldentey, J., . . . Pauleit, S. (2015). Crown size and growing space requirement of common tree species in urban centres, parks, and forests. *Urban Forestry & Urban Greening, 14*(3), 466-479. doi:10.1016/j.ufug.2015.04.006

Rachmansyah, A., Halim, L. F., & Soemarno. (2019). Sustainable Development Approach to Residential Planning in the Rapid Growth Urban Area: A Case Study in Singosari District, Malang Region, East Java Province. *Geographia Technica, 14*(Special), 3-12. doi:10.21163/GT_2019.

Sarkar, S., Butcher, J. B., Johnson, T. E., & Clark, C. M. (2018). Simulated Sensitivity of Urban Green Infrastructure Practices to Climate Change. *Earth Interact, 22*(13), 1-37. doi:10.1175/EI-D-17-0015.1

Shrestha, P., Hurley, S. E., & Wemple, B. C. (2018). Effects of different soil media, vegetation, and hydrologic treatments on nutrient and sediment removal in roadside bioretention systems. *Ecological Engineering,* **112**, 116-131. doi:10.1016/j.ecoleng.2017.12.004

Sims, A. W., Robinson, C. E., Smart, C. C., Voogt, J. A., Hay, G. J., Lundholm, J. T., O'Carroll, D. M. (2016). Retention performance of green roofs in three different climate regions. *Journal of Hydrology,* **542**, 115-124. doi:10.1016/j.jhydrol.2016.08.055

Sun, Y.-w., Li, Q.-y., Liu, L., Xu, C.-d., & Liu, Z.-p. (2014). Hydrological simulation approaches for BMPs and LID practices in highly urbanized area and development of hydrological performance indicator system. *Water Science and Engineering,* **7**(2). doi:10.3882/j.issn.1674-2370.2014.02.003

Thoeun, H., Sivakumar, M., & Dube, O. (2014). Observed and projected Changes in temperature and rainfall in Cambodia. *Weather and Climate Extremes,* **131**. doi:10.1016/j.wace.2015.02.001

Uhl, M., & Schiedt, L. (2008). Green roof storm water retention–monitoring results.

Viola, F., Hellies, M., & Deidda, R. (2017). Retention performance of green roofs in representative climates worldwide. *Journal of Hydrology, 553*, 763-772. doi:10.1016/j.jhydrol.2017.08.033

Voda, A.I., Şarpe, C.A. & Voda, M. (2018). Methods of maximum discharge computation in ungauged river basins. Review of procedures in Romania. *Geographia Technica*, **13**(1), 130-137.

Xiao, Q., & McPherson, E. G. (2011). Performance of engineered soil and trees in a parking lot bioswale. *Urban Water Journal,* **8**(4), 241-253. doi:10.1080/1573062X.2011.596213

Zabret, K., & Šraj, M. (2015). Can Urban Trees Reduce the Impact of Climate Change on Storm Runoff? *Urbani Izziv,* **26**, S165-S178.

LAND SUITABILITY FOR RICE FIELD AND CONSERVATION PLANNING IN HO WATERSHED, TABANAN REGENCY, BALI PROVINCE, INDONESIA

Ni Made TRIGUNASIH[1] , *Putu Perdana Kusuma WIGUNA[2]*

ABSTRACT:
This study aims to determine the actual extent of land use in the Ho watershed, to determine the suitability of paddy fields and their limiting factors and provide direction for land use in the Ho watershed of Tabanan Regency. Land characteristics as a determinant of land suitability observed include: annual mean temperature, water availability; rooting media; availability of oxygen; nutrient retention, CEC, BS, pH, and organic matter; nutrients available; erosion; flood hazard; land preparation. Land suitability assessment is done by matching the quality of the land with the requirements for growing rice. The results showed that the actual land suitability for rice field was classified as not suitable (N) and marginal suitable (S3) with limiting factors: erosion hazard (slope and erosion hazard) and nutrient availability (P-available). Potential land suitability for rice field is classified as very suitable (S1) to marginal suitable (S3) with temperature limiting factors and erosion (slope) hazards. Efforts to improve must be done by adding P fertilizer to areas classified as very low soil Potasium content and maintenance of terraces, especially rice fields with a slope of> 8% to overcome/prevent erosion and landslides.

Key-words: Land suitability, land characteristics, conservation planning

1. INTRODUCTION

Properly mapping agricultural land suitability is needed to manage current and future agricultural land use, and for decision makers to develop strategies for sustainable use of land resources (Li et al., 2017). There is a long history of establishing what soils are capable of (FAO, 1976), which is often described as land suitability. The occurrence of land conversion from forest land use, especially in the upstream area, into agricultural land or other uses causes a decrease in the catchment area as an effective area capable of infiltrating rainwater into the ground. The decrease in rainwater infiltration causes water reserves that can be used as water sources in the dry season to be reduced (McBratney & Field, 2015). In addition, increasing population and high economic pressures in upstream communities have led to the conversion use of land resources without regard to land suitability. The Ho Watershed is located in Tabanan Regency, Bali Province, Indonesia, as one of the largest watershed in Bali Province with total area with an area of 15,367.65 ha. The Ho Watershed consists of various landuses, namely, plantations (6117.63 ha), rice fields (4,529.15 ha), forests (2,213.31 ha), rain-fed rice fields (1,022.75 ha), settlements (894.44 ha), dry land (392.06 ha), bush (98.44 ha), water bodies such (97.80 ha) and pasture (2.05 ha). This watershed is also influenced by climate change phenomena (Suparta & Yatim, 2019).

[1]*Udayana University, Faculty of Agriculture, Kampus Bukit Jimbaran, Badung, Bali. 80361, Indonesia. trigunasih@unud.ac.id;*

[2]*Udayana University, Faculty of Agriculture, Kampus Bukit Jimbaran, Badung, Bali. 80361, Indonesia. wiguna@unud.ac.id.*

As one of the largest landuse in Ho watershed, and as the producer of rice, staple food for Indonesia people, the management of rice fields in Ho watershed must meet the principles of land suitability and soil and water conservation to avoid problems in near future. The problems that potentially occur in the Ho watershed are increased erosion which can cause siltation and silting of reservoirs, rivers, canals and other water bodies in the downstream of the watershed. This problem can have implications on decreasing water quality and reducing the potential of water resources, both surface water, springs and ground water. The accumulation of all these problems will lead to the emergence of new environmental problems such as flooding and drought. Erosion that occurs in the upstream area can further reduce the quality of land resources, loss of fertile soil layers, loss of nutrients, damage to soil structure, increased use of energy for production, deterioration of soil productivity, impoverishment of smallholder farmers, reduced alternative land use and others (Arsyad, 2010). Outside the erosion site, especially in the downstream areas of the watershed, there will be siltation and silting of reservoirs, rivers and drainage channels, accumulation of fertile agricultural land, loss of springs and deteriorating water quality, damage to aquatic ecosystems, increased frequency and periods of drought, shortened reservoir life, and increased frequency of flooding (Scholten & Seitz, 2019).

For this reason, in order to improve the welfare of the farming community in the Ho watershed, landuse in the Ho Watershed must be in accordance with the suitability of the land and its management must meet the principles of soil and water conservation. Therefore it is necessary to conduct research on "Land Suitability for Rice Fields and Conservation Planning in the Ho Watershed, Tabanan Regency".

2. STUDY AREA AND DATA

The access to agricultural fields represents the main factor which favors their spatial distribution and their mechanized exploitation (Bilasco *et al.*, 2018). The research is carried out in the Ho Watershed, Tabanan. Administratively the Ho watershed is located in two sub-districts in Tabanan Regency, Bali Provnce, Indonesia, namely Kerambitan sub-district and Penebel sub-district. Astronomically, the Ho Watershed is located at position 115º 01 '26.3 "- 115º 09' 04.9" East and 8º 16 '30.2 "- 8º 34' 03.7" South. The map of Ho watershed are presented in **Fig. 1**.

Fig. 1. Research location, Ho watershed.

The data on land characteristics observed in the field survey are physical characteristics of the soil which include texture, drainage, erosion, and effective root depth, as well as physiographic conditions namely height and slope. Soil analysis to determine soil chemical content includes CEC, BS, C-Organic, N-Total, P- Available, K- Available, salinity, and pH. Data were collected primarily by measurement in the field and secondary by literature studies and maps. This research is conducted through land suitability and soil conservation approaches. This activity consists of a series of activities which include the collection and evaluation of secondary data, surveys, data analysis, and field tests.

3. METHODOLOGY

This research was conducted through land suitability and soil conservation approaches. This activity consists of the collection and evaluation of primary data, secondary data, surveys, data analysis, laboratory analysis and field tests. Primary data and secondary data collections are shown in **Table 1**.

Table 1.
Primary Data and Secondary Data Collection.

No.	Primary Data	Source	No.	Secondary Data	Source
1	Land Unit Map	slope map, climate map, soil type maps and rice fields, field surveys	1	Bali Geological Map,	Geospatial Information Agency of Indonesia (BIG)
2	Land suitability for rice field	Overlay of land suitability factors, field surveys, laboratory analysis	2	Bali Soil Type Map,	Geospatial Information Agency of Indonesia (BIG)
3	Limiting factors for land suitability	Overlay of land suitability factors, field surveys, laboratory analysis	3	RBI Maps of Bali	Geospatial Information Agency of Indonesia (BIG)
			4	Quickbird satellite imagery of Tabanan Regency	Geospatial Information Agency of Indonesia (BIG)
			5	Rainfall and Climatology data	Meteorological and Geophysical Agency of Bali

Definition of criteria affecting the land suitability is one of the most important parts of land evaluation (Arisanti et al., 2019). Before physical data collection activities are carried out in the field, detailed land units are delineated from overlaying slope map, climate map, soil type maps and ricefields map. Land unit map functions to direct sampling in the field. Each land unit then sampled proportionally to its area. Sampling is done by transect in a sloped area and with a grid system in a flat area to the rice fields. Soil samples are taken in layers at a depth of 0 - 30 cm, whereas to determine the effective depth is continued up to a

depth of 150 cm for soils classified as deep or until lytic contact in shallow soils. All data taken from the sampling results are then evaluated in the field, to obtain representative samples. Each soil sample then analyzed in the laboratory to determine the characteristics of the soil. The characteristics of the soil to be analyzed are Soil texture, Organic C, N-Total, P- available, K- available, Cation Exchange Capacity (CEC), Base Saturation (BS), soil pH, and salinity. Land suitability analysis is calculated by comparing the requirements of growing rice field with the characteristics of existing land. The level of land suitability analysis to be used in this study is unit level.

4. RESULTS AND DISCUSSIONS

4.1. Land Unit and Land Characteristics

Detailed land units are delineated from overlaying slope map, climate map, soil type maps and rice fields map, as its function to create sampling in the field. Each land unit then sampled proportionally to its area. All data taken from the sampling results are evaluated in the field, then analyzed in the laboratory. Based on the overall process using Geographic Information Systems tool, there are six land unit and six samples to analyze. **Table 2** shows the land unit of Ho Waterhed. **Fig. 2** shows the land unit map of Ho Watershed.

Table 2.
Land Unit of Ho Waterhed.

Land Unit	Main material	Physiography	Topography	Soil Type	Slope	Landuse
SLH I	Intermediary Volkan Ash	Beach Ridge	Flat,	Grayish Brown Regosol	0-8 %	Agricultural
SLH II	Ash and Intermediary Volkan Tuff	Volcanic	Wavy until hilly	Yellowish Brown Latosol	0-8 %	Agricultural
SLH III	Ash and Intermediary Volkan Tuff	Volcanic	Wavy until hilly	Yellowish Brown Latosol	8-15 %	Agricultural
SLH IV	Ash and Intermediary Volkan Tuff	Volcanic	Wavy until hilly	Yellowish Brown Latosol	15-25 %	Agricultural
SLH V	Ash and Intermediary Volkan Tuff	Volcanic	Wavy until hilly	Yellowish Brown Latosol	25-40 %	Agricultural
SLH VI	Ash and Intermediary Volkan Tuff	Volcanic	Wavy until hilly	Grayish Brown Regosol	25-40 %	Agricultural

The characteristics/ quality data of ricefields located in Ho Watershed shows that the physical properties of the analyzed soil are soil texture dominated by a rather fine texture (clayey clay and clay), medium texture (clay). Drainage conditions are ranged from rather poor (ABr) to bad (Br). Coarse material, and surface rocks are found in the rice fields located in the upper reaches of the Yeh Ho watershed, which are located in the land units II and III in Mangesta Village and Penatahan Village, Penebel District. Rock outcrops are not found in all irrigated rice fields in the Ho Watershed.The slope of the study site ranges from

2% (flat) to> 45% (steep). Chemical properties and soil fertility including soil pH ranges from slightly acidic to neutral, salinity levels range from low to very high, C-organic ranges from very low to high, Soil CEC varies from moderate (21.79 me/100g) to high (30.59 me/100g), base saturation ranges from moderate (46.15%) to very high (107.21%). N-total is classified as low (0.18%) to moderate (0.35%), P-available is classified as very low (1.38 ppm), to high (10.03 ppm); and K-available is high (120.58 mg/100g) very high (334.08 mg/100g).
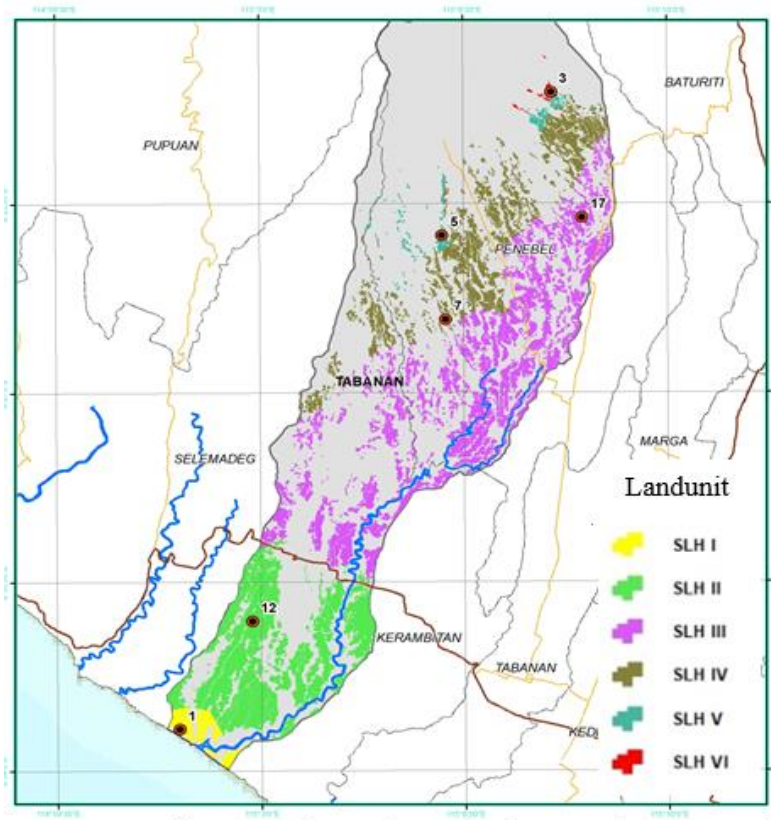
Fig. 2 Land Unit Map of Ho Watershed.

Based on agro-climate data which includes annual mean temperature, rainfall is taken from the Meteorology Climatology and Geophysics Agency of the Central Tabanan Region. Average annual temperatures range from 21.5-28.9 0C, humidity ranges from 58-82%, and annual average rainfall ranges from 1000 mm - 2000 mm. The Bali Geological Map data, the Yeh Ho watershed has soil types that are dominated by Yellowish Brown Latosol soil types, then followed by the Regosol Brown Gray and Andosol Brown Gray soils. The topography of the area in the Ho watershed is dominated by the form of a undulating to hilly area, then followed by the shape of the hilly to mountainous area in the upstream area of the Yeh Ho watershed, as well as the flat area form in the downstream area of the Ho watershed.

4.2. Actual Land Suitability

Soil and land suitability analysis is very important to identify potential agricultural areas (Rostaminia & Rahmani, 2019). Actual land suitability is land suitability based on data on the biophysical nature of the land or land resources before the land is given input input needed to overcome obstacles. The biophysical data in the form of soil and climate characteristics are related to the growth requirements of the plants being evaluated. The results of the actual land suitability assessment are assessed from matching between the quality/characteristics of the land with the conditions for growing rice, then the suitability class of ricefields can be determined. Based on the assessment of actual land suitability for rice field, the results are not suitable class (N) in SHL III (Mengesta Village), SHL IV (Penatahan village), SHL V (Wangaya Gede Village) and SLH VI (Jatiluih Village). Marginally suitable class (S3) found in SHL I (Beraban Village) and SHL II (Tangguntiti Village). The suitability of the actual land for ricefields in the Ho Watershed are affected with limiting factors in erosion hazardous land quality, namely slope characteristics and erosion hazard, nutrient availability, especially namely P-available characteristics.

4.3. Potential Land Suitability

The actual land suitability for rife fields in the Ho Watershed are classified as not suitable (N) and marginally suitable (S3) with the limiting factors are erosion hazard and land quality ie slope characteristics, erosion hazards, and soil nutrient namely P-available characteristics. By improving the limiting factors so that the actual land suitability can be increased to become the potential land suitability. The potential and actual land suitability in rice fields in the Ho Watershed is presented in **Table 3**.

Table 3.

Actual and Potential Land Suitability for Ho Watershed.

Land Unit/ Samples	Location (Village)	Agro ecosystem Land Suitability				Coordinate UTM
		Rice Field Suitability				
		Actual	Limiting factor	Potential	Limiting factor	
1	Beraban	S3eh2, na2	Hazad Erosion and P-available	S1	-	282804; 9053915
2	Tangguntiti	S3na2	P- available	S1	-	285086; 9057612
3	Mengesta	Neh1	slope	S3tc, eh1	Temperature, slope	295457; 9071430
4	Penatahan	Neh1	slope	S3, eh1	slope	291162; 9067927
5	Wangaya Gede	Neh1	slope	S3tc, eh1	Temperature, slope	291042; 9070795
6	Jatiluwih	Neh1	Slope	S3tc, eh1	Temperature, slope	294471; 9075702

Potential suitability for ricefields in the Ho Watershed is very suitable (S1) to marginal suitable (S3) with limiting factors: temperature (for Mengesta, Wangaya Gede and Jatiluwih Village), and erosion hazards. Suitability of S1 land (very appropriate) is found in

the downstream of Ho Watershed, locate in SHL I (Desa Beraban) and SHL II in Tangguntiti Village. Improvement efforts that must be made for ricefields in the Ho Watershed is by adding Phosphate element fertilizer at locations classified as very low Phosphate content. Map of actual and potential land suitability are presented in **Fig 3**.

Agricultural land is a major area with the highest soil erosion rate in Indonesia (Sumiahadi & Acar, 2019). Soil loss values are highly variable from year to year, as they sdepend on the weather and the land management (Schwilch et al., 2019). One of the most important indicators for land degradation is the progressive salinization of soils (Abidine et al., 2018). Soil conservation structures along with advanced soil loss models would be important toward land management (Bhat et al., 2019). The locations that have very steep slopes, maintenance of terraces are needed to overcome erosion. The direction of land use can be obtained from the suitability of agro ecosystem land with the limiting factors in each one homogeneous land (SHL). Directions for land use that can be recommended for using rice fields are by limiting factor of the level of erosion hazard by overcome by repairing and maintaining the existing bench terrace and planting reinforcement terrace plants and limiting factor of the low availability of P-available nutrients by overcome by adding fertilizers that contain P elements such as SP36.
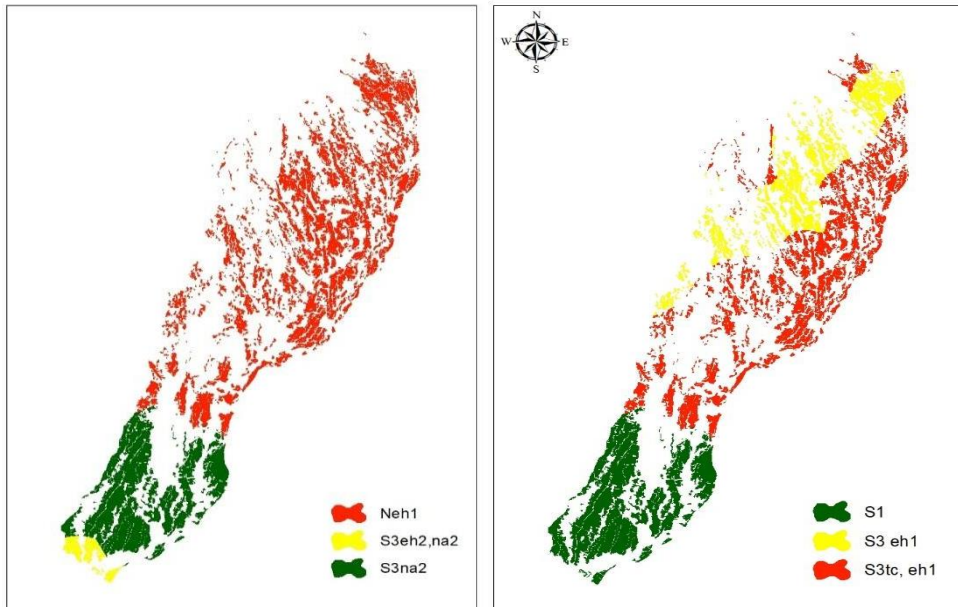
Fig. 3 Actual (left) and Potential Land Suitability (right) for Rice Fields in Ho Watershed.

5. CONCLUSIONS

Based on the results and discussion described above, it can be concluded the actual land suitability for ricefields in the Ho Watershed is classified as Not Suitable (N) in SHL III (Mengesta Village), SHL IV (Penatahan village), SHL V (Wangaya Gede Village) and SLH VI (Jatiluih Village) and marginally suitable (S3) found in SHL I (Beraban Village) and SHL II (Tangguntiti Village). The limiting factor in the actual suitability of land is the quality of the erosion hazard land, namely the slope and erosion hazard and the availability

of nutrients, P-available. Potential suitability for rice field plants in the Ho Watershed is very suitable (S1) to marginal suitable (S3) with limiting factors: temperature (for Mengesta, Wangaya Gede and Jatiluwih), and erosion (slope) hazards. Land suitability of S1 (very suitable) is found in SHL I (Desa Beraban) and SHL II in Tangguntiti Village.

Directions / recommendations that can be given on the use of rice fields are by repairing and maintaining existing bench terraces and planting reinforcing terraces and adding fertilizer containing P elements such as SP36.

ACKNOWLEDGEMENT

REFERENCES

Abidine, M.M.O., El Aboudi, A., Kebd, A., Aloueimine , B.B., Dallahi, Y., Soulé, A., Vadel, A. (2018). Modeling the spatial variability of the electrical conductivity of the soil using different spatial interpolation methods: case of the dawling national park in Mauritania. *Geographia Technica,* **13**(2), 1-11.

Arisanty, D., Adyatma, S. & Normelani, E. (2018). Land suitability evaluation for rice field: farmers' effort to decrease land limitation in Mekarsari, South Kalimantan. *10.2991/icsse-17.2018.10.*

Arsyad, S. (2010). *Soil and water conservation*. Penerbit Institut Pertanian Bogor Press, Bogor.

Bilaşco, T., Roşca, S., Păcurar, I., Moldovan, N., Vescan, I., Fodorean, I., Petrea, D. (2018). Roads accesibility to agricultural crops using GIS technology: methodological approach. *Geographia Technica,* **13**(2), 12-30.

Bhat, S., Dar, M. U., & Meena, R. M. (2019). Soil erosion and management strategies. *Sustainable Management of Soil and Environment*, DOI: 10.1007/978-981-13-8832-3_3.

FAO. (1976). A framework for land evaluation. *Soils Bulletin, 32*. FAO, Rome.

Li, G., Messina, J., Peter, B., & Snapp, S. (2017). Mapping land suitability for agriculture in Malawi: agricultural land suitability mapping. *Land Degradation & Development. 10.1002/ldr.2723.*

McBratney, A. B., Field, D. J. (2015). Securing our soil. *Soil Science & Plant Nutrition,* 61.

Rostaminia, M. & Rahmani, A. (2019). Land suitability evaluation for pistachio and saffron products in Sirvan, Ilam province. *16th Iranian Soil Science Conference, Zanjan University*.

Scholten, T. & Seitz, S. (2019). Soil erosion and land degradation. *Soil Systems.* **3,** 68. *10.3390/soilsystems3040068.*

Schwilch, G., Corsin, L., Michael, Z., Prasuhn, V. & Derungs, N. (2019). Soil erosion policy in Switzerland. *Global Symposium on Soil Erosion, FAO, Rome*

Sumiahadi, A. & Acar, R. (2019). Soil Erosion in Indonesia and Its Control. *International Symposium for Environmental Science and Engineering Research*, Konya, Turkey.

Suparta, W. & Yatim, A. N. M. (2019) Characterization af heat waves: a case study for Peninsular Malaysia. *Geographia Technica*, **14**(1), 146 - 155.

A MULTI HAZARD PERSPECTIVE IN
FLOOD AND DROUGHT VULNERABILITY: CASE STUDY OF MALAWI

Tamara F. KAMANGA[1,4] (ID)*, Sarintip TANTANEE[2]* (ID)*,*
Faidess D. MWALE[3] (ID)*, Panu BURANAJARUKORN [4]*

ABSTRACT:
The prominence of vulnerability assessments cannot be over emphasized. They are key in informing policy by supporting holistic, multi-disciplinary and evidence based policy implementation. They foster delineation of locales and sectors requiring resources and interventions. About 90% of the population in Malawi and most of sub-Saharan Africa rely on rain fed agriculture. Due to this overreliance, people's livelihoods and economy are vulnerable to hydrological hazards such as flood and droughts, which account for 70% of all the hazards in the region. This paper employs indicators to couple exposure, susceptibility, capacity measures and economic, social, physical and environmental components to measure multiple hazard vulnerability. It then utilizes the Community Based Disaster Risk Index in the analysis. Results show that Karonga is an area of medium and high multi hazard vulnerability. The lead contributor to this vulnerability is susceptibility, which manifests itself as high and very high, with predominance in the high levels. Exposure manifests on the lower end of vulnerability spectrum. Lack of capacity is predominantly medium. Socio economic and environmental aspects underlie this susceptibility. Reducing vulnerability in these economies will demand radical programs that target infrastructural investment, socio-economic empowerment, environmental management and strengthening of institutional capacity.

Key-words: *Multi hazard vulnerability, Exposure, Susceptibility, Capacity measures, Malawi, Sub Saharan Africa.*

1. INTRODUCTION

Scientific predictions and evidence affirms that global climate change is likely to increase further the exposure to multiple-risks affecting the magnitude, frequency and spatial distribution of hazardous and disastrous events (IPCC, 2014). Population growth, urbanization and the inability of poor populations to escape from vicious cycle of poverty makes it all more likely there will be an increase in the number of people who are vulnerable to natural hazards with a resulting increase of disasters and environmental emergencies (Guha-Sapir et al., 2004). In the sub-Saharan Africa (SSA), hydro-meteorological hazards tend to be the most dominant.

[1]*Malawi University of Science and Technology, Ndata School of Climate and Earth Sciences, P.O Box 5196, Limbe, Malawi* tamarakamanga@gmail.com

[2]*Naresuan University, Centre of Excellence on Energy Technology and Environment, Faculty of Engineering, Tapho Sub-District, Mueang District, Phitsanulok, 65000, Thailand,* sarintipt@nu.ac.th

[3]*University of Malawi, The Polytechnic, Department of Civil Engineering, Blantyre, Malawi,* fmwale@poly.ac.mw

[4]*Naresuan University, Faculty of Engineering, Tapho Sub-District, Mueang District, Phitsanulok, 65000, Thailand,* tamarakamanga@gmail.com, panub@nu.ac.th

Correspondingly, economies are agro-based with agriculture being primarily rain fed and supporting over 90% of the farmers (Tchale, 2009). This interplay renders people very vulnerable to any climatic shocks.

Multi hazard vulnerability assessments are encouraged in key government and inter-governmental initiatives and agencies. The Sendai Framework for Disaster Risk Reduction, states that disaster risk reduction needs to be multi hazard, and effective risk reduction is possible if all relevant stresses are taken into consideration and analyzed (UNISDR, 2015). Among many advantages, multi hazard vulnerability offers the function of highlighting locations and sectors requiring more targeted interventions and are a prerequisite for under-standing risk and the development of risk reduction and adaptation strategies to extreme events.

Researchers have utilized a wide range of approaches to measure vulnerability over the years. Several European Projects studied hazard and risk mapping techniques for different natural hazards like floods, earthquakes, landslides, forest fires, volcanoes and meteorological extreme events, climate change, etc. (Boukalova, 2005; Klemesova et al., 2014; Pashova et al., 2016). The focus of most past researches had been mainly on single hazards, ignoring the multi hazard measurement. The danger of measuring single hazards over multiple hazards is that they can mislead management priorities, increase vulnerability to other spatially relevant hazards or underestimate vulnerability (Budimir et al., 2014; Gill & Malamud, 2016; Kappes et al., 2010). Areas under study are Wasambo, Lupembe, Kilipula, Mwaka-boko, Mwirang'ombe and Karonga Town communities in Karonga district, northern Mala-wi.

2. MATERIALS AND METHODOLOGY

2.1 Study Area and Data

The study focused on communities in Karonga district in Northern Malawi. (**Fig. 1**). The district hosts a total land area of 3,416 km^2, and a population of 365,028 people (National Statistical Office, 2018). Poverty levels according to the fourth Integrated Household Survey (IHS4), collected in 2016–2017, stand at 57.1%, higher compared to the national average at 51.5 %. The main livelihoods are crop farming, livestock production and fishing (Mapoma et al., 2017). Karonga is prone to flooding with the Songwe, North Rukuru, Kibwe, Kasisi, Nyungwe, Wayi, Lufirya and Kyungu being the rivers that commonly floods (UNECA, 2015). Drought is an annual occurrence in the district, with serious impact on food security as 75% of the households are engaged in crop and animal husbandry (Manda, 2014).

The scale of analysis in this study follows the institutional framework for disaster management in Malawi. Karonga district has one District Civil Protection Committee (DCPC), 6 Area Civil Protection Committee (ACPC) and 46 Village Civil Protection Committee (VCPC) s. The ACPC level was chosen as a scale as of analysis for this study, and all six communes taken into consideration. These are Kilipula, Mwakaboko, Kilipula, Mwirang'ombe, Wansambo and Karonga Town communes.

2.2. Vulnerability framework

Vulnerability is multifaceted and definition use commonly depends on the audience and decisions in question. The IPCC defines vulnerability as the propensity or predisposition to be adversely affected (IPCC, 2014).

According to this definition, vulnerability encompasses three components of exposure, sensitivity and adaptive capacity (IPCC, 2014). UNSIDR (2017) classifies vulnerability into four main types namely: economic, social, physical and environmental. This classification indicates that each social entity has different types of vulnerability, and it is not only the result of the human actions, decisions and choices, but it is the result of the interaction of the different contexts where people live (Alcantara-Ayala, 2002).

In this study, exposure is the presence of people, livelihoods, species or ecosystems, environmental functions, services, and resources, infrastructure, or economic, social, or cultural assets in places and settings that could be adversely affected (IPCC, 2014). While susceptibility is the degree, to which a system is open, liable, or sensitive to a hazard. Capacity Measures /Resilience is the combination of all the strengths, attributes and resources available within an organization, community or society to manage and reduce disaster risks and strengthen resilience (UNSIDR, 2009).

This study assess vulnerability by coupling indicators of susceptibility, exposure, and capacity measures based on IPCC framework of which parameters in each group can be categorized to social, economic, environment and physical discourse following the sustainable development framework. **Fig. 1** shows the study process.
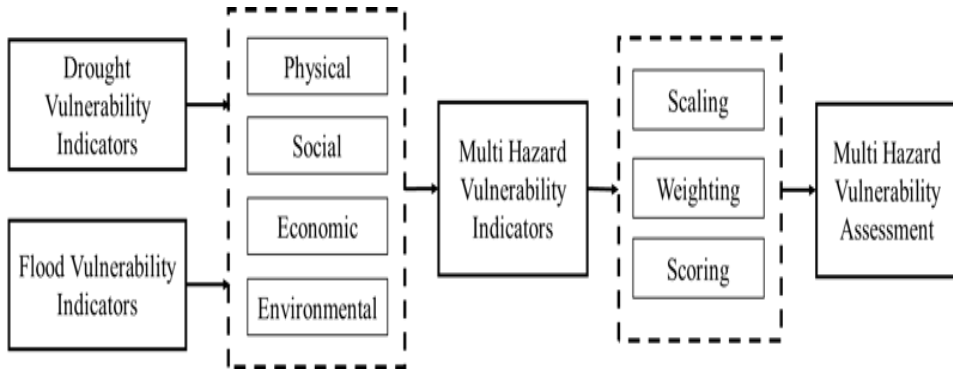
Fig. 1. Study process.

2.3. Indicators for vulnerability quantification

Vulnerability is a product of myriad factors (Suwarno *et.al.,* 2019; Fujiki & Renard, 2018). Factors that are eventually selected in measuring vulnerability are dependent on several factors such as the scale of analysis the aims of the study, relative ease of measurement, validity of the indicator, data availability and methodological approach in building the index (Mwale et al., 2015).

To assess multi hazard vulnerability in this study, flood vulnerability indicators adopted from the CBDRI were coupled with drought indicators drawn from various literature in Sub-Saharan Africa (SSA) (Ahmadalipour & Moradkhani, 2018; Ahmadalipour et al., 2019; Hahn et al., 2009; Hannaford, 2018; Malcomb et al., 2014; Muyambo et al., 2017; Naumann et al., 2014). **Table 1** presents the indicators used.

Table 1:

Multi hazard vulnerability indicators

EXPOSURE		SUSCEPTIBILITY				CAPACITY MEASURES			
Physical (Structure)	Economic	Physical	Social	Economic	Environmental	Physical	Social	Economic	Management and Institutional
• Rain fed Agriculture dependency • Livestock production • Lifelines	• Economy	• Density • Demographic pressure • Access to services	• Poverty level • Literacy • Attitude • Community Participation Dependency ratio • Average time to health facility • Percentage of households with family member with chronic illness • Percentage of households dependent on family farm for food • Average number of months households struggle to find food (range: 0–12) • Percent of households that do not save crops	• Local resource base •Diversification • Stability •Accessibility	•Environmental	• Preventive measures •Environmental management • Land use planning • Building codes • Retrofitting	• Public awareness programs • School curriculum • Public participation • Local risk • Average Crop Diversification Index range >0-1 • Average Agricultural Diversification Index (Range : 0.2 –1) •Emergency response drills	• Local emergency fund • Access to national fund • Access to International funds • Insurance market •Mitigation loans •Reconstruction loans • Public works	• Risk management /emergency • Early warning system •Institutional capacity building •Communication • Risk map •Emergency plan

2.4. Index selection

This study adapts the Community Based Disaster Risk Index (CBDRI) by Bollin et al (2013). The CBDR was chosen as is applicable in data scarce areas where data for conventional vulnerability assessment is limited. The CBDRI utilizes equations (1) and (2) in its operations.

$$CBDRI = v(H + E + V - C) \tag{1}$$

$$H = \sum_{i=1}^{h}(w_i x_i), \text{E} = \sum_{j=1}^{q}(w_j x_j), S = \sum_{k=1}^{r}(w_k x_k), \text{C} = \sum_{y=1}^{z}(w_y x_y) \tag{2}$$

Where H, E, V and C are the hazard, exposure, vulnerability and capacities (resilience) sub components with a range from zero to 100; v = 0.33.

The v factor keeps the final value within zero and 100. *w* is a weight reflecting indicator importance in the sub-component. *h q r z* ,are the total number of indicators in the hazard, exposure, vulnerability and capacity components respectively. *x* is a score allocated to the indicator in the sub-component and in the original state (equation 1) is equal to either 1 (low), 2 (medium) and 3 (high). In the adapted form used in this study, the CBDRI uses susceptibility S in place of vulnerability V in equation (1). This is because in vulnerability literature, exposure, susceptibility and capacities underlie vulnerability (Adger, 2003; Birkmann, 2013; Fussel & Klein, 2006; Smit et al., 2000). In addition, since the CBDRI, measures risk directly but as per equation (1), it is possible to disaggregate it to measure vulnerability directly as in equation (3). Thus.

$$V = 1/3 [E+S+ (1-C)] \tag{3}$$

Where (1 – C) is the lack of capacity. For example, if exposure is 0.65, susceptibility is 0.80, and lack of capacity is 0.4, then: V= (0.60 + 0.80 + 0.4) /3 = 0.6. Further, the scores in this study were stretched from 1 - 3 to 1 - 5 as follows: 1 (very low), 2 (low), 3 (medium), 4(high) and 5 (very high). In the original CBDRI, the total sum of weights per sub-component is 33.

With a maximum score of 3, this ensures that the subcomponent value does not exceed 100. In this study, with a maximum score of 5, the sum of weights per subcomponent was therefore 20. Since the weights ranged from 1 (less important) to 10 (most important) in which case their sum would exceed 20, an adjusted weight for the indicator was used. A simple mathematical proportion was the applied. For example, assuming the total number of weights in the susceptibility subcomponent is 50, and the variable 'poverty level' has a weight of 5, the adjusted weight for this indicator was 5/50 *20 = 2. To dimension single hazard vulnerability by the social, economic, environment and physical dimensions (V$_j$), variables were rearranged and then measured by equation (4) and (5)

$$V_j = [(V_{Ej} +V_{Sj}+ (1-V_{Cj}))]/3 \tag{4}$$

Where, $V_{Ej} = \sum_{i=1}^{m} \left[x_i \left(20 \frac{wi}{\sum_{i=1}^{m} wi} \right) \right]$, $V_{Sj} = \sum_{i=1}^{n} \left[x_1 \left(20 \frac{wi}{\sum_{i=1}^{m} wi} \right) \right]$,

$$V_{Cj} = \sum_{i=1}^{p} \left[x_i \left(20 \frac{wi}{\sum_{i=1}^{m} wi} \right) \right] \tag{5}$$

Where V$_{EJ}$, V$_{Sj}$ and V$_{Cj}$ are the vulnerability due to exposure (E$_j$), susceptibility (S$_j$), and capacities (C$_j$), within the social, economic, environmental and physical sub-component V$_j$. X$_i$ is the score and

w_i is the weight. m, n and p are the number of variables in the exposure (E_j), susceptibility (S_j) and capacities(C_j) respectively of the sub-component V_j. V_{EJ}, V_{Sj} V_{Cj} and V_j range from 0 to 100 (Mwale et al., 2015).

For the ultimate multi hazard vulnerability measurement, this study coupled variables from the two hazards that is flood and drought, then dimensioned them into susceptibility, exposure and lack of capacity and further into economic, physical, social and environmental aspects as explained in equations 1 - 5. Vulnerability levels obtained were scaled based on quantiles. Thus 0 - 0.2 represented very low vulnerability, >0.2 - 0.4 represented low vulnerability, > 0.4- 0.6 equated medium vulnerability, while >0.60 - 0.80 and >0.80 – 1 represented high and very high vulnerability respectively.

2.5. Data Collection

For each community, primary data was sourced through a structured questionnaire administered to a group of experts and knowledgeable people representing the community as recommended by Bollin et al., (2003). The knowledgeable people were mainly from ADC. ADC members are people with various qualifications mainly from police, Community Based Organizations (CBOs) and Government departments. This study also had local government representatives, chiefs and some ordinarily community members. For each commune, one questionnaire was administered, and members agreed on the weight and score. Nine people were interviewed in each of the six communes under study, which is about 70% of ADC composition.

Secondary data such as dependency ratio, population density, population growth rate, access to water services, and literacy levels were obtained from the fourth Integrated Household Surveys and the 2008 and 2018 population and housing census data. Agricultural and Crop diversification index were calculated using data obtained from the Ministry of Agriculture, Irrigation and Water Development. The percentage of forested area as well as land under cultivation for a community was derived with Geographic Information System (GIS), from land cover data sourced at the Regional Centre for Mapping of Resources for Development (RCMRD) geoportal.

3. RESULTS AND DISCUSSIONS

3.1 Results

3.1.1 Exposure

Exposure to multi hazards is generally low in Karonga, manifesting in the very low (0-0.2), low (>0.2-0.4) and medium (>0.4-0.6) levels, but with a predominance in the low level. Magnitudes for this vulnerability ranged 0.2 - 0.53 across communes. The low level of exposure in the district in general may arise from Karonga being predominantly rural as most districts in Malawi. Karonga Town is the commune with highest exposure, (**Fig. 2**). This can be explained from the commune being a town and thus more items in harm's way.

3.1.2. Susceptibility

The high level of vulnerability in Karonga is principally attributable to high levels of susceptibility (**Fig. 2**). Susceptibility magnitudes for multi hazard vulnerability ranged 0.79 – 0.84, manifesting as high (>0.6 -0.8), and very high (>0.80-01), but with a predominance in the very high level (**Fig. 2**).
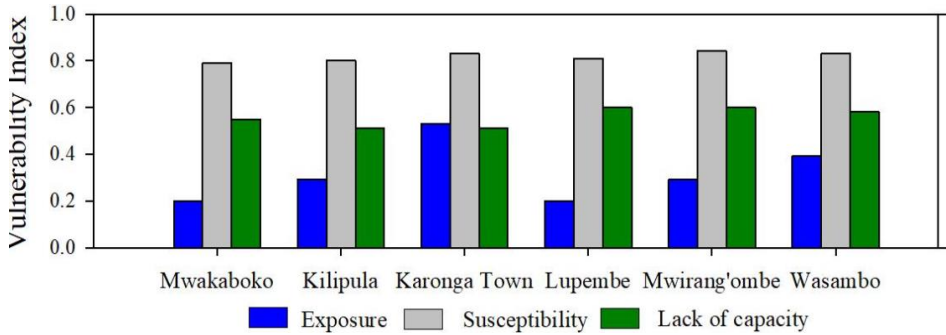
Fig. 2. Multi hazard vulnerability magnitudes.

3.1.3. Lack of Capacity

Resilience is generally medium in Karonga communes. Magnitudes ranges 0.4 - 0.49. Lupembe, Mwirang'ombe and Wasambo communes have slightly lower resilience as compared to Karonga Town, Kilipula and Mwakaboko (**Fig. 2**). The slightly higher resilience in Kilipula, Mwakaboko and Karonga Town may be attributable to the fact that these communes are considered as high flood prone areas hence, they are more targeted for programs involving disaster risk management, consequently increasing their capacity measures / resilience.

3.1.4. Total Vulnerability

Karonga depicts a medium (>0.4 -0.6) to high (>0.6 -0.8) level of vulnerability to multi hazards, with a predominance in the medium range (**Fig. 3**). The magnitudes for this vulnerability ranged 0.51- 0.62.
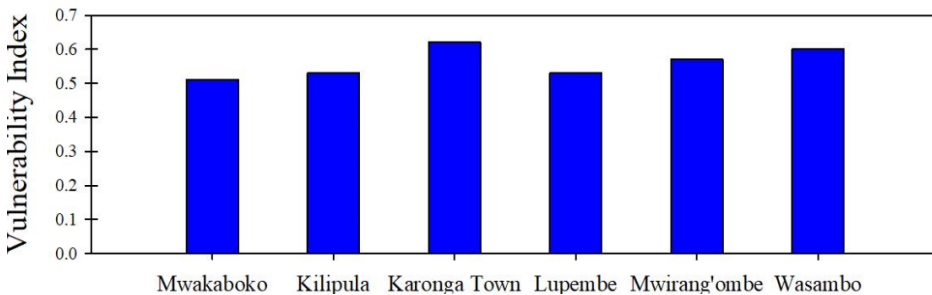
Fig. 3. Total multi hazard vulnerability

3.2. Discussion

As seen from the results, vulnerability to multi hazards in Karonga is quite significant, manifesting in the medium to high range. This high vulnerability emanates from high susceptibility levels underlined by socio economic and environmental factors, mainly originating from low levels of income. These findings are in line with vulnerability literature to climatic shocks in developing countries.

For instance, Yiran et al. (2017), mapped the vulnerability to multiple hazards in the Savannah Ecosystem in Ghana, and their study established that the high vulnerabilities in the area were because of high susceptibilities and low adaptive capacities. Similar to the current study, the underlying causes of vulnerability in the Savanna Ecosystem in Ghana

were socio economic factors. Zacarias (2019), in his quest to understand community vulnerability to climate change and variability at a coastal municipality in southern Mozambique found out that vulnerability is susceptibility driven and is especially derived from susceptibilities of physical, financial and social capitals. Comparably, Ahmadalipour et al. (2019) found out that vulnerability to drought is specifically high in the Sub Saharan countries than the Sahel region despite the latter being an area of high water stress. The underlying causes of this vulnerability were generally socio economic factors, as well as limitations in energy and infrastructure development in the region. Similarly, Mohmmed et al. (2018) substantiated that Darfur region is highly exposed and sensitive to drought risks. The high vulnerability was mainly due to susceptibility factors such as less crop diversity, higher land degradation, frequent droughts, and high poverty levels.

In contrast to susceptibility, exposure is much lower falling in the very low to medium levels but with predominance of low levels. This may be unexpected. However, the low level of exposure in comparison may be explained from the low value of assets in harm's way. It is to be noted that Karonga, as most of the country and a larger part of SSA, is predominantly rural. This is in agreement with figures on economic loses on hazards in developing countries in comparison to developed countries. For instance, CRED 2018's report on economic losses by disasters from 1998 to 2017 indicates that only US$ 21 billion were lost due to climate related disaster in the period 1998 to 2017, in comparison to US$1432 billion lost from developed countries during the same time (Wallemacq et al., 2018).

The lack of capacity was expected to be very high, but contrary to expectations, capacities are predominantly medium. It is to be noted though that except for public participation and presence of decentralized institutions, many attributes from physical, economic and to a large extent institutional aptitude are very limited. The underlying factors are limited alternative agricultural technologies, nonexistence of risk loans and other microfinances for disaster management in the communes as well as low physical capacities such as retrofitting, building codes, and other preventive measures. Thus, effectively, capacities to manage disasters in developing countries remain in a precarious state.

The Sustainable Development Framework is equally supportive of the findings. There are heightened levels in environmental, social as well as economic vulnerabilities, underscoring the socio-economic and environmental dimension of vulnerabilities in rural communities in developing countries. Socio economic aspects like poverty, makes people have limited or no access to financial support that is essential to protect them and their assets from hazards, and disaster insurance are not a priority for them, hence heightened susceptibilities. Several studies in SSA have examined income as a determinant of vulnerability using various proxies, including Gross Domestic Product (GDP), Gini index, and household income and have found high poverty levels to be the underlying causes of vulnerability in the region (Adger, 2003; Malcomb et al., 2014; Mohmmed et al., 2018; Mwale et al., 2015; Vincent, 2004).

Higher susceptibility in the environmental component, agrees with the current state of affairs for the environment in Sub-Saharan Africa. For instance, Keenan et al. (2015), documented that the highest net losses in forest area between 2010 and 2015 in Africa were in Nigeria (410 K ha y1), Tanzania (372 K ha y1), Zimbabwe (312 K ha y1) and Democratic Republic of Congo (311 K ha y1). Generally, the enterprises culprit for this are agriculture land for farmland, charcoal burning, brick making, and other small-scale businesses that puts a lot of pressure on the environment (DeFries et al., 2010; Fisher, 2010; Mwale et al., 2015).

Vulnerability literature suggests that exposure to multi-hazards or repeated exposure to single hazards modifies vulnerability magnitudes. In China for example, Tian et al. (2019) examined temporal trends in resilience to landslides, rock falls and debris flows over a 15-year period. He found that not only did community resilience generally decrease over the years, it increased in periods following catastrophic hazards and it was correlated to original adaptive capacity of the communities, their coping and adaptive capacities related to infrastructure investment, availability of television services, labor employment, medical condition and Engel coefficient.

While floods and droughts may not coincide in time, they often coincide spatially and therefore may have the compounding effect on vulnerability. However, as demonstrated in this study, multi vulnerability magnitudes fall in relatively the same ranges with single hazard vulnerability (Mwale et al., 2015).

In developing countries where such factors as infrastructural investment, poverty, employment and environmental factors are structural deficiencies, it is unlikely vulnerability may vary significantly within the span of the sequential occurrence of floods and droughts, supporting the findings herein.

4. CONCLUSIONS

Vulnerability to multi-hazards of floods and droughts in Karonga, Malawi is medium to high. It is susceptibility driven rooted in social, economic and largely, environmental factors. Measurement of vulnerability to single natural hazards including floods and droughts has been conducted in Sub-Saharan Africa (Ahmadalipour & Moradkhani, 2018; Mwale et al., 2015; Williams et al., 2018; Zacarias, 2019). More importantly, a coupled IPCC and UNISDR framework has been applied tested on floods (Mwale et al. 2015). The patterns depicted from these studies are in general agreement with a multi-hazard spectrum found herein, both in patterns and in magnitudes. This underscores the dominance of structural factors to vulnerability of people in developing countries irrespective of the type of hazard exposed to. Ultimately, radical programs that target infrastructural investments, socio-economic empowerment, and environmental protection and institutional capacity can play a vital role in reducing vulnerability to these climatic hazards.

The multi hazard assessment applied in this study is recommended to areas facing multiple hazards, such as the Yom river basin in Thailand. This approach is also highly applicable to areas with limited data and resources like most of the developing countries.

REFERENCES

Adger, W. N. (2003). Social aspects of adaptive capacity *Climate change, adaptive capacity and development* (pp. 29-49): World Scientific.

Ahmadalipour, A., & Moradkhani, H. (2018). Multi-dimensional assessment of drought vulnerability in Africa: 1960–2100. *Science of The Total Environment,* **644**, 520-535. doi: https://doi.org/10.1016/j.scitotenv.2018.07.023

Ahmadalipour, A., Moradkhani, H., Castelletti, A., & Magliocca, N. (2019). Future drought risk in Africa: Integrating vulnerability, climate change, and population growth. *Science of The Total Environment,* **662**, 672-686. doi: 10.1016/j.scitotenv.2019.01.278

Alcantara-Ayala, I. (2002). Geomorphology, natural hazards, vulnerability and prevention of natural disasters in developing countries. *Geomorphology,* **47**(2-4), 107-124.

Birkmann, J., Cardona, O. D, Carreño, Martha Liliana, Barbat, Alex H, Pelling, Mark, Schneiderbauer, Stefan, Kienberger, StefanKeiler, Margareth, Alexander, David E, Zeil, Peter, . (2013). Framing vulnerability, risk and societal responses: the MOVE framework. *Natural Hazards,* **67**(2), 193-211.

Boukalova, Z. (2005) Applied multi Risk Mapping of Natural Hazards for Impact Assessment, AR-MONIA Project.

Budimir, M., Atkinson, P., & Lewis, H. (2014). Earthquake-and-landslide events are associated with more fatalities than earthquakes alone. *Natural Hazards,* **72**(2), 895-914.

DeFries, R. S., Rudel, T., Uriarte, M., & Hansen, M. (2010). Deforestation driven by urban population growth and agricultural trade in the twenty-first century. *Nature Geoscience,* **3**(3), 178.

Fisher, B. (2010). African exception to drivers of deforestation. *Nature Geoscience,* **3**(6), 375.

Fujiki, K., & Renard, F. (2018). A Geographic Analysis of Post-Disaster Social Impacts on Municipal Scale - A Case study of potential Major Flood in the Paris Region (France). *Geographia Technica,* **13**(2), 31-51.

Fussel, H. M., & Klein, R. J. T. (2006). Climate change vulnerability assessments: An evolution of conceptual thinking. *Climatic Change,* **75**(3), 301-329. doi: 10.1007/s10584-006-0329-3

Gill, J. C., & Malamud, B. D. (2016). Hazard interactions and interaction networks (cascades) within multi-hazard methodologies. *Earth System Dynamics,* **7**(3), 659-679.

Guha-Sapir, D., Hargitt, D., & Hoyois, P. (2004). *Thirty years of natural disasters 1974-2003: The numbers*: Presses univ. de Louvain.

Hahn, M. B., Riederer, A. M., & Foster, S. O. (2009). The Livelihood Vulnerability Index: A pragmatic approach to assessing risks from climate variability and change—A case study in Mozambique. *Global environmental change,* **19**(1), 74-88.

Hannaford, M. J. (2018). Long-term drivers of vulnerability and resilience to drought in the Zambezi-Save area of southern Africa, 1505–1830. *Global and planetary change,* **166**, 94-106. doi: https://doi.org/10.1016/j.gloplacha.2018.05.001

IPCC. (2014). ANNEX II. In K. J. Mach , Planton S. Von Stechow C (Ed.).

Kappes, M., Keiler, M., & Glade, T. (2010). From single-to multi-hazard risk analyses: a concept addressing emerging challenges.

Keenan, R., Reams, G., Frédéric, A., Freitas, J., Grainger, A., & Lindquist, E. (2015). *Dynamics of global forest area: Results from the FAO Global Forest Resources Assessment 2015. Rodney J. Keenan,Gregory A. Reams, Frédéric Achard, Joberto V. de Freitas, Alan Grainger, Erik Lindquist*, **352**.

Klemesova, K., Kolar, M., & Andrask, I. (2014). Using GIS in the flood management – flood map. *Geographia Technica,* **9**(2), 44-53.

Malcomb, D. W., Weaver, E. A., & Krakowka, A. R. (2014). Vulnerability modeling for sub-Saharan Africa: An operationalized approach in Malawi. *Applied Geography,* **48**, 17-30. doi: https://doi.org/10.1016/j.apgeog.2014.01.004

Manda, M. Z. (2014). Where there is no local government: addressing disaster risk reduction in a small town in Malawi. *Environment and Urbanization,* **26**(2), 586-599.

Mohmmed, A., Zhang, K., Kabenge, M., Keesstra, S., Cerdà, A., Reuben, M., . . . Ali, A. A. (2018). Analysis of drought and vulnerability in the North Darfur region of Sudan. *Land Degradation & Development,* **29**(12), 4424-4438.

Muyambo, F., Jordaan, A. J., & Bahta, Y. T. (2017). Assessing social vulnerability to drought in South Africa: Policy implication for drought risk reduction. *Jàmbá: Journal of Disaster Risk Studies,* **9**(1), 1-7.

Mwale, F. D., Adeloye, A. J., & Beevers, L. (2015). Quantifying vulnerability of rural communities to flooding in SSA: A contemporary disaster management perspective applied to the Lower Shire

Valley, Malawi. *International Journal of Disaster Risk Reduction,* **12**, 172-187. doi: https://doi.org/10.1016/j.ijdrr.2015.01.003

Naumann, G., Barbosa, P., Garrote, L., Iglesias, A., & Vogt, J. (2014). Exploring drought vulnerability in Africa: an indicator based analysis to be used in early warning systems. *Hydrol. Earth Syst. Sci.,* **18**(5), 1591-1604. doi: 10.5194/hess-18-1591-2014

Pashova, L., Kouteva-Guentcheva, M., & Bandrova, T. (2016). *Towards Maping Multi-Hazard Vulnerability of Natural Disasters for the Bulgarian Territory* Paper presented at the 6th International Conference on Cartography and GIS.

Smit, B., Burton, I., Klein, R. J., & Wandel, J. (2000). An anatomy of adaptation to climate change and variability *Societal adaptation to climate variability and change* (pp. 223-251): Springer.

Suwarno, Sutomo & Aditama, M.R. (2019). The analysis of the Landslide Vulnerability Sub Watersheds Arus in Banyumas Regency *Geographia Technica,* **14**(2), 112-119.

Tchale, H. (2009). The efficiency of smallholder agriculture in Malawi. *AFJARE, 3*(2), 101-121.

Tian, C.-s., Fang, Y.-p., Yang, L. E., & Zhang, C.-j. (2019). Spatial-temporal analysis of community resilience to multi-hazards in the Anning River basin, Southwest China. *International Journal of Disaster Risk Reduction*, 101144.

UNECA. (2015). Assesment Reort on Mainstreaming and implementing disaster risk reduction measures in Malawi Addis Ababa , Ethiopia: United Nations Economic Commmision for Africa.

UNSIDR. (2009). Terminology on disaster risk reduction from united nations international strategy for disaster reduction.

UNSIDR. (2017). Terminology on disaster risk reduction from United Nations International Strategy for Disaster Reduction.

Vincent, K. (2004). Creating an index of social vulnerability to climate change for Africa. *Tyndall Center for Climate Change Research. Working Paper,* **56**(41).

Wallemacq, P., Below, R., & McLean, D. (2018). UNISDR and CRED report : Economic Losses , Poverty & Disasters (1998 - 2017).

Williams, P. A., Crespo, O., & Abu, M. (2018). Assessing vulnerability of horticultural smallholders' to climate variability in Ghana: applying the livelihood vulnerability approach. *Environment, Development and Sustainability*, 1-22.

Yiran, G. A., Stringer, L. C., Attua, E. M., Evans, A. J., Challinor, A. J., & Gyasi, E. A. (2017). Mapping vulnerability to multiple hazards in the savannah Ecosystem in Ghana. *Regional environmental change,* **17**(3), 665-676.

Zacarias, D. A. (2019). Understanding community vulnerability to climate change and variability at a coastal municipality in southern Mozambique. *International Journal of Climate Change Strategies and Management,* **11**(1), 154-176.

URBAN FLOOD HAZARD MAP USING GIS OF MUANG SUKHOTHAI DISTRICT, THAILAND

Charatdao KONGMUANG[1], Sarintip TANTANEE[2] iD, Kamonchat SEEJATA[3]

ABSTRACT:
Urban flood is one of the most challenge tasks for cities that needs the complex decision support system based on the integration among physical, social parameters and technical knowledge. It needs the analysis on flood hazard map to set up the emergency response plan. Most of communities in Thailand originated along the river of which urban flood is caused by both overflowing from river bank and ineffective drainage system. The most severe urban flood in Thailand occurs in Muang district of Sukhothai province. Because the city locates along Yom river basin where is no regulated dam upstream. Since there are the limitations on the technical support of local organizations. The aim of this paper, therefore, is to generate flood hazard map by coupling flood frequency analysis with GIS that the local officer can easily develop by themselves. Flood frequency analysis proves it can be an alternative method for flood hazard map generating. With the case study of Muang Sukhothai district, the accuracy of this method is 88.83%. The obtained flood hazard map will be the basic information for the decision maker not only on flood emergency response plan but also on prioritizing of budget allocation for flood protection system.

Key-words: *Urban flood, Flood emergency response plan, Flood hazard map, Sukhothai flood.*

1. INTRODUCTION

Flood is one of the most threatening and damaging natural disasters globally that impacts negatively upon the activities of human lives, with inundation leading to disastrous consequences including the loss of lives and destruction of property (Dadson et. al, 2017). Flood hazard is expected to increase in frequency and magnitude because of the impacts of climate change (Dinh et al., 2012). Then it requires various responses including construction for downstream flood defences, forecasting (for warning and evacuation), and land-use management for upstream land use changes and runoff characteristics (Kidson and Richards, 2005). Floods occur because of the rapid accumulation and release of runoff waters from upstream to downstream, caused by very heavy rainfall (Ouma and Tateishi, 2014; Şarpe and Haidu, 2017). Urban areas in particular suffer from a relatively high flood risk because of high population number and density, a lot of economic activities, infrastructure and property values (Pelling, 2003; Nusit et al., 2019).

[1]*Naresuan University, Department of Natural Resources and Environment, Faculty of Agriculture, Natural Resources and Environment, Phitsanulok, Thailand, charatdao@gmail.com;*
[2]*Naresuan University, Excellent Center on Energy Technology and Environment, Faculty of Engineering, Phitsanulok, Thailand, sarintipt@nu.ac.th;*
[3]*Naresuan University, Department of Civil Engineering, Faculty of Engineering, Phitsanulok, Thailand, kamonchatseejata@gmail.com*

Impacts of urban floods are significant in terms of economic losses. There is a direct relationship between urbanisation and hydrological characteristics; decreased infiltration, increase in runoff, increase in flood frequency and flood height (Alaghmand et al., 2010; Ouma and Tateishi, 2014, Haidu and Ivan, 2016a). Increasing discharge is directly related to the increase in urbanised areas (Phetprayoon et al., 2010; Haidu and Ivan, 2016b). Urbanisation tends to increase peak flood flows because of reduced infiltration under paved areas and rapid flow over the surface (Dadson et al., 2017, Kumar et al., 2013).

Urban flood due to overflow of the riverbank in cities is not an isolated phenomenon but closely related with overall basin characteristics. The city of Sukhothai, located in lower Yom river basin in lower northern of Thailand, frequently suffers from floods due to the low retention capability of the upstream area (lacking of the regulated dam) and the narrow basin cross section in the downstream area (Sriariyawat et al., 2013; Seejata et. al., 2019). The Yom river, a tributary of the Chao Phraya River, is approximately 736 km long with the average flow capacity of the main channel varies from 220 m^3/s to 2,000 m^3/s. As Sriariyawat et al. (2013) pointed out that the segment from Phrae province to Sukhothai province has a capacity of 1,000-2,000 m^3/s, whereas the segment from Sukhothai province to Phitsanulok province has a capacity of only 220-300 m^3/s. Therefore, when there is heavy rainfall over the upstream area, it causes an overflow of the riverbanks, erosion and severe flooding in Sukhothai urban area.

With urban development, impermeable surface areas decrease infiltration and increase the rate and volume of surface runoff (Fitzpatrick et al., 2005). Klemešová et al. (2014) noted that flood hazard map is one of the preventive instruments for assessment and management of flood risks. The problem is that there are still have limitations on technical support of local organizations in Sukhothai province. Having flood hazard and flood extent maps could help them in terms of dicision support system to prioritise the response plan and budget allocation for the protection system. The aim of this study, therefore, is to generate flood hazard map by coupling frequency analysis with Geographic Information System (GIS) that the local officer can easily develop by themselves as well as can be the information for decision maker on flood preparedness and responses.

2. STUDY AREA AND DATA

2.1 Study area

Sukhothai province is most famous for its historical city, the first capital of Thailand. Sukhothai Historical Park in Muang district is now a UNESCO World Heritage Site. Muang Sukhothai is the capital district that can be seen as an urban area of Sukhothai province. It is located in lower Yom river basin in lower northern of Thailand (**Fig.1**). It is divided into 10 sub-districts, which are further subdivided into 98 villages. Total area of Muang Sukhothai is 553.38 km^2 with the population of 104,328. It has the highest population density of 188.53/ km^2 accounting for 18.82% of the Sukhothai province that covers approximately 6,664.48 km^2 with the population of 597,257 (**Tab. 1**).

2.2 Data

According to Seejata, et al. (2019) and previous studies, eight conditioning parameters were selected for flood hazard analysis including rainfall, elevation, slope, land use, soil drainage, drainage density, distance from drainage and road density (Anucharn and

Iamchuen, 2017; Cao et al., 2016; Das, 2019; Duangpiboon et al., 2018; Khosravi et al., 2016; Lee et al., 2018; Sahana and Patel, 2019; Samanta et al.,2018; Samanta, 2018; Shafapour et al., 2019; Tehrany et al., 2015; Youssef et al., 2016). **Table 2** and **Fig. 2** give more detailed on data used in this analysis.
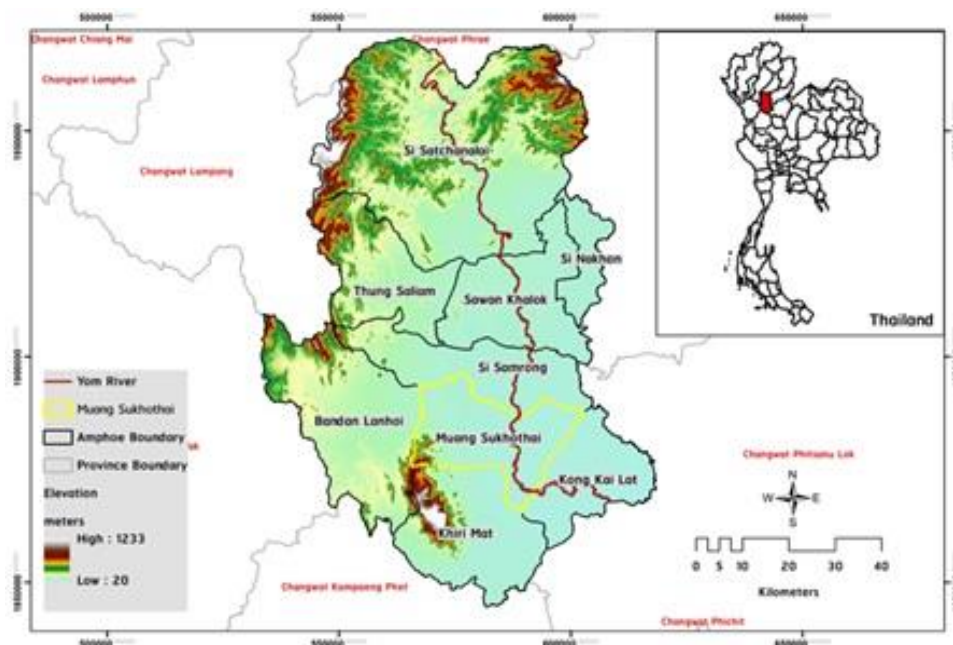
Fig. 1. Study area of Muang Suhkothai district, Thailand.

Table 1.

Area and population of Sukhothai province.

District	Area	Pop	Pop Density (per km²)	%
Muang Sukhothai	553.38	104,328	188.53	18.82
Kong Krailat	449.10	64,308	143.19	14.30
Si Nakhon	183.25	26,177	142.85	14.26
Sawankhalok	620.06	83,919	135.34	13.51
Si Samrong	558.50	71,110	127.32	12.71
Thung Saliam	583.94	49,492	84.75	8.46
Khiri Mat	679.73	56,864	83.66	8.35
Ban Dan Lan Hoi	923.24	47,960	51.95	5.19
Si Satchanalai	2,113.29	93,099	44.05	4.40
Total	**6,664.48**	**597,257**	**89.62**	**100.00**

Source: National Statistical Office of Thailand

Data and Sources.

| Data	Detailed and Sources
Rainfall	Average rainfall (Between1988-2017) obtained from Thai Meteorological Department (TMD)
Elevation	30x30 meter spatial resolution from the Digital Elevation Model of Shuttle Radar Topography Mission
Slope	Derived from the Digital Elevation Model
Land use	(1) Agricultural land (2) Forest land (3) Urban land (4) Water (5) Miscellaneous land (From Land Development Department)
Soil drainage	(1) No survey (2) Poorly to somewhat poorly drained (3) well to moderately well-drained (4) Very well-drained (5) Urban area (6) Miscellaneous area (7) Water (From Land Development Department)
Drainage density	Derived from the Geo-Informatics and Space Technology Development Agency (GISTDA)
Distance from drainage	Five concentric buffers (each of 1,000 meter width).
Road density	Derived from the GISTDA
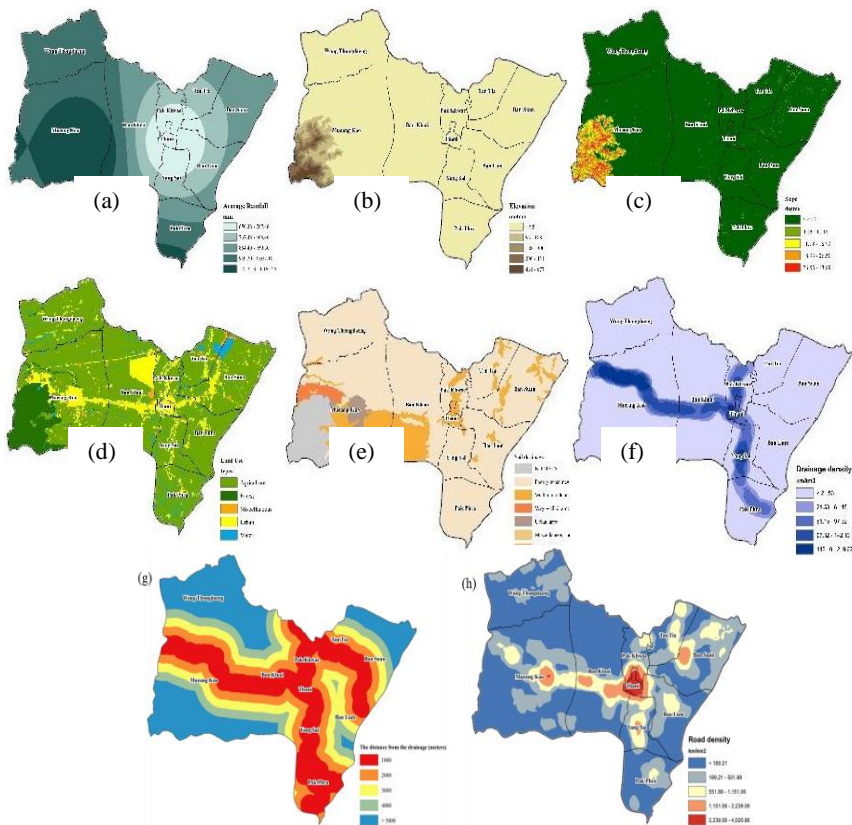
Fig. 2. Eight conditioning parameters: (a) rainfall, (b) elevation, (c) slope, (d) land use, (e) soil drainage, (f) drainage density, (g) distance from drainage and (h) road density.

3. METHODOLOGY

To generate the flood hazard map, this study applied the frequency ratio (FR) method. **Fig. 3** shows the methodology framework.
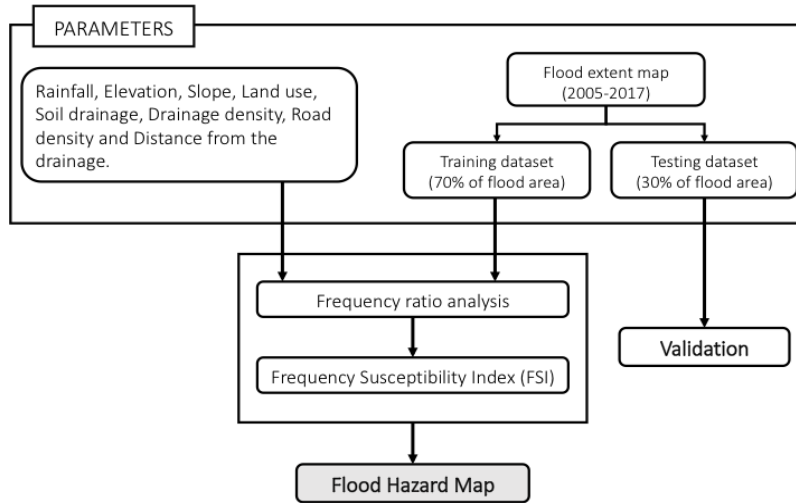
Fig. 3. Flood hazard mapping methodology framework.

3.1 Flood Extent Map

The flood extent map was generated from multi-satellite including RADARSAT-2, THAICHOTE, and COSMO-SkyMed-4 obtained from GISTDA for the period of 2005 to 2019 using Geostatistical analyst tool in GIS environment. Seventy percent of flood area was used to generate the flood hazard map while another thirty percent for validation (Seejata et al., 2019).

3.2 Flood Hazard Map using Frequency Ratio Method

Geographic Information System (GIS) and Frequency Ratio (FR) method have been used to create flood hazard map. The FR method is a bivariate statistics analysis method based on relationships between historical data and conditioning factors (AlThuwaynee, 2018). It is not only simply implemented but also easy to understand (Khosravi, 2016). The FR is calculated using the following equation (1).

$$\text{FR} = \frac{PH}{PS} \tag{1}$$

where PH is the percentage number of flood hazard in each class and PS is the percentage number of study area in each class.

If FR value is lower than 1 means weak correlation, on the other hand, if the FR value is more than 1 means strong correlation.

The Frequency Susceptibility Index (FSI) is calculated using the following equation (2).

$$FSI = \sum_{i=1}^{n} FR_i \qquad (2)$$

where FR_i is the value of FR in each factor and *n* is the number of factors.

In conclusion, the FSI value applied for flood hazard mapping and classified by Jenks natural breaks classification method into 5 classes: (1) very high, (2) high, (3) moderate, (4) low, and (5)very low.

3.3 Validation Process

The validation process had been done by the Area Under Curve (AUC). The success rate was calculated using the training flood area of 70% whereas the prediction accuracy was calculated using a testing flood area of 30%. The FSI was classified into 100 categories on the x-axis, with a cumulative of flood occurrence on the y-axis (Tehrany et al., 2019).

4. RESULTS AND DISCUSSIONS

Table 3 shows observed flood extent for the period of 2005-2019. As can be seen that flood occurred in Muang Sukhothai district almost every year with the severe events, especially in 2006, 2010, 2011 and 2017 (**Fig. 4**) Among 13 years records, flood extent in Muang district are severe as 78.94%, 38.83%, 55.10%, 49.68% of the total district area in 2006, 2010, 2011, and 2017, respectively (**Tab. 3**). This shows that it is needed to have the preparedness and response plan to cope with flood over the district.

Table 3.
Flood area during 2005-2019.

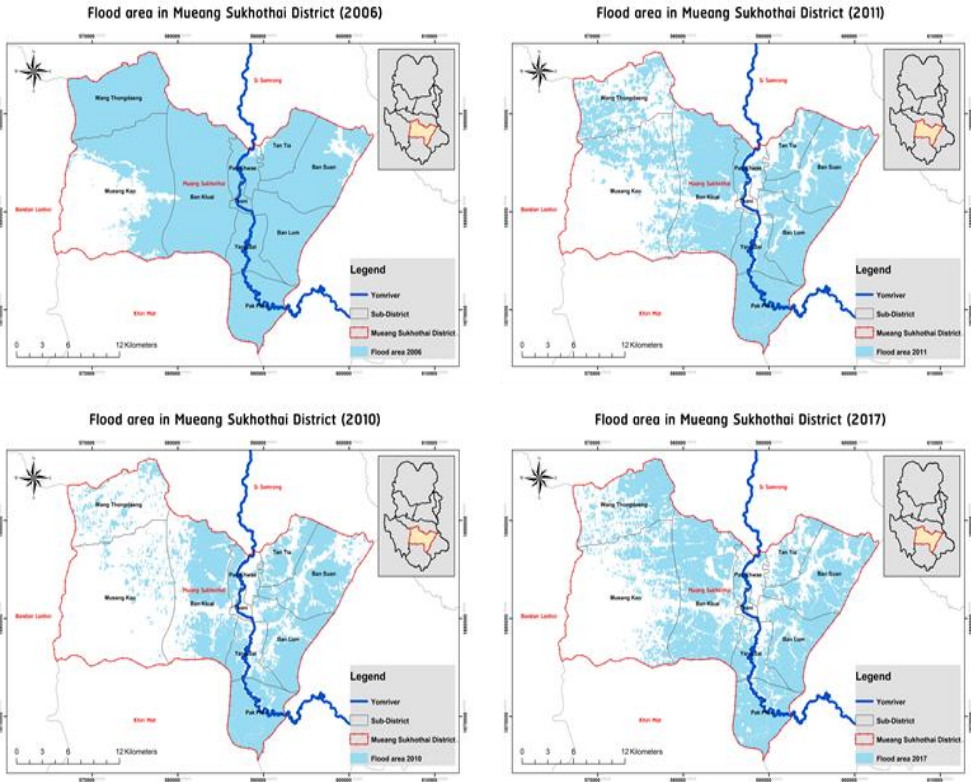| Year	Area (km^2)	% of Flooding area
2005	156.683	26.95
2006	458.996	78.94
2007	141.625	24.36
2008	85.227	14.66
2009	88.147	15.16
2010	225.807	38.83
2011	320.403	55.10
2012	170.973	29.40
2013	124.257	21.37
2014	103.867	17.86
2016	123.956	21.32
2017	288.885	49.68
2019	65.890	11.33

Fig. 4. Observed flood extent for severe events.

By using the frequency ratio method, the obtained flood hazard map is shown in **Fig. 5** and **Table 4** demonstrates the percentage of each level of flood hazard. It has been found that area with very high flood risk is 88.87% of the whole district.

Fig. 5. Flood hazard map in Muang Sukhothai District.

Table 4.
Flood hazard classification in Muang Sukhothai District.

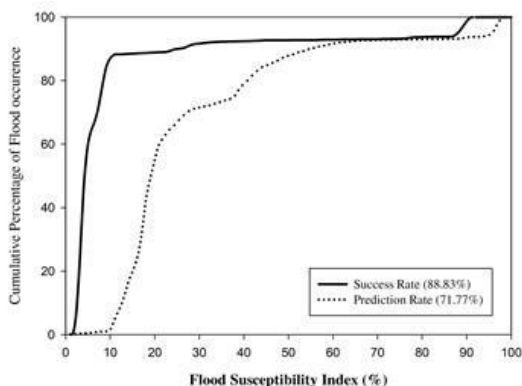| Level	Area (km2)	%
Very Low	34.24	6.19
Low	5.14	0.93
Moderate	0.91	0.16
High	21.23	3.084
Very High	491.37	88.87

Fig. 6. Success rate and prediction rate curve of the frequency ratio model.

The Area Under Curve (AUC) was used to examine the accuracy of the flood hazard map. Flood Susceptibility Index (FSI) was classified into 100 categories on the x-axis, while a cumulative of flood occurrence was shown on the y-axis. For the frequency ratio model, it has been found that AUC of the training area was 88.83% and the testing area was 71.77% (**Fig. 6**). In order to mitigate flood disaster in Muang Sukhothai district, it is important not only to promote structural measure by constructing flood control facilities such as levee or floodwall but also to prepare non-structural measures by improving ways to communicate disaster information and evacuation as well as by increasing public awareness towards disaster prevention because there is a possibility that a levee or floodwall can breach if the flood exceeds its designed capacity. For these reasons, flood extent map and flood hazard map should be disclosed as a part of flood control measures and flood emergency response plan.

5. CONCLUSIONS

The method of flood frequency analysis can be an alternative for flood hazard map generating. With the case study of Muang Sukhothai district, the obtained accuracy of this method is 88.83%. Although, Muang Sukhothai district has floodwall and sandbags to prevent the overflowing in urban area, sometimes it was at risks of collapsing. Therefore, *"Flood Hazard Mapping Manual"* will be delivered to local officer with the aims of minimizing flood damage by providing residents with inundation-related information in an easy-to-understand way. The manual will describe how to prepare a flood hazard map by coupling frequency analysis with GIS step by step. And that the local officer can easily

develop by themselves. As can be seen that flood hazard map proves it can uncover and identify risk areas that exist in the district as the basic information for risk-based decisions. However, further develop should be done as follows: evacuation information, communication system during disaster, disaster tracking system, disaster quantify process, allocate mitigation measures, as well as the effectiveness verification system.

REFERENCES

Alaghmand, S., Bin-Abdullah, R., Abustan, I. & Vosoogh, B. (2010) GIS-based River Flood Hazard Mapping in Urban Area: A Case Study in Kayu Ara River Basin, Malaysia. *Int. J. Eng. Technol*, **2**, 488–500.

AltThuwaynee, O. (2018) *How to Produce Prediction Map in GIS with ArcGIS and Excel*. Available from: https://www.udemy.com/user/omar-f-althuwaynee/. [Accessed December 2019].

Anucharn, T. & Iamchuen, N. (2017) Flood Susceptibility Map Based on Frequency Ratio Method at Songkhla Lake Basin in the Southern of Thailand. *BURAPHA SCIENCE JOURNAL,* **22**(3), 106-122.

Cao, C., Xu, P., Wang, Y., Chen, J., Zheng, L. & Niu, C. (2016) Flash Flood Hazard Susceptibility Mapping Using Frequency Ratio and Statistical Index Methods in Coalmine Subsidence Areas. *Sustainability*, **8**(9), 948.

Dadson, S. J., Hall, J. W., Murgatroyd, A., Acreman, M., Bates, P., Beven, K., & O'Connell, E. (2017) A restatement of the natural science evidence concerning catchment-based 'natural' flood management in the UK. *Proceedings of the Royal Society of London. Series A, Mathematical and Physical Sciences*, **473** (2199).

Das, S. (2019) Geospatial mapping of flood susceptibility and hydro-geomorphic response to the floods in Ulhas basin, India. *Remote Sensing Applications: Society and Environment*, **14**, 60-74.

Dihn, Q., Balica, S., Popescu, I. & Jonoski, A. (2012) Climate change impact on flood hazard, vulnerability and risk of the Long Xuyen Quadrangle in the Mekong Delta. *Int. J. River Basin Manag*, 10, 103–120.

Duangpiboon, S., Suteerasak, T., Rattanakom, R. & Towanlong, W. (2018) Flood Susceptibility Mapping Using Geographic Information System and Frequency Ratio Analysis in the Lang Suan Watershed, Southern Thailand. *The Journal of King Mongkut's University of Technology North Bangkok*, **28**(2), 259-272.

Fitzpatrick, F.A., Diebel, M.W., Harris, M.A., Arnold, T.L., Lutz, M.A. & Richards, K.D. (2005) Effects of urbanization on the geomorphology, habitat, hydrology, and fish index of biotic integrity of streams in the Chicago area, Illinois and Wisconsin. *American Fisheries Society Symposium,* **47**, 87–115.

Haidu, I., & Ivan, K. (2016a). Évolution du ruissellement et du volume d'eau ruisselé en surface urbaine. Étude de cas: Bordeaux 1984-2014, France. *La Houille Blanche*, **5**, 51-56.

Haidu I., Ivan K. (2016b) The assessment of the impact induced by the increase of impervious areas on surface runoff. Case study the city of Cluj-Napoca, Romania. *Carpathian Journal of Earth and Environmental Sciences*, **11**(2), 331-337**.**

Khosravi, K., Nohani, E., Maroufinia, E. & Pourghasemi, H. R. (2016) A GIS-based flood susceptibility assessment and its mapping in Iran: a comparison between frequency ratio and weights-of-evidence bivariate statistical models with multi-criteria decision-making technique. *Natural Hazards*, **83**(2), 947-987.

Kidson, R. & Richards, K. S. (2005) Flood frequency analysis: Assumptions and alternatives. *Progress in Physical Geography*, **29**(3), 392-410.

Lee, S., Lee, S., Lee, M. J. & Jung, H. S. (2018) Spatial assessment of urban flood susceptibility using data mining and geographic information System (GIS) tools. *Sustainability*, **10**(3), 648.

Klemešová, K., Kolář, M. & Andráško, I., (2014) Uing GIS in the flood management – Flood maps (Troubky, Czech Republic). *Geographia Technica*, **9**(2), 44-53.

Kumar, D. S., Arya, D. S. & Vojinovic, Z. (2013) Modeling of urban growth dynamics and its impact on surface runoff characteristics. *Comput Environ Urban Syst*, **41**, 124–135.

Nusit, K., Tantanee, S., Subsomboon, K., Leungvichcharoen, S. & Yiemwattana, S. (2019). The design of flood protection along Nan river, Phitsanulok Province, Thailand. *Geographia Technica*, **14**, Special Issue, 129-137.

Ouma, Y. & Tateishi, R. (2014) Urban Flood Vulnerability and Risk Mapping Using Integrated Multi-Parametric AHP and GIS: Methodological Overview and Case Study Assessment. *Water*, **6**, 1515-1545.

Pelling, M. (2003) *The vulnerability of cities: Natural disasters and social resilience*, London.

Pakorn, P., Blanken, P. D., Ekkawatpanit, C. & Hussein, K. (2010) Hydrological impacts of land use/land cover change in a large river basin in central–northern Thailand. *International Journal of Climatology,* **30**(13), 1917–1930.

Sahana, M. & Patel, P. P. (2019). A comparison of frequency ratio and fuzzy logic models for flood susceptibility assessment of the lower Kosi River Basin in India. *Environmental Earth Sciences*, **78**(10), 289.

Samanta, R. K., Bhunia, G. S., Shit, P. K. & Pourghasemi, H. R. (2018). Flood susceptibility mapping using geospatial frequency ratio technique: A case study of Subarnarekha River Basin, India. *Modeling Earth Systems and Environment*, **4**(1), 395-408.

Samanta, S., Pal, D. K. & Palsamanta, B. (2018) Flood susceptibility analysis through remote sensing, GIS and frequency ratio model. *Applied Water Science*, **8**(2), 66.

Shafapour Tehrany, M., Kumar, L., Neamah Jebur, M. & Shabani, F. (2019) Evaluating the application of the statistical index method in flood susceptibility mapping and its comparison with frequency ratio and logistic regression methods. *Geomatics, Natural Hazards and Risk*, **10**(1), 79-101.

Srijata, C., Yodying, A., Chatsudarat, S., Chidburee, P., Mahavik, N., Kongmuang, C. & Tantanee, S. (2019) Assessment of Flood Hazard using Geospatial Data and Frequency Ratio Model in Sukhothai Province, Thailand. *Proceeding of Asian Conference on Remote Sensing 2019*, South Korea.

Sriariyawat, A., Pakoksung, k., Sayama, T., Tanaka, S. & Koontanakulvong, S. (2013) Approach to estimate the flood damage in Sukhothai Province using flood simulation. *Journal of Disaster Research*, **8**(3), 406-414.

Şarpe, C.A., & Haidu, I., (2017) Temporal sampling conditions in numerical integration of hydrological systems time series*. Geographia Technica*, **12**(1), 82- 94,
DOI: 10.21163/GT_2017.121.09

Tehrany, M. S., Pradhan, B. & Jebur, M. N. (2015) Flood susceptibility analysis and its verification using a novel ensemble support vector machine and frequency ratio method. *Stochastic Environmental Research and Risk Assessment*, **29**(4), 1149-1165.

Youssef, A. M., Pradhan, B. & Sefry, S. A. (2016) Flash flood susceptibility assessment in Jeddah city (Kingdom of Saudi Arabia) using bivariate and multivariate statistical models. *Environmental Earth Sciences,* **75**, 1-16.

ASSESSMENT OF THE VEGETATION COVER CHANGE IMPACTS ON WATER EROSION, USING PAP/RAC METHOD IN UPSTREAM OF "OULJET SOLTANE" DAM, CENTRAL PLATEAU-MOROCCO

Youssef DALLAHI[1], Ahmed OUHAMMOU[1], Mohamed SBAI[2],
Ahmed El ABOUDI[2], Amal BOUJRAF[3]

ABSTRACT:
The aim of this paper is to evaluate the impact of forest cover dynamics on the erosion at Kharouba watershed in the Moroccan Central Plateau. Our methodology is based on the diachronic analysis of the land cover between 1986 and 2016, using treatments of aerial photographs from 1986 and a Google Earth satellite imagery at a high resolution from 2016. The land cover maps obtained were used to establish erosion status maps between 1986 and 2016, based on methodology PAP/RAC. Our study highlights the regressive evolution of vegetation cover. This decline has stressed the increased water erosion risk in Kharouba watershed causing the spread of the areas that are vulnerable to water erosion from 36 % in 1986 up to 41 % in 2016.

Key-words: *Vegetation cover, erosion, watershed, methodology PAP/RAC*

1. INTRODUCTION

Soil erosion is a degradation process of natural resource that has remarkably grown over time. In fact, rapid landscape changes, due to demographic pressure and climate changes, magnify the surface runoff process, and therefore, the soil degradation (Heusch, 1970; Al Karkouri et al., 2000; Naimi et al., 2005).
In Morocco, several research studies have been dedicated to understand the erosion process in the Moroccan mountains through the modeling of soil loss in several watersheds (Laouina, 1998; Moufaddal, 2002; Damnati et al., 2013; Simonneaux et al., 2015; Iaaich et al., 2016; Briak et al., 2016).
Results, at the Beht watershed, show that the area at risk amounts to 87 %, with an annual siltation rate of 1.40 Mm3 / year (El Gaatib, 2015). Kharouba watershed, located in the central part of Beht, has an average specific degradation; estimated at 4.10t / ha/year. The outlets losses are measured at 60 thousand tons per year (HCEFLCD, 2007). This situation could pose a real threat to the siltation of the under-construction Ouljet Soultane dam.

[1] *Cadi Ayyad University, Laboratory of Microbial Biotechnologies Agrosciences and Environment (BioMAgE), Faculty of Sciences Semlalia, Marrakech, dallahi.youssef1@gmail.com*
[2] *Mohammed V University, Laboratoire de Botanique et Valorisation des Ressources végétales et Fongiques (BOVAREF), Faculté des Sciences, Rabat, mohamedsbai68@gmail.com, elaboudi@gmail.com*
[3] *Ibn Tofail University, Laboratoire de Botanique, Biotechnologie et de Protection des Plantes, Département de Biologie, Faculté des Sciences, Kénitra, amal.boujraf@gmail.com*

This watershed has valuable forest resources covering more than 87 % of its area. However, this forest patrimony suffered over time significant amount of pressures: mainly illegal logging, overgrazing and climate changes, consequently intensifying erosion and land degradation. In this context, the present work aims to highlight the gravity and the erosion phenomena evolution and to evaluate impacts of vegetation cover change on water erosion at Kharouba watershed.

2. STUDY AREA AND DATA

Kharouba watershed covers an area of about 19888.5 ha and is located in the central part of Beht (**Fig. 1 and 2**). It is characterized by the dominance of primary geological formations. The area has an accentuated relief, a semi-arid to sub-humid climate, marked by strong spatial and temporal rain variability. These factors associated with land use and anthropogenic actions promote its vulnerability to erosion.
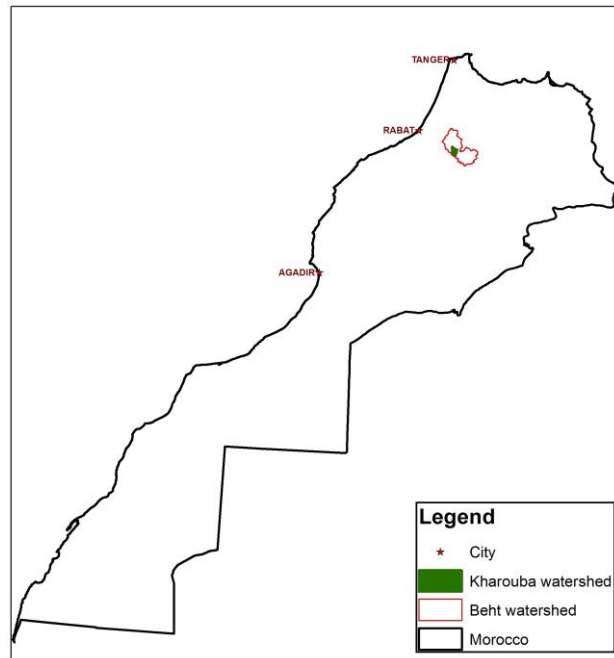
Fig. 1. Location Map of the studied area.

The average specific degradation for Kharouba watershed is estimated at 4.10t /ha/year. Losses at the watershed outlet are estimated at 60 thousand tons per year (HCEFLCD, 2007). In terms of land use, Kharouba watershed is dominated by forest formations covering more than 87 % of its area (**Fig. 3**). These formations are mainly based on *Tetraclinis articulata* and *Quercus rotundifolia* (Dallahi et al., 2016; Dallahi et al., 2017).
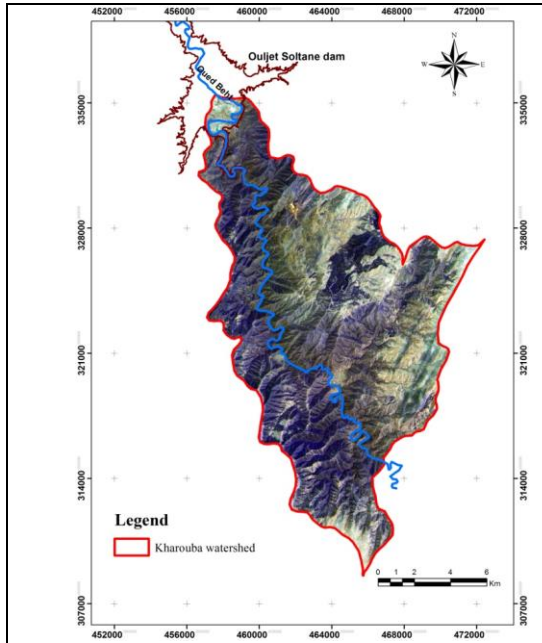
Fig. 2. Location Map of the Kharouba watershed
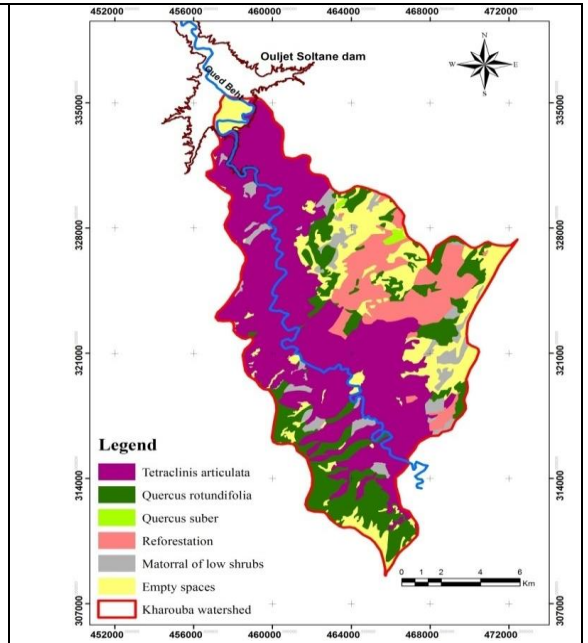
Fig. 3. Vegetation cover map (2016)

3. METHODOLOGY

From a methodological approach, this work consists, firstly, in a diachronic analysis of the vegetation cover using aerial photographs from 1986 and a Google Earth satellite imagery at a high resolution from 2016 to quantify the spatio-temporal dynamics of the vegetation cover. Secondly, we relied on the predictive approach of the PAP / CAR method (PAP/RAC, 1997), to set up an erosion status map on two different dates, providing thus the map canvas of the potential and the general patterns of erosion.

The predictive approach of the PAP/RAC method is mainly a data processing according to the following operations (**Fig. 4**):

- Slope and lithofacies mapping;
- Erodibility mapping by overlaying the slope and the lithofacies maps;
- Land and vegetation cover mapping for 1986 and 2016;
- Soil protection maping of 1986 and 2016 by overlaying the land and vegetation cover maps;
- Erosion status mapping by overlaying erodibility and soil protection level maps.
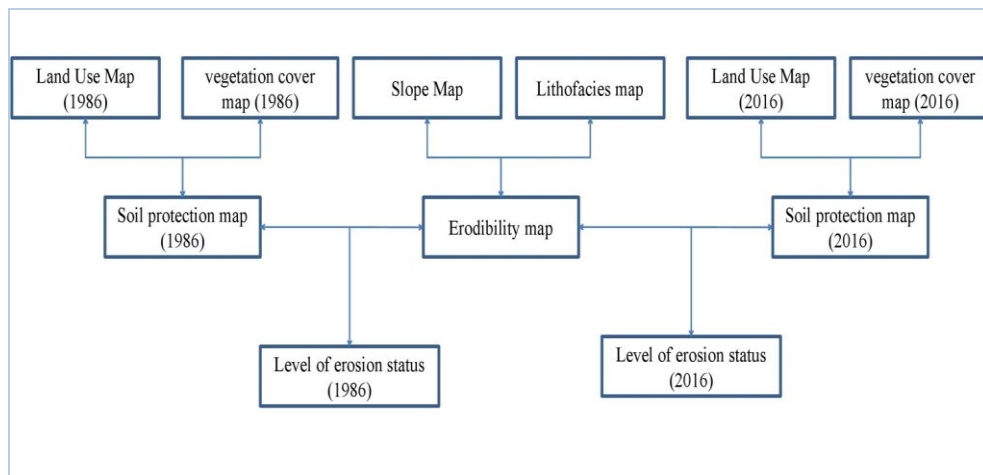
Fig. 4. Main operational sequence of erosion mapping procedures (PAP/RAC, 1997).

4. RESULTS AND DISCUSSIONS

4.1. Results of the vegetation diachronic analysis

The diachronic analysis is based on the comparison of the composition and the surface of the plant's formations on two different dates. The different area's loss and gain in term of strata are shown in **Table 1**.

Table 1.

Confusion matrix for mapping land cover change.

		1986						
	strata	Ta	Qr	Qs	R	M	V	Total (2016)
	Ta	10898	0	0	0	0	0	10898
	Qr	0	2559	0	0	0	0	2559
2	Qs	0	0	97	0	0	0	97
0	R	303	655	0	1150	54	0	2162
1	M	730	212	2	0	145	0	1089
6	V	2629	191	10	57	9	186	3082
	Total (1986)	14560	3617	109	1207	208	186	///

The table analysis exhibits the significant regression that the different plant formations have experienced. Indeed:

- The *Tetraclinis articulata* (Ta) area declined from 14560 ha in 1986 to 10898 ha in 2016, a fall of 25 %. Its average regression rate is 118 ha/year. Empty spaces and matoral of low shrubs took over this stratum superficy.

- *Quercus rotundifolia* (Qr) reported a 34 % reduction in 2016 compared to 1986. The regression pace is up to 34 ha. The majority of this stratum was planted by *Pinus Pinaster* (R).

- *Quercus suber* (Qs) declined by 12 ha, or 11 % of its area. It has been largely transformed to empty spaces.
- The matorral (M) benefited from the forest trees degradation, it gained an area of 881 ha. Their average growth rate is estimated at 28 ha/year.
- Empty land (V) increased over an area of 2896 ha. Their extension is mainly at the expense of *Tetraclinis articulata* and *Quercus rotundifolia*.

4.2. Soil protection maps analysis

Each type of vegetation cover provides a degree of soil protection that corresponds to a specific class. The Soil Protection Map reflects the type and the density of the vegetation cover in Kharouba watershed.

The diachronic analysis of Kharouba watershed's soil protection map, between 1986 and 2016, exhibit the regressive evolution that the vegetation cover has undergone a in terms of area and especially density. Indeed, the high-density vegetation is declining in favour of an average or even low vegetation cover density. This regression mainly concerned the high density *Tetraclinis articulata* whose surface area has been slashed from around 2699 to 760 ha.

This situation has led to the increase in areas of low to very low protection, which expanded from 26 % of the total watershed area in 1986 to 33 % in 2016. On the other hand, the high and very high protection levels have a regressive evolution, their percentages dropped from 51 % in 1986 to 47 % in 2016 (**Fig. 5 and 6**). This regressive evolution of the soil protection levels is the result of several factors including illegal logging, overgrazing and climate changes.

Fig. 5. Soil protection map (2016)

Fig. 6. Soil protection map (1986)
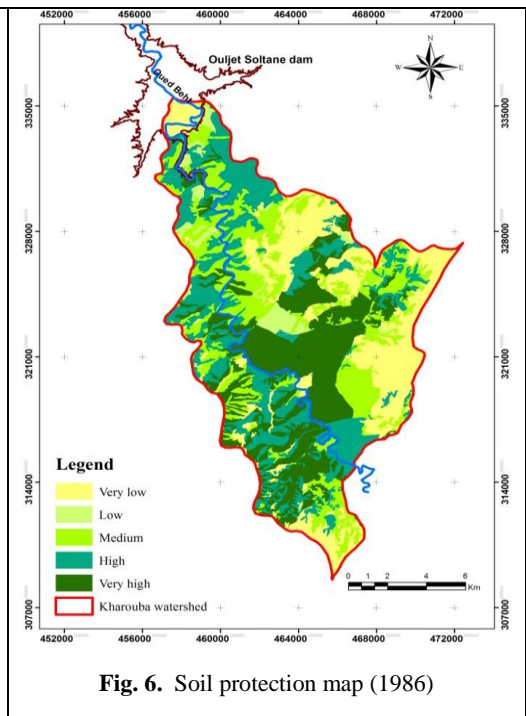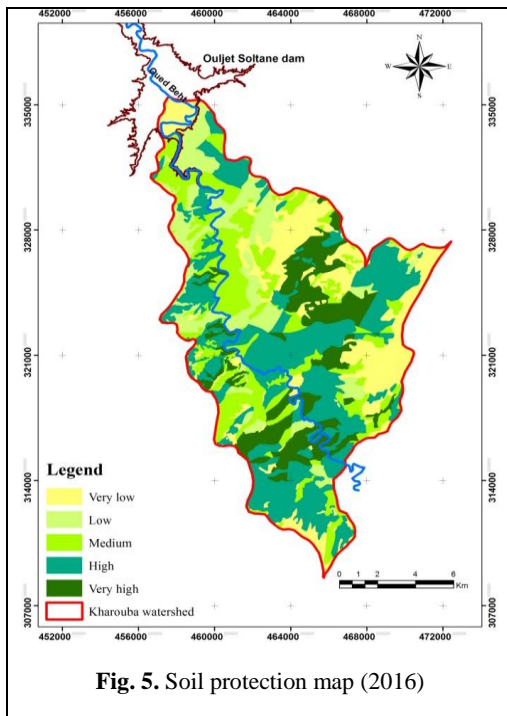
The analysis of the soil protection levels' distribution depending on the vegetation cover nature and density shows that soils with high protection are mainly located in *Tetraclinis articulata* and in dense to medium-dense *Quercus rotundifolia* forests with a very developed undergrowth. However, the low protection soil can be found in very degraded rangelands, bare soils and bad-lands.

4.3. Erodibility map analysis

The distribution analysis of the erodibility levels (**Fig. 7 and 8**) reveals that the most representative class is the one belonging to the strong class with 38 % of the total study area, followed by the class of medium erodibility whith 26 %. On the other hand, low to moderate erodibility affects only 18 % of the total kharouba Watershed area.

In addition, the erodibility map indicates that zones where the slope is steep, erodibility is always high to extreme. This can notably be observed at the southern and south-eastern part of the watershed. However, in the north, north-west and the middle of the watershed, the situation is less worrying due to the dominance of weak to moderate levels of erodibility.

Fig. 7. Erodibility map

Fig. 8. Levels of erodibility
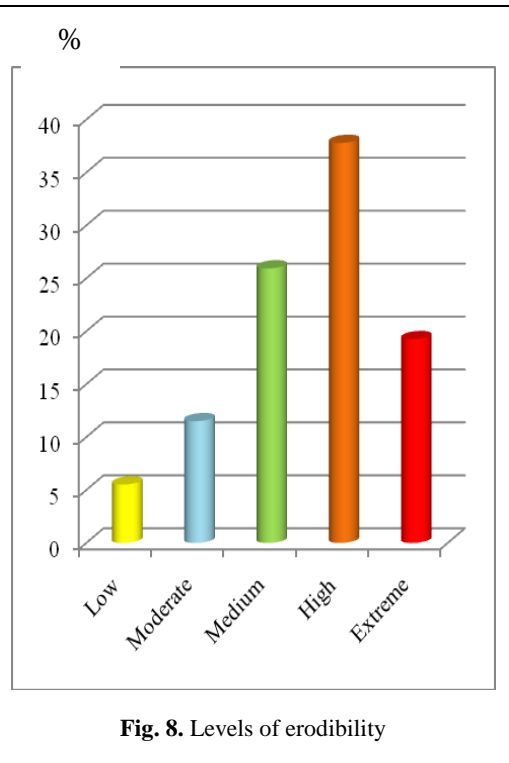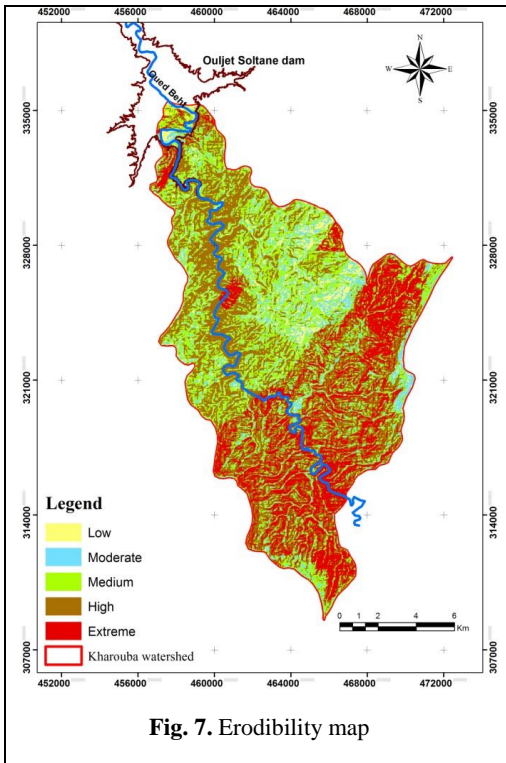
4.4. Erosion status map analysis

The mapping of the erosion states of 1986 and 2016 is obtained by overlaying erodibility and soil protection level maps of 1986 and 2016. The erosional status maps

analysis (**Fig. 9 and 10**) shows that erosion is active and apparent over more than 63 % of the total watershed area. It takes different kinds of erosion, including sheet erosion and gullying.

Areas of high erosive risk correspond particularly to rough terrain with fairly high soil friability rate and low to very low recovery rate.

The dynamics of erosion status analysis exhibit an increase of the high and extreme states expanding from 36 % of the total area in 1986 to 41 % in 2016. This increase mainly concerned the southern and northern part of Kharouba watershed, more particularly in areas where the vegetation cover and notably *Tetraclinis articulata* was severely degraded, in addition to the zones at the edge of Oued Beht. This is due to the dominance of sedimentary formations. Similarly, the erosion map analysis shows that areas marked by important vegetation cover are not very sensitive to erosion.

Our results highlight the predominant role of the vegetation cover in the overall decrease of the erosion rate. This vegetation protects the soil surface against the raindrops impact, slows down the speed of runoff water and maintains good soil porosity, making it highly resistant to erosion (Sabir et al., 1994; Zhou et al., 2008; Fletcher, 2017; Hou et al., 2016).

Fig. 9. Erosion status map (2016)   **Fig. 10.** Erosion status map (1986)
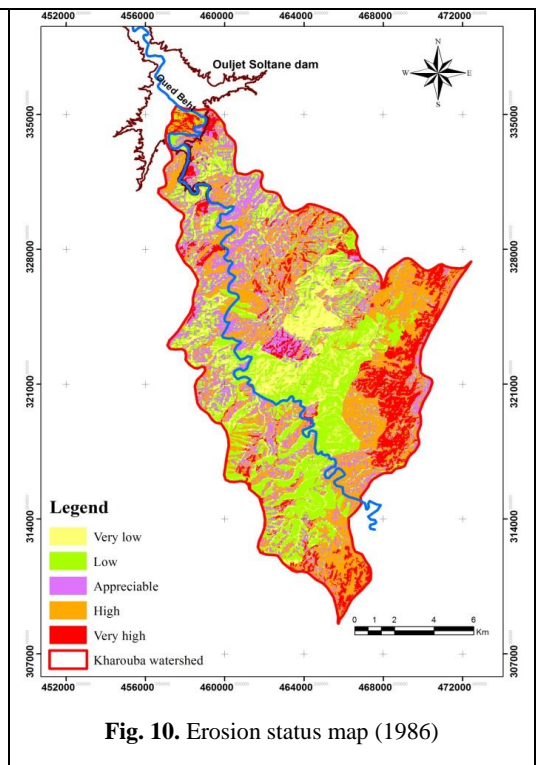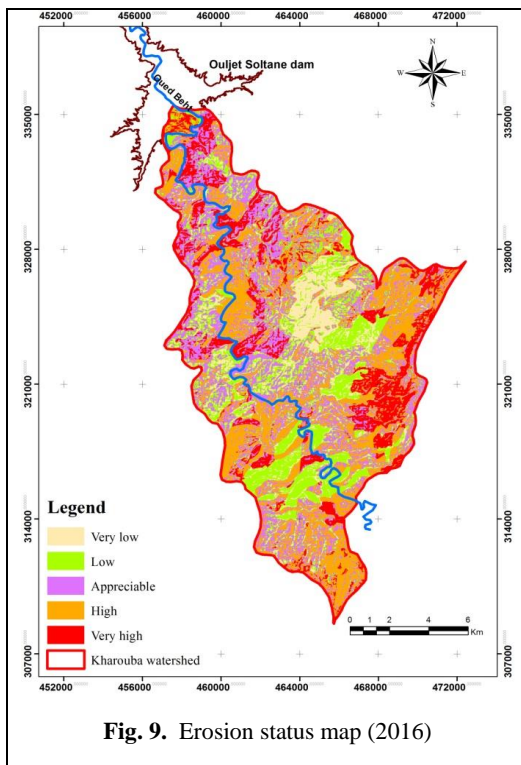
5. CONCLUSIONS

   Kharouba watershed, in upstream of "Ouljet Soltane" dam, covers an area of about 19 888.50 hectares and is largely dominated by forests along with land suitable for grazing and uncultivated land. It offers valuable forest resources due to its rich floristic diversity.

   The evaluation of the forest cover dynamics impacts on water erosion in this watershed pinpoints the regressive evolution of the vegetation cover between 1986 and 2016. This decline has stressed the increased water erosion risk in Kharouba watershed causing the expansion of areas that are vulnerable to water erosion from 36 % in 1986 to 41 % in 2016.

   Given the situation, it is necessary to intervene to fight against erosion, based on an innovative approach that relies on the improvement of the living conditions of the local population in order to reduce the pressure on the forest resources while ensuring their conservation and development.

R E F E R E N C E S

Al Karkouri, J., Laouina, A., Roose, A. & Sabir M. (2000) Capacité d'infiltration et risques d'érosion des sols dans la vallée des Beni Boufrah Rif central (Maroc). *Bulletin du Réseau Erosion*, **20**, 342-356.

Briak, H., Moussadek, R., Aboumaria K. & Mrabet R. (2016) Assessing sediment yield in Kalaya gauged watershed (Northern Morocco) using GIS and SWAT model. International Soil and Water Conservation Research. *International Soil and Water Conservation Research*, **4**(3), 177-185.

Da Cruz, D.C., Benayas, J.M.R., Ferreira, G.C., Monteiro, A.L., Schwartz, G. (2019) Evaluation of soil erosion process and conservation practices in the Paragominas-pa municipality (Brazil). *Geographia Technica*, **14**(1), 14-35, DOI: 10.21163/GT_2019.141.02

Dallahi Y., El aboudi A. & Aafi A. (2016) A contribution to the knowledge of the Moroccan Central Plateau plant communities. *Plant Sociology*, **53** (2), 41-46.

Dallahi Y., El aboudi A., Aafo A. & Belghazi B. (2016) Inventory of medicinal plants in the Site of Biological and Ecological Interest of Kharouba (Central Plateau, Morocco). *J. Mater. Environ. Sci.*,**7** (11), 3993-3999.

Dallahi, Y., Chahhou, D., El Aboudi & A., Aafi, A. (2017) Distribution Mapping and chemical composition of Tetraclinis articulata (Vahl.) Masters in the Site of Biological and Ecological Interest of Kharouba (Central Plateau, Morocco). *Journal of Materials and Environmental Science*, **8** (7), 2474-2479.

Damnati, B., Sanaa, I. & Radakovitch, O. (2013) Quantifying erosion using 137Cs and 210Pb in cultivated soils in three Mediterranean watersheds: synthesis study from El Hachef, Raouz and Nakhla (North West Morocco). *Journal of African Earth Sciences*, **79**, 50-57.

El Gaatib, R., Larabi, A. & Faouzi M. (2015) Integrated elaboration of priority planning of vulnerable areas to soil erosion hazard using Remote Sensing and GIS techniques: A pilot case of the Oued Beht Watershed (Morocco). *Journal of Materials and Environmental Science*, **6** (11), 3110-3127.

Fletcher, W.J. (2017) Anthropogenic trigger for Late Holocene soil erosion in the Jebel Toubkal, High Atlas, Morocco. *Catena*, **149** (3), 713-726.

HCEFLCD (2007) Plan d'Action du Haut Commissariat aux Eaux et Forêts et à la Lutte Contre la Désertification, 11-13.

Heusch, B. (1970) L'érosion du Pré-Rif. Une étude quantitative de l'érosion hydraulique dans les collines marneuses du Pré-Rif occidental. *Annales de la recherche forestière*, **12**, 9-176.

Hou J., Wang H., Fu B., Zhu L., Wang Y. & Li Z. (2016) Effects of plant diversity on soil erosion for different vegetation patterns. *Catena*, **147**, 632-637.

Iaaich H., Moussadek R., Baghdad B., Mrabet R., Douaik A., Derradji A. & Bouabdli A. (2016) Soil erodibility mapping using three approaches in the Tangiers province, Northern Morocco.

International Soil and Water Conservation Research. *International Soil and Water Conservation Research*, **4**, 159-167.

Laouina, A. (1998) Dégradation des terres dans la région méditerranéenne du Maghreb. *Bulletin du Réseau Erosion*, **18**, 33-53.

Moufaddal, K. (2002) Résultats des parcelles d'érosion dans le bassin versant de l'oued Nakhla,Maroc. *Bulletin du Réseau Erosion*, **21**, 244-254.

Naimi, M., Tayaa, M., Ouzizi, S. (2005) Cartographie des formes d'érosion dans le bassin-versant de Nakhla (Rif occidental, Maroc). *Secheresse*, 16, 79-82.

PAP/RAC (1997) Guidelines for mapping and measurement of rainfall-induced erosion processes in the Mediterranean coastal areas. PAP-8/PP/GL.1, Priority Actions Programme Regional Activity Centre (MAP/UNEP), with the co-operation of FAO : XII, 70 p.

Sabir, M., Merzouk, A., Berkat, O. & Roose, E. (1994) Effet du pâturage sur l'état de surface, l'infiltrabilité et la détachabilité du sol dans un milieu pastoral aride (Aarid, Haute Moulouya, Maroc). *Bulletin du Réseau Erosion*, **14**, 444-462.

Simonneaux, V., Cheggour, A., Deschamps, C., Mouillot, F., Cerdan, O. & Le Bissonnais, Y. (2015) Land use and climate change effects on soil erosion in a semi-arid mountainous watershed (High Atlas, Morocco). *Journal of Arid Environments*, **122**, 64-75.

Suwarno, Sutomo, Aditama, M.R. (2019) The analysis of the landslide vulnerability sub watersheds Arus in Banyumas Regency. *Geographia Technica*, **14**(2), 112-119, DOI:10.21163/GT_2019.142.10

Zhou, P., Luukkanen, O., Tokola, T. & Nieminen, J. (2008). Effect of vegetation cover on soil erosion in a mountainous watershed. *Catena*, **75** (3), 319-325.

CALCULATION OF THE RIVER FLOW
WITH DIFFERENT PROBABILITIES OF OCCURRENCE
USING ARTIFICIAL NEURAL NETWORK

Ioan Florin MOLDOVAN[1]

ABSTRACT:
The aim of this paper is to calculate the river flow with different necessary probabilities of occurrence, by the Artificial Neural Network (ANN) method. The studied ANN uses a radial basis function (RBF) architecture, with an input layer, a hidden layer and an output layer. Three series of maximum annual flow were used for the input layer. The series of maximum annual flow were collected from gauge stations, situated on three tributaries of the Mures river, Romania. The number of the neurons in the input layer is variable, according to the number of the flow values in the series. It means that the architecture of the ANN is different from one series to another. Consequently, the ANN has to repeat the calculation stages for each series. The results revealed that the ANN interpolates very well in the range of the values of the series. Each time, the stop condition of the target error was met. A comparison was made between the values of the flow calculated by the ANN method and by the statistical (classical) method using the Pearson type 3 distribution. The comparison showed that there are significant differences for the flow values corresponding to the 0.01% and 0.1% probabilities, and less or not significant for the rest.

Keywords: *River flow, Probabilities of occurrence, Artificial Neural Network (ANN), Romania.*

1. INTRODUCTION

In many domains, the scientists tried to imitate nature, including to imitate the functioning of the the human brain, which is a very complex "computer". The Artificial Neural Networks (ANNs) are inspired by the human nervous system and their architecture is based on parallel processing (Aichouri et al, 2015).

In the last decades, the Artificial Neural Networks (ANNs) were developed on a large scale, in different domains, like arts, natural sciences, social sciences, industry, agriculture, sports, entertainment. The development was due to the features that makes the ANNs very effective. The ANN is an interpolation-approximation model. An important feature is that in an ANN the information is distributed along the artificial neural network, being stored in the synaptic weights between the neurons. This property gives the possibility of the ANN to be tolerant to input data with distortions. That makes ANN very effective for distorted character recognition (Enăchescu, 1998). A well-known application of this property is used in the field of the optical character recognition (OCR).

Another important propriety is that an ANN is able to simulate non-linearity in a system. This way it can distinguish between relevant and irrelevant data characteristics (de Vos & Rientjes, 2005).

---
[1]*Babes-Bolyai University, Faculty of Geography, 400084, Cluj-Napoca, Romania, moio13898@studmail.ubbcluj.ro*

These features recommend the ANNs to be used in hydrology, as well. Good results were obtained for rainfall-runoff models, as mentioned in many studies (e.g. Dar, 2017; de Vos & Rientjes, 2005; Dounia, Sabri, & Yassine , 2014; Firuzi et al 2011; Kashiwao et al, 2017; Lallahem & Mania, 2003; Sarkar & Kumar, 2012).

There are many architectures types for the ANN models. A very common neural network architecture is the Multi-Layer Perceptron (MLP). A MLP consists of three types of layers: input, hidden, and output. The input data are introduced via the input layer. The processing is done in the hidden layers, and the result is presented to the output layer. In a MLP the data flows in one direction, from input to output, and due to this property it is named feed forward neural network (Tanty & Desmukh, 2015).

For this study more appropriate is another type of architecture, the radial basis function (RBF). It is, also, a feed forward neural network. The structure of the RBF network is similar, with three layers, in which the hidden layer performs a fixed nonlinear transformation with no adjustable parameters (Leonard et al, 1992, as cited by ASCE Task Committee, 2000). The hidden layer has nodes and a ''center'' which can be considered the weight vector of the hidden layer. To measure the distance between the input vector and the center, it is used the standard Euclidean distance. For each node is computed the distance between the input vector and the center, and the result is transformed by the activation function, wich is a nonlinear function (ASCE Task Committee, 2000).

A very important field in hydrology is the calculation of the river flow value for a certain probability of occurrence. These values are used for practical applications (e.g. hydrotechnical construction designs or bridge designs). Thus, it could be necessary to calculate the flow for the corresponding probabilities: 0,01%, 0,1%, 1%, 2%, 5% and 10% for the maximum flow, respectively 80%, 90%, 95% and 99% for the minimum flow. This study will analyze only the maximum flow series.

The annual maximum flow value represents the peak of the highest flood during the year, which can be very destructive, with loss of human life and huge damages. For this reason, the hydrologists are highly interested in calculating the maximum river flow with different probabilities of occurrence, in order to use the maximum flow value in the domain of flood protection. Usually, the standards in each country establishes what probabilities have to be calculated according the type of the construction that to be designed. It is the case for the Romanian legislation, too.

The most used method for calculations is the statistical (classical) method. Still, the advantage of the ANN method is that it can reach very low interpolation error, as presented in this study.

2. STUDY AREA AND DATA

The Mureș river basin has 28310 km^2 and a length of 761 km of the main river. It represents about 12% of the surface of Romania.

For this study data from three gauging stations were analyzed on three tributaries: Ampoi, Aries and Strei (**Fig. 1**).

Barabant gauge station is situated on the Ampoi river. The surface of the catchment area is 576 km^2, the length of the river is 57 km and the average altitude is 700 m. Petreni gauge station is situated on the Strei river, the surface of the catchment area is 1983 km^2 and the average altitude is 911 m. Finally, Turda gauge station is situated on the Aries river, the surface is 3005 km^2, the length of the river is 166 km and the average altitude is 818 m.

The number of the values in each series is variable as can be seen in Table 2.
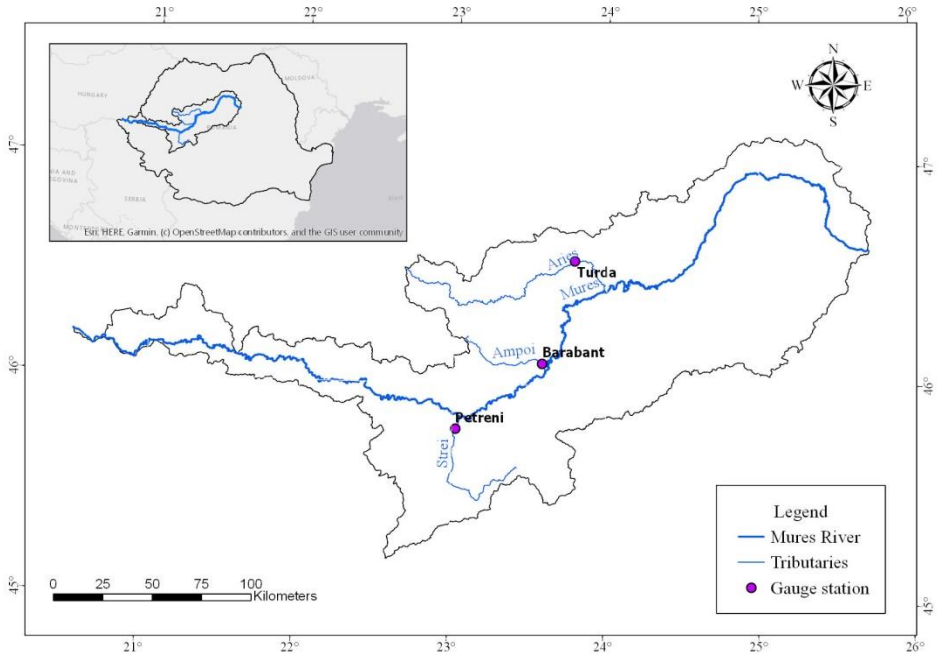
Fig. 1 – The Mureș River Basin location in Romania.

3. METHODOLOGY

3.1 Theoretical aspects of the ANNs

The general theoretical aspects of the ANNs are described in many articles and books.

In general, an ANN is composed of neurons disposed in layers. A neuron "j" in a layer (**Fig. 2**) computes an output, based on the weighted sum of all its inputs (S_j), and based on the activation function ($f(S_j)$).
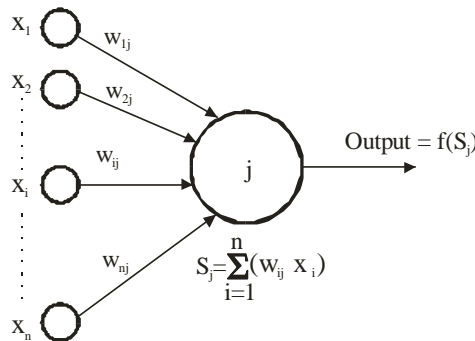
Fig. 2 - Activation of a single neuron "j" (according to Dawson & Wilby, 2001).

The activation functions and their derivative are simple to calculate. They can be identical, logistic sigmoid, linear, threshold, Gaussian or hyperbolic tangent functions and they depend on the type of network used. The most common functions are the logistic sigmoid and the hyperbolic tangent.

In the logistic sigmoid activation function (1), x represents the weighted sum of inputs to the neuron and f(x) represents the neuron's output (Dawson & Wilby, 2001):

$$f(x) = \frac{1}{1 + e^{-x}} \qquad (1)$$

The ANN used in this study has a RBF architecture with three layers: the input layer, one hidden layer and the output layer. It is a feed-forward with back-propagation (FFBP) ANN. The activation of the neuron "j" is the same as already mentioned (**Fig. 2**).

Some proprieties of the RBF architecture will be presented in the following (according to Enăchescu, 1998).

The input layer has n neurons (2), based on the number of values in the series:

$$\mathrm{x}_i = \left(x_i^{(1)}, x_i^{(2)}, ..., x_i^{(n)} \right) \qquad (2)$$

where: - i represents the i-th series of data
- x_i represents the input data vector of the i-th series
- n is equal to the number of values in the input data series

The Bias term (the red circle in **Fig. 3**) can be considered implicitly or explicitly in the model. In this study it was considered implicitly.

The hidden layer has the number of neurons equal to the number values N of the training set T (3):

$$T = \left\{ \left(\mathrm{x}_i, f\left(\mathrm{x}_i\right) \right) \middle| i = 1, 2, ..., N \right\} \qquad (3)$$

where the training set is a subset of the entire set of input data. In our case, $N=n$, because there are no subsets of the data series.

The activation functions (4) for the hidden layer are:

$$f(x) = \sum_{i=1}^{N} w_i G(x; x_i) \qquad (4)$$

and are different for each neuron, for example the k-th neuron has the activation function centered in the point x_k, and the function is (5):

$$G(x; x_k) = G(x - x_k) \qquad (5)$$

The output layer has one neuron, because the ANN will calculate one value of flow at a time.

Because of the small number of values in each data series, we will consider the following: the number of the neurons in the input layer is equal to the number of the input values in each series of annual maximum flow; the number of the neurons in the hidden layer is equal to the number of the neurons in the input layer.
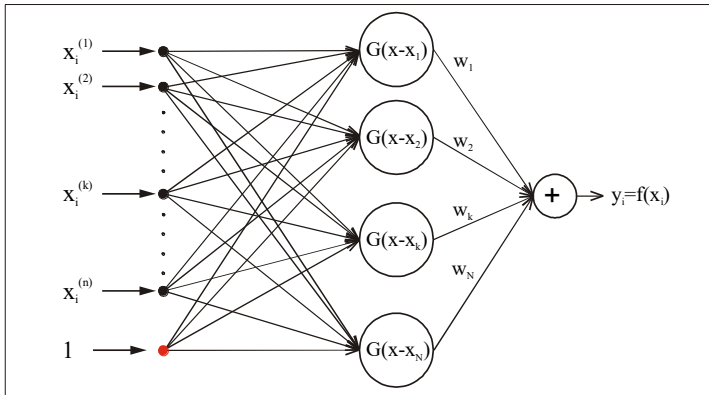
Fig. 3 - The architecture of the RBF (according to Enăchescu, 2008).

In this study, the identical function (7) was considered for the activation function of the hidden layer:

$$f(x_i^{(k)}) = x_i^{(k)} \tag{7}$$

where: $x_i^{(k)}$ represents the *k*-th data value in the *i*-th series of data.

The activation functions in the output layer are Radial Basis Functions (RBF) of Gaussian type (8):

$$G(x - x_i) = e^{-\frac{(x-x_i)^2}{\sigma_i^2}}, \quad i = 1,2,...,N \tag{8}$$

where: σ_i represents the diameter of the *i-th* cluster.

The number of the clusters (K) is equal to the number of the input values (K = N = n). It means that each data is a cluster and the activation functions are „centered" on the data values. According to this consideration (9), $\sigma_i = 1$:

$$G(x - x_i) = e^{-(x-x_i)^2}, \quad i = 1,2,...,N \tag{9}$$

The final value of the neuron in the output layer is weighted by the function (10):

$$y = \frac{\sum_{i=1}^{K} w_i G(x - x_i)}{\sum_{i=1}^{K} G(x - x_i)} \tag{10}$$

Based on the above considerations, the architecture for this study is represented in **Fig. 4**.
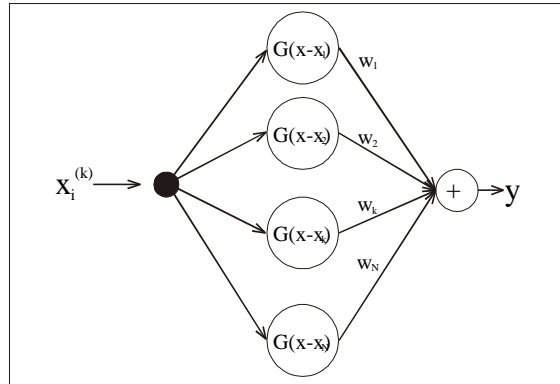
Fig. 4 - The RBF architecture for this study, corresponding to the *k*-th value
from the *i*-th input series.

A descendant gradient algorithm was proposed for the model. The learning error E_l was calculated by formula (11), the root mean square error - RMSE (Sarkar & Kumar, 2012):

$$E_l = RMSE = \sqrt{\frac{\sum_{i=1}^{n}(z_i - y_i)^2}{n}} \tag{11}$$

where:
- z_i represents the *i*-th input value in the annual maximum flow series
- y_i represents the *i*-th corresponding value of the flow calculated by the ANN
- n represents the number of values in the annual maximum flow series

The algorithm stops when the condition for the error E_l is met (12):

$$E_l \rightarrow \min \tag{12}$$

Practically, the stop condition (12) can be written as follows (13):

$$E_l = \sqrt{\frac{\sum_{i=1}^{n}(z_i - y_i)^2}{n}} \leq \varepsilon \tag{13}$$

where: ε is the target error (e.g. $\varepsilon = 10^{-10}$)

After the calculation of the error E_l, the Back-Propagation algorithm, which uses the derivative of the function (9), will propagate the error back to the neurons in the hidden layer, by modifying the weights. Then a new epoch (iteration) starts, which will stop when the condition (13) is reached again.

A supplementary stop condition was imposed, by limiting the number of the learning epochs to 10.000, in case that the program cannot reach the target error. This can happen if the function E_l is blocked in a local minimum value of the Equation (13).

There are many programs for ANN models, including free versions. For this study, it was preferred to design a program in C# language (with Microsoft Visual Studio Community 2015), because it gives more flexibility to test different versions of architecture and methodology and to plot the results in a desired manner.

For instance, the results of the ANN were compared with the results given by the statistical (classical) method. A Pearson type 3 density probability function was calculated for each series of input data and plotted on the same graphics, as presented in paragraph 3.2.2 and in Chapter 4.

3.2 Practical considerations

In general, there are 2 main stages necessary to obtain the results from an ANN. The first is the "learning" stage and the second is the „generalization" stage.

3.2.1 The learning stage

In this study, the input values are the empirical probabilities. The output values are the annual maximum flows. After each series has been sorted in descending order, for each annual maximum flow the empirical probability (pe_i) is calculated, based on the Weibull formula (14), in general used to calculate the probabilities for the maximum flow:

$$pe_i = \frac{i}{n+1}, \tag{14}$$

where:
- i represents the position in the sorted series of the *i*-th value
- n represents the total number of the values in the series

This way, n pairs (pe_i, z_i) can be obtained, composed by the annual maximum flow value z_i and its corresponding empirical probability pe_i .

Due to the fact that the activation functions (9) have the results in the range of [0, 1], before starting the learning stage, the normalization (McCaffrey, 2014) of the z_i values was made by the Min-Max Normalization formula (15):

$$z_i = \frac{z_i^{ini} - z_{min}}{z_{max} - z_{min}} \tag{15}$$

where:
- z_i is the normalized value based on the initial z_i^{ini} value
- z_{max} and z_{min} are the maximum respectively the minimum values of the series

Due to the fact that the input data consists of the pairs (pe_i, z_i) where the output values are known (z_i), the proper learning method for the ANN is the supervised learning. Also, because the number of values in each series is different, the architecture of the ANN, meaning the number of neurons in the input layer, is different for each series of data. Consequently, the architecture is modified when the series is changed, and the ANN has to repeat the calculation stages for each series. The architecture is not modified during the calculation stages.

In the supervised learning stage, the input values are presented to the input layer of the ANN, the known output values are presented to the output layer, and the ANN will learn to calculate the output values with a given target error, based on the Back-Propagation algorithm.

At the beginning of the learning stage, the weights are initiated with random values comprised in the interval (0, 1). In each epoch (iteration) the learning error (11) is calculated, and the weights w_k (**Fig. 4**) are modified accordingly by the Back-Propagation algorithm. The learning stage stops when the condition (13) is met. Now, the ANN has "learned" to calculate the values of the annual maximum flow, based on the pairs (pe_i, z_i). Practically, the "learning" consists in the fact that the values of the weights were fine-tuned during this stage. The final values of the weights will be used during the generalization stage.

3.2.2 The generalization stage

Based on the learning stage, in which the ANN has learned to calculate the output values, the ANN can calculate the annual maximum flow for the necessary probabilities, other than the empirical probabilities (14) that were used in the learning stage. This is done by running the program with the final weights calculated in the learning stage, for the necessary probabilities, by presenting to the input layer the series of the necessary probabilities, and obtaining at the output layer the corresponding flow values. In the generalization stage, the weights will no longer be modified.

The representation of the data is made on Normal probability paper. This representation has the propriety that it "zooms out" the distances between the extreme values of the graphics (on the left and right sides).

4. RESULTS AND DISCUSSIONS

For all three series of data the program has reached the target error in less than 2000 epochs (**Fig. 5**).

The processing duration was less than 1 second, for each series, on a computer with Microsoft Windows 8.1, Intel i7 processor and 4 GB RAM memory. In **Fig. 5**, can be seen that the input data (red "X") are very well approximated in the learning stage (the blue dots). The results are similar for all series of data provided by the other two gauging stations (**Table 1**).

In the generalization stage the ANN has calculated the corresponding flow for the probabilities mentioned in the introduction. On the graphics, these probabilities were represented by the green dots.

Table 1.

The results of the ANN model.

Gauge station	River	Learning error (RMSE)	Generalization error (GE)	Number of epochs[1]	Processing duration[2] (seconds)
Barabant	Ampoi	$9,95 \times 10^{-11}$	0,29	1395	0,65
Petreni	Strei	$9,86 \times 10^{-11}$	0,34	1292	0,85
Turda	Aries	$9,99 \times 10^{-11}$	0,29	1280	0,65

[1] It can vary due to the random initialization values of the weights

[2] It can vary due to the momentary running tasks of the processor
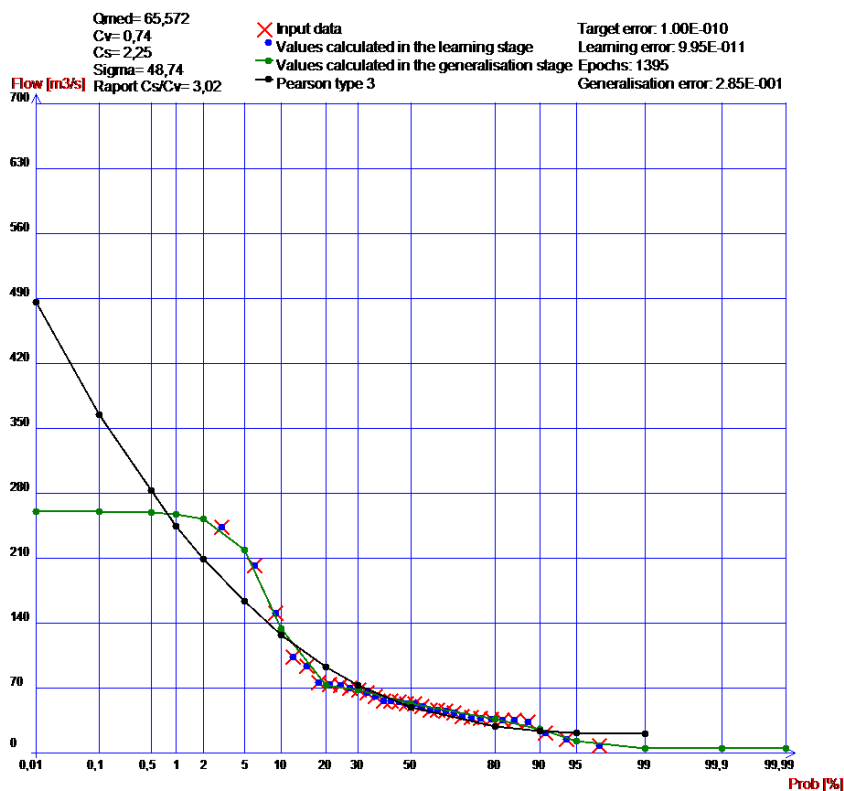
Fig. 5 – Graphical representation of the result for the Barabant gauge station.

The statistical parameters (**Table 2**): $Q_{average}$ (average flow of the series), C_v (coefficient of variation), C_s (coefficient of asymmetry), σ (standard deviation) and C_s/C_v report were calculated in order to plot the Pearson type 3 density probability function on the same graphics (the black dots). Pearson type 3 is often used for the Romanian rivers, because in general, it approximates the river flow well. The calculations were made according to the studies presented by Drobot, R. (1997).

Table 2.

Statistical data of the annual maximum flow series.

Gauge station	River	$Q_{average}$ (m³/s)	C_s	C_v	C_s/C_v	σ (Sigma)	Number of values
Barabant	Ampoi	65,572	2,25	0,74	3,02	48,74	32
Petreni	Strei	211,61	0,6	0,47	1,27	99,82	40
Turda	Aries	260,724	2,09	0,77	2,73	199,54	34

The comparison between the ANN results and the Pearson type 3 values reveals that there are significant differences for the flow values corresponding to the 0.01% and 0.1% probabilities, and less or not significant for the rest.

5. CONCLUSIONS

The ANN model used in this study proved that it can interpolate very well a series of data, according to the target error. On the present generation of computers, for small number of values in the series, the duration of the calculations is very short.

In this study, the target error value of 10^{-10} was reached each time, without exceeding the limit of the number of epochs. From the physical point of view, the target error has the unit measure of a flow, consequently the value is 10^{-10} m^3/s. One can say that the error of the calculation made by the ANN is very low. For the generalization error (GE) the situation is similar, because GE represents less than 1% from the $Q_{average}$, for all studied gauge stations.

A disadvantage of the ANN model is that for a certain gauge station, if the data series has to be added with at least one more value, the ANN model has to pass the 2 main stages again, because the addition will modify the architecture of the ANN.

The comparison between the ANN results and the Pearson type 3 values reveals that there are significant differences for the flow values corresponding to the 0.01% and 0.1% probabilities, and less or not significant for the rest. This is due to the fact that the ANN has no flow values for the learning stage in those areas of probability. Still, this is the area of interest for hydrologists, because the flow with these probabilities of occurrence are necessary to dimension the constructions (like bridges), according to the national standards. The statistical method gives the possibility to extrapolate in this area of probability.

This study is in an incipient stage. It should be repeated on the main river and on different other tributaries to observe if the conclusions have a general aspect. Another direction of research is to find a way for the ANN to be able to extrapolate in the mentioned area of interest for probabilities (possible by extending the data series with other parameters). Also, a further study should verify if there is an influence from the geographical parameters (e.g. from the elevation).

R E F E R E N C E S

Aichouri, I., Hani, A., Bougherira, N., Djabri, L., Chaffai, H. & Lallahem, S. (2015) River flow model using artificial neural networks, *Energy Procedia,* 74, 1007 – 1014. [Online] Available from: https://doi.org/10.1016/j.egypro.2015.07.832

ASCE Task Committee on Application of Artificial Neural Networks in Hydrology (2000 I) Artificial Neural Networks in hydrology: I: preliminary concepts, *Journal of Hydrology Engineering,* 5(2), 115-123. [Online] Available from:
   https://pdfs.semanticscholar.org/439b/ca74d7b1240d218d69e6b55539b52a489f57.pdf

Dar, L. A. (2017) Rainfall-runoff modeling using artificial neural network technique, *International Research Journal of Engineering and Technology (IRJET),* 04, 11. [Online] Available from: https://www.researchgate.net/publication/321706414

Dawson, C. W., & Wilby, R. L., (2001) Hydrological modeling using artificial neural networks, *Progress in Physical Geography*, 25, 1, 80-108. [Online] Available from: DOI: 10.1177/030913330102500104

de Vos, N. J. & Rientjes, T. H. M. (2005) Constraints of artificial neural networks for rainfall-runoff modelling: trade-offs in hydrological state representation and model evaluation, *Hydrology and Earth System Sciences,* 9, 111−126. [Online] Available from: DOI: 10.5194/hessd-2-365-2005

Drobot, R. (1997) *Bazele statistice ale hidrologiei,* ISBN 973-30-4832-1, Bucharest, Romania, Ed. Didactică și Pedagogică R.A.

Dounia, M., Sabri, D., & Yassine, D. (2014) Rainfall-Rainoff Modeling Using Artificial Neural Network, *APCBEE Procedia* 10 , 251 – 256. [Online] Available from:
   https://doi.org/10.1016/j.apcbee.2014.10.048

Enăchescu, C. (1998) *Bazele teoretice ale rețelelor neuronale*, Ed. Casa Cărții de Știință, Cluj-Napoca, Romania

Enăchescu, C. (2008) Approximation capabilities of neural networks, *JNAIAM - Journal of Numerical Analyses, Industrial and Applied Mathematics*, 3, 3-4, 221-230, [Online] Available from: https://pdfs.semanticscholar.org/3139/611a145f3319382951fe283c810e8cc7501c.pdf

Firuzi, S., Sharifi, M., Borna, K. & Rajabi, M. (2011) Using Empirical Relationships and Neural Network in GIS for Developing Rainfall-Runoff Model, TS09E - Engineering Surveying - Software, 5264. [Online] Available from: https://www.researchgate.net/publication/316154879

Kashiwao, T., Nakayama, K., Ando, S., Ikeda, K., Lee, M. & Bahadori, A. (2017) A neural network-based local rainfall prediction system using meteorological data on the Internet: A case study using data from the Japan Meteorological Agency, *Procedia Engineering* 154, 1110 – 1115. [Online] Available from: http://dx.doi.org/10.1016/j.asoc.2017.03.015

Lallahem, S. & Mania, J. (2003) A Nonlinear Rainfall-Runoff Model using Neural Network Technique: Example in Fractured Porous Media, *Mathematical and Computer Modeling*, 37, 9-10, 1047-1061. [Online] Available from: https://doi.org/10.1016/S0895-7177(03)00117-1

McCaffrey, J. (2014) Neural Networks Using C# - Succinctly, 2501 Aerial Center Parkway, Morrisville, NC 27560. [Online] Available from: www.syncfusion.com

Sarkar, A. & Kumar, R. (2012) Artificial Neural Networks for Event Based Rainfall-Runoff Modeling, *Journal of Water Resource and Protection,* 4, 891-897. [Online] Available from: http://dx.doi.org/10.4236/jwarp.2012.410105

Tanty, R. & Dr. Desmukh, T. S. (2015) Application of Artificial Neural Network in Hydrology-A Review, *International Journal of Engineering Research & Technology (IJERT)*, 2278-0181, 4, 6. [Online] Available from: DOI: 10.17577/IJERTV4IS060247

A GIS-BASED MULTICRITERIA SPATIAL DECISION SUPPORT SYSTEM MODEL TO HANDLE HEALTH FACILITIES RESOURCES. CASE OF CRISIS MANAGEMENT IN BATNA, ALGERIA

Belkacem LAHMAR[1] , *Hadda DRIDI[2], and Ahmed AKAKBA[3]*

ABSTRACT:
The city of Batna is exposed to risks of different natures and varied occurrences and cannot be avoided, the available resources to face up the results of catastrophes become very limited, especially the healthcare system, that must be flexible and take care all wounded fast as possible but also it should take in consideration their capacity and managing their resources, but it suffers from structural problems which has a negative effect on its resilience that help to rebound and assume to the normal functioning after a disaster. This paper aims is to develop a spatial model and present the possibility of the implementation inside GIS (Geographic Information System) environment to handle the problem of health resources (workforces and medical supply), and evaluate the evacuation plane in crisis management by find and the closest health centre that can take care the wounded within an acceptable distance, and in the same time the model should chose the center with available capacity.

Key-words: *Model, health services, crisis management, Capacity.*

1. INTRODUCTION

The prevention of major risks represents one of four principal phases in PPRR model (**Fig. 1**), and the management of disasters within the framework of sustainable development constitute a global system initiated and led by the State, implemented by public institutions and local authorities.

Like many counties, Algeria is ranked height vulnerable to risks, and as result every few years one the major risks cause huge human losses and damages in infrastructure, economic and materials; specially risks related to:

- earthquakes and geological risks,
- flooding, climate risks,
- forest fires,
- industrial and energy risks,
- risks related to human health.

Historically Algeria knows number of disasters most of them are naturals but with significant losses and economic damages. The **Table 1** (Disaster history 1962-2012 in Algeria) shows some of them.

1 University of Batna 2, Laboratory of Natural Hazards and Spatial Planning (LRNAT), Batna, Algeria, b.lahmar@univ-batna2.dz / Belkacemlahmer05@gmail.com, ORCID ID: 0000-0002-8479-8982 Tel:(+213)657221097.

2 University of Batna 2, Laboratory of Natural Hazards and Spatial Planning (LRNAT), Batna, Algeria, Hadda.dridi@gmail.com

3 University of Batna 2, Laboratory of Natural Hazards and Spatial Planning (LRNAT), Batna, Algeria, dja_aka@yahoo.fr

Fig. 1. Crisis management model (PPRR). Source (Rogers and others 2011).

To avoid this problem, Algeria created a disaster management system, this program consists of emergency planning and responses which is relief planning called the ORSEC plan and special intervention planning. ORSEC is a territory plan and every city's local government assure execution of this plan in their territory during of major risks to ensure tents, chalets, or any other means of temporary accommodation, food and clean water, emergency medical; it composed of multiple modules to support and manage every particular aspect of a disaster, and must identify the following priorities:

- Rescue of people.
- The establishment of secure temporary hosting sites.
- The safety and health of the victims and their property.
- The establishment of energy supply.
- Internal intervention plans.
- Special intervention plans.

Table 1.

Disasters history 1962-2012 in Algeria. Source (protection 2017).

Date	Location name	Type of risks	Damages
10.10.1980	Chlef	Earthquake	2633 deaths, 8369 injured,70\% of building destroyed
18.08.1983	Jijel	Forest fire	11 deaths,19 burned person, burned area of 27000 hectare
10.11.2001	Bab El-Oued	Flood	900 deaths
21.05.2003	Boumerdess	Earthquake	2278 deaths,11000 injured,18000 without shelter
11.08.2008	Ghelizan	Gaz explosion	21 deaths
22.02.2012	El-Taref	Flood	2 deaths, significant material damage

One of the most important ORSEC module is the health module, but this last comprises several structural problems, such as random health facility distribution to population distribution, financing problems and difficulty adapting to new challenges which reflected in their functions (Chachoua 2014; Bouyoucef barr 2015), despite the decentralization of the national health system (SNS) and the dualism of health (Oufriha 2006), for better adaptation to local issues and reaction speed against local diseases and in case of significant risks; in addition, more than 48% of patients don't respect the graduation of care even in the

case of very simple ailments that do not require hospital care (Nasereddine 2016), so there is a random of distribution of patient, and the hospital capacity is overload and rich its maximum capacity, this situation decrease its efficiency and healthcare quality. Also, the health system in Algeria is not updated to adapt new spatial planning technologies like GIS.

The aim of this paper is to create a model for crisis management and implement in GIS environment, this model will deal with health module emergency needs and manages their capacity (workforces, medical supply…etc) in the response phase of crisis management model, in the same time it will assure the evacuate plane of wounded during a crisis to the closest health facility that has the ability to handle them.

3. STUDY AREA

The city of Batna is strategically located in eastern Algeria. Its geographical location represents an important crossroads connecting the east, west, north, and south of the country. Batna has experienced since its foundation (1844) a strong but random urban dynamic in terms of demography and space, which results a functional imbalance in public services. This affects the health service quality of over 301,708 inhabitants who live in the city (DSPB 2017). The city is located in a high-temperature zone (+35C° in summer) and moderate precipitation and low slope (3%-5%), these parameters increase the vulnerability of transmission epidemic problems whereas (Bendib *et al.* 2016; Issam and Said 2017) indicates that 48.89% of the total area of Batna is highly vulnerable to risks related to human health. To avoid this problem the local health department creates fourteen of health facilities to ensure primary healthcare and focus on optimizes the public health in the city and increase the accessibility to health care services (DSP 2017) (**Fig. 2**).
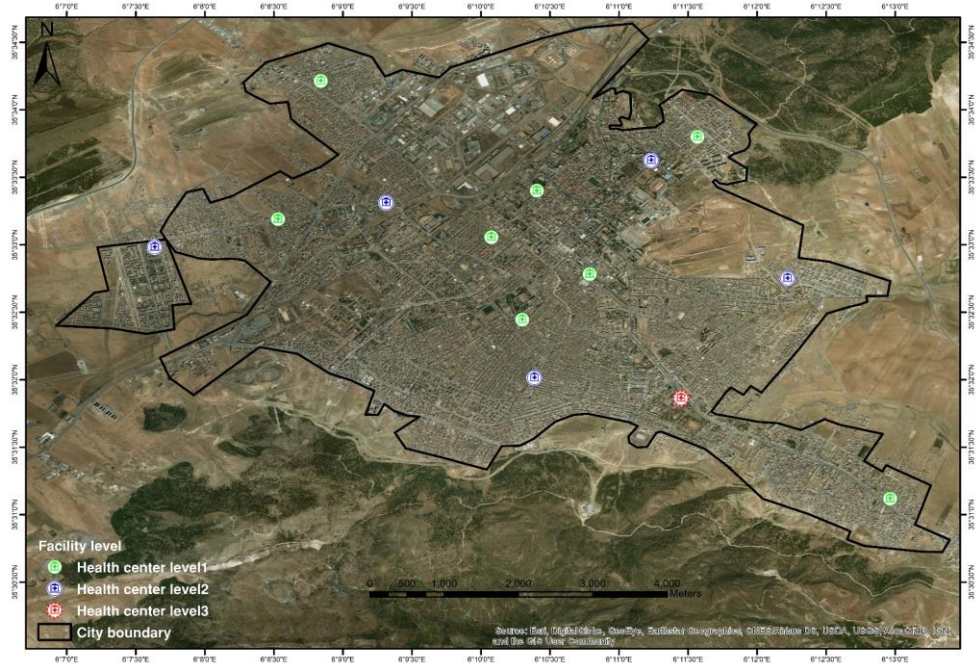

Fig. 2. Study area and health facilities distribution.

3. METHOD AND APPROACH

3.1. GIS in healthcare and crisis management

A GIS is a framework for gathering, managing, and analysing data, rooted in the science of geography, it integrates many types of data. It analyses spatial location and organizes layers of information into visualizations using maps (ESRI 2008). This unique capability helping user to make smarter decisions. It provides a strong and dynamic technique that allows us to model, manage geographic relationships, make a better decision, improve functional performance, generate more cost-effective citizen plans, evaluate spatial details, and modify information and maps (Meika 2010) .

In Addition, GIS push forward the health geographer to use range methods (quantitative, qualitative, spatial analysis) with answer the who gets what, where and why with respect to illness and appropriate care (Cromley and McLafferty 2011), also it can provide answers to the following questions, such as: How many paramedic units are required and where should they be located? What evacuation routes should be selected? does the storage facility is sufficient? Will the road networks handle the traffic? What quantity of supplies, bed space, and so forth (Johnson 2000), also it's a helpful tool for decision makers and they would enable them to make the appropriate decisions in the real time? There are also various functions which GIS can provide in the response missions such as: prepare maps, briefs, and status reports (ESRI 2008).

3.2. Spatial Decision Support Systems (SDSS)

SDSS has grown dramatically over the last few decades but there is still no universally accepted definition (Sugumaran and Degroote 2010), however we choose the definition of (Malczewski 1999) "The Spatial Decision Support Systems is an interactive computer based system designed to support a user or group of users in achieving a higher effectiveness of decision making while solving a semi-structured spatial decision problem". So basically, it's the application of Decision Support Systems (DSS) to solve problems and find the best actions (solutions) to move from an initial situation to a desired goal situation where the spatial and the geography in general are important (**Fig. 3**).

SDSS is technique executes mostly in GIS environment and widely in emergencies (Cova 1999; Gunes and Kovel 2000), but this classic operation of crisis management is focus on geographical part like scenario of evacuation and choose best street path in emergency situations (Nicoară and Haidu 2014; FILALI and KALLA 2016; Cadar *et al.* 2017; HASNAT *et al.* 2018), or focus on supply chain (medical supply, workforces) and the capacity of health (bed, The operating rooms...etc), but SDSS is a combined analytical tools with GIS environment and ensure multi criteria analyses, iterate the problem solving, have interactive user interface, offer the report generation and visualization, spatial analysis and spatial modelling capability (Mora *et al.* 2003; Sugumaran and Degroote 2010) (**Fig. 3**), so it represents a platform where the crisis management is done by taking the advantage of spatial data management and analysis, interactive user interface and semi or ill-structured problem solving for better decision in real time.
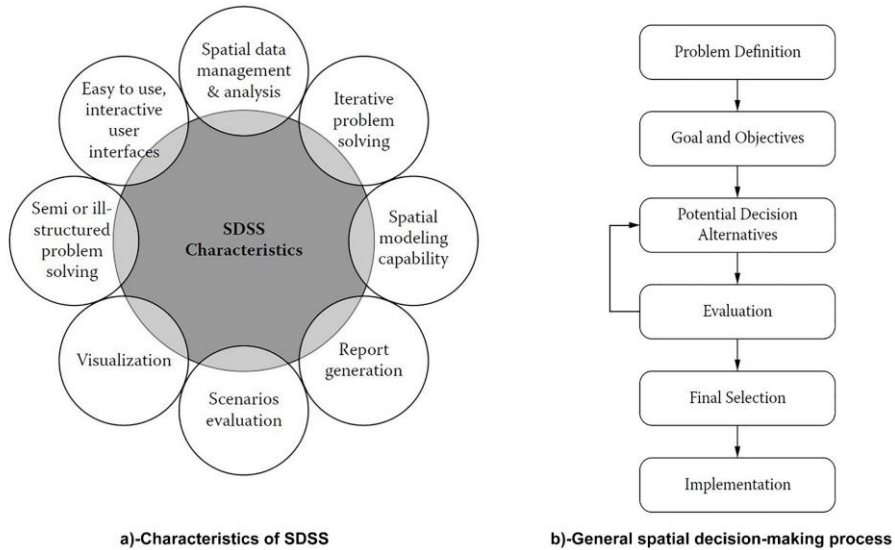
a)-Characteristics of SDSS   b)-General spatial decision-making process

Fig. 3. Characteristics of SDSS.

SDSS has several utilization combined with GIS and database management system (DMS) in different domain whether urban and planning field, agriculture or in housing (Coutinho-Rodrigues *et al.* 2011; Sultani *et al.* 2009; Makropoulos *et al.* 2003; Ayeni 2003; Zhang *et al.* 2009; Ascough *et al.* 2002) or in logistics and transportation domain (RUDA 2014); and it's a main part as well in risks and health (Wangdi *et al.* 2016). Even government agencies uses this technique like Hazus ([n.d.]) which is multi-hazard analysis software suite for the US Federal Emergency Management Agency (Schneider and Schauer 2006), CommunityViz is also a SDSS extension for ESRI ArcGIS, it offers the ability of analysis tool used for, among other applications, urban planning, land use planning, geodesign, transportation planning and resource management applications (2003). The SDSS is not just for crisis and urban management but it can be used for various domain like iGLASS which an open source SDSS for public school location-allocation (Chen *et al.* 2018).

4.3. Health facilities data

The city of Batna counts a total of fourteen functional health centre divided into three categories (DSP 2017):

(1)   Treatment room: represent the lowest level in the (SNS), it offer basic health services only, with a low number of physicians and their availability is limited for 8 hours per day, it's for small area geographically and to serve a low number of population (refers to health facility from the level 1 in our paper).We count eight treatment room in the city.

(2)   Multi-service clinic: represent the 2nd level, it offers some advanced services with a higher number of physicians with and resources like dentists and biological analyst compared to the treatment room, availability services is 12 hours per day and in some cases 24/24 hours, In Batna we have five health facility from this level.

(3)   Hospital: The city has one hospital, it includes number of services such emergency service, it offers a 24/24 hours and 7/7 days services and has a large geographically cover all the state of Batna, it represents the 3rd level.

3.4. The capacity

As capacity can sometimes change over time, it should be assessed at the time that consent is required. This will usually be done by an appropriately trained and experienced healthcare professional who's either: recommending the treatment or investigation, involved in carrying it out. The capacity may refer to medical, or any resources that can be an obstacle to health care service. In our case the capacity refers to available medical staff who will caring the wounded.

3.5. Software and tools

The tools used is ModelBuilder which is a powerful graphical interface allows us to use different tools, variable to create models inside ArcGIS environment. The models are workflows that string together sequences of geoprocessing tools, feeding the output of one tool into another tool as input. ModelBuilder can also be thought of as a visual programming language for building workflows. While ModelBuilder is very useful for constructing and executing simple workflows, it also provides advanced methods for extending ArcGIS functionality by allowing you to create and share your models as tool (Institute 2018).

4. RESULT

4.1. Spatial health model for crisis management

The proposed model is organized into layers and every layer has an input part, a processing part and an output (**Fig. 4**), so every layer has a specific task like below:

(1)   Layer 1: the input part (input 1) initialize all required parameters in the model and start the first step of the processing:
- Variables in layer 1:
    - Field_FacilityLayer: The attribute field of the health facility level.
    - Field_Catastrophe_Cas: The attribute field of the wounded health condition.
    - Facility level: The health centre feature layer.
    - Catastrophe: result victims and wounded feature layer.
- The Processing in layer 1: it has four sub processing tools:
    - 'Iterate Field value': the first order process is iterating through all values of the wounded health condition in catastrophe feature layer.
    - 'Select Facility Layer by Attribute': get all health facility feature that match the value from Iterate Field value process.
    - 'Select Catastrophe Layer by Attribute': find all catastrophes feature that match the value from Iterate Field value process.
    - 'Calculate Value': prepare a name to assign it to solved route in layer 3.

(2)   Layer 2: The objective of this layer is to find the closest health facility that match the casualty level in the capacity. The input part (input 2) is the output of the first layer as explained in the follow:
- Variables in layer 2:
    - 'FDB.GDB': the geodatabase location path where we will store the final results.

      o 'X Barriers parameters': barriers are feature classes in network analysis layers that restrict or alter costs of the underlying edges and junctions of the associated network dataset.

      o 'Dataset': the network dataset to execute the network analysis tool.

      o 'Catastrophe_Filter' and 'Facility_Filter': the outputs of the first layer, represent a selected feature from previous layer (Layer 1).

• The Processing in layer 2: The processing part in this layer is 'Find Closest Facility' which find the closest facility (evacuation path) based on the street map of the city.

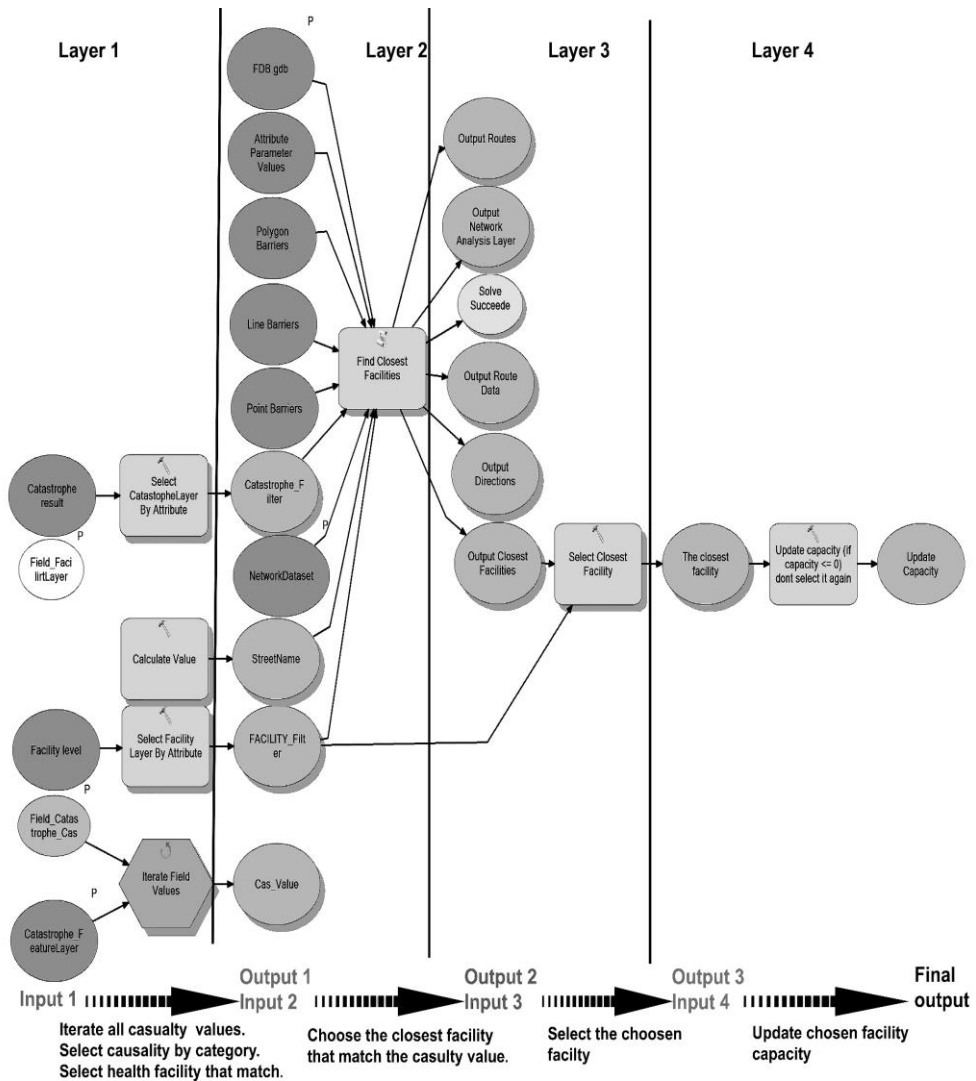(3)   Layer 3 and 4: are simply update the capacity of the chosen health centre.

Fig. 4. Spatial health model for crisis management.

4.2. Spatial health model for crisis management python code

Since the ModelBuilder uses python as the main programming language, the python code of Spatial health model for crisis management was generated with respect to the python syntax and format like the following: green colour represent comments, blue represent the reserved keywords in python, red is the argument and parameters and black colour represent the variable name (See the Model.py code file at supplement material).

```python
# Import arcpy module
import arcpy
# Load required toolboxes
arcpy.ImportToolbox("Model Functions")
# Script arguments
Field_Catastrophe_Cas = arcpy.GetParameterAsText(0)
if Field_Catastrophe_Cas == '#' or not Field_Catastrophe_Cas:
    Field_Catastrophe_Cas = "Cas" # provide a default value if unspecified
Catastrophe_FeatureLayer = arcpy.GetParameterAsText(1)
if Catastrophe_FeatureLayer == '#' or not Catastrophe_FeatureLayer:
    Catastrophe_FeatureLayer = "FDB.gdb\\Catastrophe" # provide a default value if unspecified
Field_FacilirtLayer = arcpy.GetParameterAsText(2)
Dataset = arcpy.GetParameterAsText(3)
if Dataset == '#' or not Dataset:
    Dataset = "Dataset" # provide a default value if unspecified
FDB_gdb = arcpy.GetParameterAsText(4)
if FDB_gdb == '#' or not FDB_gdb:
FDB_gdb = "FDB.gdb" # provide a default value if unspecified
```

This first part initiates the environment and load necessary package 'arcpy' that contain the main core functionalities, after import 'arcpy' package the declaration of arguments and data location and default values for every parameter is the second step.

```python
# Local variables:
Cas_Value = Catastrophe_FeatureLayer
Catastrophe_result = "Catastrophe result"
Catastrophe_Filter = Catastrophe_result
Facility_level = "Facility level"
FACILITY_Filter = Facility_level
The_closest_facility = FACILITY_Filter
StreetName = "Cas3"
Point_Barriers = "in_memory\\{B62375D9-0E03-4E3A-AB40-DD1EECA92C7E}"
Output_Routes = Point_Barriers
Output_Directions = Point_Barriers
Output_Closest_Facilities = Point_Barriers
Line_Barriers = "in_memory\\{ED87C092-03B8-4616-83B7-E1D7AEBB244C}"
Polygon_Barriers = "in_memory\\{803582EC-323C-478F-954B-35E590976E40}"
Attribute_Parameter_Values = "in_memory\\{1EE55C2C-CDD3-4B4B-8B47-A376215B4871}"
Solve_Succeeded = "true"
Output_Network_Analysis_Layer = ""
Output_Route_Data = ""
Update_Capacity = The_closest_facility
```

The second part declares all local variables used in the spatial health model for crisis management, and assignment value to every variable. There is three variable type:

- A feature variable: represent a vector layer in the geodatabase, stored in the hard drive.
- In memory variables: they are feature layer stored in memory because the model needs them temporary but not stored in the hard drive.
- Constant and real time variable: the values of this type assigned in real time (dynamic) or as constant value before executing the code.

```
# Process: Iterate Field Values
arcpy.IterateFieldValues_mb(Catastrophe_FeatureLayer, Field_Catastrophe_Cas, "String", "true", "false", "")
```

Iterate field values part using 'IteratorFieldValues_mb' tool which iterate over each value in a given field (Iterate Field Values—Tools | Documentation), the first parameter is 'Catastrophe_FeatureLayer', represent the data table that will be iterated over, the second parameter is the field name for iteration, since the model will uses the injured case to choose the best health facility, the injured case is stored in 'Field_Catastrophe_Cas' field, the third parameter is 'String' which represent a text represent the data type of the output value.

Since we want get the type of injured, we choose 'true' for the fourth parameter that represent a 'boolean' value to determine if the iteration values will be based on the unique value of the specified field or will run for each record in the input table,The fifth and last parameters determines if null values in the field will be skipped or not, and specify the null value to skip.

```
# Process: Select CatastopheLayer By Attribute
arcpy.SelectLayerByAttribute_management(Catastrophe_result, "NEW_SELECTION", "%Field_Catastrophe_Cas% = '%Cas_Value%'")
```

```
# Process: Select Facility Layer By Attribute
arcpy.SelectLayerByAttribute_management(Facility_level, "NEW_SELECTION", "Level = '%Cas_Value%' AND Capacity>0")
```

Select the injured by attribute that match the 'Cas_Value'. The 'cas_Value' represent the injured case that selected from previous code, 'Field_Catastrophe_Cas' represent the field that contain information about injured. Every case is grouped into new selection that contain the case that a facility can accept and has the ability to take care.

The same thing for health facilities, the select layer by attribute selects the health facilities that candle the selected case and in the same has a capacity above 0 so as example if we get 'value1' from previous code then the selection of facility will be all facilities of level = value1 and the selection of injured will be Fielcatatropheccas = value1 and so on.

Process: Calculate Value
```
arcpy.CalculateValue_management("'%Cas_Value%'", "", "String")
```

Process: Find Closest Facilities
```
arcpy.FindClosestFacilities_na(Catastrophe_Filter, FACILITY_Filter, "Meters", Dataset, FDB_gdb,
StreetName, "D3", "D4", "1", "", "TRAVEL_TO", "", "NOT_USED", "GEO_LOCAL",
"ALLOW_UTURNS", Point_Barriers, Line_Barriers, Polygon_Barriers, "Length_2", "Seconds", "Length",
"Meters", "NO_HIERARCHY", "", Attribute_Parameter_Values, "", "20 Kilometers", "\"g_osm_pt\"
#;\"g_osm_ln\" #;\"g_ND_Junctions\" #", "TRUE_LINES_WITHOUT_MEASURES", "10 Meters",
"DIRECTIONS", "en", "Miles", "NA Desktop", "", "", "", "", "", "", "", "NO_SAVE_OUTPUT_LAYER",
"CUSTOM", "", "NO_SAVE_ROUTE_DATA")
```

This part is simply finding the closest facility to injured person locations. The health facilities layer is the result of 'selectlayerbyattribute' from previous code and the same thing for injured.

Process: Select Closest Facility
```
arcpy.SelectLayerByLocation_management(FACILITY_Filter, "ARE_IDENTICAL_TO",
Output_Closest_Facilities, "", "NEW_SELECTION", "NOT_INVERT")
```

Process: Update capacity (if capacity <= 0) dont select it again
```
arcpy.CalculateField_management(The_closest_facility, "Capacity", "[Capacity]= [Capacity]-1", "VB", "")
```

The final part is updating the capacity of selected health facility. This done on two steps: select the closest facility, then use 'CalculateField_management' to update field capacity of the selected health facility.

4.3. Mapping the evacuation plane

The objective of the model is to manage the health module in response phase during crisis management geographically and the capacity and resources, the model should fit the following objectives:
- select all facilities with capacity and resources as a first step,
- the second step is finding the closest facility to injured,
- in the last update the capacity and resources immediately.
- Detect the health centres with capacity and level the handle every injured condition.

To test the proposed model, we simulate a risk that result 70 victims with different health conditions and we execute the model to check if the model can find the closest facilities (with good capacity). In the 2nd step we execute the model again just after the first execution, because after evacuate the injured persons in first execution the capacity of the selected health centres has been updated (**Fig. 5**).
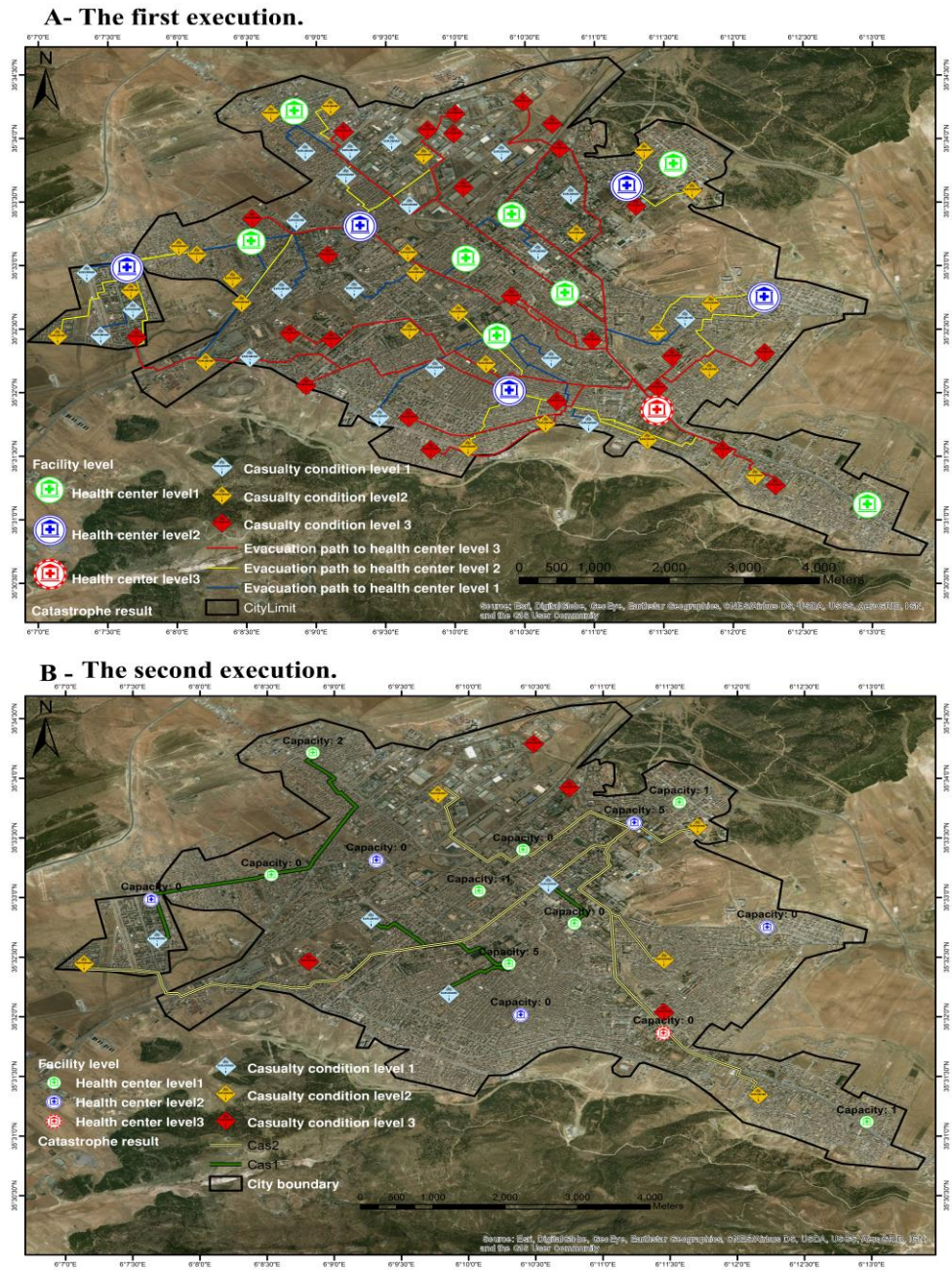
Fig. 5. Result of testing Spatial health model for crisis management.

5. DISCUSSION

The crisis management model shows very interesting results in the side of management of risks result and evacuation plane, and it's clearly fit our objective and could be using in crisis management cell and it's offered the following possibilities:

- management the data flow problem in real time.
- The geographical distribution of wounded and victims between available health centres, which mean increase the effectiveness of the evacuation plane and the health system in the city.
- Avoid the overload problem since the city has only one hospital.
- Managing data capacity in the health centres in real time so we can detect any overload or low capacity, medical supply or workforces.
- in case of any health centre is reached its maximum capacity, the management cellule crisis can reinforce it by send workforces.

After testing the crisis management model, we detect that the health system of Batna city is weak and is not effective, since evacuate 70 victims in the same time overload all health centres and they reached maximum capacity by 100%, and in case of significant risk the city need reinforcement from outside the city.

R E F E R E N C E S

Ascough, J., Rector, H., Hoag, D., McMaster, G., Vandenberg, B., Shaffer, M., … Ahjua, L. (2002). Multicriteria spatial decision support systems for agriculture: Overview, applications, and future research directions. *Integrated Assessment and Decision Support Proceedings of the 1st Biennial Meeting of the IEMSS*. U.S. DEPARTMENT OF AGRICULTURE: Agricultural Research Service, pp. 175–180.

Ayeni, B. (2003). The design of spatial decision support systems in urban and regional planning. *Decision Support Systems in Urban Planning*. London: Routledge, pp. 20–33.

Bendib, A., Dridi, H., Kalla, M. and Baziz, N. (2016). Spatial analysis of typhoid fever vulnerability in the city of Batna (eastern Algeria). *Environnement, Risques & Santé,* **15**(3), 228–237.

Bouyoucef barr, D. (2015). L'organisation territoriale de l'offre de soins : quelles réalités en Algérie. *La Revue des Sciences Commerciales,* **14**(1), 70–85.

Cadar, R.D., Boitor, M.R. and Dumitrescu, M. (2017). Effects of traffic volumes on accidents: The case of Romania's national roads. *Geogaphia. Technica,* **12**(2), 20–29.
DOI: 10.21163/GT_2017.122.03.

Chachoua, P.L. (2014). Le système national de santé 1962 a nos jours. *Colloque International Sur Les Politiques de Santé Alger.* Algeria : Ministère de la Santé, de la Population et de la Réforme Hospitalière en collaboration avec Ecole Nationale Supérieure en Sciences Politiques.

Chen, M., Thill, J.-C. and Delmelle, E. (2018). iGLASS: An Open Source SDSS for Public School Location-Allocation. *GeoComputational Analysis and Modeling of Regional Systems.* Switzerland AG: Springer, Cham, pp. 325–353.

Coutinho-Rodrigues, J., Simão, A. and Antunes, C.H. (2011). A GIS-based multicriteria spatial decision support system for planning urban infrastructures. *Decision Support Systems,* **51**(3), 720–726.

Cova, T.J. (1999). GIS in emergency management. *Geographical information systems,* **2**(12), 1999.

Cromley, E.K. and McLafferty, S.L. (2011). *GIS and Public Health.* 2nd ed. The Guilford Press.

Direction de la Programmation et du Suivi Budgétaires (2017). *Monograhie de Batna.* Wilaya de Batna.

Direction de santé et de population, Wilaya de Batna. (2017). *Rapport Annuale de Santé.* Wilaya de Batna.

Environmental Systems Research, I. (2008). *Geographic Information Systems Providing the Platform for Comprehensive Emergency Management.* Available at: https://www.esri.com/library/whitepapers/pdfs/gis-platform-emergency-management.pdf.

Filali, A. and Kalla, M. (2016). Scenario de gestion des crises en milieu urbain – cas d'El Eulma (Algérie). *Romanian Journal of Geography,* **60**(2), 203–211.

Gunes, A.E. and Kovel, J.P. (2000). Using GIS in emergency management operations. *Journal of Urban Planning and Development* **126**(3), 136–149.

Hasnat, M., Islam, M., Hadiuzzaman, M. (2018). Emergency response during disastrous situation in densely populated urban areas: a GIS based approach. *Geographia Technica,* **13**(2), 74–88. DOI: 10.21163/GT_2018.132.06.

Institute, E.S.R. (2018). *What Is ModelBuilder? — Help ArcGIS Desktop.* Available at: https://desktop.arcgis.com/en/arcmap/latest/analyze/modelbuilder/what-is-modelbuilder.htm [Accessed: 1 February 2020].

Issam, K.M. and Said, G.M. (2017). Using geomatics for assessing vulnerability to cutaneous leis hmanisais. Application to the wilaya of Batna (Algeria). *International Journal of GEOMATE* **13**(40), 9–15.

Johnson, R. (2000). GIS technology for disasters and emergency management.

Makropoulos, C., Butler, D. and Maksimovic, C. (2003). Fuzzy logic spatial decision support system for urban water management. *Journal of Water Resources Planning and Management* **129**(1), 69–77.

Malczewski, J. (1999). *GIS and Multicriteria Decision Analysis.* Us: John Wiley & Sons.

Meika, J. (2010). *The Benefits of GIS.* Available at: https://www.gislounge.com/the-benefits-of-gis/ [Accessed: 4 August 2019].

Mora, M., Forgionne, G.A. and Gupta, J.N. (2003). *Decision Making Support Systems: Achievements, Trends, and Challenges for the New Decade.* Hershey, PA: Idea Group Pub.

Nasereddine, A. (2016). The conditions of risk management in health facilities-Case study of public institutions nearby care of Algéria/EPSP. *Ru'á Iqtişadīyah* **6**(10), 283–301. doi: https://doi.org/10.12816/0034060.

Nicoară, P.-S. and Haidu, I. (2014). A GIS based network analysis for the identification of shortest route access to emergency medical facilities. *Geographia Technica,* **9**(2), 60–67.

Oufriha, F.Z. (2006). Les réformes du système de santé en Algérie. In: Oufriha, F. Z. (ed.). *De Réforme En Réforme: Un Système de Santé à La Croisée Des Chemins.* Algeria: Ed. CREAD, pp. 103–116.

Protection, civil (2017). *Disaster History 1962-2012*. Algeria: Protection civile Algeria.

Rogers, P. and others (2011). Development of resilient Australia: enhancing the PPRR approach with anticipation, assessment and registration of risks. *Australian Journal of Emergency Management,* **26**(1),54.

Ruda, A. (2014). Spatial decision making for logistics centre allocation. *Geographia Technica* **9**(2), 85–97.

Schneider, P.J. and Schauer, B.A. (2006). HAZUS—its development and its future. *Natural Hazards Review,* **7**(2), 40–44.

Sugumaran, R. and Degroote, J. (2010). *Spatial Decision Support Systems: Principles and Practices*. Crc Press.

Sultani, R., Soliman, A. and Al-Hagla, K. (2009). The Use of Geographic Information System (GIS) Based Spatial Decision Support System (SDSS) in Developing the Urban Planning Process. *Architecture & Planning Journal,* **20**, 97–115.

Wangdi, K., Banwell, C., Gatton, M.L., Kelly, G.C., Namgay, R. and Clements, A.C. (2016). Development and evaluation of a spatial decision support system for malaria elimination in Bhutan. *Malaria journal* **15**(1),180.

Zhang, Z., Liu, Y., Li, J. and Chen, B. (2009). Application of GIS and spatial decision support system for affordable housing. *Proceedings of 2009 4th International Conference on Computer Science and Education, ICCSE 2009*. pp. 1110–1115.

CommunityViz City Explained, Inc. (2003). Available at: https://communityviz.city-explained.com/communityviz/index.html [Accessed: 1 February 2020].

Hazus | FEMA.Gov. Available at: https://www.fema.gov/hazus [Accessed: 1 February 2020].

Aims and Scope

Geographia Technica is a journal devoted to the publication of all papers on all aspects of the use of technical and quantitative methods in geographical research. It aims at presenting its readers with the latest developments in G.I.S technology, mathematical methods applicable to any field of geography, territorial micro-scalar and laboratory experiments, and the latest developments induced by the measurement techniques to the geographical research.

Geographia Technica is dedicated to all those who understand that nowadays every field of geography can only be described by specific numerical values, variables both oftime and space which require the sort of numerical analysis only possible with the aid of technical and quantitative methods offered by powerful computers and dedicated software.

Our understanding of *Geographia Technica* expands the concept of technical methods applied to geography to its broadest sense and for that, papers of different interests such as: G.I.S, Spatial Analysis, Remote Sensing, Cartography or Geostatistics as well as papers which, by promoting the above mentioned directions bring a technical approach in the fields of hydrology, climatology, geomorphology, human geography territorial planning are more than welcomed provided they are of sufficient wide interest and relevance.

Targeted readers:

The publication intends to serve workers in academia, industry and government.
Students, teachers, researchers and practitioners should benefit from the ideas in the journal.

Guide for Authors

Submission

Articles and proposals for articles are accepted for consideration on the understanding that they are not being submitted elsewhere.

The publication proposals that satisfy the conditions for originality, relevance for the new technical geography domain and editorial requirements, will be sent by email to the address editorial-secretary@technicalgeography.org.

This page can be accessed to see the requirements for editing an article, and also the articles from the journal archive found on www.technicalgeography.org can be used as a guide.

Content

In addition to full-length research contributions, the journal also publishes Short Notes, Book reviews, Software Reviews, Letters of the Editor. However the editors wish to point out that the views expressed in the book reviews are the personal opinion of the reviewer and do not necessarily reflect the views of the publishers.

Each year two volumes are scheduled for publication. Papers in English or French are accepted. The articles are printed in full color. A part of the articles are available as full text on the www.technicalgeography.org website. The link between the author and reviewers is mediated by the Editor.

Peer Review Process

The papers submitted for publication to the Editor undergo an anonymous peer review process, necessary for assessing the quality of scientific information, the relevance to the technical geography field and the publishing requirements of our journal.

The contents are reviewed by two members of the Editorial Board or other reviewers on a simple blind review system. The reviewer's comments for the improvement of the paper will be sent to the corresponding author by the editor. After the author changes the paper according to the comments, the article is published in the next number of the journal.

Eventual paper rejections will have solid arguments, but sending the paper only to receive the comments of the reviewers is discouraged. Authors are notified by e-mail about the status of the submitted articles and the whole process takes about 3-4 months from the date of the article submission.

5 948422 015163